

Cover Page



Universiteit Leiden



The handle <http://hdl.handle.net/1887/37129> holds various files of this Leiden University dissertation

**Author:** Wink, Steven

**Title:** Systems microscopy to unravel cellular stress response signalling in drug induced liver injury

**Issue Date:** 2015-12-22

**Systems microscopy to unravel  
cellular stress response signalling  
in drug induced liver injury**

**Steven Wink**

**Systems microscopy to unravel cellular stress response signalling in drug induced liver injury**

Steven Wink

December 2015

Cover design: Steven Wink

Printing: CPI/Wöhrmann Print Service, Zuthpen

ISBN: 978-94-6203-963-6

© 2015 Steven Wink

No part of this thesis may be reprinted, reproduced or utilized in any form or by any electronic, mechanical or other means, now known or hereafter invented, without written permission of the author.

# **Systems microscopy to unravel cellular stress response signalling in drug induced liver injury**

**Proefschrift**

ter verkrijging van  
de graad van Doctor aan de Universiteit Leiden  
op gezag van de Rector Magnificus, prof. mr. C.J.J.M. Stolker,  
volgens besluit van het College voor Promoties  
te verdedigen op dinsdag 22 december 2015 klokke 11:15

door

**Steven Wink**

geboren op 2 april 1980 te Warnsveld, Nederland



## **Promotor**

Prof. Dr. B. van de Water

Leiden University

## **Promotion committee**

Prof. Dr. P.H. van der Graaf

Leiden University

Prof. Dr. J. Kuiper

Leiden University

Prof. Dr. A.P. Ijzerman

Leiden University

Prof. Dr. G. M. M. Groothuis

University of Groningen

Prof. Dr. J. Kleinjans

University Maastricht

This research was conducted at the Division of Toxicology of the Leiden Academic Centre for Drug Research, Leiden University, Leiden, The Netherlands

## Table of contents

<b>Chapter 1</b>	<b>1</b>
General introduction and background.	
<b>Chapter 2</b>	<b>13</b>
Quantitative High Content Imaging of Cellular Adaptive Stress Response Pathways in Toxicity for Chemical Safety Assessment.	
<b>Chapter 3</b>	<b>37</b>
High Content Imaging-based BAC-GFP Toxicity Pathway Reporters to Assess Chemical Adversity Liabilities.	
<b>Chapter 4</b>	<b>59</b>
Drug-induced Endoplasmic Reticulum and Oxidative Stress Responses Independently Sensitize Towards TNF $\alpha$ -mediated Hepatotoxicity.	
<b>Chapter 5</b>	<b>85</b>
Activation of the Nrf2 response by intrinsic hepatotoxic drugs correlates with suppression of NF- $\kappa$ B activation and sensitizes towards TNF $\alpha$ -induced cytotoxicity.	
<b>Chapter 6</b>	<b>113</b>
Automated live cell imaging of adaptive stress responses for assessment of drug-induced liver injury (DILI) liabilities.	
<b>Chapter 7</b>	<b>139</b>
User friendly high-content imaging big-data analysis on a single desktop: R package H5CellProfiler.	
<b>Chapter 8</b>	<b>155</b>
Overall discussion and conclusions.	
<b>Appendix</b>	
References	<b>162</b>
List of abbreviations	<b>174</b>
Samenvatting	<b>175</b>
List of publications	<b>180</b>
Curriculum Vitae	<b>182</b>



# Chapter 1

## General introduction and background.

---

### **1. Drug-induced liver injury: a major problem in drug development.**

#### **1.1. The liver.**

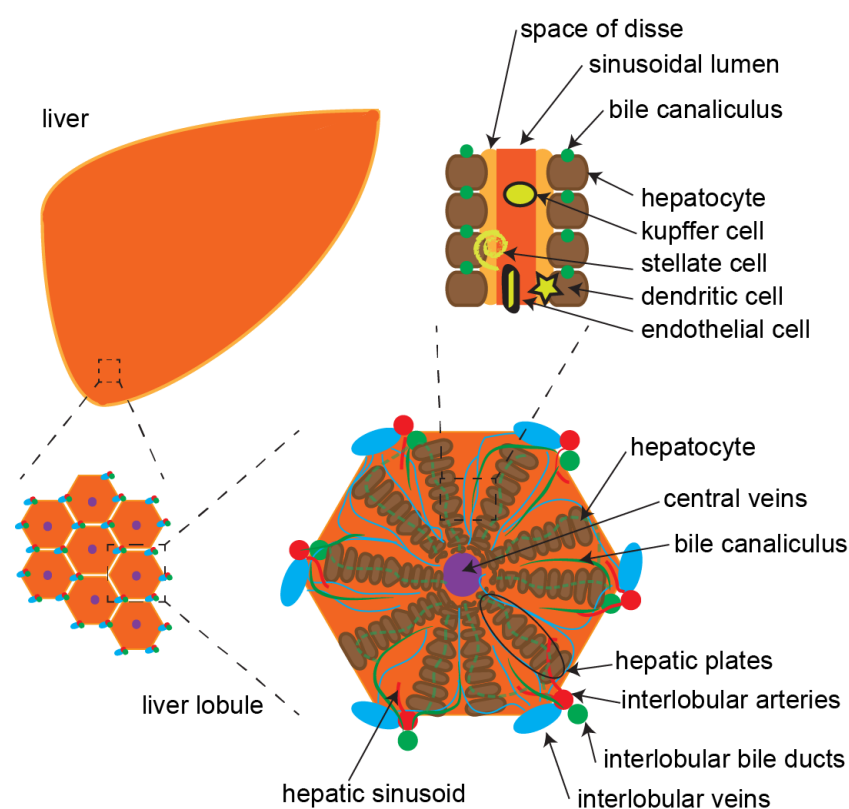
The liver is the main metabolizing organ and the first organ encountered by nutrient rich blood delivered by the hepatic vein which originates from the gastrointestinal tract. The liver consists of millions of functional subunits: individual hexagon lobules made up of the parenchyma surrounded by portal triads (Fig. 1). The portal triads consist of bile ducts, hepatic arteries and portal veins. The liver consists of the parenchyma and non-parenchyma cell types. More than 70% of the liver is composed of the parenchyma: the hepatocytes. Hepatocytes are responsible for most of the liver metabolizing capacity and contain the drug metabolizing enzymes and transporters responsible for xenobiotic transformation. Non parenchymal cells are cholangiocytes (bile duct epithelial cells), sinusoidal cells (which form triad walls) and several immune related cells such as the stellate cells, Kupfer cells and pit cells. Because hepatocytes are by far the most abundant cell type and responsible for the liver metabolizing capacity and detoxification/xenobiotic metabolism these cells are typically used for in vitro toxicity testing.

#### **1.1. Drug-induced liver injury.**

Drug-induced liver injury (DILI) constitutes liver injury as the result of drug treatments with potentially fatal adverse events. DILI can be classified into a hepatic, cholestatic or mixed phenotype. Hepatic DILI involves damage and cell death of the parenchyma which are the hepatocytes. Cholestasis involves perturbations due to altered bile acid metabolism and transport culminating in accumulation of bile in the liver or damaged bile canaliculi. Additional DILI pathophysiological phenotypes include: steatosis, the accumulation of fat droplet in the liver due to fatty acid metabolism; phospholipidosis, the accumulation of phospholipids in the liver; inflammation, the infiltration of leucocytes in the liver; and fibrosis, the increase of scarred fibrotic tissue in the liver.

#### **1.2. Societal impact of DILI.**

The market for pharmaceutical compounds in the EU is estimated at a yearly turnover of 205 billion Euro (Eurostat data 2015) with an estimated average of 0.6 % (1.2 billion) spent on drug safety (European Commission pharmacovigilance report, 2008). However the social financial impact of preventable adverse drug reactions (ADR's) in the same report is estimated at 24 billion annually for the European population. This estimated cost is based on a 5 % incidence of ADR's during hospitalization [1], a 5% ADR related hospital admission [2] and drug-related morbidity and mortality other than hospital admission or prolonged hospitalization [3]. Moreover, the public



health importance of ADR's is estimated at 200,000 deaths annually in the EU alone [1]. In addition ADR's lead to preclinical discontinuation and post market withdrawals.

**Figure 1: Cell types within a liver and structure of a liver lobule.** The smallest functional unit of a liver is the lobule which each has a set of interlobular -veins, -arteries and -bile ducts attributed to it and a single central vein. The liver is built up of parenchymal and several non-parenchymal cell types.

Hepatic and cardiac toxicity has contributed disproportionately to drug withdrawals: of 47 drugs withdrawn during the period 1975 - 2007, 21 were related to cardiotoxicity and 15 involved hepatic toxicity [4]. DILI is responsible for 30% of drug withdrawals from the market [5] and non-approvals by regulatory authorities.

Often no changes in hepatocellular toxicity parameters such as alanine or aspartate aminotransferase (ALT/AST) levels or increased total bilirubin are found in pre-clinical settings and drugs are marketed until more than 1 in 10,000 drug users demonstrate signs of liver failure [6].

Severe DILI in the clinical setting is most typically caused by a so called idiosyncratic reaction which by definition means dose independent and rare ( $<1:10,000$ ) and thus highly unpredictable. Preclinical studies often miss these rare idiosyncratic reactions due to limitation on the feasible number of test animals and species specific differences. In addition to idiosyncratic reactions also 'normal' DILI found in preclinical animal studies or during human trials is difficult to predict and as such causes many compounds to be terminated and thus imposes significant costs for the pharmaceutical industry [7]. For these reasons major efforts are being made by industry and academia to obtain better biomarkers to better understand and predict DILI pre-clinically.

## 2. In vitro toxicity testing methods.

### 2.1. Safety assessment and the Adverse Outcome Pathway (AOP) paradigm.

The current preclinical testing paradigm has improved drug safety over the last 30 years; it is estimated that 70% of human toxicity is predicted pre-clinically [8]. Typically animal experiments are performed pre-clinically to rule out as much toxic compounds as possible. For the liver these animal studies are used to determine histopathological endpoints after acute or repeated dosing of the drug. Pathologists then determine if the liver toxicity shows signs of acute, cholestatic, steatotic, necrotic or fibrotic phenotypes. However such endpoints unfortunately do not provide

much information on the mechanism of the observed drug-induced liver toxicity. In addition to this scientific shortcoming, public pressure against animal testing, exemplified by the ban on animal testing for cosmetics in Europe, and increasing societal momentum to implement more modern scientific methods for pre-clinical testing is apparent. Several multimillion funded consortia have worked on human relevant alternatives such as SEURAT-1 and MIP-DILI in Europe and ToxCast and Tox21 in the U.S. to work on these issues. Thus there is a strong incentive for consortia to focus on implementing modern scientific methodologies which are focused on human-relevant concepts. These methodologies are founded on developing a mechanistic understanding of adverse drug reactions in *in vitro* based models for evidence and read across-based approaches for risk assessment. One such methodology developed by the OECD in 2012 being the initiation and population of the Adverse Outcome Pathway (AOP) framework. The AOPs framework is described as a “sequential chain of causally linked key events at different levels of biological organization that together culminate in an adverse health outcome or ecotoxicological effect”. While several AOPs have been established, a next important step is to translate AOP-related mechanistic understanding in advanced, preferably quantitative, high throughput assays that reflect pathways essential in target organ toxicity. Such an AOP framework is highly suited as an evidence-gathering-based approach in which affected (adaptive stress) pathways can be included as a fundamental cellular response following biochemical perturbation due to chemical exposure, also branded as the molecular initiating events (see Fig. 2).

## 2.2. Overall *in vitro* methods for safety assessment.

What is the diversity of *in vitro* methods that are available? Firstly, several *in vitro* and *in silico* methods currently exist that can predict the pharmacokinetic properties and clearance of compounds [9]. Compounds that are metabolized or affect liver metabolic enzymes can be identified by *in vitro* methods. Secondly, cytotoxic endpoint assays have been developed to determine *in vitro* EC<sub>50</sub>-values for apoptosis and necrosis using colorimetric assays.

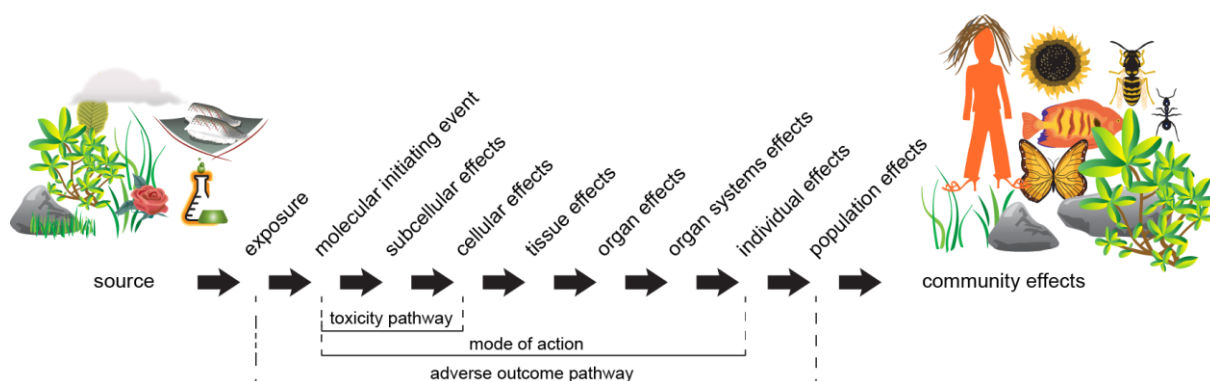


**Figure 2: The AOP framework.** An evidence gathering based approach starting from the source to the final adverse effects. Figure adapted from K. Crofton 2010, OECD AOP Meeting Definitions

Thirdly, more mechanism-based *in vitro* methods exist that can give insight into the type of toxicity in cells such as the MTT assay which reflects NAD(P)H dependent metabolic activity of cells, MitoSOX-red which is a mitochondrial superoxide indicator [10], lipid dyes which visualize phospholipid accumulation e.g. Bodipy 493/503, and the fluorescent phospholipid probe NBD-PE [11] or Fluo-4 AM to detect cytoplasm free-calcium levels [12]. In addition certain dyes are

capable of selectively binding to certain organelles or substructures such as the mitochondria, golgi, chromosomal DNA or cell membranes and perturbation of these structures after chemical exposure can be detected in this manner. Antibodies are often used in *in vitro* toxicity assays to detect perturbations of protein levels or to visualize organelles and cellular structures such as actin to detect cell-cell junctions or bile canaliculi. Polymerase chain reaction (PCR) or luciferase assays are used to monitor changes in transcript levels of certain key transcripts such as the nuclear receptors [13], anti-oxidant response element transcripts or phase I, II and III drug metabolism enzymes. Fourthly, most *in vitro* assays using the above approaches are based on monolayer cultures that do not fully mimic the *in vivo* context. More complex *in vitro* testing strategies are in development which try to mimic the 3D structure [14], multiple cell type interactions and mechanical flow and shear stress based on microfluidic reactors [15, 16].

Development of all these functional assays, largely based on an improved understanding of the cellular pathways involved on chemical induced toxicity, is increasingly based on mechanistic concepts. Within the development of these assays one of two broad routes can be defined: on the one hand the more physiological relevant liver models and on the other hand the more detailed mechanism-based predictive models. The physiological mimicking of the liver has obtained increased interest in recent years, and models such as liver slices [17], 3D models [18], pluripotent stem cell-derived differentiated cell lines [19] and liver bioreactors [16] are being developed in many investigations and some are already utilized in safety testing strategies. Mechanism-based toxicological readouts and throughput from these models are often more limited due to several technical limitations such as the inability to perform high resolution high content imaging or single cell type quantification of proteins or metabolites. Often general macro-phenotypic profiling, measurements in culture supernatant of metabolites or secretion and leakage of specific proteins from these models is performed. The more detailed mechanism-based models under development focus more on detailed mechanistic insight of molecular networks and the molecular initiating events as well as key events that eventually lead to cellular adversity (see the AOP framework earlier). More robust models that can be cultured easily and are highly reproducible are used, including the cancer-derived cell lines HepG2 and HepaRG. These models also enable functional genomics assessment of molecular mechanisms using e.g. small interfering RNA knock down approaches and the generation of genetically modified (often knock-out or tagged) cell lines; this is not possible with primary human hepatocytes. It is the combination of these two different approaches that will take science to the next level of understanding chemical-induced toxicity. This thesis focuses on the second approach: application of genetically modified hepatoma cell lines to unravel mechanism of action in the context of DILI.

### **3. From molecular mechanisms to DILI prediction.**

#### **3.1. Mechanisms of DILI.**

For only several drugs the underlying mechanisms leading to DILI is by and large elucidated. The best known example is acetaminophen, which induces acute liver injury after overdosing. The cytochrome-P450 enzyme system metabolizes acetaminophen into more hydrophilic and reactive metabolites including N-acetyl-p-benzoquinone imine (NAPQI) [20]. At lower concentrations NAPQI does not accumulate because antioxidant molecules such as glutathione act as a redox buffer clearing the reactive NAPQI before it can bind and damage macromolecules and elicit

further significant cellular damage. However after an overdose acetaminophen, glutathione becomes depleted and cellular damage caused by NAPQI leads to acute liver damage. The ultimate cell death involves many cellular perturbations, including mitochondrial injury, increased reactive oxygen formation, activation of cellular stress pathways, that all individually contribute to the onset of cell death [21, 22].

A second well-known example is the dose-dependent toxicity of valproic acid. Valproic acid is a simple fatty acid and therefore a substrate of the  $\beta$ -oxidation pathway. Valproic acid and its metabolites can cause interference with e.g. mitochondrial  $\beta$ -oxidation, oxidative phosphorylation, and depletion of CoA culminating in the accumulation of fatty acids in liver cells eventually resulting in microvesicular steatosis [23-25].

Unfortunately for most compounds that induce severe DILI the exact molecular mechanisms are not fully understood and various plausible mechanisms for individual drugs have been proposed that could contribute to DILI. Below various molecular mechanisms that contribute to DILI are discussed in more detail with a focus on several key adaptive stress response programs.

### **3.2. Mitochondria injury, oxidative stress & apoptosis: an intricate interplay.**

Mitochondrial dysfunction is considered a key component to the overall mechanism of many DILI related drugs [26]. In the literature many examples can be found involving drug-induced impairment of mitochondrial fatty acid oxidation (see above the example of valproic acid), electron transfer within the respiratory chain, oxidative phosphorylation and mitochondrial DNA damage [27]. The mitochondria are central to cellular metabolism as the reduction of oxygen to water fueled by organic catabolic processes provides the necessary energy in the form of ATP. With limited ATP supply the overall cell function will be severely affected as most cellular metabolic processes require energy; eventually cells will die. Importantly, mitochondrial function is linked to the cellular redox state of the cell as the mitochondrial respiratory chain is critical in the  $\text{NAD(P)}^+/\text{NAD(P)H}$  ratio. Therefore, mitochondrial dysfunction will inherently lead to oxidative stress and overproduction of reactive oxygen species and lipid peroxidation [28].

In addition, mitochondria function as a central hub in programmed cell death. Cell death signals, such as mediated by the mitochondrial translocation of the pro-apoptotic Bcl2 family member Bax, leads to the formation and opening of mitochondrial permeability transition (MPT) which leads to the release of mitochondrial calcium and loss of mitochondrial membrane potential and therefore ATP production [29] as well as release of cytochrome c. A second mechanism related to mitochondrial control of programmed cell death is the formation of mitochondrial outer membrane pores (MOMP) that do contain BAX/BAK dimers. These pores mediate the release of mitochondrial proteins such as cytochrome c and other pro-apoptotic factors such as apoptosis inducing factor (AIF), and Smac/Diablo [30]. The release of the pro-apoptotic proteins defines the formation of the apoptosome, containing cytochrome c, APAF1 and pro-caspase-9 as well as dATP, resulting in activation of caspase-9 followed by downstream activation of caspase-3. Since ATP is required for apoptosis, severe impairment of cellular metabolism caused by chemical-induced mitochondrial damage will inhibit the onset of programmed cell death. In this more severe and uncontrolled manner cell death will occur by necrosis. Following necrosis so-called damage activation molecular patterns (DAMPs) are released from cells into the extracellular space resulting in attraction and activation of innate immune cells which in turn will release cytokines



such as TNF $\alpha$ . These cytokines in turn act as a signal to recruit additional immune cells. Additionally, TNF $\alpha$  will activate intracellular NF- $\kappa$ B signalling in a paracrine manner on the hepatocytes, which may also affect overall cell survival.

In contrast to mitochondrial impairment that may indirectly cause oxidative stress, direct chemically-induced oxidative stress either in the form of pro-oxidants, alkylating agents or reactive metabolites, can directly affect the antioxidant status in cells by reducing the free (non)-protein thiol status and initiating oxidative stress. The decreased cellular antioxidant status, as mentioned earlier, can impair the mitochondrial oxidative phosphorylation; reactive oxygen species (ROS) can also damage mitochondrial DNA. ROS in general is an often cited mechanism for drug-induced liver injury [31]. ROS causes DNA damage, protein oxidation and lipid peroxidation which impairs normal cellular function and cell death. Given the fact that control of oxidative stress is of paramount importance for overall cell maintenance and cell survival, the KEAP1/Nrf2-mediated antioxidant adaptive stress program has evolved as a universal mechanism across cell types and species to control ROS-levels. It is for this reason that we established several BAC-GFP reporter cell lines to quantitatively monitor the Nrf2-mediated oxidative stress response at the single cell level using automated live cell imaging (see Chapter 2 and 3 for further details).

### **3.3. The unfolded protein response in the endoplasmic reticulum.**

In the context of molecular toxicology the endoplasmic reticulum (ER) is most well-known for the xenobiotic enzymes located in the membrane folds such as P450 enzymes, UDP-glucuronosyltransferases (UGTs) and glutathione S-transferases and for its ability to store large amounts of intracellular calcium. Therefore the ER is a source of xenobiotic transformation and resultant reactive intermediates. Moreover, upon impairment of the ER membranes large amounts of calcium are released into the cytosol resulting in activation of pro-apoptotic signalling via the previously mentioned mitochondrial perturbations [32].

The main cell physiological role of the ER is protein folding and post translational protein modification. Compounds that interfere with these processes cause the activation of the so-called Unfolded Protein Response (UPR). The UPR consists of three major branches regulated via three transmembrane transducer proteins: activating transcription factor 6 (ATF6), protein kinase R-like ER kinase (PERK) and inositol-requiring enzyme 1- $\alpha$  (IRE-1 $\alpha$ ) [33]. The activation level of these three distinct routes determines the balance of the resultant unfolded protein response. Thus, ATF6 and IRE-1  $\alpha$  activation lead to a more pro-survival physiologic response such as increased chaperone production; in contrast PERK activation leads to translation inhibition and with prolonged activation of downstream target Chop (DDIT3) and can sensitize cells to pro-apoptotic signalling [34]. Further details regarding on the ER-stress/ unfolded protein response are presented in chapter 2.

### **3.4. Inflammatory signalling and DILI.**

The involvement of the immune system in DILI has been suggested for several drugs such as diclofenac, carbamazepine and methimazole [35] and are often known as hypersensitivity reactions. Several hypothesis have been suggested such as the hapten hypothesis, genetic disposition of HLA alleles or direct binding of the (parent) compound to T-cell receptors [36]. Recent work has demonstrated the importance of drug reactive metabolite-mediated adaptive

stress response signalling and cytokine-induced pro-apoptotic signalling in DILI [37, 38]. Following liver damage immune cells infiltrate the liver and secrete pro-inflammatory cytokines which can further exacerbate inflammation and liver damage.

Tumor necrosis factor- $\alpha$  (TNF $\alpha$ ) is the main pro-inflammatory cytokine excreted by liver resident macrophages known as Kupffer cells. TNF $\alpha$  has been shown to increase liver damage caused by various drugs [39]. TNF $\alpha$  activates the tumor necrosis factor receptor (TNF receptor) which in turn activates pro-apoptotic signalling via its death domain and also activates NF- $\kappa$ B signalling. Upon activation NF- $\kappa$ B transiently translocates to the nucleus to activate downstream target genes mainly involved in cytoprotective (anti-apoptotic proteins) and inflammatory (cytokines) mechanisms (Liu et al. 1996). Reactive metabolites from DILI-related drugs typically provoke a cellular oxidative stress environment thereby initiating the stabilization and activation of the transcription factor Nrf2 (Li et al. 2005). Downstream antioxidant genes contribute to adaptation and protection of cells against the reactive metabolite induced oxidative stress. Several studies indicate that Nrf2 activation can act to suppress NF- $\kappa$ B-based immune signalling responses (Chen et al. 2006) which would indicate Nrf2 could be involved in NF- $\kappa$ B dysregulation in DILI. This is also part of our own investigations described in Chapter 5.

### 3.5. Toxicogenomics legacy data: TG-GATES

The above adaptive stress response pathways are not the only cellular responses to toxic insults. In the past decade major progress within the toxicology field has been made to unravel a multitude of cellular responses that are initiated by xenobiotic exposure using omics technologies with the focus on transcriptomics and to lesser extent metabolomics and proteomics. More recently the attention has shifted to epigenomics and regulation by the microbiome [40] as well as the more recently developed transcriptomic technology RNA-sequencing [41]. Many gene-set based biomarkers have been reported in literature originating from omics-research [42, 43]; here optimized gene-, metabolic- or protein fingerprints/profiles were developed based on training compound sets. Several examples indicate that such profiles can add to hazard identification early in the drug development process [44]. The major benefit that emerged from these omics efforts is more likely to be the increased understanding of the biological pathways involved in the cellular, organ and organism adversity [45]. Omics-based technologies provide novel insights into the type of cellular processes initiated following chemical exposure. These insights are then followed up by more detailed mechanistic investigations. Thanks to the increased understanding of xenobiotic-induced toxicity it has become possible to create evidence-based frameworks (e.g. the AOP framework, see above) based on mechanistic understanding that can be implemented in safety testing strategies.

Throughout this thesis we used the legacy toxicogenomics dataset TG-GATES [46]. The TG-GATES dataset is available in the public domain in the form of Affymetrix .CEL files (<http://toxico.nibio.go.jp/>). The TG-GATES dataset originates from the Japanese Toxicogenomics Project which ran from 2004 to 2014 as a joint government-private sector project organized by the National Institute of Biomedical Innovation (NIBIO), the National Institute of Health Sciences (NIHS) and 18 pharmaceutical companies [46]. The main bulk of the data consists of Affymetrix microarray obtained transcript profiles from liver rat *in vivo* (acute and repeated dosing), primary rat hepatocytes (PRH) and primary human hepatocytes (PHH) at several time points and

concentrations. In total over 170 compounds were tested of which the majority are DILI-related drugs but also some kidney injury-related drugs and negative controls were included. In addition to the liver models a subset of the data consists of *in vivo* rat kidney repeat and acute dosing samples. The TG-GATES dataset is one of two examples of DILI-relevant and rich (encompassing large compound sets with various mechanisms of toxicity) datasets that are publicly available; DrugMatrix [47] being the second, and most large pharmaceutical companies maintain their own private rat (microarray) databases. Thus, the whole-genome transcriptomic profile of the majority of DILI related drugs is already known. Since time and dose-response relationship transcriptomic profiles are generally unavailable, due to the cost of performing microarray experiments, the TG-GATES data has paved the way to understanding general and specific responses of cells to DILI-related drugs. In addition, these transcriptomic datasets can be utilized for biomarker discovery as well as be the starting point for more functional and mechanistic understanding of DILI. In this thesis the TG-GATES dataset has extensively been used for several purposes: 1) the comparison of the HCl derived HepG2 reporter-protein levels with the transcript level in primary human hepatocytes; 2) data mining the TG-GATES data for suitable candidate BAC-reporter genes; 3) mapping of the transcriptomic profiles to more biological interpretable pathways to better understand the role of adaptive stress response pathways and inflammatory signalling to subsets of DILI-related compounds. In essence, the utilization of a previously established dataset and integration with HCl-derived data is a systems toxicology approach to efficiently combine diverse sets of models and datatypes to better understand cellular biology underlying DILI.

#### **4. From mechanisms of toxicity to fluorescent reporters for high content imaging.**

##### **4.1. The BAC-GFP reporter platform.**

To better assess the underlying mechanisms of chemical-induced liver toxicity we established a large set of reporter cell lines that quantitatively define the mode-of-action of chemicals. For this we have used the Bacterial Artificial Chromosome (BAC) cloning technology [48]. A BAC is a large plasmid containing double-strands genomic DNA and therefor includes regulatory sequences such as endogenous promoters and endogenous splicing mechanisms due to the inclusion of intron sequences. A BAC is selected based on the target gene of interest, and an additional requirement that on both sides of the outer exons of the gene of interest at least 10,000 base pairs must be situated to include regulatory elements. With homologous recombination a fluorescent tag, typically GFP, and resistance marker are cloned in the BAC plasmid, usually in frame at c-terminal side of the last intron of the gene of interest, resulting in the generation of a fusion of the gene-product of interest and GFP. The modified BAC can be introduced in cell lines. For this purpose we use the HepG2 cells, a hepatocellular carcinoma cell line with some human hepatocyte characteristics that is often used for early pre-clinical assessment of cytotoxicity liabilities. The introduction of the BAC-GFP constructs into HepG2 by transfection is followed by selection of monoclonal modified HepG2 cells which can be further selected based on suitability for imaging and homogeneity of the fluorescence level of the individual cells. HepG2 cells were selected based on several considerations. Firstly the HepG2 cell has several properties similar to that of hepatocytes. Secondly HepG2 cells are easy to culture and remain viable up to 30 passages and proliferate fast enough (doubling time of around 1 day) to allow selection after genetic modification. The application of this BAC-GFP technology in mechanistic toxicology is further

introduced in chapter 2, while throughout the thesis BAC-GFP reporter cell lines have been applied for interrogation of pathway of toxicity activation.

#### **4.2. High content imaging of key adaptive stress networks.**

As discussed briefly above the primary repair and defense mechanism of cells following chemical exposure are the adaptive stress response programs (Fig. 3). The key rationale to monitor in particular these adaptive stress response pathways follows from the paradigm that the molecular initiating events result in an altered (intracellular) biochemical environment that, as a first step, provokes activation of the various adaptive stress response pathways. Which pathways are activated depends on the mode-of-action as well as the concentration of individual compounds.

The cell senses these environmental changes via upstream biochemical sensors (e.g. Keap1 for the Nrf2-activated oxidative stress response) and responds via signalling networks called adaptive stress response pathways. These pathways are physiological pathways and as such activation does by itself not correspond to or imply toxicity. We anticipate that it is essential to monitor the magnitude of the response of all individual adaptive stress response pathways and to understand at which point a threshold, or breaking point, is reached when the cell can no longer cope with the chemically-imposed stress. At this stage cells would die by either apoptosis, necrosis, necroptosis or in milder cases where only organelles are damaged autophagy. By monitoring the concentration and time relationships of chemical-induced stress responses, it is possible to separate the initial (causative) adaptive stress type from secondary adaptive stress-types. To illustrate this, imagine the following: some compound affect proper folding of proteins in the endoplasmic reticulum resulting in the activation of the unfolded protein response (UPR), translation initiation inhibition and selective protein translation of chaperones. At a certain concentration the UPR is unable to re-establish homeostasis in the endoplasmic reticulum and proper protein folding and transport is impaired as well as release of  $\text{Ca}^{2+}$  from the lumen of the ER. Due to this impairment, secondary effects, such as oxidative stress, are expected to occur. Only by obtaining detailed maps of the concentration and time course relationships of the activation of the various adaptive stress response networks can such time resolved primary and secondary mechanistic insights be uncovered.

During the live cell imaging-based assessment of pathway activation one can simultaneously monitor the fate of the cells, the onset of necrosis or apoptosis, cell proliferation, and cell migratory behaviour. This allows the evaluation the relationship between mode and magnitude of toxicity pathway activation and cell fate caused by xenobiotic exposure. These relationships inform us on the mechanism of toxicity. Such combinations of biological readouts can be interpreted as a dynamic biological 'fingerprint'. Importantly, such fingerprints allow unsupervised clustering methods to define sets of compounds with similar mode of action and cell fate. Such strategies can aid in prediction of toxic liabilities.

#### **5. High content imaging.**

High content imaging (HCI) has evolved greatly in the past two decades due to the technological advancement of microscopy technology. Automated microscopes can be fitted with incubation systems enabling live cell imaging. Robotic arms for multi-well imaging plate loading in combination with robotic liquid handlers lead to high throughput imaging-based experimentation.

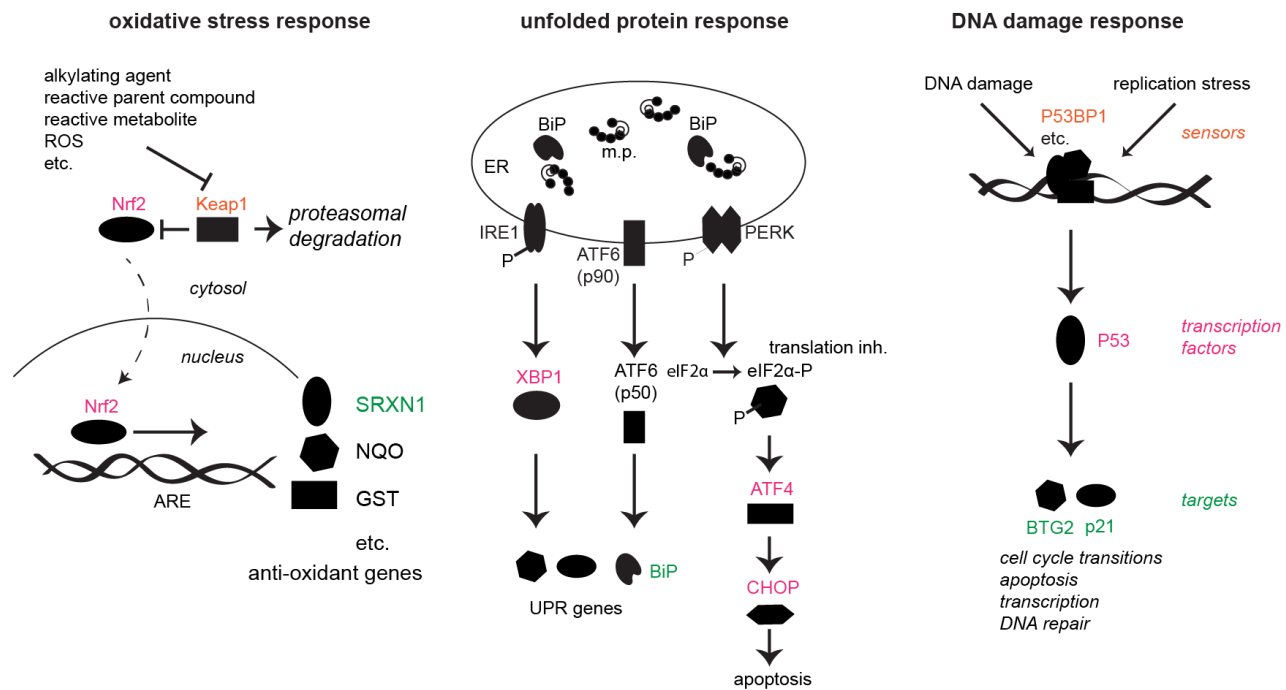


**Figure 3: Primary adaptive stress response programs.** Left) The oxidative stress response program which is activated by the translocation of Nrf2 to the nucleus where it binds to the antioxidant response element (ARE). Middle) The three arms of the unfolded protein response activated by misfolding (m.p.) or overload of proteins in the ER. Right) The DNA damage response which involves a sensory and repair machinery and main regulator p53. Each adaptive stress response pathway consists of sensor proteins, transcription factors and down stream targets.

Confocal microscopes allow a high level of detail of in practice up to four different fluorescence emission wavelengths. In addition, most confocal microscopes allow simultaneous image acquisition of transmitted light, phase contrast or other non-fluorescence based image modalities. Because of the high throughput applications and enormous amount of imaging data, proper and efficient file storage systems are essential. Moreover, all images contain massive amount of information regarding the level and localization of fluorescence at the single cell level. The analysis of these data in an efficient manner requires specific informatics-based automated strategies. The development of an image analysis pipeline to enable current efforts in high throughput HCI is described in chapter 2 and chapter 7.

## 6. Tool development for datamining in HCI.

As indicated, HCI efforts results in enormous amounts of quantitative data. Due to technological development and automation of HCI hardware data output can be staggering which requires software in the form of data base management systems (DBMS) and application interfaces and computational hardware in the form of a storage file system and sufficient computational power. To enable datamining of large datasets one must consider two important physical aspects of a “dataset”; the size and the computational load the desired operations on the data require. A database engine based on structure query language (SQL) such as MySQL allows unlimited storage of data in relational tables. The organization of HCI data in a relational database is quite intuitive as each object will have a primary index as well as secondary indexes linking the parent-child relationships which allows the join-operations to be performed on multiple table to, for example,

query all measurements for a certain cell containing multiple objects such as the nucleus, organelles, cytoplasm over several frames in time. CellProfiler utility allows the output data derived from the image analysis to be stored in such databases [49]. This is often the recommended approach for handling large and complex datasets resulting from image analysis pipelines of single cell data and screens. Yet, this also requires informatics expertise to maintain a server-side database, or keep track of lots of small local databases. CellProfiler also allows run-time data dumps to the HDF5 file storage system [50]. Several applications (e.g. HDFView) allow easy browsing through this file system making it more intuitive. Memory wise it is possible to load subsets of data from the HDF5 file to analyze determined by the amount of memory available on the local system. After the user selected data is loaded into R-memory, speed is a non-issue as no more read/writing operations to hard drives have to be performed. By using a binary-ordered indexed table structure provided by the R-package 'data.table' all further data analysis operations are near-instant. Calculations on millions of data entries involving very small subsets of large datasets can still require a lot of time on a single CPU. R provides parallel computation with for example 'doSNOW' and 'parallel' packages without data duplication resulting in trivial additional memory usage. As many modern desktops prove 8-24 cpu-threads, this speeds up computations considerably.

The work presented in this thesis involves HCI data representing high throughput experiments for various reporters exposed to >170 compounds at the different concentrations with up to 50 time points per condition. Each condition would capture information of 100-200 individual cells. This type of data is no longer suited for detailed analysis using spreadsheet software tools as a single overnight experiment can easily lead to several GB of numeric data. The memory of spreadsheet tools is insufficient and the computational load too severe for even a single over-night HCI dataset. Often such data types will be analyzed by computational/informatics-oriented staff which will perform the analysis based on the requests of the biologist. The output from the analysis is then interpreted by the biologist who will then usually return to the (bio)-informatician who will optimize the analysis. Meanwhile more data will be produced. This leads to a cycle which is very time consuming and leads to communication problems as biologists and informaticians have to understand the jargon and science from two different worlds.

For the above reason a user-friendly R-package was developed (H5CellProfiler) that allows biologists to analyze their own large datasets such as perform aggregations, statistics, plate-normalizations and basic table manipulations such as selection, filtering, division and counting. In addition, live-cell tracking specific operations can be performed on the single cell data such as making the data suitable for single cell tracking by creating unique track labels for each time-lapse movie and also reconnecting "broke" tracks based on user defined thresholds. After appropriate data summarization H5CellProfiler allows interactive plotting of selected treatments to create time course or dose response graphs or the user can plot all data in a single graphic using the faceting utility provided by the R-package 'ggplot2'. The described utilities are provided in the form of a browser based menu; a graphical user interface which sends commands to the (local) R-server. A detailed description of H5CellProfiler architecture is provided in chapter 7.

## **7. Overall aim and objectives of this thesis.**

Our long term vision is to establish an imaging-based platform that can quantitatively assess the activation of individual key events relevant to AOPs. The initial focus in this thesis is on adaptive stress response pathways, that are typically part of AOPs and related to adverse drug reactions. In this thesis, we have established and characterized various reporter cell lines. We have established the infrastructure for automated imaging and image analysis of these reporters cell lines. We have integrated these reporter cell lines in mechanistic understanding of DILI. We have used these reporter cell lines to improve the prediction of DILI. These topics are described in the following chapters:

**Chapter 2** provides an overview of the background of adaptive stress responses, the development of reporter cell lines to monitor these pathways, and examples of the application of these reporters.

**Chapter 3** details the generation and characterization of pathway reporters that reflect the KEAP1/Nrf2 pathways, the unfolded protein response and the DNA damage response.

**Chapter 4** describes the interaction between the Nrf2 pathway and the NF- $\kappa$ B pathway in relation to DILI. I present how DILI compounds with strong Nrf2 activation affects the NF- $\kappa$ B signalling pathway and susceptibility to DILI.

**Chapter 5** deals with the role of oxidative stress and the unfolded protein response in the control of DILI compound-mediated cytotoxicity. I present how the activation of these pathways by DILI compounds affect the susceptibility to TNF $\alpha$ -induced cell death. Here we applied different BAC-GFP reporters to monitor the UPR.

**Chapter 6** involves the application of adaptive stress response reporters in the prediction of DILI. Here we used >170 different compounds, that largely cover most DILI types, and demonstrate the applicability of the reporter systems in DILI prediction.

**Chapter 7** describes the HDF5CellProfiler pipeline for the datamining of high content imaging data.

**Chapter 8** provides an overall summary of the work and discussion on future perspectives and further challenges on the application of the reporter cell lines in DILI safety assessment.

# Chapter 2

## **Quantitative High Content Imaging of Cellular Adaptive Stress Response Pathways in Toxicity for Chemical Safety Assessment.**

---

**This chapter has been published as:**

Steven Wink<sup>‡</sup>, Steven Hiemstra<sup>‡</sup>, Suzanna Huppelschoten<sup>‡</sup>, Erik Danen<sup>‡</sup>, Marije Niemeijer<sup>‡</sup>, Giel Hendriks<sup>§</sup>, Harry Vrieling<sup>§</sup>, Bram Herpers<sup>‡</sup> and Bob van de Water<sup>‡,\*</sup>

<sup>‡</sup>Division of Toxicology, Leiden Academic Centre for Drug Research (LACDR), Leiden University, The Netherlands

<sup>§</sup>Department of Toxicogenomics, Leiden University Medical Center (LUMC), Leiden, The Netherlands

*Quantitative High Content Imaging of Cellular Adaptive Stress Response Pathways in Toxicity for Chemical Safety Assessment*

Chem Res Toxicol. 2014 Mar 17;27(3):338-55. doi: 10.1021/tx4004038



## 1. Abstract

Over the past decade major leaps forward have been made on the mechanistic understanding and identification of adaptive stress response landscapes underlying toxic insult using transcriptomics approaches. However for predictive purposes of adverse outcome several major limitations in these approaches exist. Firstly the limited number of samples that can be analyzed reduces the in depth analysis of concentration-time course relationships for toxic stress responses. Secondly these transcriptomics analysis have been based on the whole cell population, thereby inevitably preventing single cell analysis. And thirdly, transcriptomics is based on the transcript level - totally ignoring (post)translational regulation. We believe these limitations are circumvented with the application of high content analysis of relevant toxicant-induced adaptive stress signalling pathways using bacterial artificial chromosome (BAC) green fluorescent protein (GFP) reporter cell-based assays. The goal is to establish a platform that incorporates all adaptive stress pathways that are relevant for toxicity, with a focus on drug-induced liver injury. In addition, cellular stress responses typically follow cell perturbations at the subcellular organelle level. Therefore we complement our reporter line panel with reporters for specific organelle morphometry and function. Here we review the approaches of high content imaging of cellular adaptive stress responses to chemicals and the application in the mechanistic understanding and prediction of chemical toxicity at a systems toxicology level.

## 2. Introduction

The mode of action of a chemical entity encompasses its on-target but also off-target effects and both of these effects can lead to adverse outcomes such as drug induced liver injury,[51] [52] renal failure,[53] skin allergies,[54] adverse respiratory arrhythmia,[55] neurotoxicity[56] [57] or in the case of constitutively activated mitogenic signalling or mutagenic or inflammatory properties of the chemical entity ultimately leading to cancer.[58] [59] Chemicals react or interact with cellular components leading to a perturbation of signal transduction networks as the cell tries to reestablish homeostasis. In case these perturbations are detrimental to cells adaptive stress responses are activated. However, if cellular stress is too severe these adaptive stress responses are unable to reestablish homeostasis; a threshold will be reached where the cell activates cell death responses to avoid cell community-level detrimental effects. Understanding these cellular adaptive stress responses to chemicals in detail is key for better drug development and safety assessment.[60] [61] However, these adaptive stress responses are composed of a multitude of biochemical reactions and molecular events and are always in a dynamic flux to maintain cellular homeostasis in an ever changing environment. In addition, these responses exist at the intra- and inter-cellular level and must be fine-tuned and coordinated for cells to be able to perform their role in reestablishing tissue homeostasis. Such responses have been also named 'toxicity pathways [62] or fully cover or are part of 'adverse outcome pathways (AOPs)'. [63] We prefer the term 'adaptive stress response pathways', since this relates to the evolutionary defined genetic programs that are meant to adapt to new harmful environments. Ideally one would want to capture the central network hubs underlying these stress responses. We propose that high content imaging of key events that are pivotal in the development of specific toxicities will be essential. In this review we will address the different key adaptive stress response pathways in the context of chemically-induced liver injury and how components of these stress response pathways

can be used in high content imaging approaches. Moreover we will discuss how such tools can then be incorporated in further studies to assess the molecular mechanisms of toxicity as well as in more advanced high content analysis and modeling studies.

### 3. Drug-induced liver injury: concepts of adaptation and adversity of pathways of toxicity.

A research focus in our laboratory is on drug-induced liver injury (DILI). Liver toxicity is an important reason for drug attrition and a major cause of hospital admissions due to adverse drug reactions. Improved preclinical prediction of drug toxicities is essential for effective development of new and safer drugs. Classically, histopathology data and data on alanine aminotransferase (ALT) and total bilirubin increase obtained from animal models is the golden standard for identification of DILI, but will tell little about the molecular mechanisms involved in the pathogenesis after chemical exposure. Using these animal models for pre-clinical toxicity testing has led to poor predictions: hepatotoxicity is most often cited as the cause of withdrawal of a drug from the market.[8] Several reasons for the low predictivity of animal models for hepatic toxicities are thought to exist including the low occurrence of human toxicity (idiosyncratic DILI), the involvement of the immune system, differences in the metabolic capacities between animals and humans, genetic sensitivities and disease mediation.[64] At the cellular level indications for the type of injury can be resolved, *i.e.* phospholipidosis, steatosis, apoptosis or necrosis, but this does not lead to better mechanistic understanding of the initial cause of adverse outcomes. Biochemical analysis has allowed insight into major metabolic programs including cellular redox status, citric acid cycle metabolism and energy generation. Major developments in metabolomics now allow the detailed analysis of chemical-induced perturbations of the metabolome in close detail.[65] Such changes are likely rather reflections of earlier cellular perturbations that will then define and/or characterize the cellular status, *e.g.* steatosis or mitochondrial dysfunction than that they constitute the prime initiating event (Fig. 1). The initial cell state changes that are closest to the molecular initiating events are probably best described by the assessment of either key (cell-specific) biochemical or cell biological programs. This may include the measurement of enzyme activities in key programs or the evaluation of activation of cellular stress response pathways that will allow the cells to adjust to a new stressful situation. When these cell state changes cannot be met with a new rheostat, key breaking points in the cellular response programs may trigger the onset of adverse outcome and determine the fate of individual cells and eventually overall liver function. Only when exceeding certain concentrations adaptation cannot be met with cellular adaptive stress response programs and cell death or senescence will be initiated. In such a conceptual thinking, the monitoring of the activated adaptive stress response pathways after toxicant exposure would be an improved strategy to assess the underlying molecular mechanisms that link the initial molecular initiation events to toxic outcome. Preferably one would then follow individual markers of the activation status of such key adaptive programs including key-nodes of signalling events that are initiated once the threshold of the adaptive stress response has been met.

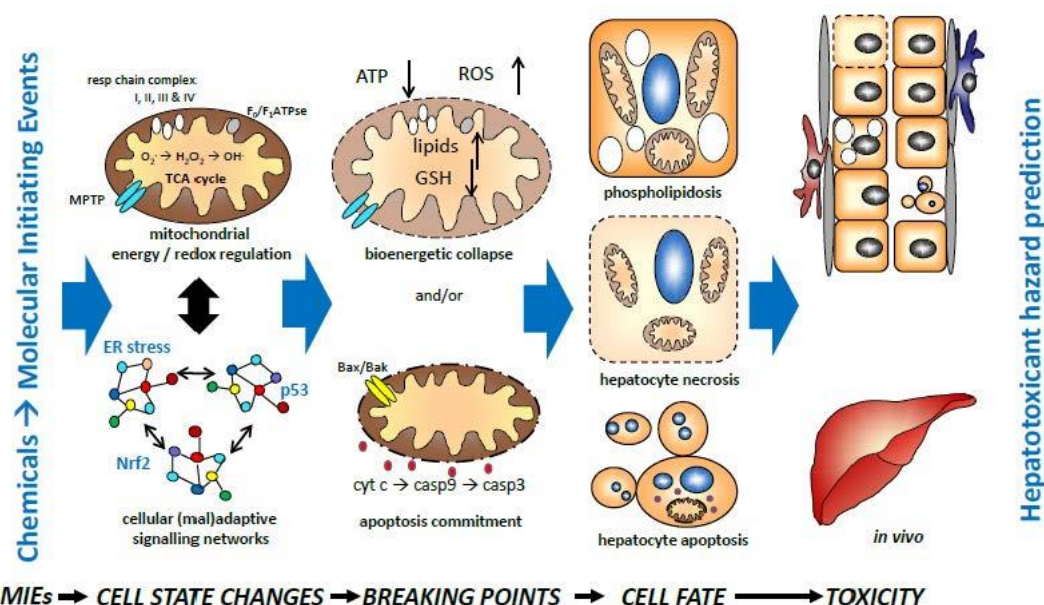


**Figure 1: A model for integrated understanding of chemical-induced liver injury.** Cellular adaptive stress response pathways sense and respond to environmental changes induced by the molecular initiating events of chemical induced toxicity. If the adaptive stress response programs cannot maintain a healthy homeostasis (breakpoint threshold is exceeded) cells will commit to *e.g.* apoptosis resulting in adverse outcome phenotypes such as phospholipidosis, massive hepatocellular necrosis and/or apoptosis leading to organ damage.

#### 4. From toxicogenomics to predictive classifiers of toxicity.

Toxicogenomics forms an excellent tool to identify key stress response pathways.[45] Over the past decade an overwhelming number of toxicogenomics studies have been performed both in industrial settings as well as within the academic environment in the U.S., Europe and Japan (reviewed in).[66] While initially the promises and expectations of toxicogenomics were high and suggested to establish predictive tools for diverse types of organ toxicities, so far only limited success stories have been reported.[66-69] Regardless of the overall application of toxicogenomics in the industry and academia, in its current state it has been difficult to tie the gap between transcriptomics to the actual biological understanding. The reason for this has in particular been the cost factor and thereby the limitations for in depth concentration time course experiments for a wide range of target organ toxicities to establish direct cause-effect relationships between target gene expression and toxic outcome. An exception has been the detailed TG-GATES and DrugMatrix data for establishing in particular DILI toxicogenomics datasets.[70] These datasets have so far allowed the establishment of classifiers for specific types of DILI,[71-73] however the relationship between these classifiers and the molecular mechanisms of the phenotypes is still largely unclear. Moreover, there remains a wealth of information in these datasets that allows for hypothesis generation.[66] This should eventually lead to the identification of (additional) predictive classifiers that have more direct biological relevance to the mode of action of toxicity. We anticipate that some of such candidate genes could be excellent for establishing reporter cell systems, for which we propose to use GFP-based technology (see below). In particular the TG-GATES data is suited for this, as this dataset will allow the extraction of gene sets and/or biological (toxicity) pathways that are associated with DILI outcome. Genes that are part of these pathways

and expressed at low levels under control situation, but clearly upregulated after chemical treatment could serve as excellent markers to establish reporter models. Alternatively already available or future novel small molecular fluorescent probes could be applied in simple high content imaging approaches. Yet for further identification of transcriptomics-based reporters more detailed concentration-time resolved toxicogenomic studies are required, in particular where possible targeting specific cell types in relevant organs of toxicity, using human donors or if necessary alternatively in conjunction or replaced by improved *in vitro* models that recapitulate the human target organs. Clearly this should involve the latest next generation sequencing technology and should preferably be tightly integrated with direct assessment of additional critical markers of cellular function at the biochemical or phenotype level as well as toxicological outcome, including assessment of intracellular parent compound and metabolite concentration analysis to allow for future *in vitro* to *in vivo* extrapolations. Moreover, it will be essential to determine whether the eventual candidate markers of toxicity are an integral part in the regulation of adaptive stress response pathways using RNA interference-based functional genomics approaches.[74]

In the past years also alternative omics approaches have been used to better understand the initial mode of action of chemicals. In particular advanced SILAC-based proteomics (stable isotope labeling by amino acids in cell culture) has now uncovered a plethora of early post-translational signalling events through protein kinase-mediated phosphorylation which contributed to an improved molecular understanding of *e.g.* the DNA damage response.[75, 76] While such proteomics approaches are tedious and costly, they may lead to the identification of novel phosphorylation events in signalling networks that are key in the target organ specific toxicities. This would allow the generation of phospho-state specific antibodies as an extra type of event that could be integrated in high content imaging approaches and may facilitate bridging of the gap between the *in vitro* and *in vivo* (human) situation.

Besides toxicogenomics several additional efforts have been made on monitoring the underlying signalling pathways based on for example qRT PCR.[77] The primers for these high throughput assays are designed for profiling the expression of sets of genes that are proven or expected classifiers for the mode of action of chemicals, typically derived from toxicogenomics studies. Another approach to detect specific signalling events is the use of phosphorylation state-specific antibodies *e.g.* with phospho-specific flow cytometry.[78] The number of alternative non-animal testing methodologies have increased substantially, many improving on a number of substantial issues regarding *in vitro* toxicity screening like metabolic capacity and tissue-context structural attributes This review focuses on cellular stress response signalling based readouts for chemical safety evaluation; for an in depth review on recent developments on alternative testing methods see for example reviews by Hengstler *et al.*[16] and LeCluyse *et al.*[79]

## 5. High content imaging of adaptive stress response pathways.

Today's state of the art high content imaging systems combine (semi) high throughput (High Throughput Screening – HTS) with a high level of detail (High Content Screening/Imaging – HCS/HCI) which allows capturing the phenotypic cellular responses to many environmental conditions at the subcellular (organelle) and protein signalling level. This technology should overcome the past classical biochemical cell toxicity readouts that so far have captured different

types of cell dysfunction but usually give little information on causality, *i.e.* the mode of action of the chemical entity and the underlying chemical-pathway interactions and resultant cellular signalling events. The most well-known classical biochemical cell toxicity readouts include reduced activity of mitochondrial respiration (MTT and MTS assays),[80][81] cellular ATP content depletion (e.g. ATPlite assay),[82] leakage of the enzyme lactate dehydrogenase (LDH) upon cell death[83] and quantitation of the fraction of surviving cells with or without intercalating DNA-staining dyes such as DAPI or Hoechst 33342 for living cells and propidium iodide [PI] for necrotic cells.

Now for the first time investigators are able to visualize the central signalling hubs controlling the adaptive cellular stress responses in a systematic manner, which allows its integration in toxicity screening strategies.[84-86] The true power of HCS using automated imagers lies in its ability to capture when and where specific molecular signalling events are taking place, enabling characterization of cellular responses to many different changes in the environment in a high time and spatial resolution, relatively high throughput (depending on exact setup) and on a single cell basis enabling detection of heterogeneity within populations.

Automated imaging systems can be roughly divided into four groups of increasing complexity: wide-field imagers for fixed cell samples, (spinning disk) confocal imagers to scale up the detail of the fixed images, imagers equipped with temperature and CO<sub>2</sub> control and confocal systems adapted for HCS and equipped with an environment chamber, reviewed in.[87] The latter two systems can be combined with a robotic plate exchange system to enable imaging of multiple multi-well plates containing living cells in parallel thus vastly increasing the throughput of high content live single-cell based imaging.

When current efforts of high content imaging in the context of the adverse outcome pathway concept[63] is viewed in relation to establish assays for adaptive stress response pathways, it becomes apparent that most assays are based on the final outcome of an adverse effect within a cell: the observed phenotype is the end result or downstream observable effect of the mode of action and adverse outcome molecular initiating event in the chemical- biological space. For example in a high content imaging assay utilizing cell viability stains like propidium iodide and annexin V-FITC[88] the readout is in effect based on dead cells only discriminating between the type of cell death, necrotic or apoptotic. Already a more detailed view of the type of cellular toxicity leading to cell death is obtained using for example mitochondrial membrane potential assays (*e.g.* TMRM, Rhodamine123 or JC-1), mitochondria superoxide detection (MitoSOX), reagents allowing mitochondrial permeability transition detection (calcein-acetoxymethyl ester (AM)) or detection of intracellular calcium levels (calcium binding probes), excess lipid droplet formation (nile red and BODIPY 493/503)[89] or an accumulation of phospholipids in the lysosomes during drug-induced phospholipidosis (*i.e.* LipidTOX Red or NBD-PE).[89, 90] One example of an implementation of such a HCI effort has been performed using several dyes and markers (calcium (Fluo-4 AM), mitochondrial membrane potential (TMRM), DNA content (Hoechst 33342) and plasma membrane permeability (TOTO-3)) on HepG2 cells to predict DILI.[91] This study mentions a sensitivity of 93% and specificity of 98% using 243 drugs, in comparison with 7 more conventional in vitro toxicity assays with a sensitivity of 25% and specificity of 90% for 611 compounds. However the underlying signalling events culminating in these adverse phenotypes are still not part of HCI. A step forward is the use of reporter cell lines. These can be on the genetic level (luciferase reporters) or on the protein level (fluorophore

coupled proteins) and even on interactome,[92] phosphor-proteomic[93] and metabolic level,[94] using fluorescence resonance emission transfer indicators (FRET). In toxicology luciferase reporters and fluorophore coupled protein reporters have been used and several are commercially available. A good example comes from the efforts within the Tox21 and ToxCast consortia where a set of 2870 compounds was screened using a  $\beta$ -lactamase reporter gene assay with reporter cell lines from GeneBLAzer®. These cell lines constitutively co-express a fusion protein comprised of the ligand-binding domains (LBD) of related human nuclear receptors coupled to the DNA-binding domain of the yeast transcription factor GAL4.[95] In addition more simple luciferase and GFP reporters are used in these large collaborative efforts. A drawback of these different reporter-based systems is that several critical endogenous regulation mechanisms are lacking including the entire promoter region as well as introns. This can often lead to less specific and or less sensitive readouts. In addition for many genes the promoter sequence is not entirely known, therefore fusion constructs are often based on CMV driven promoters leading to several factors of overexpression of the protein of interest which can lead to perturbed homeostasis in the reporter cell line. With the introduction of bacterial artificial chromosome (BAC) transgene-based cell lines these shortcomings are circumvented. By application of BAC transgenomics a large panel of BAC-reporter cell lines can be generated with relatively little effort.[48] The basic principle is based on the use of BACs that contain a genomic copy of a particular human gene including all exons and introns and at least 10 kB flanking DNA on each end of the gene which most likely encompasses the entire promoter region and other regulatory elements ensuring its normal physiological regulation of expression. A fluorescent or luciferase reporter construct can be introduced into the BAC by homologous recombination making use of homology arms on each end of the reporter construct. So far we showed that a small panel of BAC transgenic engineered mouse embryonic stem cells in combination with flow cytometry analysis could distinguish oxidative stress inducing chemicals from DNA damage inducing chemicals using the *Srxn1* and *Bcl2* genes.[13] This demonstrates how key nodes of stress response signalling networks can reveal mechanistic information on the mode of action of chemicals.

The next step is to utilize state of the art high content automated imaging coupled to automated image analysis with panels of reporter cell lines, enabling high throughput identification of specific key signal transduction nodes being perturbed by chemicals. We envision that high content automated imaging combined with a panel of endogenously regulated reporter cell lines will prove to be a powerful tool in early chemical safety assessment and will improve mechanistic understanding of chemicals in an early stage.

#### **6. Key adaptive stress response pathways in chemical toxicity as BAC reporter systems.**

Stress responses and the cellular signalling network in general cannot be regarded as an independent set of linear signal transduction routes. Therefore a panel of reporter cell lines to monitor multiple key nodes of adaptive stress response pathways is key. The major stress signalling routes activated in response to adverse chemical reactions that can be discerned from toxicogenomics studies include the antioxidant response element activation, heat shock response, unfolded protein response, metal stress response, the DNA damage response and CYP and other phase I, II and III enzyme/transporter induction by nuclear receptors. Time lapse analysis of these responses programs, where possible at a single cell level, would give valuable information on the

mode of action of novel chemical entities. Typically these programs would involve the activation of sensors that recognize the cell injury or stress followed by activation of single or networks of specific downstream transcription factors that modulate the expression of specific gene sets thereby affecting the outcome of the cellular stress response at the cell biological level (see Fig. 2 for examples). Below we will address the selection steps for reporters of the most relevant stress response pathways by describing in more detail their molecular activation as well as their involvement in liver injury. This then allows the identification of ‘sensors’, ‘effectors’ and downstream ‘targets’ that may be appropriate for DILI.

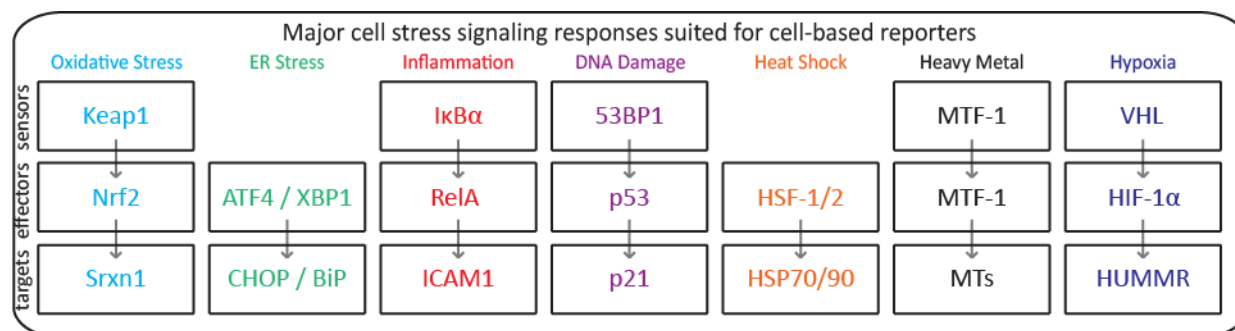


**Figure 2: Key stress reporter pathways for chemical safety assessment.** Key players in major adaptive stress response pathways that could be chosen for BAC reporter cloning – the early signalling ‘sensors’, ‘effectors’ transcription factors and downstream ‘targets’.

### 6.1. KEAP1/Nrf2 signalling pathway.

Cellular redox homeostasis can be disrupted by internal metabolism, xenobiotic exposure, environmental factors and host immune cell defense mechanisms.[96-98] Although drug-metabolizing enzymes metabolize and detoxify electrophiles and oxidants,[99] metabolism of xenobiotics by *e.g.* P450 CYP enzymes can also lead to bio activation resulting in the formation of electrophiles. The most well-known example being acetaminophen overdose toxicity, which depletes cellular anti-oxidant glutathione levels and increases the levels of reactive oxygen species (ROS) in cells.[100] ROS are controlled by various constitutively expressed detoxifying enzymes such as glutathione-S-transferases, NADP(H):quinone oxidoreductase, glutathione peroxidases, catalase, superoxide dismutases, epoxide hydrolases, heme-oxygenase, UDP-glucuronosyl transferases, gamma-glutamylcysteine synthase and sulfiredoxin-1.[101-104] These ROS detoxifying genes are controlled by anti-oxidant response elements (ARE) in their promoter regions which are activated by so called xenobiotic-activated receptors (XARs) or by the nuclear factor erythroid 2-related factor 2 (NFE2L2 or Nrf2), which in turn are activated in response to specific chemicals or other environmental perturbations involving redox biology. Nrf2 is the key transcription factor required for ARE dependent drug metabolizing enzymes.[105] Many chemicals and substances induce ARE-dependent genes. Nrf2 mRNA is readily detectable in a wide range of cells, implying that transcription of Nrf2 is not a major mechanism by which Nrf2 is regulated.[106] The main mechanism of activation of the anti-oxidant response occurs by modification of specific cysteine thiol groups on Kelch-like erythroid cell-derived protein with CNC homology-associated protein (Keap1)[107] and Nrf2 – the cysteine groups function as electrophile and oxidant sensors.[108][109] Under non oxidizing conditions Nrf2 is bound by homo-dimerized Keap1 acting as an adaptor protein for the Cul3-dependent ubiquitin ligase (E3) complex.[110] Cul3 is a scaffold protein for the binding with RING box protein 1 (Rbx1) which in turn recruits ubiquitin-conjugating

enzyme (E2) for polyubiquitination and degradation by 26S-proteasomes. Upon alkylation or oxidation of specific cysteine thiol groups on Keap1[111] Nrf2 translocates to the nucleus where it binds to promoter enhancer regions containing the ARE consensus sequences.[112] The Nrf2 signalling as adaptive stress response pathway has emerged as a vital signalling node. Nrf2-null mice are more sensitive to a wide range of chemicals, including butylated hydroxytoluene (BHT). Nrf2 protects against liver injury produced by numerous hepatotoxicants including acetaminophen *in vivo* and *in vitro*. [113-115] While constitutive Nrf2 activation can be detrimental in particular in cancer progression and drug resistance.[116] [117] We anticipate monitoring the anti-oxidant response using BAC transgene reporters combined with high content imaging will reveal important early clues to unexpected off-target effects and possible toxicity by *e.g.* reactive metabolites for early toxicity screening of chemicals and drugs. The magnitude and time dynamics of the Nrf2 pathway in relation to other adaptive stress response pathways is likely a relevant marker for early toxicity evaluation in pre-clinical compound screens. We have generated a set of oxidative stress BAC-GFP reporters (Fig. 3A) in a strategic manner to be able to monitor the oxidative stress 'sensor' Keap1, the transcription factor Nrf2 acting as the 'effector' and downstream 'target' anti-oxidant enzyme sulfiredoxin-1 (Srxn1). The latter is specifically controlled by Nrf2 and highly responsive to a wide range of DILI compounds in primary human hepatocyte transcriptomic analysis (unpublished results). After exposure to iodoacetamide the Keap1 accumulation in foci identified as autophagosomes is followed by the translocation of Nrf2 to the nucleus. Several hours later this is followed by a strong increase in the levels of Srxn1 (see Fig. 3A and supporting information 1).



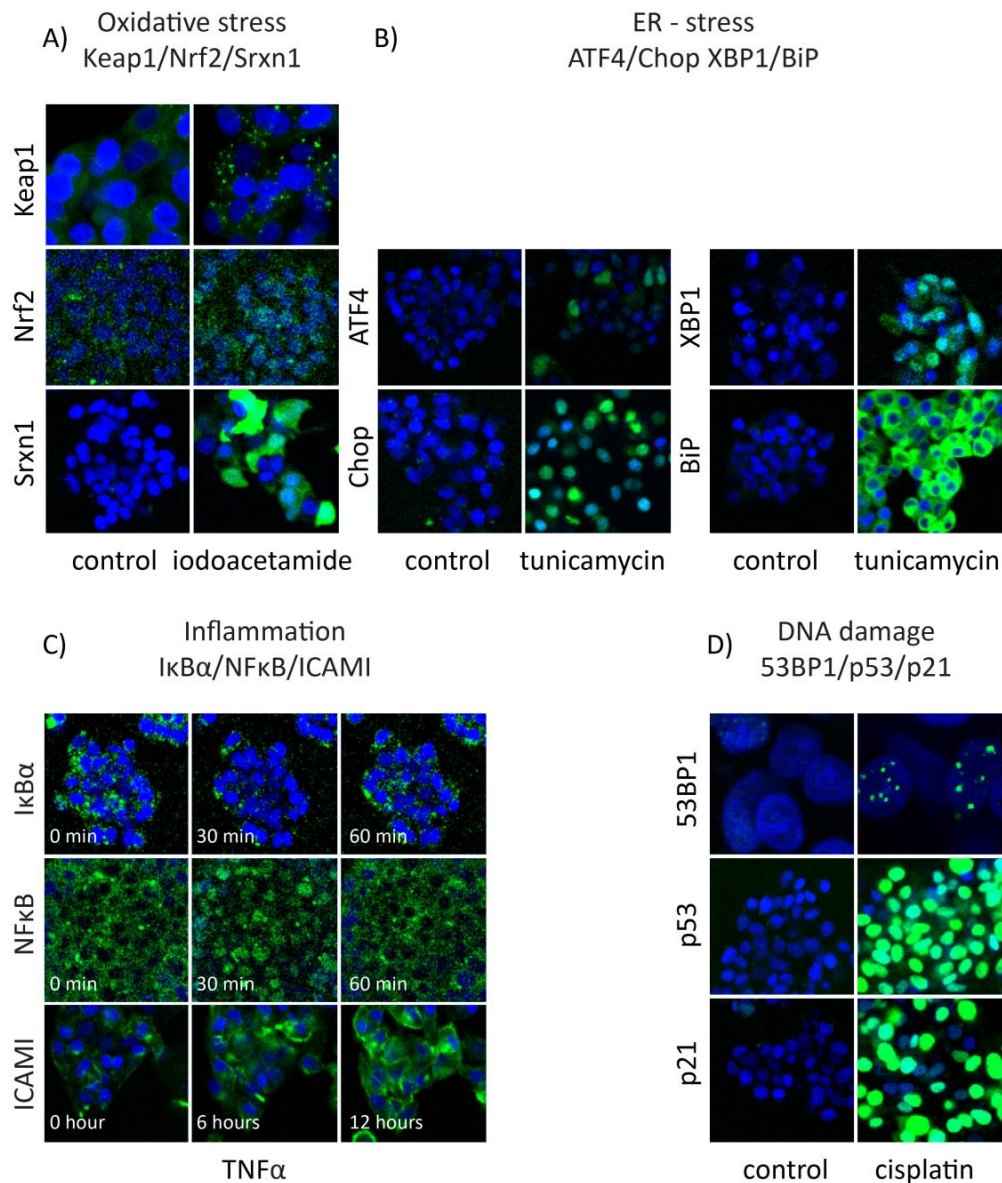


**Figure 3: Examples of BAC reporter cell lines of toxicity pathways in HCl.** **A)** Oxidative stress signalling: Keap1 as sensor; treatment with 10  $\mu$ M iodoacetamide (an electrophile for covalent modification of nucleophilic residues on proteins, *e.g.* cysteines) leads to formation of Keap1 foci – these foci correspond to autophagosomes where the Keap1 proteins are degraded. Nrf2 as transcription factor: Endogenous Nrf2 levels are extremely low but the nuclear translocation after treatment is still quantifiable. Srxn1 as downstream target: Following Keap1 degradation and Nrf2 nuclear translocation downstream target Srxn1 protein levels are increased. **B)** ER-stress signalling: The apoptosis related ER-stress signalling arm of transcription factor ATF4 and downstream target CHOP v.s. the acute protective arm consisting of transcription factor XBP1 and downstream target BiP. Both signalling arms are activated after 8 hours of 10  $\mu$ M tunicamycin treatment. **C)** Inflammation signalling: The maximum and minimum of the first peak of the oscillatory NF- $\kappa$ B response after a 10 ng/ml TNF $\alpha$  treatment is shown. At 30 minutes the level of NF- $\kappa$ B inhibitor IkB $\alpha$  is decreased – followed by NF- $\kappa$ B translocation to the nucleus. The first peak has disappeared after 60 minutes. As a consequence downstream target ICAM1 levels steadily increase. **D)** DNA damage response: cisplatin-induced bulky lesions lead to formation of DNA-repair protein foci (*e.g.* 53BP1) which act as sensors for further DNA-damage repair signalling. This is followed by the nuclear translocation of transcription factor p53 leading to an increase in the level of non-apoptotic senescence downstream target p21.

## 6.2. Unfolded protein response (UPR) and endoplasmic reticulum (ER) damage.

The endoplasmic reticulum (ER) is the major cellular organelle involved in protein synthesis, modification, folding and sorting.[118] Cells have evolved an adaptive protective mechanism to cope with perturbations in the protein processing capacity of the ER called the unfolded protein response (UPR). The UPR is separated in three branches: the inositol requiring enzyme 1 $\alpha$  (IRE1 $\alpha$ ) branch, the activating transcription factor 6 (ATF6) branch and the protein kinase RNA-like ER kinase (PERK) branch.[119] They all have one sensing molecule in common: the ER-resident chaperone BiP. Under normal conditions, BiP binds to the transmembrane transducers IRE1 $\alpha$ , ATF6 and PERK on the ER luminal membrane. BiP has a relatively strong binding affinity with unfolded proteins, when unfolded proteins start to accumulate in the ER lumen the transducers are thought to go through a conformational change because of the resultant free BiP binding sites. Dissociation of BiP triggers PERK to homodimerize and autophosphorylate.[33, 120] Activated PERK phosphorylates eukaryotic translation initiator factor 2 $\alpha$  (eIF2 $\alpha$ ). This leads to an attenuation of general translation, however also leads to increased translation of a specific mRNA species that encodes the transcription factor ATF4. ATF4 in turn activates genes involved in amino acid metabolism, redox balance, protein folding and autophagy.[121, 122] IRE1 $\alpha$  is also activated via homodimerization and autophosphorylation triggered by BiP dissociation. The activated ribonuclease domain of IRE1 $\alpha$  catalysis the excision of a 26 nucleotide intron from ubiquitously expressed XBP-1 mRNA which causes a frame shift in the XBP-1 coding sequence resulting in its translation. X-box binding protein 1 (XBP1) then translocates to the nucleus and induces transcription of ER-associated degradation (ERAD), phospholipidosis to promote ER-membrane expansion, and protein folding by expression of chaperones like p58, ERdj4 and BiP.[123] In addition activated IRE1 $\alpha$  activates programs including regulated IRE1 dependent decay (RIDD; selective degradation of mRNA of proteins located in the ER), macroautophagy and inhibition of translocation of proteins into the ER-lumen.[124-126] Following BiP dissociation ATF6 translocates to the golgi apparatus where it is cleaved into the transcriptionally active form (ATF6f).[127] ATF6f subsequently activates genes involved in ERAD (endoplasmic reticulum associated degradation) and protein folding.[128] Thus, all three UPR axes (PERK, IRE1 $\alpha$  and ATF6) initially contribute to the adaptation of the cell to overcome the overload of unfolded proteins. However, when the amount of unfolded proteins keeps accumulating during sustained stress conditions, the UPR switches to pro-apoptotic mechanisms. A key transcription factor in this switch is C/EBP-homologous protein (CHOP, also known as GADD153). CHOP is mainly activated via the PERK-ATF4 axis,[129] however, there is also evidence for a non-specific activation via (one of) the other two branches.[130, 131] CHOP regulates transcription of a variety of pro-apoptotic genes including Death Receptor TRAIL receptor 2 (DR5)[132] and Bcl-2 family member Bim,[133] thereby sensitizing cells to apoptosis. In addition CHOP also de-attenuates the general translation program by inducing expression of GADD34 which dephosphorylates eIF2 $\alpha$ . This can result in an accumulation of premature proteins in the ER, which is shown to induce accumulation of reactive oxygen species (ROS) and subsequent mitochondrial damage and apoptosis.[134] Recent publications demonstrate a crucial role for ER-stress in hepatosteatosis, cholestasis and hepatotoxicity. Elevated levels of ATF4 and spliced XBP1 were observed in fatty liver samples compared to normal and steatotic liver samples.[135] Also *in vivo* evidence for a role of UPR in cholestasis was recently observed where CHOP-null mutants developed much less liver fibrosis

compared to wild type livers.[135] In addition, CHOP knock-out mice are less susceptible to acetaminophen-induced liver injury.[136] Altogether there is clear evidence for different UPR/ER stress programs in liver injury responses. Concurrently it is critical to establish reporters for the different anti-apoptosis and pro-apoptosis UPR/ER stress signalling pathways. We have established BAC-GFP reporters for ATF4 and CHOP on the one hand, and XBP1 and BiP/HSPA5 on the other hand (Fig. 2 and Fig. 3B) which are highly responsive for prototypical UPR inducers, such as tunicamycin. These individual reporters would be valid to be incorporated in advanced high throughput microscopy approaches to assess chemically-induced UPR onset.

### **6.3. Inflammatory signalling through the cytokine-NF- $\kappa$ B pathway.**

The liver contains around 20-40% non-parenchymal cells including resident immune cells from both the adaptive and innate immune system (Kupffer cells (KC), Natural Killer (NK) cells and dendritic cells (DCs)) and as such has a unique immunological environment. Paradigmatically, this ensures both the tolerogenic nature of the liver and defense against bacterial or viral infections.[137-139] Pro-inflammatory cytokines like TNF $\alpha$  and IL1 are produced mainly by immune cells and facilitate intercellular communication within the liver to mediate (immune) cell activation, migration and recruitment. TNF $\alpha$  is produced by Kupffer cells upon pathogen challenge and danger-associated molecular pattern (DAMP) exposure and has been convincingly shown *in vivo* to be a key-component in the development of DILI, for instance in trovafloxacin and sulindac liver injury.[140, 141] Stimulation with TNF $\alpha$  activates the TNF receptor and induces the formation of a receptor complex activating kinase TAK1 and the IKK kinase complex. Phosphorylation of I $\kappa$ B $\alpha$  followed by its ubiquitination and subsequent proteasomal degradation[142] leads to NF- $\kappa$ B nuclear translocation. Nuclear NF- $\kappa$ B can activate gene transcription of early, middle and late target genes, including I $\kappa$ B $\alpha$  and A20 establishing a strong negative feedback loop.[143] Similarly, IL1 $\beta$  stimulation induces NF- $\kappa$ B translocation by activating TAK1 and the IKK complex. However, signalling upstream of TAK1 differs and ultimately NF- $\kappa$ B translocation by IL1 $\beta$  signalling leads to transcription of a different set of target genes. In both cases NF- $\kappa$ B nuclear translocation is a dynamic process which involves an oscillatory response where the duration of the overall nuclear localization time is one of the factors determining the transcriptional activity and downstream effects. Either drug exposure itself or drug exposure combined with pathogen challenge can lead to liver inflammation and pro-inflammatory cytokine production.[144-146] Current research suggests that drug-mediated perturbations in cytokine or DAMP signalling pathways cause synergistic drug/cytokine-induced cell death.[38, 147] Therefore, unraveling cytokine signalling in DILI will form one of the corner stones in the understanding of DILI. We have approached this by measuring drug-induced effects on NF- $\kappa$ B translocation using high content live cell microscopy using BAC-GFP reporter cell lines of a signal 'sensor' I $\kappa$ B $\alpha$ , an 'effector' protein RelA and several 'target' genes including ICAM1. Such experiments provide information in a time-resolved, quantitative and single cell fashion on NF- $\kappa$ B activation.

### **6.4. The DNA damage response.**

Cells in our body are exposed to exogenous and endogenous sources of DNA damage inducing agents, *e.g.* UV light, genotoxic substances and metabolic processes causing single or double strand breaks, base modification or intra or inter-strand crosslinks.[148] A set of highly conserved

cell cycle check point and DNA damage repair systems has evolved that allows cells first to repair inflicted DNA damage before replication commences with the risk of mutation induction.[149] The signalling involved in sensing the types of DNA damage, halting cell division at the cell-cycle check point and repairing the damaged DNA is fitted to the various types of lesions. DNA damage is detected by specific damage sensing mechanisms and by enzymes involved in DNA replication and transcription.[150] Crucial early regulators in the DNA damage response are the PI3-K-related protein kinases ataxia-telangiectasia mutated (ATM), ATM and RAD3 related (ATR) and DNA-dependent protein kinase (DNA-PK).[151] From these proteins the DNA damage signal is thought to be transmitted via CHK and CHK2 (check point kinase 1 and 2, respectively), aided by scaffold proteins such as MDC1 (mediator of DNA-damage checkpoint 1), 53BP1 (p53-binding protein 1) and BRCA1 (breast cancer 1 early-onset).[152-154] Among others ATM and ATR can activate p53 by phosphorylation of p53 or its inhibitor - the E3 ubiquitin ligase Mdm2.[155, 156]

p53 is mainly known as a tumor suppressor, but numerous additional roles have been reported. At least 129 direct transcriptional targets of p53 exist.[157] Under conditions of severe stress, p53 tumor suppression activity leads to irreversible apoptosis programs by activating extrinsic and intrinsic apoptosis targets including *BAX*, *FAS*, *NOXA* and *PUMA*. [158] The best-studied pro-apoptotic protein required for apoptosis induction by p53 is PUMA, a p53 target gene that is required to release cytoplasmic p53 from the antiapoptotic protein Bcl-X<sub>L</sub>, followed by mitochondria outer membrane permeabilization.[159] Alternatively, under conditions of low-level stress, p53 mediates its tumor suppression function via cellular growth arrest by activating the expression of cyclin-dependent kinase inhibitor p21, giving individual cells the possibility to repair DNA damage.[160] The most well described downstream targets of p53 have been reviewed by *e.g.*[161, 162] It is important to note that p53 also mediates numerous roles under non-stressed conditions which involves diverse cellular process including cellular migration, metabolism, cellular redox state, autophagy, angiogenesis inhibition, innate immunity and differentiation.[160] This is likely related to sub-lethal stress conditions that can also activate p53. Thus stress severity and type leads to different functional roles of p53. Functionality of p53 is modulated by its concentration, conformation and translocation into the nucleus. p53 contains nuclear localization-(NLS) and nuclear export signals (NES) that are located adjacent to and within the oligomerization domain of p53, respectively, leading to the possibility that p53 oligomerization is an important mediator of nucleo-cytoplasmic transport.[163] Nucleo-cytoplasmic shuttling is controlled by Mdm2, which interacts with p53 in the nucleus targeting it for nuclear export and degradation.[163] [164] Moreover, phosphorylation of p53 by kinases such as ATM, ATR, DNA-PK, and casein 1-like kinase (CK1) regulates p53 nuclear import or export.[155, 165-168] To monitor the DD response in individual cells using fluorescent reporter imaging several candidate genes can be proposed. In the case of double strand breaks or stalled replication forks the ATR, ATM and DNA-PK kinases are activated followed by recruitment of a large variety of DNA repair proteins that localize to the damaged sites forming distinct DD foci.[169] Well known markers of these foci are phosphorylated histone variant H2AX and p53 binding protein 1 (53BP1).[152, 170] 53BP1 undergoes nuclear relocation to focal structures of unknown architecture at double strand breaks or large adduct loci, presumably to facilitate the checkpoint and repair functions.[152] 53BP1 based foci formation are a useful high content imaging readout to identify candidate genes that modulate the DD response and allowed the identification of NUP153 as a novel factor

specifically required for 53BP1 nuclear import.[171] Therefore 53BP1 can perform a role as early DD response 'sensor'. Next, the nucleo-cytoplasmic translocation and concentration of p53 as one of the most relevant 'effectors' in the DD response. Finally, well known downstream 'targets' of p53 could be monitored, including Mdm2 which functions as a feedback loop inhibitor of p53 activity[172] [173] or p21 which is known to be very sensitive to small increases in p53 levels.[160]

### **6.5. Additional stress response pathways.**

There are additional known stress response pathways in drug-induced liver injury that we will only briefly touch. These include hyperthermia (heat shock response), heavy metal insult, hypoxia and nuclear hormone receptors. The heat shock protein family (HSP) is currently recognized for their role in reaction to a broad variety of physical and chemical insults, including drug-induced liver injury inducers.[174]

Physical and chemical insults may cause an accumulation of unfolded and denatured cellular proteins. This triggers heat shock factors (HSF-1 or HSF-2) to trimerize and translocate to the nucleus.[175] HSFs induce expression of five different heat shock protein families: the HSP70 family, HSP90 family, HSP110 family, HSP40 family and the small HSP family.[176] The heat shock proteins function as chaperones and bind proteins to prevent denaturation and to refold denatured proteins.[177]

Cells are also able to adapt to heavy metal stress. Heavy metals, like zinc, copper and cadmium, are sensed by MTF-1. A conserved cysteine cluster is responsible for the homodimerization of MTF-1 after activation with heavy metals.[178] MTF-1 translocates to the nucleus where it induces transcription of metallothioneins. Metallothioneins are responsible for the detoxification of heavy metals.[179] MTF-1 is shown to be essential for adult liver detoxification in mice.[180] This indicates an important role for the heavy metal stress pathway in drug-induced liver injury.

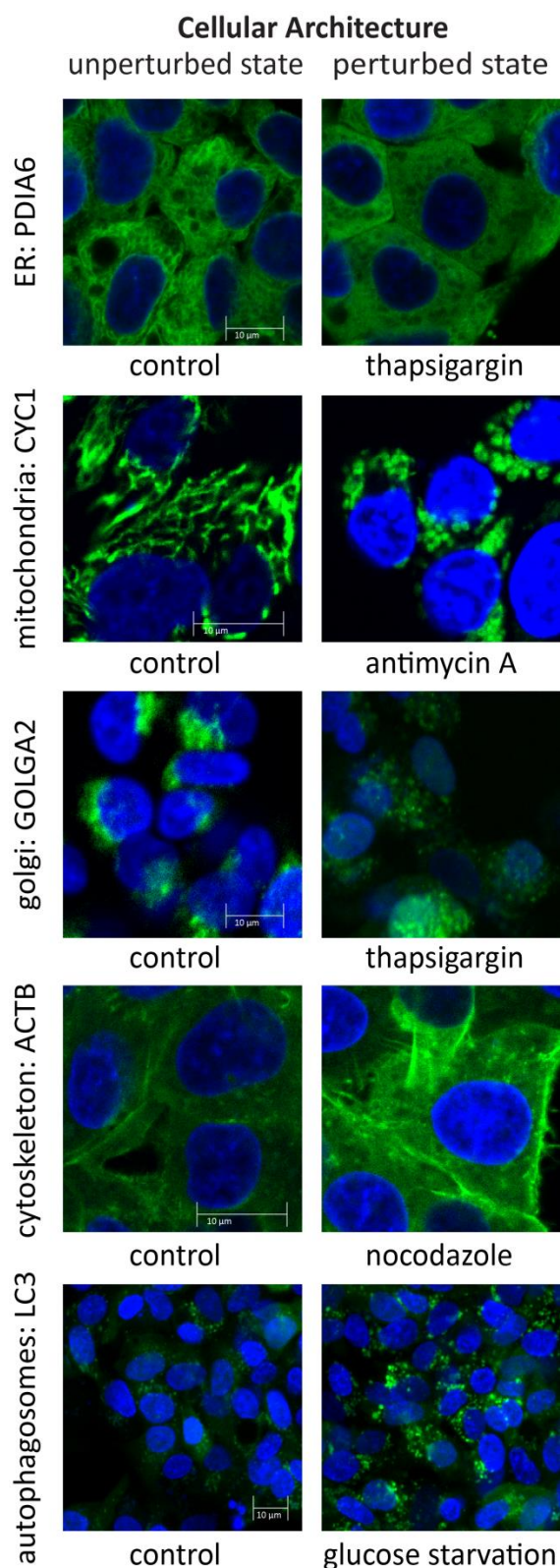
Reduced oxygen tension (hypoxia) in cells can induce cell perturbations and cell death. Therefore, the intracellular oxygen tension is constantly monitored by prolyl hydroxylases, which catalyze the hydroxylation of proline residues of transcription factor hypoxia-inducible factor 1 $\alpha$  (HIF1- $\alpha$ ). The hydroxylation of HIF-1 $\alpha$  enables the Von Hippel-Lindau (VHL) protein to bind to HIF-1 $\alpha$ . This complex translocates to the autophagosomes where it is degraded under conditions of normal oxygen tension. Under hypoxic conditions, hydroxylation of HIF-1 $\alpha$  proline residues ceases, enabling HIF-1 $\alpha$  to translocate to the nucleus and activating downstream targets.[181] One such target is HIF-1 $\alpha$ -inducible protein (HUMMR) which alters mitochondrial distribution and transport.[182] HIF-1 $\alpha$  is shown to play a role in DILI; HIF-1 $\alpha$  deficient mice exposed to an acetaminophen overdose showed significantly less hepatotoxicity in the early stages after administration.[183]

Finally, another protein family which is essential in hepatotoxicity is the nuclear hormone receptor family.[184] The members of this family are highly expressed in the liver and include PXR, RXR, CAR, AHR and HXR. They can bind a broad spectrum of ligands, including various xenobiotics. When bound, the nuclear receptors are released from their co-repressors and bound by their co-activators. Together, these complexes activate gene transcription of cytochrome P450 enzymes, and other phase I, II and III enzymes responsible for bile salt and fat metabolism and which are very well known for their drug metabolizing capabilities.[16] We consider the components of the



above pathways, including HSFs, Hsp family members, MTF-1, metallothioneins, HIF1 $\alpha$  and xenobiotic nuclear hormone receptors and some of their downstream target genes, also likely candidates for BAC-GFP reporter constructs. These can then contribute to monitor stress response pathways related to toxicity, in particular DILI.

### 6.6. Markers for critical cellular organelles and cell function.



Transcriptomics analysis has revealed the detailed cellular adaptive stress response landscapes and the diversities of organelles that are likely involved. Indeed, various organelles undergo cellular perturbations and/or remodelling upon injury such as the mitochondria (fission/fusion),[185] endoplasmic reticulum (ER)[186, 187] and the actin cytoskeleton[188], which are critical in the onset of cytotoxicity. We found that such phenotypic alterations occur well before the typical ultimate outcome of cell stress: cell death by apoptosis.[189] It seems essential to classify the cellular perturbations also on the basis of imaging-based analysis of disruption of cell organelle morphology and function. Similar as for the stress response reporters, specific target genes used for BAC tagging enable visualization of these organelles and their perturbations as response to diverse cellular stress conditions and can serve as markers for sub-cellular compartments and cell organelle function. Such reporters should preferably be selectively localized in these organelles and remain associated with the organelle membrane or lumen even under stress conditions. Several relevant markers are indicated in figure 4.

**Figure 4: Examples of morphology markers and cell death markers.** Panel 1 to 5 (top to bottom): **1)** endoplasmic reticulum folds disperse after a 8 hour treatment with 1  $\mu$ M thapsigargin, a endoplasmic reticulum  $\text{Ca}^{2+}$  ATPase inhibitor; **2)** Mitochondria swelling and network disintegration after 8 hour treatment with 5  $\mu$ M Antimycin A, Cytochrome reductase inhibitor; **3)** golgi polarization is dispersed after a 8 hour treatment with 1  $\mu$ M thapsigargin; **4)** formation of stress fibers after a 4 hour treatment with 5  $\mu$ M nocodazole (microtubuli polymerization inhibitor); and **5)** autophagosome increase after 8 hours of glucose starvation.

### **7. From microscope images to quantitative data.**

How can one derive the relevant quantitative data that describes all the relevant toxicological features from high throughput microscopy experiments to assess chemical safety? The simultaneous imaging capabilities of several high content live cell imagers in a screening laboratory easily leads to 100 GB of images (20,000-30,000 images) overnight. Therefore automated high content image acquisition must be coupled to an integrated automated multiparameter-image analysis tool for fast and accurate quantification of the acquired images, for a review on popular tools see.[145] As an example of how to handle such large data streams and computational overhead we describe our own customized automated image analysis pipeline based on an integration of custom made ImageJ[190] plugins, CellProfiler,[191] HDF5[192] and quantitative data processing R-scripts (Fig. 5). Image loading, image metadata definitions, intensity- and most morphological feature measurements, and the initial tracking of single cells is performed by standard CellProfiler modules. The segmentations are performed by a custom made ImageJ plugin based on the Watershed Masked Clustering Algorithm,[193] in addition some morphological (*e.g.* skeleton measurements) are also performed by ImageJ plugins. These plugins have been integrated in the CellProfiler environment by making use of the python-javabridge utility provided by CellProfiler. The latest version of CellProfiler includes the option to store quantitative data output in a hierarchical data format: HDF5.[192] An often overlooked aspect is data format standardization for accessibility and inter laboratory data exchange, for a promising implementation for the high content imaging community see cellH5.[194] CellH5 is based on the HDF format – a hierarchical file based system to store (biological) data.[195] Together with a plate layout text file the quantitative data is analyzed and graphically displayed in an automated fashion using R-scripts, which will become available as a R-package in the near future. The automated analysis includes reorganization and modification of the tracked objects and linkage of cellular features/phenotypes to cell mobility on the single cell level. In addition a database for storage and accessibility of imaging data and preferably a pipeline to streamline the workflow is needed. Several tools exist for this purpose the most well-known open source variations are the database, analysis and management package OMERO[196] and for analysis pipeline and software tool integration KNIME.[197] However quicker and easier to implement database-management systems originate from commercial vendors.

### **8. Examples of the application of cellular stress response fluorescent reporter systems.**

The BAC GFP cellular stress response reporter cell lines can be applied in various settings. Firstly, this may involve large compound screens using end-point measurements to simply monitor overall activation a cellular stress response pathway after chemical exposure. Secondly, it can include the live cell imaging of dynamic signalling responses of for example transcription factor activation and the consequences of chemicals on such a response. Thirdly, for those signalling routes that are of high relevance in toxicology large scale RNA interference approaches may address the underlying signalling networks that control the respective cellular stress responses and thereby the cellular outcome, *e.g.* enhanced activation of adaptive programs with limited cytotoxicity, or suppression of adaption with increased susceptibility for cell killing. Below we will describe in more detail these applications.

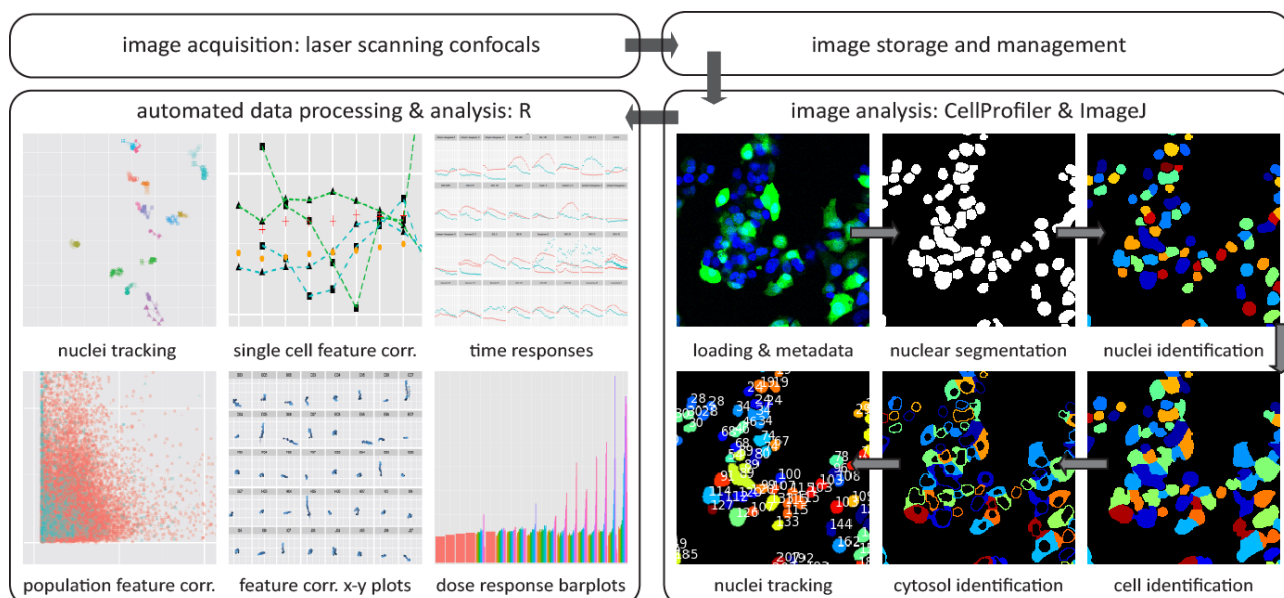


**Figure 5: Pipeline of high content imaging of BAC-GFP reporter cell lines.** Image acquisition by laser scanning confocal microscopes is followed by storage in a central data storage utility including a database management system. Image analysis is performed using CellProfiler and integrated ImageJ plugins. Raw images are loaded and metadata (*i.e.* well locations) is defined. After image processing (*e.g.* noise filtering) the nuclei are segmented using the nuclei-stained channel followed by single nuclei identification to enable analysis of population distributions. These identified nuclei are used as seeds to detect the cell-boundaries using the GFP channel. Further image objects can be defined (*e.g.* foci, cytoplasm, and organelles). Single-cell tracking is usually included to enable single-cell based analysis over time. Image analysis output (*i.e.* quantitative data) is stored in HDF5 files. R is used to interact with the data in HDF5 in an automated manner; several summary statistical output text files are generated and in addition a collection of plots to investigate the quantitative data are generated. Legend: Nuclei tracking: for quality control purposes of the tracking performance, the x & y-axis represent the x and y coordinates in the original images; single cell feature corr.: single cells are followed in time(x-axis) for two selected measurements(y-axis), the two selected measurements are for example cell speed and cytosolic intensity of the reporter cell lines; time responses: the selected percentile of all the single-cell measurements(y-axis) in each well in the multi-well plate are plotted over time(x-axis). Population feature corr.: two selected measurements(x & y-axis) can be compared on a single cell basis on the entire plate – for identifying dependencies (*e.g.* cell density and cytosolic intensity measurement); feature corr. x-y plots: linear regression analysis for two selected measurements for each condition in the multi-well plate to identify correlations; dose response barplots: area under the time-curve summary statistic of a selected measurement(y-axis) for each condition(x-axis) in the multi-well plate with increasing concentration(sub parts x-axis).

### 8.1. Compound screening to assess chemically-induced cellular stress response activation.

The application of the above described and proposed reporter systems can be positioned in mechanistic toxicology, early pre-clinical drug discovery for compound classification or compound ranking. Alternatively they can be applied in more large compound screening campaigns to build reference databases for future compound classification or as part of for example large consortia such as ToxCast[198] to complement the current set of HT assays. Such large compound screens could then be integrated with QSAR analysis. We have so far evaluated the feasibility of such an approach by testing the effect of the Spectrum Collection compound library including 2,350 FDA



approved drugs and active natural product compounds on the modulation of the Srxn1-GFP reporter in HepG2 cells. HepG2-Srxn1-GFP cells were exposed to individual drugs at 10  $\mu$ M and then treated with a specific activator of the Keap1/Nrf2 route, CDDO-Me,[199] and then fixed after 7 hr or left untreated and then fixed after 24 hr. We quantified the effect of all compounds Srxn1-GFP activation and determined the Z-scores to rank all compounds compared to control conditions. We observed compounds that strongly enhance the Nrf2/Srxn1 response induced by CDDO-Me, which interestingly contained colchicine, vincristine and vinblastine that all effect microtubule polymerization as a common pharmacological effect (Fig. 6). In addition, we observed compounds that inhibit the CDDO-Me-mediated GFP-Srxn1 upregulation, which also included compounds from the same pharmacological class that inhibit Na<sup>+</sup>/K<sup>+</sup>-ATPase ion channels. Such reference compound data allow the identification of off-target effect related to modulation of adaptive stress response pathways. Also QSAR analysis of such a dataset may allow the identification of toxicophores that affect the Nrf2/Srxn1 response.

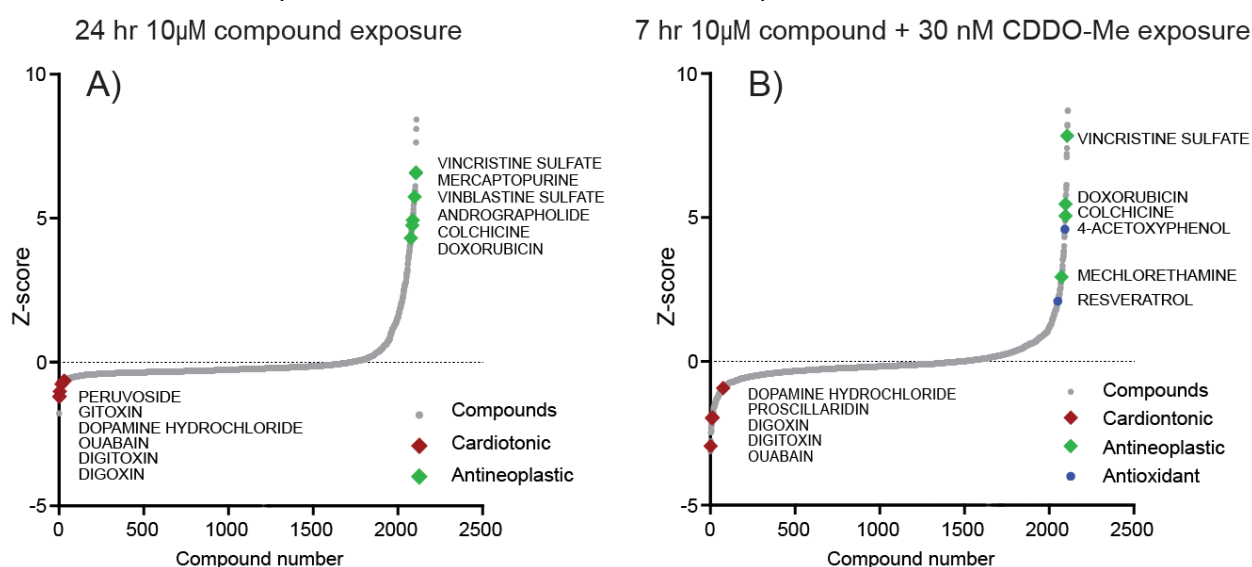


**Figure 6: Compound screen for Nrf2-mediated Srxn1 induction.** To monitor NRF2 activity upon drug exposure, BAC Srxn1-GFP HepG2 cells were used. Imaging was performed three days after cell seeding in 96-well  $\mu$ -clear imaging plates, Spectrum library compounds were transferred by automated pipetting to a final concentration of 10  $\mu$ M in 6 replicate plates. A) Three plates were incubated for 24hr, fixed and imaged by automated confocal microscopy. B) Three other plates were co-exposed to 30 nM CDDO-Me, a potent Nrf2 activator, and fixed after 7h incubation; this set of plates allowed us to identify compounds that inhibit or enhance the Nrf2 response. The average cellular Srxn1-GFP intensity was determined by ImageJ-based image analysis. The Z-score was calculated based on the population average. Per well, on average 5000 cells were quantified. If this number was less than 500, a compound was marked as severe toxic and excluded from the analysis. For a detailed description of the screen see supporting information 2.

## 8.2. Effects of chemical exposure on the dynamics of cellular signalling.

A good example of a highly dynamic adaptive signalling response is the nuclear translocation the transcription of factor NF- $\kappa$ B after inflammatory cytokine signalling. This is highly relevant in DILI as already described above and therefore monitoring the effect of chemicals on this oscillatory response is highly relevant. We have previously demonstrated such an effect for the drug diclofenac, a widely used non-steroidal anti-inflammatory drug, which causes hospitalization upon

liver failure in 23/100000 users according to a prospective study among arthritis patients.[200] Diclofenac is hepatotoxic in animal models at very high doses,[201] yet a combination of very low

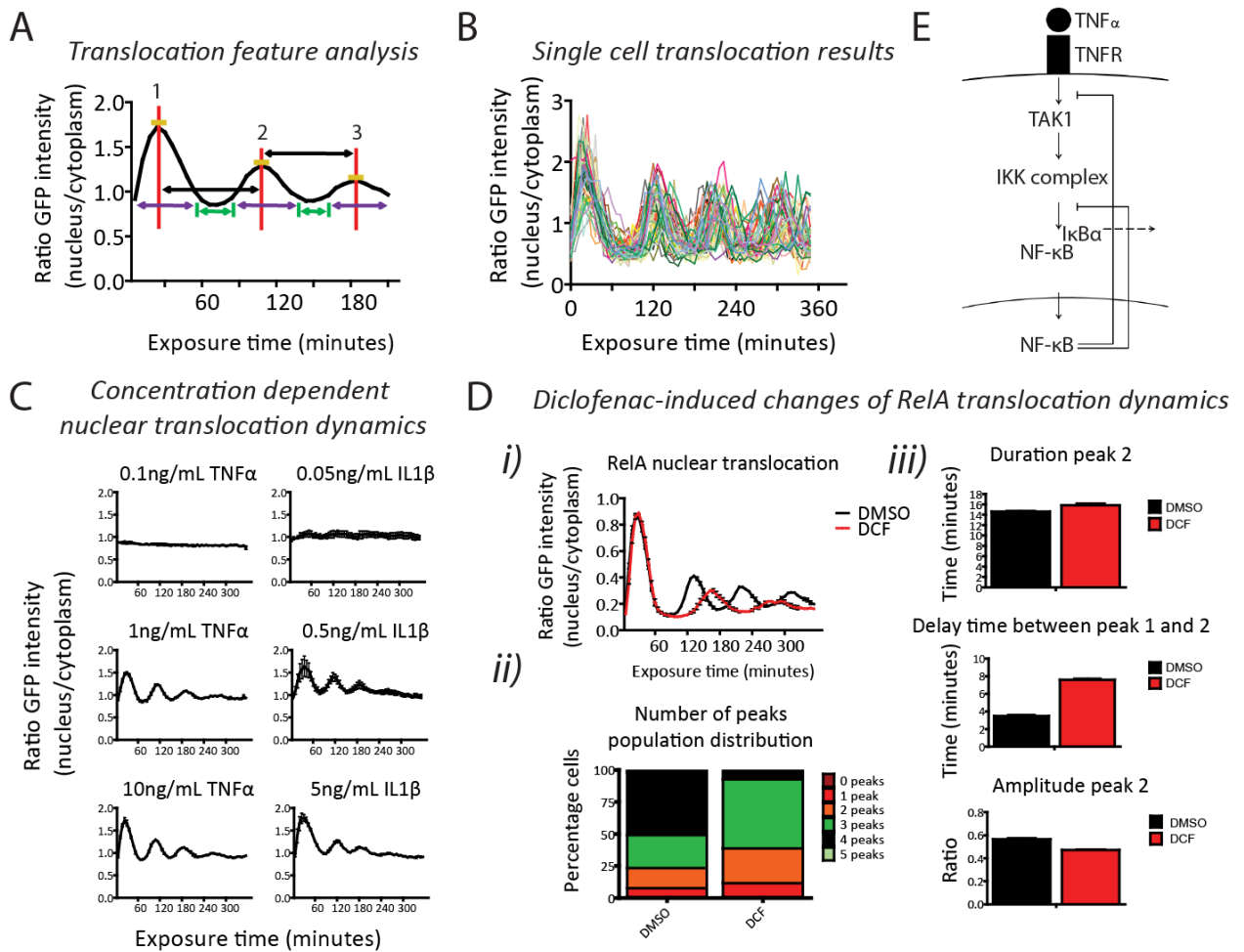


**Figure 7: Multiparametric analysis of BAC RelA-GFP HepG2 cells for nuclear translocation.** **A)** Characterization of nuclear oscillation features. Per single cell the time of the peaks, the duration of the peaks, the delay time between peaks, the time between peaks, the peak amplitude and the slopes of nuclear entry and exit kinetics. **B)** Single cell nuclear oscillation plots of cells with 4 nuclear translocation events. **C)** Nuclear translocation dynamics of RelA-GFP under a concentration range of TNF $\alpha$  and IL1 $\beta$ . **D i)** Normalized RelA-GFP nuclear translocation upon 10ng/mL TNF $\alpha$  stimulation. Cells were pre-incubated under 2% DMSO control or 500  $\mu$ M diclofenac (DCF) conditions. **ii)** Population distribution of the number of peaks under 2% DMSO control or 500  $\mu$ M diclofenac (DCF) conditions. **iii)** Nuclear oscillation features of cells under 2% DMSO control or 500  $\mu$ M diclofenac (DCF) conditions. Duration of peak 2, the delay time between peak 1 and 2 and the amplitude of peak 2 are displayed. **E)** Schematic overview of NF- $\kappa$ B signalling pathway including feedback loops. For a detailed description of the experiment see supporting information 3.

doses of diclofenac and LPS exposure in rats leads to the exposure of DAMPs and pro-inflammatory cytokines IL1 $\beta$ , TNF $\alpha$ , and CINC1.[147] Furthermore, in vitro assays showed that in HepG2 cells TNF $\alpha$  stimulation and in primary human hepatocytes a mixture of TNF $\alpha$ , IL1 $\alpha$ , IL6 and LPS leads to synergistically induced apoptosis or cell death, respectively.[38, 146] To assess this interaction further we established a high content analysis assay in HepG2 cells to measure the activation status of NF- $\kappa$ B induced by TNF $\alpha$ . For this we generated BAC-GFP-RelA HepG2 cells. TNF $\alpha$  exposure results in a concentration dependent nuclear translocation of the NF- $\kappa$ B complex

containing the GFP-RelA subunit (Fig. 7). NF- $\kappa$ B transcriptional activity leads to I $\kappa$ B $\alpha$  expression and subsequent shuttling of NF- $\kappa$ B back into the cytoplasm. Continuous TNF $\alpha$  stimulation however stimulates NF- $\kappa$ B to a second nuclear translocation, characterized by the typical nuclear oscillation pattern. Importantly, diclofenac inhibits the oscillatory response. Multiparametric analysis of NF- $\kappa$ B oscillation at single cell level allows the identification of different parameters, accurately describing the cell- population distributions of the nuclear translocation responses and the effect of diclofenac (Fig. 7). Our current data fit the mathematical models of feedback mechanisms that control NF- $\kappa$ B activity.[202] High throughput microscopy will now allow us to integrate this quantitative single cell NF- $\kappa$ B oscillation data in mathematical models to predict the mechanism by which chemicals interfere with the NF- $\kappa$ B signalling pathways and thereby suppress overall survival signalling. Indeed, depletion of NF- $\kappa$ B in HepG2 cells sensitizes cells towards diclofenac-induced cell death [38].

### **8.3. RNA interference to unravel signalling networks that control cellular stress responses.**

Above we described the regulatory mechanisms by which various physiological adaptive stress response pathways are controlled. This is based on the current scientific knowledge and may not per se establish how chemicals affect these pathways. Chemical cell injury is associated with extensive activation of various protein kinases and ubiquitinases that mediate post-translational modification of various proteins and thereby affect their activity. This may impinge as well on the modulation of these adaptation programs. Hence understanding the entire complexity of the signalling networks that drive adverse drug reactions requires functional genomics RNA interference-based approaches as well. The integration of RNA interference with HCI of the GFP-reporters is a powerful approach. We first addressed this concept to assess the role of alternative mechanisms by which the Keap1/Nrf2 pathway is controlled. Indeed alternative mechanisms of Nrf2 regulation have been reported: *e.g.* binding of selective substrate for autophagy p62 to the KIR motif on Keap1 leads to activation of Nrf2 [203] or a Keap1 independent degradation of Nrf2 possibly by phosphorylation of specific Nrf2 serine sites, *e.g.* by glycogen synthase kinase 3 (GSK-3) and protein kinase C (PKC).[204]'[205] We sought to identify novel candidate signalling molecules that control the activation of Srtn1-GFP expression by a specific activator of Keap1, CDDO-Me. As a first step we evaluated the role of epigenetic modifiers (~150 target genes) and performed knockdown of individual genes by Dharmacon siRNA smartpool mixes followed by CDDO-Me treatment for 7 hr. Nrf2 knock down as a positive control blocked CDDO-Me-induced Srtn1 expression as expected, while Keap1 knockdown enhanced the response. Interestingly, SMARCA2 was found to almost fully block the adaptive stress response program, while LRCH4 enhanced the response (Fig. 8). These results exemplify that RNAi screens can further contribute our understanding which signalling networks control pathways of toxicity. Genetic polymorphism in candidate regulators may determine the amplitude of cellular adaptive stress response programs and thereby the susceptibility to particular adverse drug reactions. Much work will be required in this area.

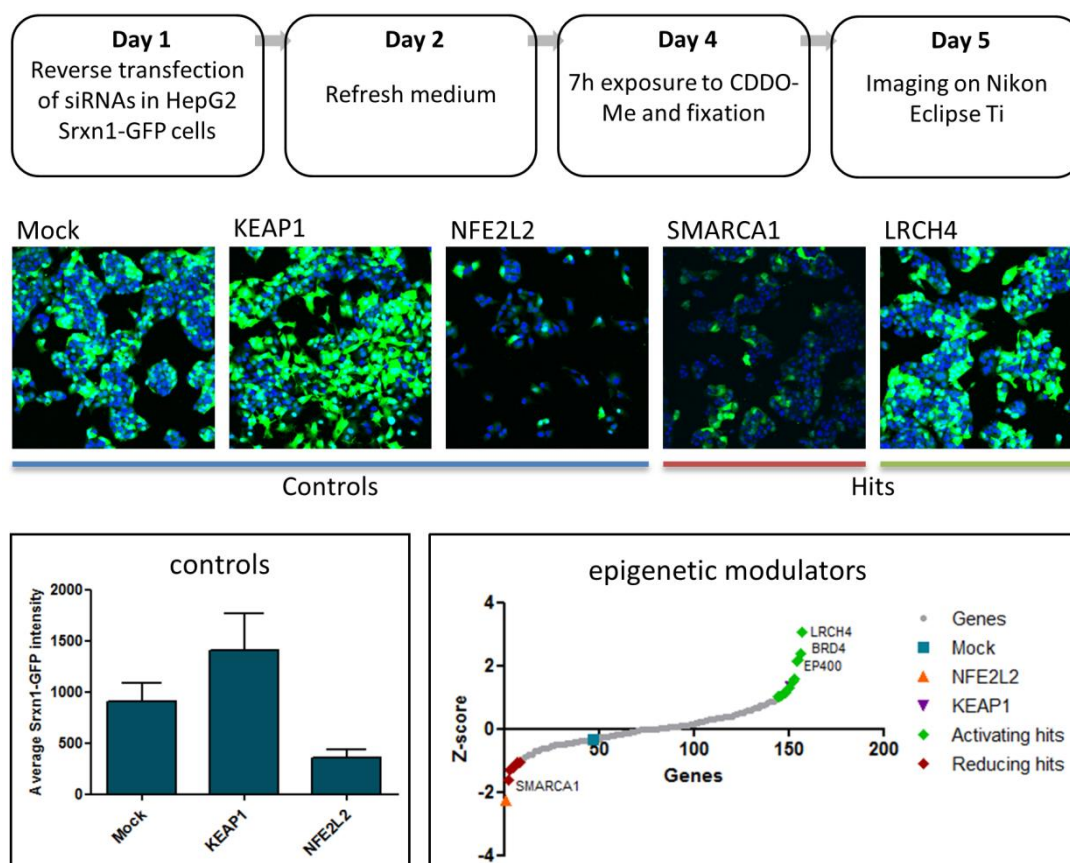


**Figure 8: siRNA screen for Nrf2-mediated Srxn1 induction.** To monitor the epigenetic modifiers that modulate Nrf2 activity we performed a siRNA screen of in total ~150 candidate genes in BAC Srxn1-GFP HepG2 cells. Cells were transfected with siRNA for 72 hr followed by exposure to CDDO-Me for 7 hr. Then cells were fixed and imaged on a Nikon confocal microscope and image analysis of Srxn1-GFP expression in individual cells using Image-J. Z-score was determined for the effect of individual genes. Note that SMARCA2 knock down inhibits Srxn1 expression while LRCH4 is enhanced Srxn1 expression. NFE2L2 (Nrf2) and Keap1 were used as controls. For a detailed description of the experiment see supporting information 4.

## 9. Future perspectives.

In this review we described the approaches and advantages to apply high content imaging to monitor the dynamics of adaptive stress response pathways that are critical in toxicity in relation to compound screening, mechanistic RNAi studies and dynamic modeling of such responses. So far these studies are based on the analysis of 2D cell culture of HepG2 cells. While such systems are likely fit for purpose for various applications, these cells contain limited reminiscence with human hepatocytes in the *in vivo* situation and have for example limited xenobiotic metabolism capacity.[206, 207] Nevertheless, there are improved methods to culture HepG2 cells in 3D cultures which will improve their differentiation and increase their metabolic capacity.[208] When such 3D cultures, in combination with other relevant liver cells, are applied to the HepG2 reporter cell lines, we may well get better prediction of liver toxicity. Automated live cell imaging of 3D cultures requires fast confocal imaging approaches and is rather in its infancy.

Alternatively, for improved modeling of the stress responses in relation to toxic outcome, the above reporter assays could be combined with alternative fluorescent probes that detect various biochemical parameters such as mitochondrial membrane potential, ROS or cell death.

This will then allow to more closely dissect the relationship between levels of stress activation and ultimate onset of cytotoxic events and help to assess the safety window of stress response activation.

An ultimate goal for an efficient monitoring of stress response signalling would be to integrate different reporters in one cell system, by labeling the different reporters with different fluorescent proteins. This would then allow the evaluation of the relationship between activation of different stress responses at the cellular level, and again to determine the maximal levels of stress responses in relation to toxic outcome. Alternatively, different cell reporters that contain different colors could be mixed into a 'rainbow' cell stress reporter platform that would capture the different stress response in one well, yet not in the same cells.

Certainly HepG2 may on the long run not be the optimal cell model and stem cell technology seems to be the future. While current differentiation protocols are at the most feasible to generate hepatocyte-like cells from either human pluripotent stem cells or induced-pluripotent stem cells,[209] it will be of high relevance to generate iPS cells with critical stress response markers. These can then be differentiated in hepatocyte-like cells and used in high content imaging approaches.

How can we eventually integrate these models in compound screening? As mentioned, these HepG2 reporter systems could be a highly valuable tool in large screening efforts including the ToxCast and Tox21[210] efforts. In particular the single cell analysis of stress responses as well as the evaluation of dynamic responses using live cell imaging will be a major asset to better dissect the principal mode of action of chemicals. Since these reporter systems allow fixation, large compound screens are feasible. On a more limited scale these reporter systems can be used in a pre-clinical drug development program to classify smaller compound library for lead prioritization: *i.e.* compounds that in a concentration escalation response provide minimal activation of various stress responses are likely to have also the least interference with the normal cellular physiological homeostasis and hence a reduced liability for adverse drug reactions.

**Funding Information**

This work was supported by a grant from the Netherlands Genomics Initiative to the Netherlands Toxicogenomics Center, Top Institute Pharma project D3-201, IMI MIP-DILI project grant agreement number 115336 and the EU FP7 Seurat-1 Detective project grant agreement number 266838.

**Acknowledgement** We would like to acknowledge lab members Sylvia Le Dévédec and Hans de Bont for their helpful discussions.

**Supporting information 1**

[Movies of several BAC-reporter cell lines have been uploaded. The DNA-damage response BAC-reporters 53BP1-GFP, p53-GFP & p21-GFP were exposed to 25 $\mu$ M Etoposide. The UPR BAC-reporters ATF4-GFP, XBP1-GFP, BiP-GFP and Chop-GFP were exposed to 10  $\mu$ M tunicamycin. The oxidative stress BAC-reporters Nrf2-GFP, Keap1-GFP and Srxn1-GFP were exposed to 10 $\mu$ M iodoacetamide. The inflammatory BAC-reporters RELA-GFP, ICAM1-GFP and IKBalpha-GFP were exposed to 10 ng/ml TNF $\alpha$ . All movies are over a time course of 24 hours with equidistant time intervals between consecutives frames]. This material is available free of charge via the Internet at <http://pubs.acs.org>.

**Supporting information 2**

[Figure 6: Human hepatoma HepG2 cells were obtained from American Type Culture Collection (clone HB-8065, ATCC, Wesel, Germany). HepG2 cells stably expressing Srxn1-GFP were created by 500 $\mu$ g/mL G418 selection upon transfection of GFP tagged Srxn1 cloned into bacterial artificial chromosome (BAC) construct, using Lipofectamine<sup>TM</sup> 2000 (Invitrogen, Breda, Netherlands). For all experiments the cells were maintained in Dulbecco's modified Eagle's medium (DMEM) supplemented with 10% (v/v) fetal bovine serum, 25 U/mL penicillin and 25  $\mu$ g/mL streptomycin between passages 5 and 20. The screening was performed on  $\mu$ Clear Greiner 96 well plates on a Nikon TI eclipse A1 MP confocal microscope. Spectrum library compounds were transferred by automated pipetting to a final concentration of 10  $\mu$ M in 6 replicate plates. Three of these plates were incubated for 24hr, fixed and imaged by automated confocal microscopy. The three remaining plates were co-exposed to 30 nM CDDO-Me, a potent Nrf2 activator, and fixed after 7h incubation. The spectrum library 2320 was obtained from Microsource Discovery Systems, Gaylordsville. This collection consists of 2320 compounds of which 60% drug components, 25% natural products and 15% other bioactive components. The compounds are dissolved in DMSO at 10 mM and diluted to 10  $\mu$ M final concentration (0.1% DMSO)]. This material is available free of charge via the Internet at <http://pubs.acs.org>.

**Supporting information 3**

[Figure 7: Human hepatoma HepG2 cells were obtained from American Type Culture Collection (clone HB-8065, ATCC, Wesel, Germany). HepG2 cells stably expressing RelA-GFP were created by 500 $\mu$ g/mL G418 selection upon transfection of GFP tagged RelA cloned into bacterial artificial chromosome (BAC) construct, using Lipofectamine<sup>TM</sup> 2000 (Invitrogen, Breda, Netherlands). For all experiments the cells were maintained in Dulbecco's modified Eagle's medium (DMEM) supplemented with 10% (v/v) fetal bovine serum, 25 U/mL penicillin and 25  $\mu$ g/mL streptomycin between passages 5 and 20.

Prior to imaging, nuclei were stained with 100ng/mL Hoechst 33342 in complete DMEM for 45 minutes. Next, cells were exposed to 500 $\mu$ M Diclofenac (Sigma-Aldrich, Zwijndrecht, The Netherlands) or 0.2% DMSO for 8 hours. Then, the cells were stimulated with the indicated amount of human TNF $\alpha$  (R&D Systems, Abingdon, UK). Nuclear translocation was followed for 6 hours by automated confocal imaging every 6 minutes (Nikon TiE2000, Nikon, Amstelveen, Netherlands). Quantification of the nuclear/cytoplasmic ratio of GFP-RelA intensity in individual cells was performed using an algorithm for imageJ. This material is available free of charge via the Internet at <http://pubs.acs.org>.

#### **Supporting information 4**

[Figure 8: Human hepatoma HepG2 cells were obtained from American Type Culture Collection (clone HB-8065, ATCC, Wesel, Germany). HepG2 cells stably expressing Srxn1-GFP were created by 500 $\mu$ g/mL G418 selection upon transfection of GFP tagged Srxn1 cloned into bacterial artificial chromosome (BAC) construct, using Lipofectamine<sup>TM</sup> 2000 (Invitrogen, Breda, Netherlands). For all experiments the cells were maintained in Dulbecco's modified Eagle's medium (DMEM) supplemented with 10% (v/v) fetal bovine serum, 25 U/mL penicillin and 25  $\mu$ g/mL streptomycin between passages 5 and 20. Knock down of a certain gene was done by performing reverse transfection. For the transfection mix, pooled siRNAs (50nM) where mixed with INTERFERin (0.3% end dilution, Polyplus, Leusden, Netherlands) and serum free medium. The used siRNAs were siNFE2L2, siKEAP1 and the libraries kinases, ubiquitinases, deubiquitinases, epigenetic modulators, transcription factors and toll-like receptors which were all derived from Dharmacon (Lafayette Colorado, USA). As control, Mock was used in which no siRNA was added to the transfection mix. Medium was refreshed 24 hours after transfection or 100  $\mu$ L medium was additionally added 7 hours after reverse transfection]. This material is available free of charge via the Internet at <http://pubs.acs.org>.

# Chapter 3

## High Content Imaging-based BAC-GFP Toxicity Pathway Reporters to Assess Chemical Adversity Liabilities

---

**This chapter has been submitted to Archives of Toxicology as:**

Steven Wink<sup>\*‡</sup>, Steven Hiemstra<sup>\*‡</sup>, Suzanna Huppelschoten<sup>\*</sup>, Bram Herpers<sup>\*</sup>, Bob van de Water<sup>\*§</sup>

<sup>‡</sup>Both authors contributed equally

<sup>\*</sup>Division of Toxicology, Leiden Academic Centre for Drug Research, Leiden University, Leiden, The Netherlands

*High Content Imaging-based BAC-GFP Toxicity Pathway Reporters to Assess Chemical Adversity Liabilities*



## 1. Abstract

Adaptive cellular stress responses are paramount in the healthy control of cell and tissue homeostasis and generally activated during toxicity in a chemical-specific manner based on the mode-of-action. Here we established a platform containing a panel of distinct adaptive stress response reporter cell lines based on BAC-transgenomics GFP tagging in HepG2 cells. Our current panel of ten BAC-GFP HepG2 reporters together contain i) upstream sensors, ii) downstream transcription factors, and iii) their respective target genes, representing the oxidative stress response pathway (KEAP1/Nrf2/Srxn1), the unfolded protein response in the endoplasmic reticulum (XBP1/ATF4/HSPA5/DDIT3), and the DNA damage response (53BP1/p53/p21). Using automated confocal imaging and quantitative single cell image analysis we established that all reporters allowed the time-resolved, sensitive and mode-of-action specific activation of the individual BAC-GFP reporter cell lines as defined by a panel of pathway specific training compounds. Implementing the temporal pathway activity information increased the discrimination of training compounds. For a set of >30 hepatotoxins the induction of Srxn1, HSPA5, DDIT3 and p21 BAC-GFP reporters correlated strongly with the transcriptional responses observed in cryopreserved primary human hepatocytes. Together our data indicate that a phenotypic adaptive stress response profiling platform will allow a high throughput and time-resolved classification of chemical-induced stress responses, thus assisting in the future mechanism-based safety assessment of chemicals.

## 2. Introduction

In the past decades hepatic toxicity has contributed disproportionately to drug withdrawals [4]. Nowadays drug-induced liver injury (DILI) is still notoriously difficult to predict in as well preclinical and clinical trial settings because of the often idiosyncratic nature. There is a strong incentive to integrate human-relevant mechanistic understanding of adverse drug reactions in *in vitro* based data for evidence and read across based approaches for risk assessment. Transcriptomics has contributed much to our mechanistic understanding and has helped to initiate and populate the adverse outcome pathway (AOP) framework [63, 211]. AOPs are described as a sequential chain of causally linked events at different levels of biological organization that together culminate in the adverse health outcome. While some AOPs have so far been established, a next important step is to translate AOP-related mechanistic understanding in advanced preferably quantitative high throughput assays that reflect pathways essential in target organ toxicity. Our vision is to establish an imaging-based platform that can quantitatively assess the activation of individual key events relevant to AOPs. Our initial focus is on adaptive stress response pathways, that are typically part of AOPs and related to adverse drug reactions.

Chemicals may interact with cellular components leading to an altered cell biochemical status. Cells sense these biochemical changes and activate specific adaptive stress response pathways. These pathways are activated to combat detrimental conditions under which cells cannot function normally. Classical adaptive stress response pathways are the anti-oxidant pathways (OSR) mediated by activation of the Nrf2 transcriptional program [212], the endoplasmic reticulum (ER) unfolded protein response (UPR) mediated by XBP1, ATF4 and ATF6 transcription factor activation [213], and the DNA damage repair (DDR) pathway typically related to activation of the p53 transcriptional program [214, 215]. We propose that the quantitative dynamic monitoring

of the activation of these adaptive stress response pathways at the single cell level in high throughput systems will significantly contribute on the hand to chemical safety assessment.

All above mentioned adaptive stress response pathways can roughly be conceived as three consecutive steps: i) 'sensing' of the biochemical perturbations; ii) downstream transcription factor activation through either stabilization and/or nuclear translocation; and iii) downstream target gene activation. For the OSR this involves: i) KEAP1 modulation, ii) Nrf2 stabilization and nuclear translocation, followed by iii) target gene expression including *Srxn1* [216, 217]. The UPR involves i) sensing of unfolded proteins in the lumen of the ER by IRE1, PERK and ATF6, followed by ii) downstream transcription factor stabilization and nuclear translocation of ATF4, ATF6 and XBP1 and iii) subsequent activation of the expression of the chaperone BiP/Grp78/HSP5A and the transcription factor CHOP/DDIT3 [218]. Finally the DDR involves i) recognition of DNA damage sites and DNA damage foci formation with accumulation of e.g. 53BP1 in these foci, subsequent ii) stabilization of p53 through phosphorylation by kinases activated after DNA damage, and iii) expression key p53 target genes upon translocation of p53 to the nucleus including p21 and BTG2 [219, 220] (see Figure 1A). We anticipate that the integration of all these different sensors, transcription factors and downstream targets in fluorescent protein reporters would facilitate the evaluation of the dynamic activation of adaptive stress responses at the single cell level using high content imaging approaches. Therefore the aim of the current work was to establish and systematically evaluate the application of GFP-reporters using HepG2 cell lines for these three pivotal adaptive stress response pathways using bacterial artificial chromosome (BAC) cloning technology [48] targeting individual "sensor" proteins, transcription factors as well as downstream target proteins. Since DILI prediction remains a major problem, we focused on the integration of these reporters in the liver hepatoma cell line HepG2, which is routinely used for high throughput first tier liver toxicity liability assessment [221-223].

Here, we established, characterized and evaluated in total 10 BAC-GFP HepG2 reporter cell lines reflecting three adaptive stress response pathways for the application in live cell high content imaging in relation to a set of DILI reference compounds. Our data indicate that these reporter cell lines consistently selective monitor the dynamic activation of the OSR, UPR and DDR at the single cell level for pathway specific compounds. Moreover, we demonstrate that these HepG2 BAC-GFP reporter cell lines can identify the activation of these stress response pathways that are typically seen by DILI drugs in primary human hepatocytes. Interestingly, the live cell acquisition data allow the improved classification of DILI compounds based on dynamic stress pathway activation.

### **3. Material and Methods**

#### **3.1. Generation of GFP-tagged cell lines**

Human KEAP1, NFE2L2 (Nrf2), CDKN1A (p21), TP53 (p53), BTG2, TP53BP1, XBP1, DDIT3 (CHOP), ATF4, HSPA5 (BiP) and mouse *Srxn1* BAC clones were selected and GFP tagged as described previously [48] and stably introduced into HepG2 cells by transfection and 500µg/ml G-418 selection. At least 20 of the monoclonal BAC transfected HepG2 colonies were separately grown out and GFP positive clones suitable for imaging were selected to complement the BAC-GFP stress response reporter platform.

#### **3.2. RNA interference**

siRNAs against human NFE2L2 (NRF2), TP53 (P53), ATF4, ATF6 and EIF2AK3 (PERK) were acquired from Dharmacon (ThermoFisher Scientific) as siGENOME SMARTpool reagents, as well as in the form of four individual siRNAs. HepG2 cells were transiently transfected with the siRNAs (50nM) using INTERFERin (Polyplus) as described previously [38]

#### **3.3. Western blotting**

Samples were collected by direct cell lysis (including pelleted apoptotic cells) in 1x sample buffer supplemented with 5% v/v β-mercaptoethanol and heat-denatured at 95°C for 10 minutes. The separated proteins were blotted onto PVDF membranes before antibody incubation in 1% BSA in TBS-Tween20. Antibodies: mouse-anti-GFP (Roche) and mouse-anti-tubulin (Sigma) and mouse-anti-GAPDH (Santa Cruz). Horseradish Peroxidase detection was performed by Pierce® ECL (ThermoScientific) using the ImageQuant LAS4000 (GE HealthCare). Cy5 was detected by the ImageQuant LAS4000(GE HealthCare).

#### **3.4. Microscopy**

Accumulation of target protein-GFP levels, localization or foci formation and propidium iodide staining was monitored using a Nikon TiE2000 confocal laser microscope (lasers: 647nm, 488nm and 408nm), equipped with an automated stage and perfect focus system. Prior to imaging at 20x magnification and either 1X, 2X or 4X zoom, HepG2 cells were loaded for 45 minutes with 100ng/mL Hoechst33342 to visualize the nuclei, upon which the Hoechst-containing medium was washed away to avoid Hoechst phototoxicity [224]. The time interval was dependent on the required resolution for the corresponding reporter cell line and on the number of reporter types plated simultaneously on the imaging plates. Cell death was determined by monitoring the accumulation of PI stained cells after a 24 hour time period.

#### **3.5. Quantitative image analysis**

Image quantification was performed with CellProfiler version 2.1.1 [49] with an in house developed module implementing the watershed masked algorithm for segmentation [193]. The watershed separates an image in regions with single cells followed by pixel classification for each region as fore- or background and this method performs well detecting the Hoechst33342 stained nuclei of the closely packed HepG2 cells. The binary mask containing the segmented nuclei was fed to the identify-primary-objects module, overlap-based-tracking module and intensity-nuclei-size-shape-measurement modules of CellProfiler. For the cytosol location of the *Srxn1*-GFP, *Btg2*-GFP and *BiP*-GFP reporters the nuclear objects were used as seeds for the identify-secondary-objects

module set to a propagation method with the MCT algorithm on adaptive (window size approximately 20 pixels) segmentation. The Keap1 and TP53BP1 reporters are based on foci detection. The nuclei are segmented and used as seeds for the cytosol identification using the cytosolic GFP signal for the KEAP1-GFP cell line. The foci detection is performed with the fociPicker3D plugin [225] in ImageJ and each individual foci is assigned to either the nuclei (for P53BP1) or cytosol (KEAP1) using the CellProfiler assign parent-child relationship module. The p21, p53, Nrf2, Xbp1, Atf4 and CHOP reporters are based on quantifying the GFP signal in the nuclei. The nuclei signal is segmented and these regions are directly used to quantify the GFP intensity. Segmentation results were stored as png files for quality control purposes and CellProfiler pipelines were stored for reproducibility. Image analysis results were stored on the local machine as HDF5 files.

### 3.6. Data analysis

Data analysis, quality control and graphics was performed using the in house developed R package H5CellProfiler (Wink *et al.*, 2015, manuscript in preparation).

The features of interest were extracted from the HDF5 files and further analyzed using the graphical user interface of the H5CellProfiler package. The mean of the features for each compound, concentration, cell line and replicate combination was calculated. To account for PI background staining and noise the segmented PI segmentations were masked by a 2 pixel dilated nuclei. The area of these nuclei and the PI were divided to obtain the cell death stain to cell area ratio. These ratios were filtered to be at least 10% of the cell size and following this procedure each cell was either flagged as alive or dead in the final time point of the 24 live imaging session. In this manner the fraction of dead cells could be accurately determined. All resultant summarized data was stored as tab delimited text files and further processed for normalization and graphical presentation using R.

Due to automated confocal imaging over a one year period, the time course data required intensity variation plate normalization as well as modeling of the time course-data. The mean and integrated intensity features and the foci were first transformed to fold change with respect to the plate- specific DMSO controls at time point 1. Afterwards these value were scaled between 0 and 1 over the entire dataset with the formula  $(x - x_{\min\_screen}) / (x_{\max\_screen} - x_{\min\_screen})$  for the purpose of proper heatmap display. Prior validation of negative and positive control responses preceded this scaling procedure. After the normalization steps the response specific features were fit separately per replicate with the b-splines method with a degree of freedom of 10 and 3<sup>rd</sup> degree polynomials using the base-r lm function and bs function of the splines package. This allowed resampling the data with equidistant time points for replicate statistics and higher density time point sampling (200 points) for smooth heatmap display. All b-spline fits were stored for verification purposes.

### 3.7. Data representation

All HCI data representations were generated or modified with Illustrator CS6, Fiji, ggplot2 [226], the aheatmap function of the NMF package [227]. For response data clustering the equidistant sample time profile features from the b-spline model were used to calculate a distance matrix for each feature separately using Euclidean distance. A mean distances matrix was calculated and subjected to clustering with the ward.D method of the hclust function.

### **3.8. Reagents**

All compound drugs were acquired from Sigma-Aldrich, except for Cisplatin (Ebewe), CDDO-me (kind gift from Dr. Ian Copple, University of Liverpool), Bendazac (kind gift from Dr. Anita Dankers, Janssen Pharmaceuticals), Metformin (MIP DILI consortium), Propylthiouracil, Captopril, Tacrine, Thioridazine, Azathioprine and Sulindac (all a kind gift from Dr. Weida Tong, NCTR-FDA). All compounds were freshly dissolved in DMSO, except for Metformin, Venlafaxine, Methapyrilene, Fluphenazine, Buthionine Sulfoxamine, Bromoethlyamine, Lomustine (all PBS), Acetaminophen, 2,4-dinitrophenol and Phenobarbital (all DMEM).

### **3.9. Cell culture**

Human hepatoma HepG2 cells were acquired from ATCC (clone HB8065) and maintained and exposed to drugs in DMEM high glucose supplemented with 10% (v/v) FBS, 25U/mL penicillin and 25µg/mL streptomycin. The cells were used between passage 5 and 20. For live cell imaging, the cells were seeded in Greiner black µ-clear 384 wells plates, at 20,000 cells per well.

### **3.10. Gene expression analysis.**

CEL files were downloaded from the Open TG-GATEs database: "Toxicogenomics Project and Toxicogenomics Informatics Project under CC Attribution-Share Alike 2.1 Japan" <http://dbarchive.biosciencedbc.jp/en/open-tggates/desc.html>. Probe annotation was performed using the `hthgu133pluspmhsentrezg.db` package version 17.1.0 and Probe mapping was performed with `hthgu133pluspmhsentrezgcdf` downloaded from NuGO ([http://nmg-r.bioinformatics.nl/NuGO\\_R.html](http://nmg-r.bioinformatics.nl/NuGO_R.html)). Probe-wise background correction (Robust Multi-Array Average expression measure), between-array normalization within each treatment group (quantile normalization) and probe set summaries (median polish algorithm) were calculated with the `rma` function of the Affy package (Affy package, version 1.38.1 [228]). The normalized data were statistically analyzed for differential gene expression using a linear model with coefficients for each experimental group within a treatment group. A contrast analysis was applied to compare each exposure with the corresponding vehicle control. For hypothesis testing the empirical bayes statistics for differential expression was used followed by an implementation of the multiple testing correction of Benjamini and Hochberg using the LIMMA package.

## 4. Results

### 4.1. GFP-tagged stress-reporter proteins respond to corresponding chemically induced stress.

To enable live cell imaging of the chemically induced dynamics of cellular adaptive stress response programs a panel of reporter cell lines was created using BAC cloning technology [48]. For each adaptive stress response pathway an upstream 'sensor', a transcription factor and a downstream target was chosen (Fig. 1A). For the oxidative stress response program (OSR) kelch-like ECH-associated protein 1 (KEAP1) was selected as upstream sensor, nuclear factor, erythroid 2-like 2 (Nrf2/NFE2L2) as transcription factor and *Srxn1* as downstream target [217, 229]. For the UPR heat shock 70kDa protein 5 (BiP/HSPA5) regulates the endoplasmic reticulum (ER)-stress/unfolded protein response (UPR) pathway through binding to accumulated unfolded proteins and consequently dissociating from the transmembrane transducers ATF6, PERK and IRE-1 [230]; as such BiP acts as a sensor of the UPR. However, BiP is also induced strongly after ER stress [231] and also reflects UPR activation. We labeled two arms of the UPR: for the pro-survival route we labeled the transcription factor XBP1 and downstream target chaperone BiP; and for the translation inhibition and pro-apoptotic arm we labeled the activating transcription factor 4 (ATF4) and DNA-damage-inducible transcript 3 (CHOP/DDIT3). For the DNA damage response program (DDR) the upstream sensor tumor protein p53 binding protein 1 (TP53BP1) was chosen based on its ability to sense double strand breaks [232] and activate the Ataxia Telangiectasia Mutated Protein pathway (ATM). As transcription factor for the DDR tumor protein p53 (p53/TP53) was chosen as the pivotal transcription factor in the DDR; two p53 downstream targets selected were cyclin-dependent kinase inhibitor 1 (p21/CDKN1A) and BTG family member 2 (BTG2). To ensure near-endogenous protein-fusion levels and normal regulation of these adaptive stress response programs eGFP and selection markers were cloned in bacterial artificial chromosome (BAC) vectors which consist of genomic DNA which still contain the endogenous promotor, enhancers and introns. BACs were selected that contained at least 10k bp on either side of the exon domains.

The BAC-GFP construct was used to transfect HepG2 cells using electroporation together with pRED/ET recombinase enzyme as described previously [13]. Viable HepG2 colonies were passaged separately to obtain monoclonal BAC-GFP cell lines. For each target gene a single monoclonal BAC-GFP cell line was selected based on fluorescent intensity and protein size (Figure 1B). All selected reporter lines were evaluated on fusion-protein size, responsiveness to selective pathway activators and targeted knock down by RNAi (Fig. 1C and 1D). The GFP-tagged protein sizes for all targets were in line with reported values (<http://www.genecards.org/>). While KEAP1-GFP levels were not induced by the pro-oxidant DEM, as expected, the levels of NRF2-GFP and SRXN1-GFP were clearly induced by DEM. The ER-stress reporters ATF4-GFP, CHOP-GFP, XBP1-GFP and BiP-GFP clearly responded to the ER-stress inducer thapsigargin. The DDR reporters p53-GFP, p21-GFP and Btg2-GFP are clearly induced after 24 hr exposure of the topoisomerase inhibitor etoposide; the large size of TP53BP1-GFP (241 kDa) prohibited qualitative assessment by Western blotting. Cellular localization of GFP-fusion products for all reporters was evaluated by confocal microscopy for control and 5 hr (Nrf2) or 24 hr (all others) compound treatment (Figure 2).

A clear increase in levels of all downstream targets GFP-Srxn1, GFP-Btg2 and GFP-BiP in the cytosol was seen. For the transcription factors GFP-Nrf2, GFP-Xbp1, GFP-CHOP and GFP-p53 as well as GFP-p21 an increase in nuclear intensity was observed.

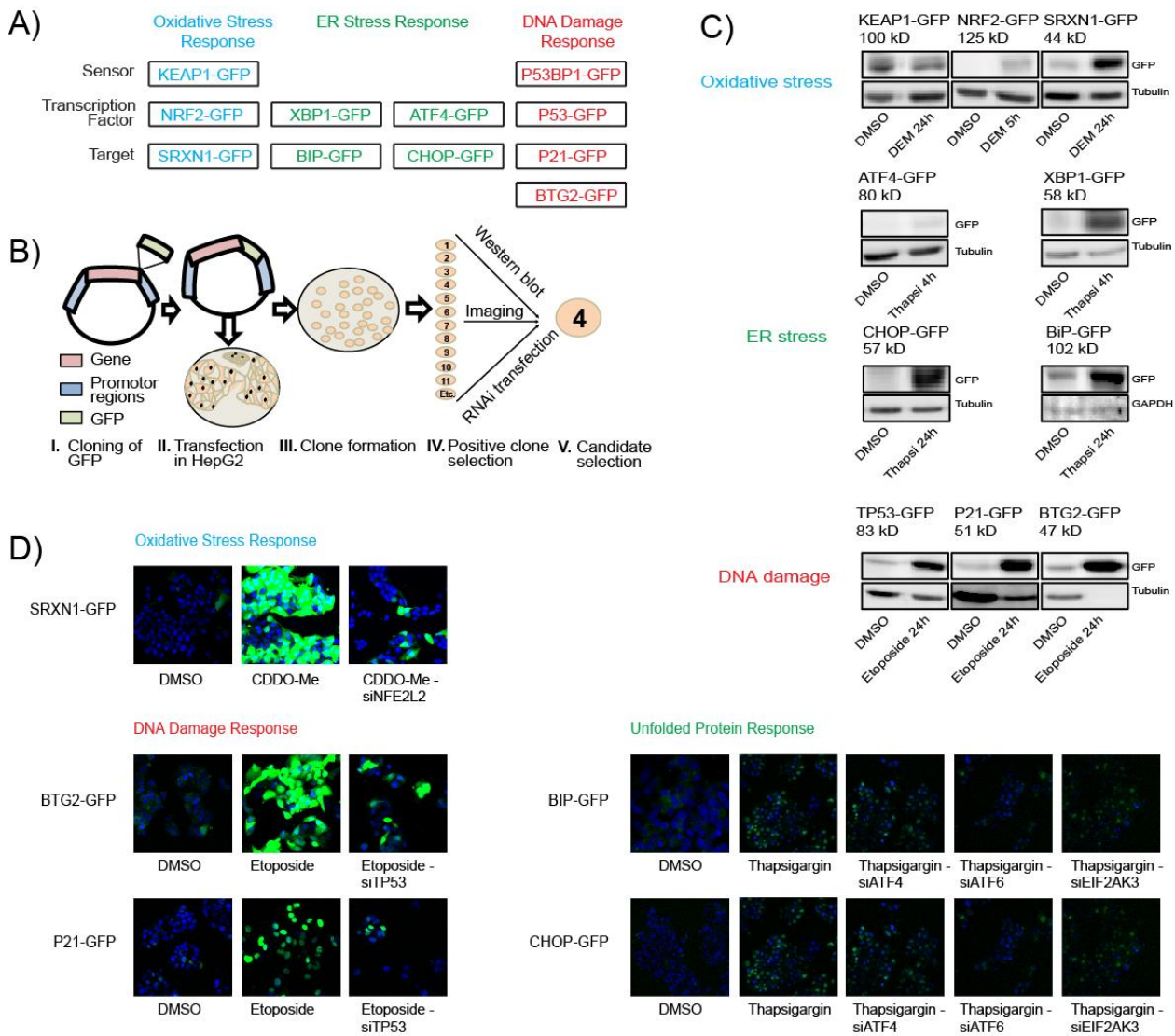
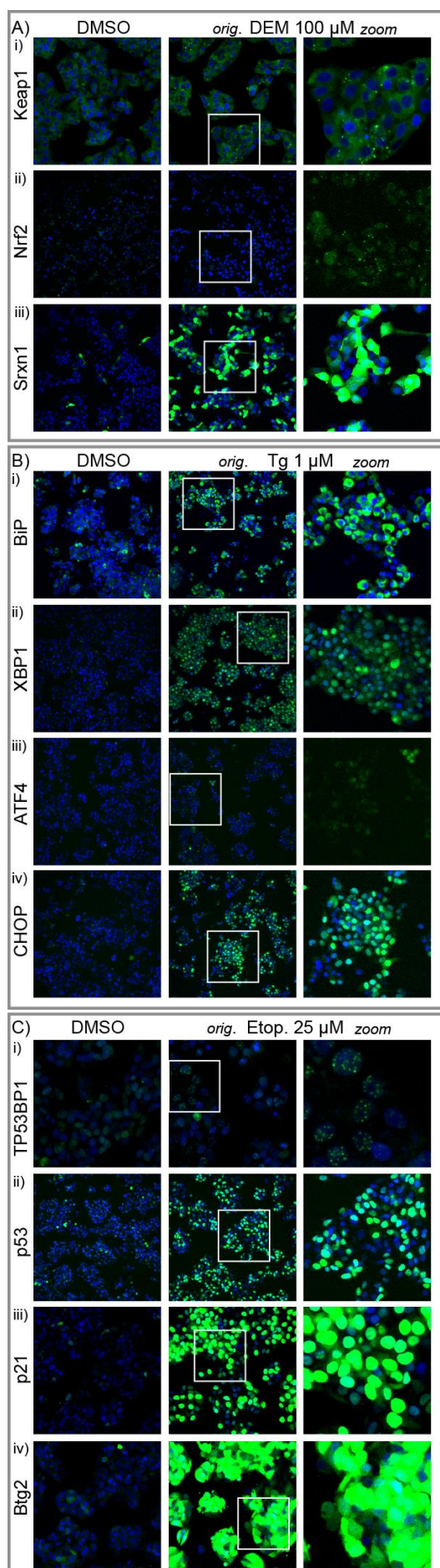


**Figure 1: Selection and characterization of adaptive stress response pathway markers for OSR, UPR and DDR.** A) Selection of the individual reporters for the respective pathways representing ‘sensor’, transcription factor and target genes. B) Insertion of GFP into BAC plasmid is followed by transfection and selection of the (monoclonal) HepG2 reporter. The selection process involves 1) imaging of 10-24 transfected HepG2 clones to determine suitability (fluorescence intensity and cell-cell variability) as a reporter cell line, with or without exposure to a stress-inducing compound depending on the reporter type, 2) determining the size of the target protein GFP fusion and induction level after stress-inducing exposure by western blot. C) Western blot analysis of reporter expression under control conditions and treatment conditions. Reporters for oxidative stress (Keap1, Nrf2 & Srxn1), ER-stress (Atf4, Xbp1, CHOP & BiP), DNA damage (p53, p21 & Btg2). The size and responsiveness to chemical stress of the GFP-fusion protein product was evaluated. Cells were treated with 100  $\mu$ M DEM (oxidative stress), 25  $\mu$ M etoposide (DDR) and 1  $\mu$ M thapsigargin (UPR) for the either 5 hr (Nrf2-GFP) or 24 hours (all others) followed by WB analysis. D) Responsiveness of target genes was assessed by knock down for Nrf2 (Srxn1 activation), p53 (p21 and BTG2 activation) and UPR transcription factors Xbp1, ATF4 or ATF6 (BiP and CHOP activation).

An increase in the number of nuclear DNA damage foci for GFP-TP53BP1 and cytosolic autophagosome-related foci for GFP-Keap1 is also evident. Little increase in Atf4-GFP was visible, yet image analysis revealed a clear and selective increase (see later Figure 4).





Next for all individual BAC-GFP reporters an automated multi-parameter imaging analysis pipeline was established using CellProfiler [49] software and ImageJ plug-ins (Figure 3). Depending on the BAC-GFP reporter type the different imaging readouts were determined using automated image analysis. For 53BP1-GFP and KEAP1-GFP we quantified foci formation in the cytosolic (KEAP1-GFP translocation with autophagosomes) and nuclear compartment (53BP1-GFP localization in DNA damage foci), respectively. For Srxn1, BiP and BTG2 we quantified the integrated GFP intensity in the cytosol. For Nrf2, Xbp1, ATF4, CHOP, p53 and p21 we determined the mean GFP-intensity in the nucleus. The different quantitative measurements reflect the altered expression and localization of our stress reporters.

Altogether we have established a functional panel of adaptive stress response reporters that allows us to quantitatively assess the dynamic activation of individual pathway components in living cells at the single cell level population level.

**Figure 2: Representative confocal images of BAC-GFP adaptive stress response reporters.** Representative confocal images are shown for OSR: Keap1, Nrf2 and Srxn1 (panel A); UPR: BiP, Xbp1, Atf4 and CHOP (panel B), and DDR: TP53BP1, p53, p21 and Btg2 (panel C). Left column reflects vehicle treatment for 24 hours or 5 hours for Nrf2; the two right panels reflect model compound treatment for 24 hr or 5 hr for Nrf2 (middle column overall image; right column zoomed image): OSR, 100  $\mu$ M DEM; UPR, 1  $\mu$ M thapsigargin; DDR, 25  $\mu$ M etoposide. Images of most reporters are captured at 20 or 40 times magnification on 512X512 pixels, however the reporters Keap1 and TP53BP1 require a higher resolution to be able to count the number of foci per cell and as such these were captured at 40X magnification on 1024X1024 pixels. Hoechst channel is omitted for low intensity level reporters in the right column (zoom) panel.



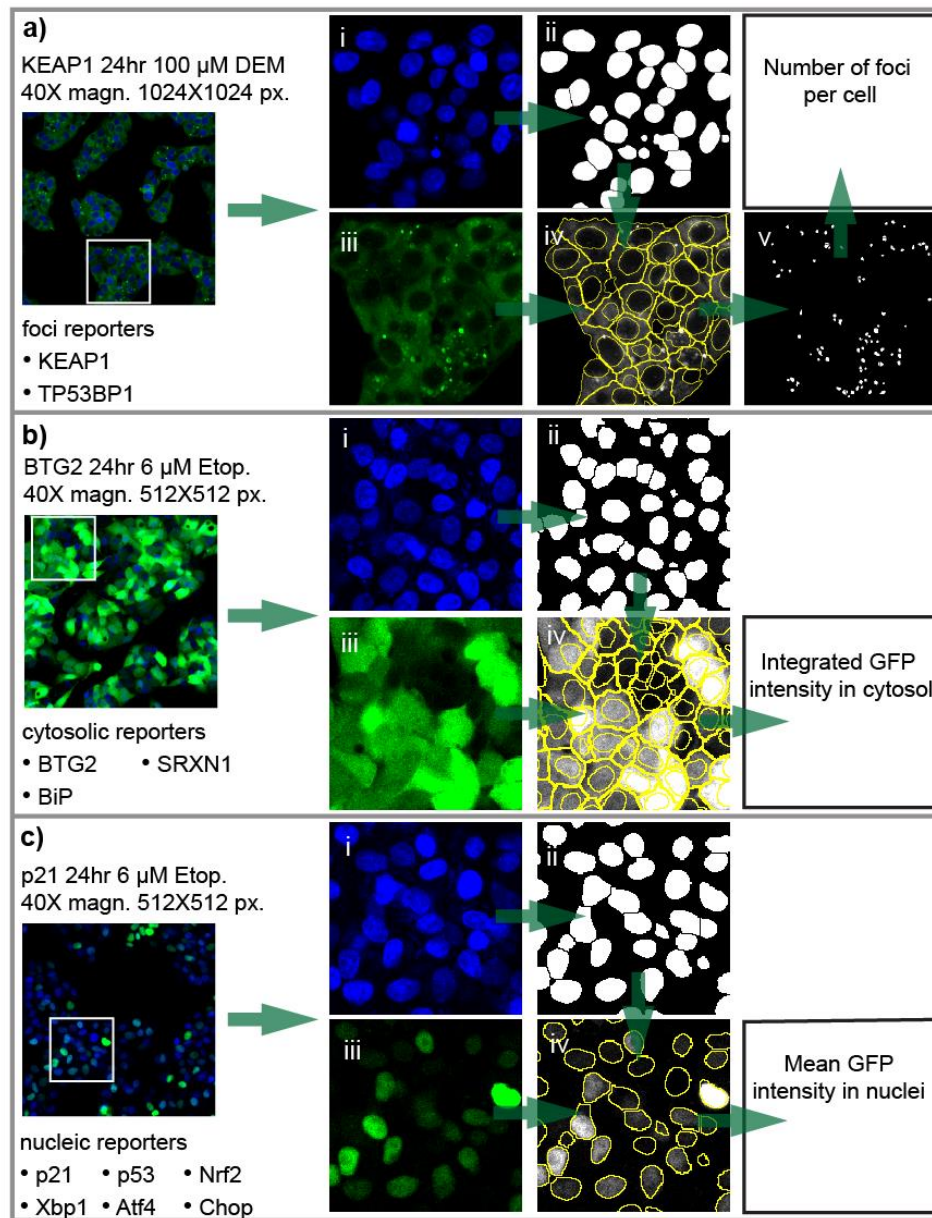


**Figure 3: Automated image analysis of BAC-GFP reporter cell lines.** Automated imaged analysis was performed using CellProfiler and ImageJ-based algorithms as described in material and methods section. A) The Keap1 and P53BP1 reporters were based on foci detection. Left panel: A 1024X1024 pixel 40 times magnified image of KEAP1-GFP reporter after 24 hours exposure to 100  $\mu$ M DEM. Blue staining corresponds to the nuclei (i) and green corresponds to the KEAP1-GFP fusion protein (iii). The nuclei are segmented (ii) and used as seeds for the cytosol identification using the GFP signal (iv), the outlines of the nuclei and cytosols are displayed as yellow lines. Next, the GFP-signal foci corresponding to KEAP1-GFP being degraded in autophagosomes are segmented (v) and assigned to individual cells. B) The Btg2, Srxn1 and BiP reporters are based on quantifying the GFP signal in the cytosolic region of cells. First the nuclei signal (i) is segmented (ii) and used as seeds for the cytosol identification (iii & iv). C) The p21, p53, Nrf2, Xbp1, Atf4 and CHOP reporters are based on quantifying the GFP signal in the nuclei. The nuclei signal (i) is segmented (ii) and these regions (iv) are directly used to quantify the GFP intensity (iii).

#### **4.2. Adaptive stress response BAC-GFP reporters respond in sensitive and selective manner to reference compounds**

As a next step we set out to test the responsiveness and selectivity of the panel of stress-reporter cell lines to: i) oxidative stress inducing agents hydrogen peroxide ( $H_2O_2$ ), DEM, CDDO-Met (a pharmacological inducer of Nrf2 activity, [233]) and iodoacetamide (IAA); ii) DNA damage inducing agents topoisomerase II inhibitor and cisplatin; and iii) UPR-inducing agents brefeldin A (BFA), tunicamycin (Tc) and thapsigargin (Tg). To monitor signalling programs well before any significant cytotoxicity occurs and thereby deduce causative relationships for the onset of cytotoxicity, compound concentrations were chosen that would not lead to significant cell death after 24 hours as well as two additional concentrations that were 2- and 4-fold lower to assess the overall sensitivity of the reporter panel. Reporter cell lines were imaged for a period of 24 hours using live cell confocal imaging and evaluated for onset of cytotoxicity by propidium iodide (PI) exclusion (Supplemental Figure 1). Little cell death was observed and no major differences between cell lines were discernable.

We set out to obtain mechanistic information on the mode of activation of our different reporters and anticipated a selective activation by our reference compounds. We first evaluated whether as a simplified method only the final time point of the live imaging dataset would be sufficient to determine reporter activation. The endpoints from the different quantitative features of each reporter (see Figure 3) were collected for each reference compound concentration range and subjected to an unsupervised hierarchical clustering and displayed as a heatmap (Figure 4).

The heatmap showed a clear clustering of the reporter cell lines and reference compound groups within the corresponding adaptive stress response pathway. This was reflected by a significant activation of the GFP-reporters. Intriguingly, at this 24 hr time point GFP-Nrf2 did not show enhanced nuclear localization and for any of the reference compounds, possibly related to an earlier activation. The DNA damage and UPR reporters were all activated by their corresponding reference compound sets. Interestingly, the UPR reference compound thapsigargin also strongly activated the oxidative stress reporters Keap1 and Srxn1, in accordance with observations in neuronal cells [234]; yet, brefeldin A and tunicamycin selectively induced the UPR response. Brefeldin A slightly activated the GFP-TP53BP1 reporter, while the GFP-p53, GFP-Btg2 and GFP-p21, were not activated. This underscores the possibility to identify compound specific responses.

#### **4.3. Live cell imaging of HepG2 reporters define temporal ranked adaptive stress response profile.**

We obtained detailed live cell imaging data over a 24 hr time course for the entire reference data set. Next we investigated whether live imaging adds value in quantifying adaptive stress response programs. For most reference compounds reporter activation occurred within the first hours after treatment, dependent on the reporter (Figure 5). Also the dynamics of the response differed per reference compound and reporter. Thus, the live cell data demonstrate a rapid accumulation of GFP-Nrf2 starting around 2 hours and returning to close to baseline levels after 15 hr for CDDO-Me, DEM as well as IAA (Figure 5). IAA exposure caused early activation of several adaptive stress response programs: the OSR reporters Keap1, Nrf2 and Srxn1 but also UPR reporter XBP1 and DDR reporter TP53BP1. Interestingly, while thapsigargin showed strong activation of all UPR reporters as well as the Keap1 and Srxn1 reporter, no clear stabilization of GFP-Nrf2 was observed. Next the

entire set of quantitative time course data of the reference compounds for all reporters was subjected to cubic hierarchical clustering, thus taking into consideration the time dynamics of each

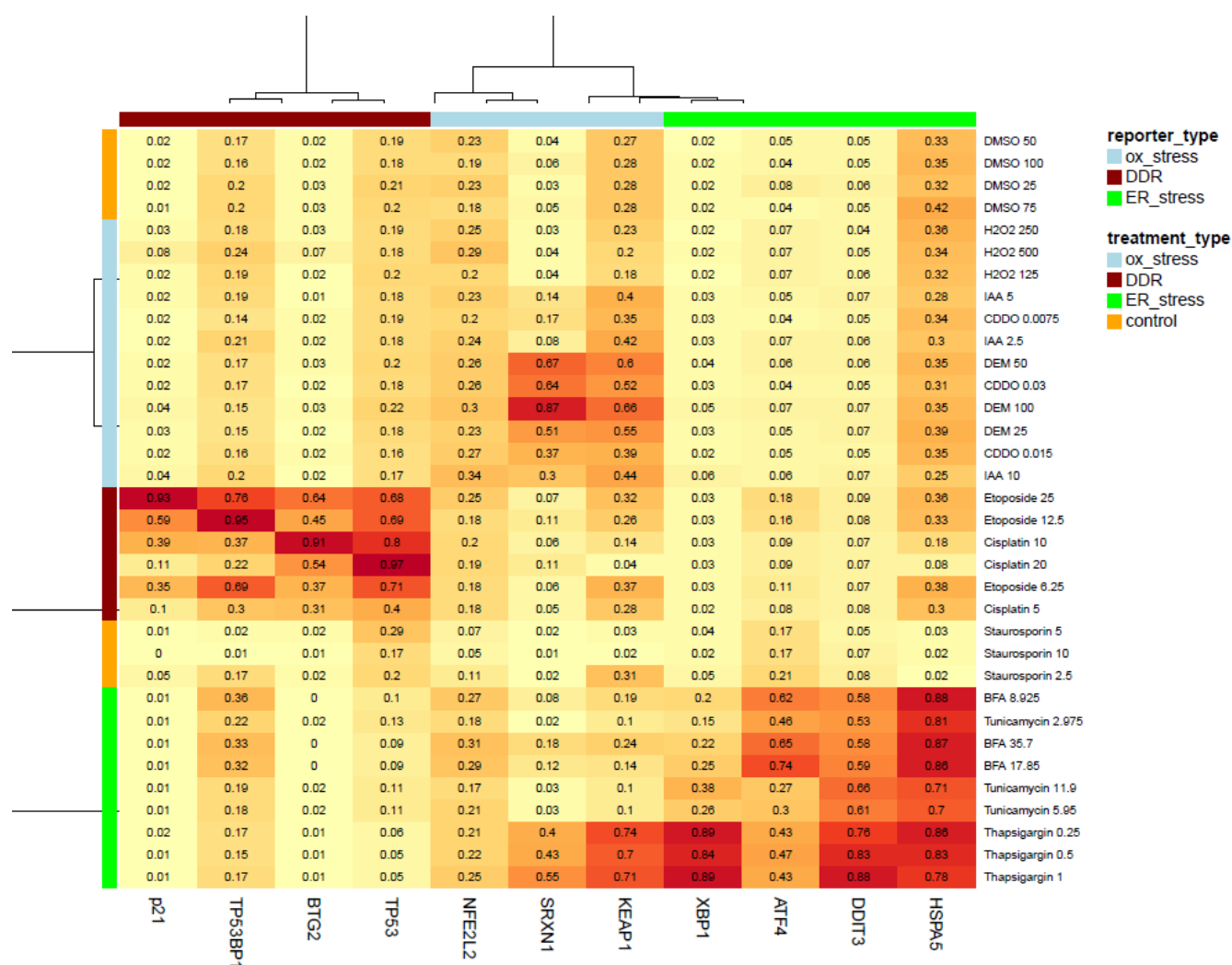


**Figure 4. Effect of reference compounds on adaptive stress GFP-reporter response.** Heatmap displays the individual GFP-reporter and compound measurements of the various reference compounds in all reporter cell lines. Shown are the 24 hr end-point measurements as the average of three independent experiments. Color intensity corresponds to plate-cell line-normalized feature values, these values are also displayed in the boxes. Data shown were subjected to unsupervised hierarchical clustering. Side bars correspond to stress pathway reporter type (top bar) and reference compound treatment class (side bar).

reporter-treatment combination. The reporter- and treatment stress-types again cluster fully together (Figure 6). However by inclusion of the time dynamics into the clustering algorithm compounds with similar time dynamics cluster together within the reference and model compound blocks and thus reveals distinct response-type sub-clusters. This is most evident as the different compounds induce responses with distinct time dynamics and, therefore, the concentration ranges for each compound (except IAA 10  $\mu$ M) cluster together, in contrast to the end-point clustering of figure 4. Altogether this supports the notion that the entire time course dynamics of compound responses on reporter cell lines provides added value for classification of compounds.



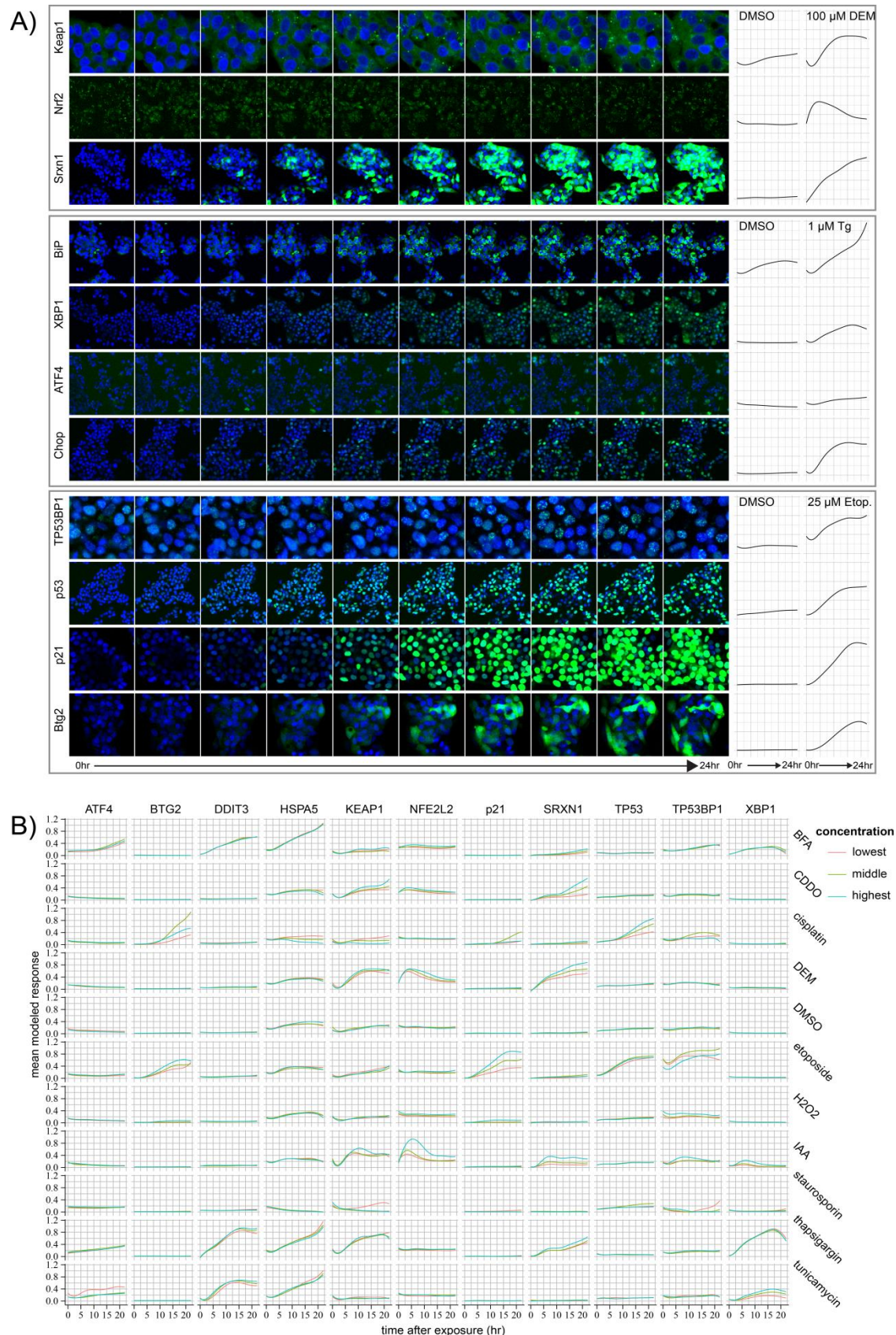


**Figure 5: Dynamic GFP-reporter activation for different adaptive stress response pathways.** A) Representative images of the dynamic activation of the various stress response pathway reporter cell lines by different reference model compounds: OSR, DEM; UPR, Tg; DDR, Etop). B) Time dynamics of all reference compounds on the different stress response reporters. Data shown are the normalized values for individual reporters. Different colors indicate low (red), medium (green) and high (blue) concentrations.

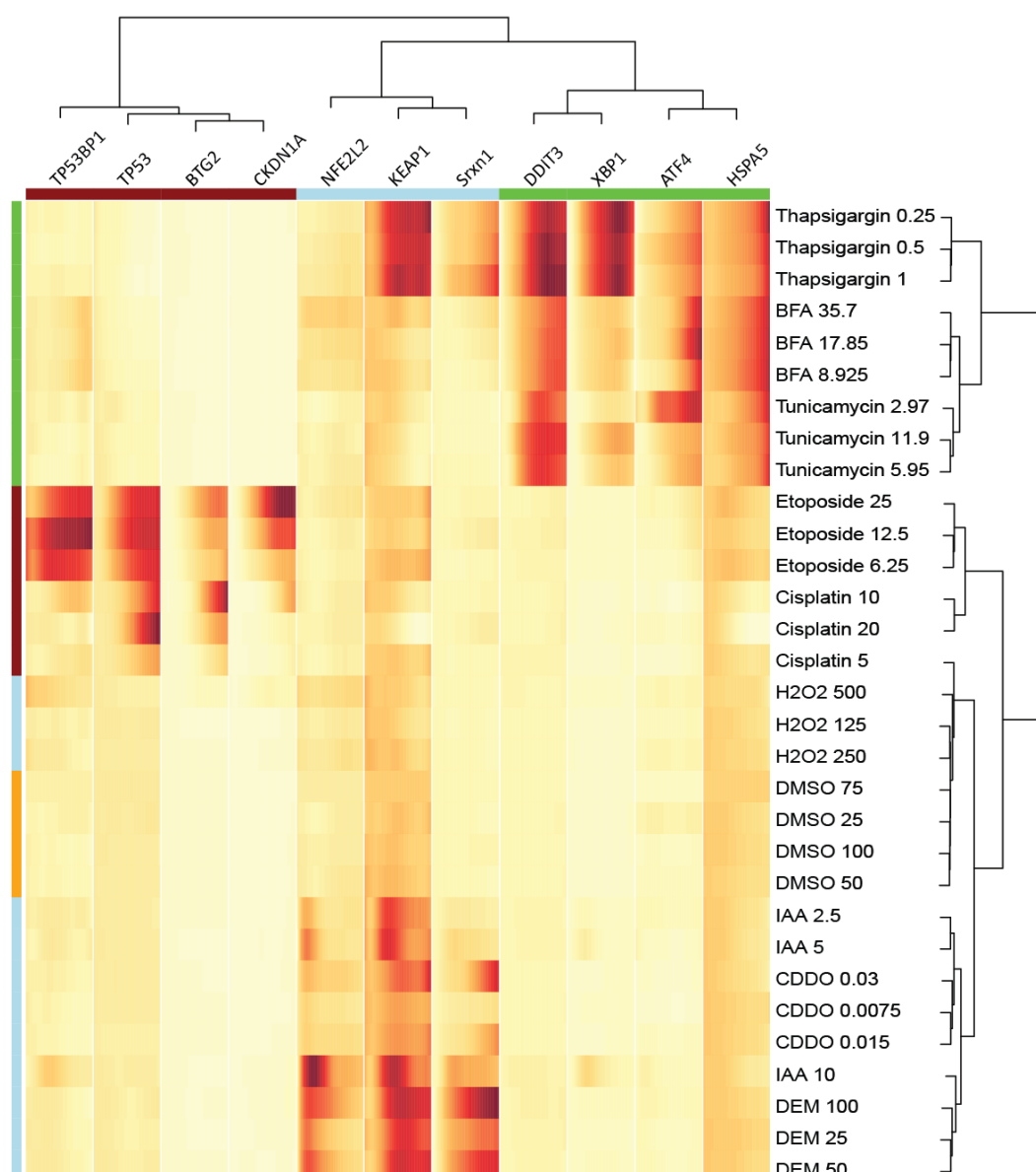


**Figure 6: Cubic hierarchical clustering of the time courses of the reporter panel and reference compounds.** Time dynamics of all reference compounds on the different stress response reporters was used for cubic hierarchical clustering as described in Material and Methods. Data shown are the normalized values for individual reporters of >3 independent experiments.

#### 4.4. DILI compounds mainly activate OSR and UPR reporter genes in primary human hepatocytes (PHH).

As a next step we set out to test the reporter platform in a more DILI-relevant setting. First we calculated the log<sub>2</sub> fold changes for all DILI compounds from the PHH data from the TG-GATES dataset for all our 11 reporter genes. We next subjected this data to hierarchical clustering (Figure 7A). The oxidative stress transcript levels were increased by a set of 39 compounds with NFE2L2, KEAP1 and SRXN1 correlation over all treatments being high (pearson correlation KEAP1-NFE2L2 0.64, KEAP1-SRXN1 0.58, NFE2L2-SRXN1 0.45). The transcript level responses of the UPR genes was diverse; 53 compounds activated the DDIT3/CHOP of which 33 (62%) negatively regulated HSPA5/BiP. ATF4 seemed to slightly correlate with oxidative stress (pearson correlation SRXN1-



ATF4 0.4). Hardly any changes in transcript levels of XBP1 were seen likely due to its mechanism of post-transcriptional regulation [235].

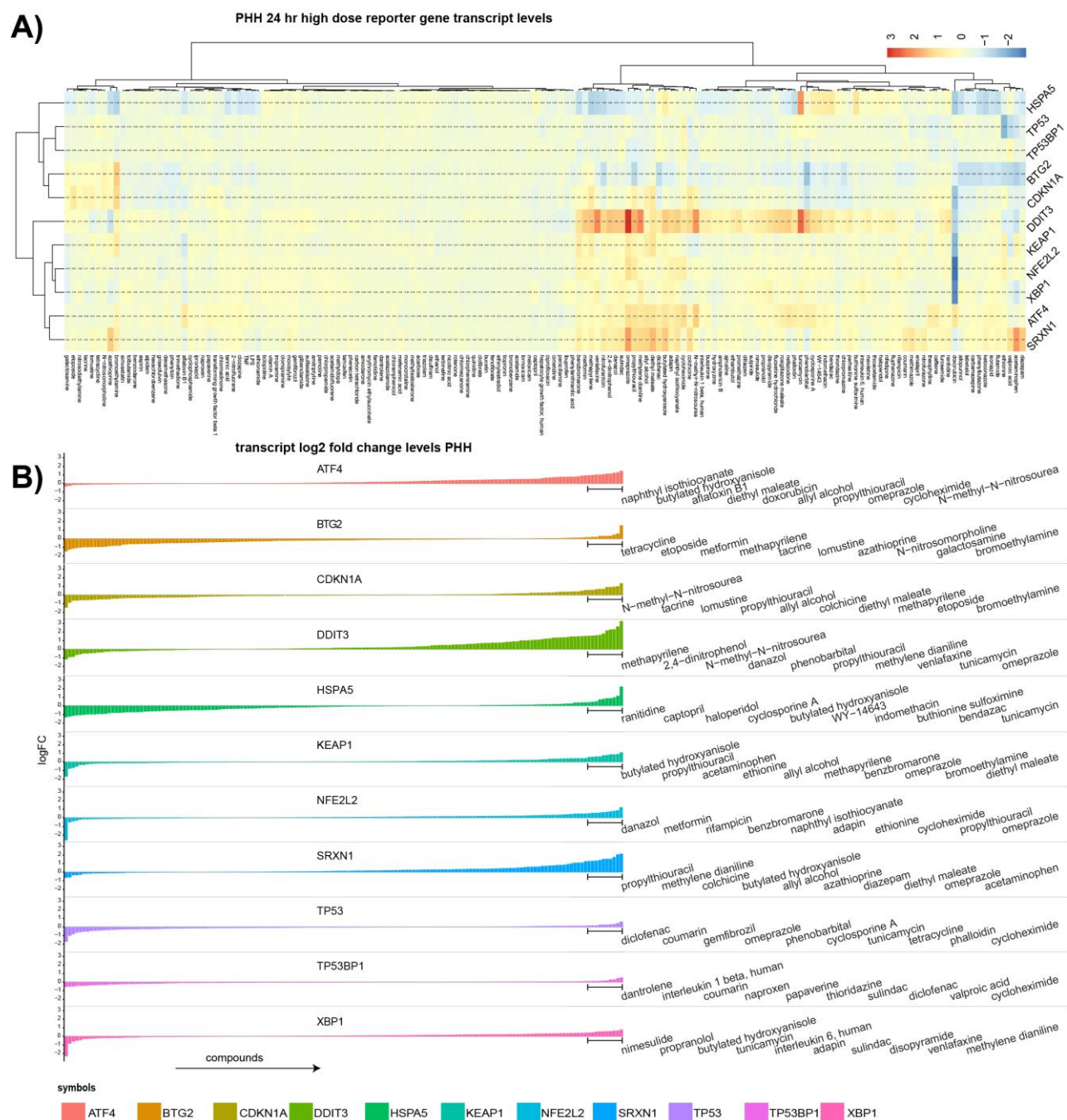


**Figure 7: Primary human hepatocyte data from TG-GATES.** A) Unsupervised hierarchical clustering of log2 fold change values of primary human hepatocyte transcripts in PHH. B) Rank ordered transcript fold changes for each reporter gene. Top 10 upregulated compounds per reporter gene were selected for HCI and are displayed on the right.

A very small number of DILI compounds affected TP53, TP53BP1, CDKN1A or BTG2 transcript levels in PHH; this reflects the thorough screening for DNA damage effects of pharmaceuticals. A small cluster of compounds activated the CDKN1A and BTG2 expression but not TP53 and TP53BP1.

To assess the correlation between adaptive stress pathway activation in PHH and that observed in our BAC-GFP reporters we decided to focus on four downstream targets that showed

the most prominent responses in PHH: OSR, Srxn1; UPR, CHOP/DDIT3 and BiP/HSPA5; DDR, p21. To select a set of DILI compounds that selectively affect individual reporters we rank ordered the PHH fold change transcript level data for each reporter gene and the top 10 were selected as DILI-compound test set (Figure 7B), in total resulting in 29 different DILI compounds that partly had overlap between downstream targets.

#### **4.5. HepG2 reporters define temporal ranked adaptive stress response profiles of DILI relevant compounds.**

Next we tested the 29 DILI compounds in the GFP-Srxn1, GFP-CHOP, GFP-BiP and GFP-p21 cell line. For comparative purposes the same concentrations were used as in the PHH TG-GATES high-dose data. All four reporter cell lines were imaged live for 24 hr (Supplemental Figure 2). The resultant reporter-response time courses were subjected to the same cubic hierarchical clustering which lead to several distinct clusters of response-types (Figure 8). Different response-types were defined based on the intensity of the response, the response type, and the order of the response types. Based on the Srxn1-intensity level clusters of no-induction (S-0), weak-induction (S-1), middle-induction (S-2) and strong induction (S-3) can be defined. The S-0 group of compounds includes a set of 4 treatments which are negative among all 4 reporters. The remaining S-0 treatments showed a weak p21 activation. The S-1 cluster of slightly increased Srxn1 levels are preceded by p21 activation and in the case of cyclosporin A GFP-BiP levels increased markedly in time preceding GFP-Srxn1 activation. Within the strong Srxn1 activation cluster (S-3) a subset of treatments oxidative stress co-occurred with p21 as well, most notably etoposide and colchicine. A distinct adaptive stress response profile was related to strong GFP-CHOP induction by tacrine, omeprazole and thioridazine treatments which cluster together with the positive controls thapsigargin and tunicamycin. However no increase of GFP-BiP chaperone is evident, in contrast to azathioprine and sulindac which have a low to no GFP-CHOP activation but a strong GFP-BiP activation.

Finally we assessed the positive co-occurrence of reporter gene activation between reporter transcript levels in PHH and GFP-reporter levels in the four reporter cell lines. The correlation was 10/10 for GFP-SRXN1, 8/10 for GFP-p21 and 5/10 for GFP-CHOP and 4/10 for GFP-BiP.

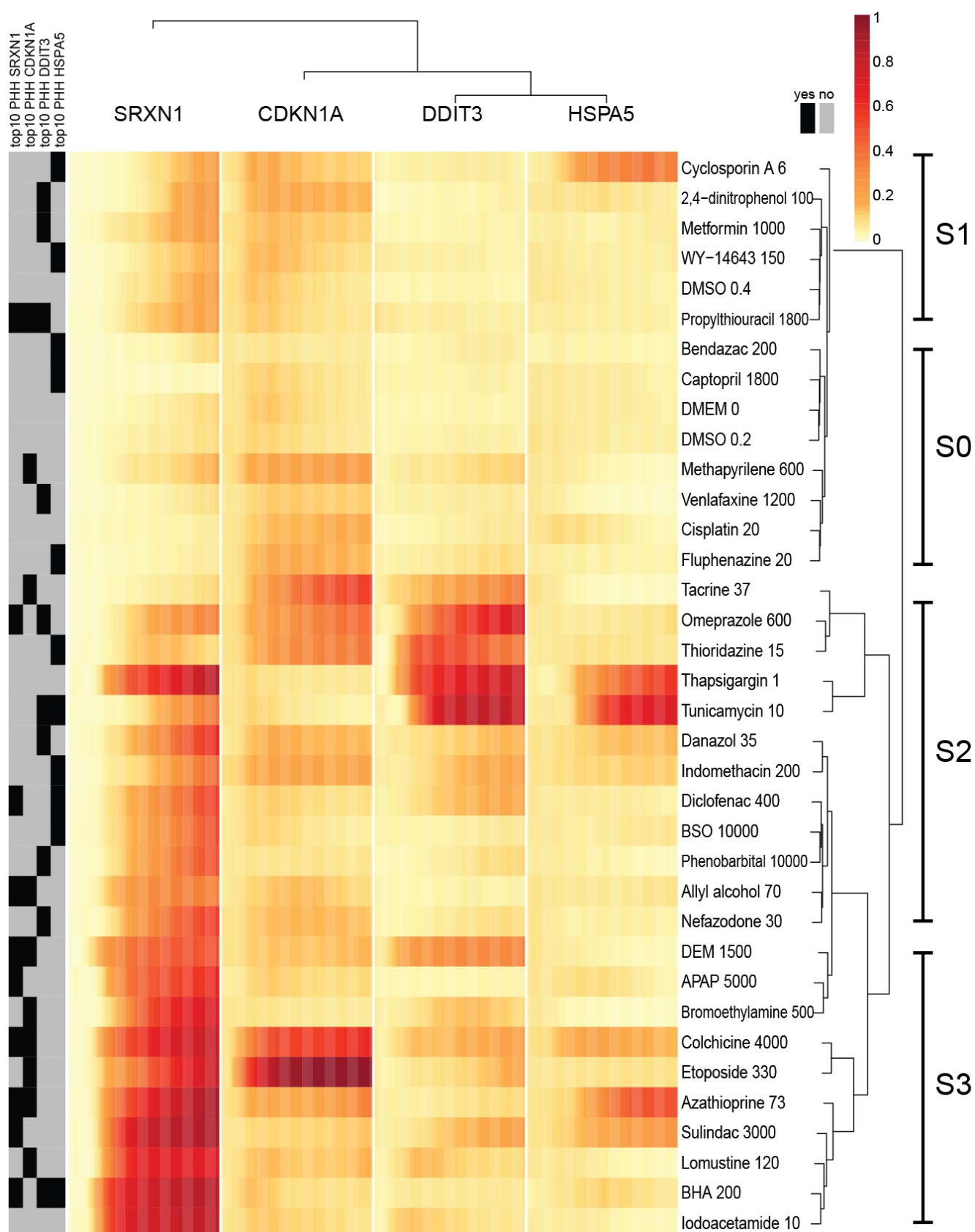


**Figure 8: Effect of selected DILI test compounds on stress response activation.** DILI compound selection origin is labeled black (left legend), 24 hour time course corresponds to the 4 individual columns, each column representing a time course for 1 of 4 reporter cell lines. Response magnitude is labeled as orange intensity and according to the legend (top right). Compounds and concentrations are displayed as rows and labeled on the right. The time course profiles were subjected to cubic clustering as described in the materials and methods section.



## 5. Discussion

In the current study we established a panel of fluorescent protein reporter HepG2 cell lines using BAC cloning technology to follow the dynamics of several adaptive stress response pathways essential in chemical-induced cytotoxicity. We focused on target genes that are central in the regulation of three key adaptive stress response programs; for each pathway we successfully established reporters for the sensory machinery, downstream transcription factor and one of the transcription factors downstream target. Our results show that the adaptive stress response reporters are selective and sensitive to their corresponding reference training compounds. Moreover, live cell imaging enabled us to define the temporal order of activation of the adaptive stress response programs initiated after chemical exposure. Furthermore, DILI-related compounds that are strong inducers of our selected adaptive stress response pathways in PHH were positively identified in the HepG2 reporter cell models with *Srxn1*, *CHOP* and *p21*.

Monitoring of adaptive stress response pathways as a predictive tool for chemical safety prediction has gained considerable attention in systems toxicology [45, 236]. So far the approaches have largely used transcriptomics-based strategies [45, 237]. Transcriptomics provides a comprehensive analysis to monitor cellular stress responses to chemicals at a single time point and average population level. The application of our GFP-based reporter cell lines as presented here, in conjunction with high content live cell imaging provides various advancements in chemical safety assessment that are not feasible with and/or complementary to transcriptomics. Firstly, here we can quantitatively assess the regulation of the entire adaptive stress response pathway irrespective of transcriptional regulation. Thus, we can monitor the modulation of upstream regulators such as *KEAP1* and *53BP1*, that are constitutively expressed and translocate to the autophagosomes and DNA damage foci, respectively, upon activation. Moreover, we can observe post-translational regulation of reporter expression of in particular transcription factors due to protein stabilization, e.g. *Nrf2*, or *p53*, or alternative processing of mRNA (e.g. *Xbp1*). Secondly, our GFP-based reporters allow a more mechanistic evaluation of the relationship between stress pathway activation and cytotoxicity since we can follow the onset of stress responses at the real protein expression level, the cell physiology relevant molecules in cells, in single cells with the subsequent assessment of cell viability (e.g. onset of necrosis or apoptosis). Thirdly, it is more cost- and technically feasible to monitor the response in a high time resolution to determine temporal orders of stress pathway activation. It is of critical importance to define the detailed oscillatory dynamics from e.g. *NF-κB* [238] that are generally controlled by genetically defined negative feedback loops. Fourthly, the GFP-reporters allow the possibility to assess the overall cell and cell organelle morphological perturbations as well as foci formation from e.g. autophagosomes or DDR repair foci [236].

In comparison to previous high content imaging studies, to our knowledge we developed the first high content imaging assay able to monitor the response of cells to chemical exposure on a signalling level. Previous high content imaging studies were based on either cytotoxic parameters such as cell death, ROS, mitochondrial potential and  $\text{Ca}^{2+}$  based dyes which measure toxic outcome measures and not the cellular responses that combat these adversities, or on morphological features which capture morphological changes of cells or organelles and correlate these indirectly to mechanisms or classify morphology based perturbations due to chemical exposure with the use of training data [239-241].

Our data indicate that our BAC-GFP-based reporter approach can clearly reveal subtle differences in the mode-of-action of compounds. Our UPR reference compounds thapsigargin and tunicamycin both induced the onset of two key UPR reporters, e.g. CHOP-GFP and BiP-GFP, to a similar extent and with a similar temporal profile (see Fig. 5). Yet, while thapsigargin also induced a strong induction of the *Srxn1* reporter, tunicamycin did not. Thapsigargin causes ER-stress due to its inhibition of the SARC/ER  $\text{Ca}^{2+}$  ATPase thereby lowering  $\text{Ca}^{2+}$  levels in the lumen of the ER. Tunicamycin blocks protein glycosylation in the ER. While both conditions initiate the UPR response, ER calcium perturbations also induce an oxidative stress response. Yet, the latter response is different from compounds that directly target protein thiols, including iodoacetamide and DEM; although thapsigargin caused KEAP1-GFP foci formation, this was not associated with a strong accumulation of Nrf2-GFP, which is observed with iodoacetamide and DEM. These results clearly illustrate the strength of the temporal single cell live cell analysis of adaptive stress responses for mode-of-action clarification. Likewise, such reporter systems may also contribute to the adverse outcome pathway (AOP) toolbox and as such quantify the activation of individual key events that reflect and are critical in toxicological relevant AOPs [63].

An important asset of our reporter systems is the temporal information on the activation of cellular defense programs after toxicological insult. This allows the definition of a detailed stress-response fingerprint for individual compounds. Since our methods also marks the onset of cell death, this would include the identification of a point-of-no-return or tipping point, reflecting both the concentration as well as time point after which a certain fraction of cells dies because the defensive programs cannot cope with the level of stress induced by the toxicant. Together, the activation of certain adaptive stress response programs, the order of activation of these programs, the concentration or time after which the tipping point is reached will be of great benefit for risk assessment early in the toxicity testing pipeline and for realization of more mechanistically defined AOPs.

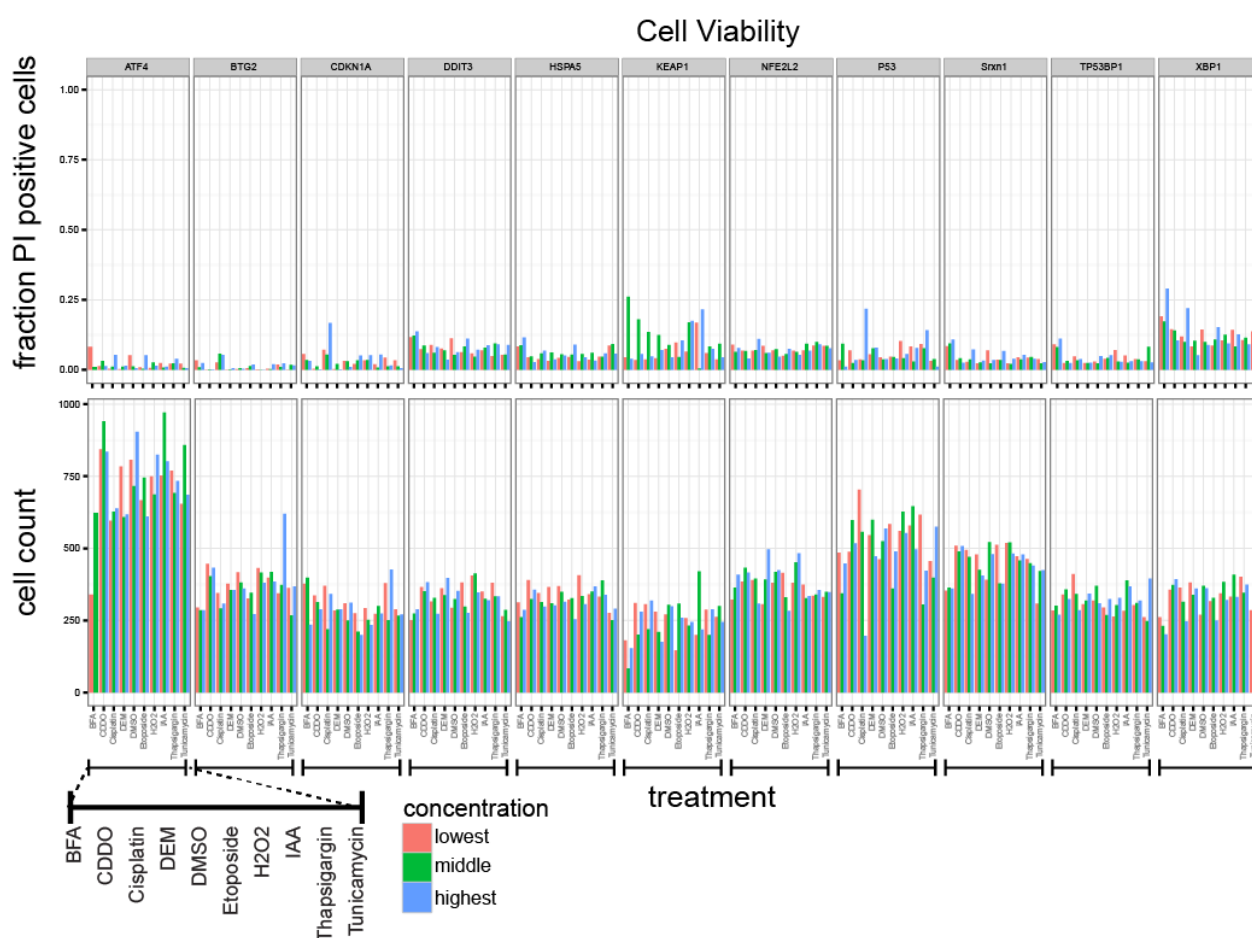
An important feature of our reporter cell systems is that we can detect DILI compound stress responses that are observed in primary human hepatocytes. For a proof-of-concept, we concentrated on four downstream target genes for oxidative stress (*Srxn1*), UPR (*HSPA5*/BiP, *DDIT3*/CHOP) and DDR (*p21*). We observed a strong concordance for in particular *Srxn1*-GFP and *p21*-GFP reporters, and a reduced concordance for the *HSPA5*-GFP and CHOP-GFP reporters. This suggest that our HepG2 reporter models translate very well to responses in PHH. This is in particular of interest since the PHH responses were based on transcriptomics and not protein expression. Our finding would be in agreement with recent observations that the onset of cytotoxicity caused by a broad set of DILI compounds is comparable between HepG2 and PHH (Park and Goldring, personal communication). Discrepancies between PHH and HepG2 reporters could be due to this difference, since it is established that the correlation between transcriptomics and proteomics in the same model does not correlate well. Alternatively, ADME and/or cell physiological differences between HepG2 reporters and PHH could explain the differences. The *Srxn1*-GFP reporter showed the highest concordance with PHH, also suggesting a conservation of the KEAP1/Nrf2/*Srxn1* pathway activation in HepG2 cells compared to PHH.

We have established our reporters in HepG2 cells. The adaptive stress response pathways that we have incorporated in these cells are not specific to liver cells, and involved in the regulation of toxicity in most if not all cells in the body, albeit most likely with different set points.

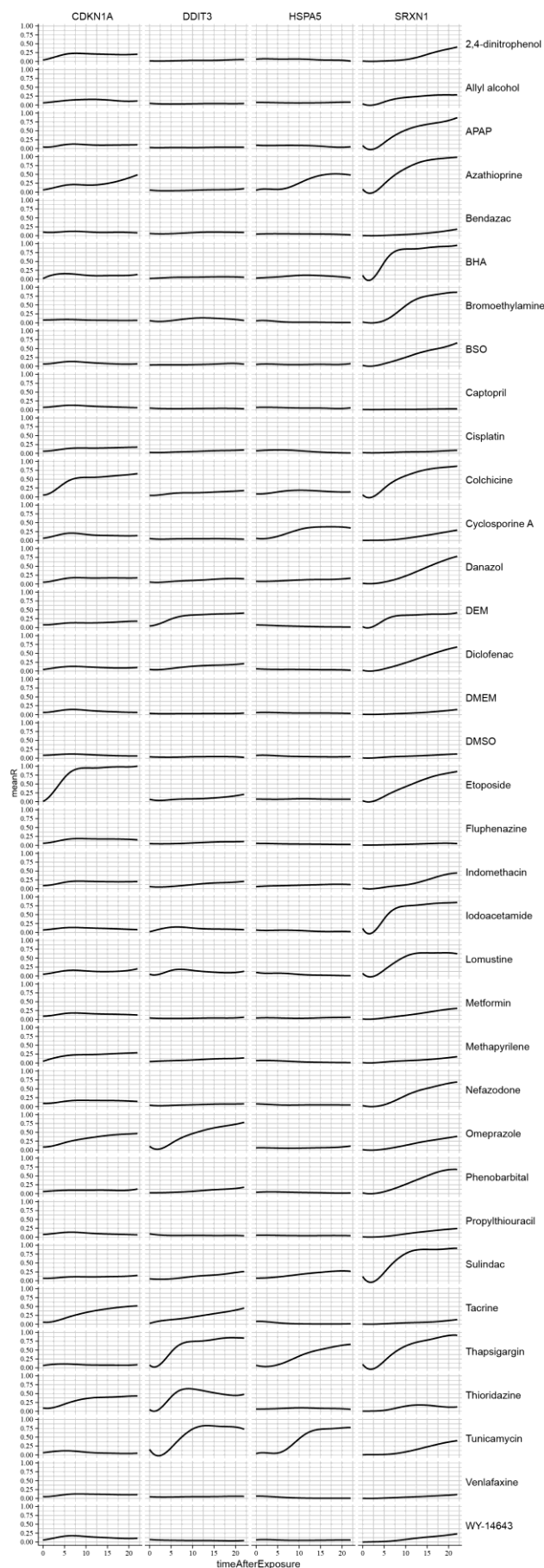
As such our HepG2 reporters could be representative for general toxicity. Induced pluripotent stem cell technology in combination with genetic recombineering strategies will allow the integration of the GFP-reporters in iPSC followed by the differentiation in any cell type. This would open the way for the assessment of the adaptive stress pathway activation in any differentiated cell type as well as the precise quantitative understanding of the differences in control and activation between the various cell types in a same genetic background.

In conclusion, we established a robust high throughput imaging-based platform for the single cell assessment of adaptive stress response pathway activation in a temporal fashion. This platform can contribute to a mechanism-based chemical safety assessment in both an industry and regulatory setting.

### Supplemental figures



**Supplemental Figure 1: Cytotoxicity measurements after exposure to reference compounds.** The percentage of dead cells was determined by analysis of the overall Hoechst 33452 positive nuclei in an image that was positive for propidium iodide (PI). The fraction of PI-positive cells for all compounds dose combinations for each individual reporter cell line is shown. (Bars indicate concentrations: lowest = red; middle = green; highest = blue). The number of cells after the overnight imaging session was determined by cell counting Hoechst 33452 positive cells, as the average per image for that compound dose combinations.



**Supplemental Figure 2: Time course responses of OSR reporter SRXN1, UPR reporters DDIT3 & HSPA5 and DDR reporter CDKN1A of top 10 selected TG-GATES PHH compounds.** Compounds (rows) and reporters (columns) are ordered alphabetically. Reported responses are average of three replicates.



# Chapter 4

## Drug-induced Endoplasmic Reticulum and Oxidative Stress Responses Independently Sensitize Towards TNF $\alpha$ -mediated Hepatotoxicity

---

**This chapter has been published as:**

Lisa Fredriksson\*§, Steven Wink\*§, Bram Herpers\*§, Giulia Benedetti\*, Mackenzie Hadi†, Hans de Bont\*, Geny Groothuist†, Mirjam Luijten‡, Erik Danen\*, Marjo de Graauw\*, John Meerman\*, and Bob van de Water\*

§ Both authors contributed equally

\*Division of Toxicology, Leiden Academic Centre for Drug Research, Leiden University, 2333 CC, Leiden the Netherlands

†Division of Pharmacokinetics, Toxicology and Targeting, Department of Pharmacy, University of Groningen, 9713 AV, Groningen, the Netherlands

‡The National Institute for Public Health and the Environment (RIVM), 3720 BA, Bilthoven, the Netherlands

*Drug-induced Endoplasmic Reticulum and Oxidative Stress Responses Independently Sensitize Towards TNF $\alpha$ -mediated Hepatotoxicity*

Toxicol Sci. 2014 Jul;140(1):144-59. doi: 10.1093/toxsci/kfu072

### 1. Abstract

Drug-induced liver injury (DILI) is an important clinical problem. Here we used a genomics approach to in detail investigate the hypothesis that critical drug-induced toxicity pathways act in synergy with the pro-inflammatory cytokine tumor necrosis factor  $\alpha$  (TNF $\alpha$ ) to cause cell death of liver HepG2 cells. Transcriptomics of the cell injury stress response pathways initiated by two hepatotoxicants, diclofenac and carbamazepine, revealed the endoplasmic reticulum (ER) stress/translational initiation signalling and nuclear factor-erythroid 2 (NF-E2)-related factor 2 (Nrf2) antioxidant signalling as two major affected pathways, which was similar to that observed for the majority of ~80 DILI compounds in primary human hepatocytes. Compounds displaying weak or no TNF $\alpha$  synergism, namely ketoconazole, nefazodone and methotrexate, failed to synchronously induce both pathways. The ER stress induced was primarily related to protein kinase R-like ER kinase (PERK) and activating transcription factor 4 (ATF4) activation and subsequent expression of C/EBP homologous protein (CHOP), which was all independent of TNF $\alpha$  signalling. Identical ATF4 dependent transcriptional programs were observed in primary human hepatocytes as well as primary precision cut human liver slices. Targeted RNA interference studies revealed that while ER stress signalling through inositol-requiring enzyme 1 $\alpha$  (IRE1 $\alpha$ ) and activating transcription factor 6 (ATF6) acted cytoprotective, activation of the ER stress protein kinase PERK and subsequent expression of CHOP was pivotal for the onset of drug/TNF $\alpha$ -induced apoptosis. While inhibition of the Nrf2-dependent adaptive oxidative stress response enhanced the drug/TNF $\alpha$  cytotoxicity, Nrf2 signalling did not affect CHOP expression. Both hepatotoxic drugs enhanced expression of the translational initiation factor EIF4A1, which was essential for CHOP expression and drug/TNF $\alpha$ -mediated cell killing. Our data support a model in which enhanced drug-induced translation initiates PERK-mediated CHOP signalling in an EIF4A1 dependent manner, thereby sensitizing towards caspase-8-dependent TNF $\alpha$ -induced apoptosis.

*Keywords:* drug-induced liver injury; transcriptomics; RNA interference, high content microscopy

## 2. Introduction

Drug-induced liver injuries (DILIs) constitute an important problem both in the clinic as well as during drug development. The underlying cellular mechanisms that determine the susceptibility towards developing DILI are incompletely understood. Recent data indicate that the crosstalk between drug reactive metabolite-mediated intracellular stress responses and cytokine-mediated pro-apoptotic signalling are important components in the pathophysiology of DILI [38, 242]. Tumor necrosis factor- $\alpha$  (TNF $\alpha$ ) severely enhances liver damage caused by various xenobiotics [38, 243-245] and it is the major cytokine to be excreted by the liver stationary macrophages (Kupffer cells) upon exposure to bacterial endotoxins such as LPS or as a response to hepatocyte damage [39]. In addition, reactive drug metabolites covalently modify cellular macromolecules leading to intracellular biochemical perturbations and the induction of various intracellular stress signalling or toxicity pathways, which have been termed the overall human toxome. These toxicity pathways set in motion, and a decreased adaptive response for cell damage recovery and protection, will predispose cells to cell death. Furthermore, it is likely that the onset of diverse sets of stress signalling pathways is causal for the sensitization of the crosstalk with the cytokine signalling. Cosgrove *et al.* previously identified that the Akt, p70 S6 kinase, MEK-ERK, and p38-HSP27 signalling pathways play a role in drug-cytokine synergistic cytotoxicity [246]. Yet, systematic transcriptomics of hepatocytes of both human and rodent origin both *in vitro* and *in vivo* have revealed a diversity of toxicity pathways that are activated by hepatotoxic drugs [242, 247]. The exact functional contribution of these pathways to DILI has only limitedly been studied and so far it remains unclear which drug-induced toxicity pathways modulate the pro-apoptotic activity of TNF $\alpha$  signalling in drug-induced liver cell injury. Here, based on our own transcriptomics, we have focused on the Kelch-like ECH-associated protein 1 (Keap1)/ nuclear factor-erythroid 2 (NF-E2)-related factor 2 (Nrf2) antioxidant response pathway and the endoplasmic reticulum (ER) stress-mediated unfolded protein response (UPR).

The Keap1/Nrf2 pathway is important in the recognition of reactive metabolites and/or cellular oxidative stress [248]. Under normal conditions Nrf2 is maintained in the cytoplasm and guided towards proteasomal degradation by Keap1 [249]. Nucleophilic reactions with the redox-sensitive cysteine residues of Keap1 releases Nrf2 followed by its nuclear entry and transcriptional activation of antioxidant genes [248]. Nrf2 signalling is critical in the cytoprotective response against reactive metabolites both *in vitro* and *in vivo* [115, 250], but its role in regulating TNF $\alpha$  pro-apoptotic signalling in relation to DILI is unclear.

The ER stress-mediated UPR is an adaptive stress response to ER protein overload due to enhanced translation and/or perturbed protein folding [118]. It involves expression of molecular chaperones such as the heat shock family member HSPA5 (also known as BiP or Grp78) [118]. When adaptation fails, a pro-apoptotic program to eliminate the injured cell is initiated [251]. The ER stress response contains three signalling arms: the protein kinase R-like ER kinase (PERK), the activating transcription factor 6 (ATF6) and the inositol-requiring enzyme 1 $\alpha$  (IRE1 $\alpha$ ) [118]. Activation of IRE1 $\alpha$  and ATF6 initiates protective responses, while activation of PERK leads to attenuation of global protein synthesis and favored translation of activating transcription factor 4 (ATF4) by phosphorylation of eukaryotic initiation factor 2  $\alpha$  (eIF2 $\alpha$ ), resulting in expression of the ATF4 downstream target gene DDIT3 encoding the C/EBP homologous protein (CHOP) [121]. CHOP initiates a pro-apoptotic program by modulation of Bcl2-family proteins [118, 251]. Although ER



stress has previously been implicated in DILI [252], the role and mechanism of individual ER stress signalling components in controlling DILI in relation to TNF $\alpha$ -induced apoptosis remains undefined.

Here we demonstrate that two different hepatotoxic drugs, diclofenac and carbamazepine, show a synergistic apoptotic response with the pro-inflammatory cytokine TNF $\alpha$ . Genome-wide transcriptomics revealed an activation of the Nrf2-related oxidative stress response and translation initiation signalling pathway in conjunction with ER stress responses as the most important cell toxicity pathways, which were activated independent of, and preceding TNF $\alpha$ -mediated cell killing. A systematic short interfering RNA (siRNA) mediated knockdown approach of genes related to these stress-induced pathways allowed a detailed functional evaluation of the mechanism by which oxidative stress, ER stress and translational regulation are interrelated in the sensitization towards pro-apoptotic TNF $\alpha$  signalling during DILI.

### **3. Materials and methods**

#### **3.1. Reagents and antibodies**

Diclofenac sodium (DCF), carbamazepine (CBZ), nefazodone (NFZ) and ketoconazole (KTZ) were obtained from Sigma (Zwijndrecht, the Netherlands). Methotrexate (MTX) was from Acros Organics (Geel, Belgium). Human recombinant tumor necrosis factor  $\alpha$  (TNF $\alpha$ ) was acquired from R&D Systems (Abingdon, United Kingdom). AnnexinV-Alexa633 was made as previously described (Puigvert *et al.*, 2010). The antibody against caspase-8, cleaved poly ADP-ribose polymerase (PARP), C/EBP homologous protein (CHOP), and translation initiation factor EIF4A1 were from Cell Signalling (Bioké, Leiden, Netherlands). The antibody against tubulin was from Sigma and the antibody against phosphorylated protein kinase R-like ER kinase (PERK; Thr 981) was from Santa Cruz (Tebu-Bio, Heerhugowaard, the Netherlands). The antibody against nuclear factor-erythroid 2 (NF-E2)-related factor 2 (Nrf2) was a kind gift from Dr. Goldring (Liverpool University, United Kingdom).

#### **3.2. Liver cells and slices**

Human hepatoma HepG2 cells were obtained from American Type Culture Collection (ATCC, Wesel, Germany), cultured in Dulbeccos's modified Eagle medium (DMEM) supplemented with 10% (v/v) fetal bovine serum (FBS), 25 U/ml penicillin and 25  $\mu$ g/ml streptomycin and used for experiments between passage 5 and 20. Primary mouse hepatocytes were isolated from 8-10 weeks old male C57BL/6J mice by a modified two-step collagenase perfusion technique (collagenase type IV, Sigma-Aldrich, Zwijndrecht, The Netherlands) and treated as described previously [253]. The source of human liver tissue and the preparation and incubation of human precision-cut liver slices were described previously [17]. In brief, liver slices (diameter 4 mm, thickness 250  $\mu$ m) were pre-incubated at 37°C for 1 hour individually in a well containing 1.3 ml Williams' medium E with glutamax-1 (Gibco, Paisley, UK), supplemented with 25 mM D-glucose and 50  $\mu$ g/ml gentamicin (Gibco, Paisley, UK) (WEGG medium) in a 12-well plate with shaking (90 times/minute) under saturated carbogen atmosphere.

#### **3.3. Gene expression profiling**

For HepG2 cells drug (500  $\mu$ M DCF, 500  $\mu$ M CBZ, 75  $\mu$ M KTZ, 30  $\mu$ M NFZ and 50  $\mu$ M MTX) or vehicle (DMSO) exposure was performed for 8 hours followed by the addition of 10 ng/ml TNF $\alpha$  or solvent and incubation for another 6 hours. For primary mouse hepatocytes, 46 hours after isolation, cells were exposed to either 300  $\mu$ M DCF or the solvent DMSO for 24 hours. For human liver slices, the slices were treated with 400  $\mu$ M DCF or the solvent DMSO and incubated for 24 hours. RNA was isolated using the RNeasy<sup>®</sup> Plus Mini Kit (Qiagen, Venlo, the Netherlands) and RNA integrity and quality was assessed using the Agilent bioanalyser (Agilent Technologies, Palo Alto, CA, USA). The Affymetrix Human Genome U133 plus PM arrays and Affymetrix Mouse Genome 430 2.0 GeneChip arrays were used for microarray analysis of human and mouse liver cell samples, respectively, and all performed at ServiceXS B.V. (Leiden, The Netherlands). BRB Array Tools software was used to normalize the CEL data using the Robust Multichip Average (RMA) method. Significantly differentially expressed genes (p-value < 0.001) between the various experimental conditions were identified with an ANOVA test followed by calculation according to Benjamini and Hochberg [254]. Classification of the selected genes according to their biological and toxicological functions was performed using the Ingenuity Pathway Analysis (IPA<sup>®</sup>) software (Ingenuity<sup>®</sup> Systems, Redwood, CA, USA). Heatmap representations and hierarchical clustering (using Pearson correlation) were performed using the MultiExperiment Viewer software [255]. The data discussed in this publication have been deposited in NCBI's Gene Expression Omnibus [256] and are accessible through GEO Series accession number GSE54257 (<http://www.ncbi.nlm.nih.gov/projects/geo/query/acc.cgi?acc=GSE54257>).

### **3.4. Gene expression analysis from primary human hepatocytes using the TG-GATEs data set.**

CEL files were downloaded from the Open TG-GATEs database: "Toxicogenomics Project and Toxicogenomics Informatics Project under CC Attribution-Share Alike 2.1 Japan" <http://dbarchive.biosciencedbc.jp/en/open-tggates/desc.html>. Probe annotation and probe mapping was performed using the hgu133plus2.db and .cdf packages version 2.9.0 available from the Bioconductor project (<http://www.bioconductor.org>) for the R statistical language (<http://cran.r-project.org>). Probe-wise background correction and between-array normalization was performed using the vsn2 algorithm (VSN package version 3.28.0) [257]. Probe set summaries were calculated with the median polish algorithm of RMA (robust multi-array average) (LIMMA package, version 1.22.0) [228]. The normalized data were statistically analyzed for differential gene expression using a linear model with coefficients for each experimental group (fixed) [258, 259]. A contrast analysis was applied to compare each exposure with the corresponding vehicle control. For hypothesis testing the moderated t-statistics by empirical Bayes moderation was used followed by an implementation of the multiple testing correction of Benjamini and Hochberg using the LIMMA package [260].

### **3.5. RNA interference**

Transient knockdowns (72 hours) of individual target genes were achieved in HepG2 cells before CBZ/TNF $\alpha$  (500  $\mu$ M/10 ng/ml) and DCF (500  $\mu$ M/10 ng/ml) exposure, using siGENOME SMARTpool siRNA reagents and siGENOME single siRNA sequences (50 nM; Dharmacon Thermo Fisher Scientific, Landsmeer, the Netherlands) with INTERFERin<sup>™</sup> siRNA transfection reagent (Polyplus

transfection, Leusden, the Netherlands). The negative controls were siGFP or mock transfection. The single siRNA sequences were used to exclude any off target effects of the SMARTpools resulting in a significant biological effect. The experiments were performed in fourfold and SMARTpool was considered on target when 2 or more of the 4 singles showed a similar significant effect. All siRNA-targeted genes can be found in Supplementary Table S1.

### **3.6. Cell death assays in HepG2 cells**

Induction of apoptosis in real time was quantified using a live cell apoptosis assay essentially the same as previously described [261].

### **3.7. Western blot analysis**

Western blot analysis was essentially performed as previously described [262] using above-mentioned antibodies. Images were processed in Adobe Photoshop CS5 (Adobe, Amsterdam, the Netherlands).

### **3.8. Live cell imaging of GFP-tagged proteins in HepG2 cells**

Reporter HepG2 cells for Nrf2 activity (Srxn1 [mouse]) and endoplasmic reticulum (ER)-stress (ATF4 and CHOP/DDIT3 [human]) were generated by bacterial artificial chromosome (BAC) recombineering [13, 48]. Upon validation of correct C-terminal integration of the GFP-cassette by PCR, the BAC-GFP constructs were transfected using Lipofectamine<sup>TM</sup> 2000 (Invitrogen, Breda, the Netherlands). Stable HepG2 BAC-GFP reporters were obtained by 500 µg/ml G418 selection. Prior to imaging, nuclei were stained with 100 ng/ml Hoechst<sub>33342</sub> in complete DMEM. The induction of Srxn1-GFP, ATF4-GFP and CHOP-GFP expression was followed for a period of 24 hours, by automated confocal imaging (Nikon TiE2000, Nikon, Amstelveen, the Netherlands). Quantification of the GFP intensity in individual cells was performed using Image Pro<sup>TM</sup>.

### **3.9. Statistical analysis**

All numerical results are expressed as the mean  $\pm$  standard error of the mean (S.E.M.) and represent data from three independent experiments. Calculations were made using GraphPad Prism 5.00 (GraphPad software, La Jolla, USA). Significance levels were calculated using 2-way ANOVA, \* =  $P < .05$ , \*\* =  $P < .01$ , \*\*\* =  $P < .001$ .

## 4. Results

### 4.1. Hepatotoxic drug synergy with TNF $\alpha$ is preceded by oxidative stress, ER stress and death receptor signalling gene expression networks.

First we treated HepG2 cells for 8 hours with different compounds associated with unpredictable idiosyncratic drug-induced liver injury (DILI) in humans, carbamazepine (CBZ), diclofenac (DCF), ketoconazole (KTZ), nefazodone (NFZ) and methotrexate (MTX), at concentrations around  $100 \times C_{\max}$  for each drug [91, 263], followed by an additional incubation with or without tumor necrosis factor  $\alpha$  (TNF $\alpha$ ; 10 ng/ml) for 16 hours. CBZ, DCF and KTZ showed a significant enhanced apoptosis when combined with TNF $\alpha$  (Fig. 1A). A slight trend towards synergy was observed for NFZ, while hardly any toxicity was observed for MTX with or without TNF $\alpha$  (Fig. 1A).

To find the mechanism behind TNF $\alpha$  synergy we next we performed a gene expression analysis on HepG2 cells exposed to DCF (500  $\mu$ M), CBZ (500  $\mu$ M), KTZ (75  $\mu$ M), NFZ (30  $\mu$ M) and MTX (50  $\mu$ M) for 8 hours to investigate which intracellular signalling pathways were perturbed by the drugs prior to TNF $\alpha$  addition (Fig. 1B). The concentrations were chosen based on minimal drug-induced toxicity with, if any, maximal TNF $\alpha$  apoptotic synergism (Fig. 1A, in bold). While MTX only mildly affected the gene expression (503 differentially expressed genes [DEGs] at 8 hours), which was related to the very limited cytotoxicity (Fig. 1A), KTZ caused the strongest gene expression changes (4,678 DEGs at 8 hours; Fig. 2A) in association with greater onset of cell death (Fig. 1A). Not many additional changes in DEGs were observed after treatment for an additional 6 hours, a time-point where synergism with TNF $\alpha$  is apparent (data not shown), with the compounds either in presence or absence of TNF $\alpha$  (Fig. 1C and D). To identify likely candidate genes that contribute to this synergy we determined the overlap in DEGs for all synergizing drugs (DCF, CBZ and KTZ; see Venn-diagrams in Fig. 1B-D). Since the most significant TNF $\alpha$  synergy was observed for CBZ (Fig. 1A) we considered this a relevant model compound for further comparisons. DCF showed the highest overlap with CBZ in DEGs when taking into account that the direction of regulation (up or down) should be the same between the two compounds (Fig. 1B-D), and therefore these two drugs were chosen for further detailed analysis.

Next we employed Ingenuity Pathway Analysis (IPA<sup>®</sup>) software to identify the toxicity-related signalling pathways that were affected by both CBZ and DCF as early as 8 hours after treatment (Fig. 2A). Three prominent toxicity pathways were found: “*EIF2-signalling/Endoplasmic reticulum stress pathway*”, “*NRF2-mediated oxidative stress response*”, and “*Apoptosis/Death receptor signalling*”. We have previously reported the involvement of death receptor signalling under DCF/TNF $\alpha$  conditions [38] and we have observed the same effect for CBZ/TNF $\alpha$  (data partially reported in Supplementary Table S1).

Subsequently we obtained all the individual genes from IPA<sup>®</sup> that determine the significant pathways described in Figure 2A. Unsupervised hierarchical clustering of all these selected genes allowed identification of three main gene clusters that were up-regulated after 8 hours CBZ and/or DCF but not MTX treatment (Supplementary Fig. S2). Interestingly, these contained almost exclusively genes representing the three prominent toxicity pathways (compare Figs 2A and Supplementary Fig. S1). For further gene selection we used a threshold of 1.5-fold change for any CBZ or DCF treatment time point (Fig. 2B).

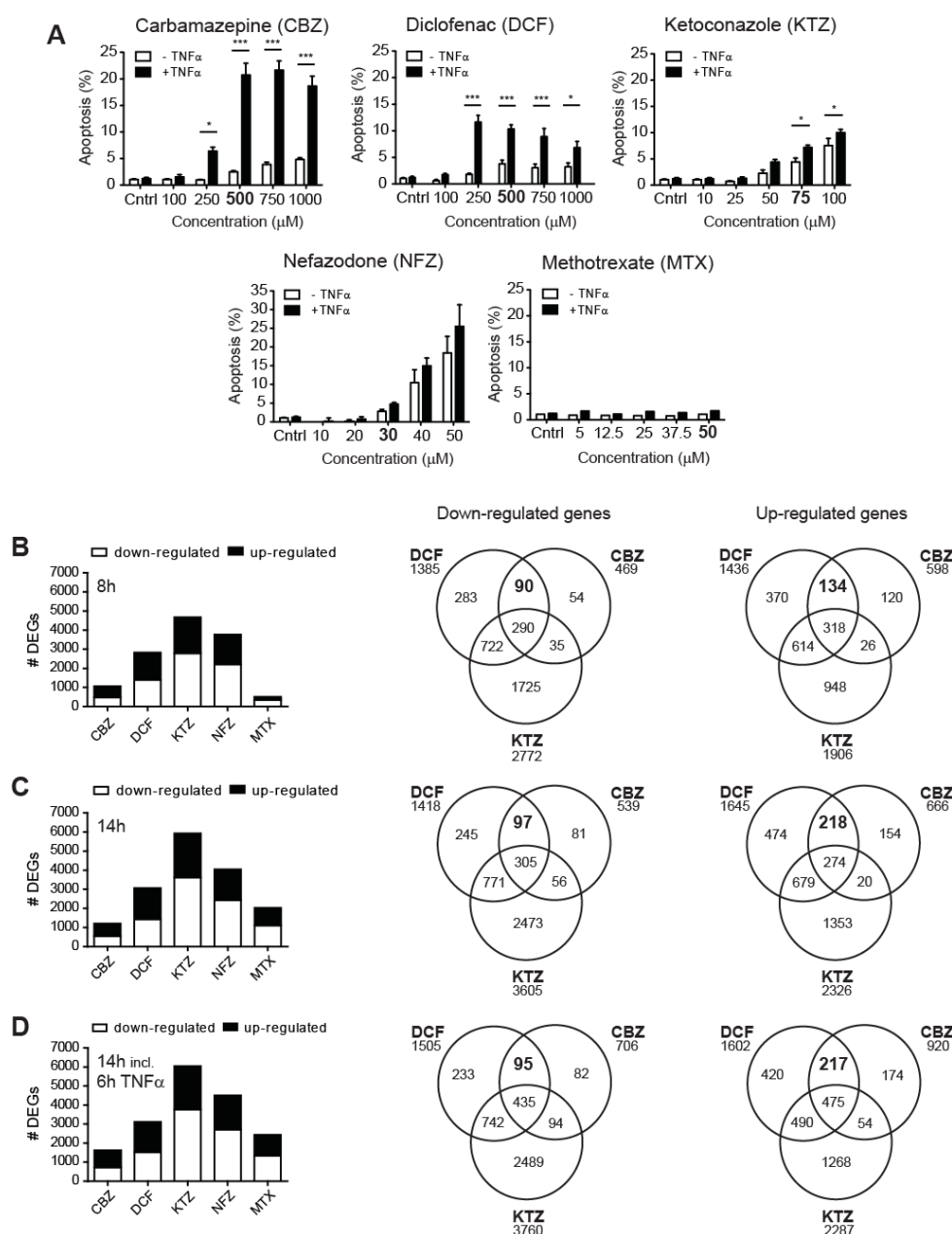


**Figure 1. Apoptosis and gene expression profiling of hepatotoxic drugs and TNF $\alpha$  in HepG2 cells.** (A) The apoptosis after drug exposure was followed in real time from 8 to 24 hours using automated imaging and AnnexinV (AnxV)-Alexa633 binding to apoptotic cells. The end-points (24h) are presented as relative AnxV-Alexa633 intensities and the concentrations used for gene expression analysis are marked in bold. The data shown are means of three independent experiments  $\pm$  SEM. \*\*\* $P < 0.001$ , \* $P < 0.05$ . The gene expression after 8 (B), 14 (C) and 14 hours including 6 hours of TNF $\alpha$  (10 ng/ml; D) exposure to diclofenac (DCF), carbamazepine (CBZ), ketoconazole (KTZ), nefazodone (NFZ) and methotrexate (MTX) is presented as number of genes differentially up- (black) or down-regulated (white) compared to control. The total number of genes overlapping among the TNF $\alpha$ -synergizing drugs is shown in the corresponding Venn-diagrams with the overlap between DCF and CBZ in bold.

We wanted to ensure that the genes that were significantly regulated in HepG2 cells as presented in Fig. 2B after CBZ and DCF exposure were also significantly regulated in primary human hepatocytes after exposure to ~80 drugs, including a large diversity of hepatotoxicants [264]. In Figure 3, the expression of these genes after drug exposure in the primary human

hepatocytes is presented. We also included classical downstream target genes known to be essential in the ER-stress and oxidative stress: XBP1, CHOP/DDIT3, BiP/HSPA5 and SRXN1. The target genes reflecting EIF2-signalling/endoplasmic reticulum (ER) stress/unfolded protein response (UPR) pathway and Nrf2-mediated oxidative stress pathway were mostly affected by the DILI compounds, unlike the death signalling genes, with Bim being the exception. Importantly, carbamazepine, diclofenac as well as ketoconazole strongly affected the set of these 34 genes in primary human hepatocytes (see Figure 3 and Supplementary Fig. S1). Moreover, unsupervised clustering of altered expression levels of these 34 genes for all DILI compounds revealed a single cluster with our synergizing compounds with an important addition of sulindac which has previously been reported to synergize with TNF $\alpha$  in another *in vitro* model of idiosyncratic liver injury [265]. Thus, we confirmed the regulation by CBZ and DCF of a large proportion of the target genes that are central in the EIF2-signalling/ER UPR response and nuclear factor-erythroid 2 (NF-E2)-related factor 2 (Nrf2)-mediated oxidative stress response in primary human hepatocytes.

#### 4.2. Oxidative stress sensitizes to diclofenac and carbamazepine mediated apoptosis.

Nrf2-mediated oxidative stress response was significantly affected by CBZ and DCF (see Fig. 2). Stabilization of Nrf2 after oxidative stress allows its nuclear translocation and transcriptional activation of antioxidant genes [248]. DCF caused a stabilization of Nrf2 in HepG2 cells (Fig. 4A), which was less clear for CBZ; TNF $\alpha$  addition did not affect the stabilization of Nrf2 (Fig. 4A). Sulfiredoxin (Srxn1) is a direct target of Nrf2 [266] and we monitored the activity of Nrf2 using live cell imaging of a BAC-Srxn1-GFP HepG2 reporter cell line. In line with the microarray data and the Nrf2 stabilization, Srxn1-GFP expression was strongly induced following both DCF and CBZ treatment (Fig. 4B). We validated that the siRNA-mediated knockdown of Nrf2 (Supplementary Fig. S2A) completely inhibited the GFP-Srxn1 expression, while Kelch-like ECH-associated protein 1 (Keap1) knockdown enhanced the Srxn1-GFP response, supporting the functionality of the Keap1/Nrf2 pathway in these cells (Supplementary Fig. S2B). The Nrf2 pathway was also critically involved in the protection against drug/TNF $\alpha$ -mediated cell killing. Knockdown of Keap1 led to enhanced protein levels of Nrf2 (Supplementary Fig. S2A), which was associated with a protection against CBZ/TNF $\alpha$ - and DCF/TNF $\alpha$ -induced cytotoxicity and inhibition of caspase-8 activation (Fig. 4C and 4D and Supplementary Fig. S2C). Importantly, knockdown of Nrf2 itself led to enhancement of the apoptosis (Fig. 4C and Supplementary Fig. S2C).

These data collectively illustrate the importance of oxidative stress in CBZ/TNF $\alpha$ - and DCF/TNF $\alpha$ -induced cytotoxicity

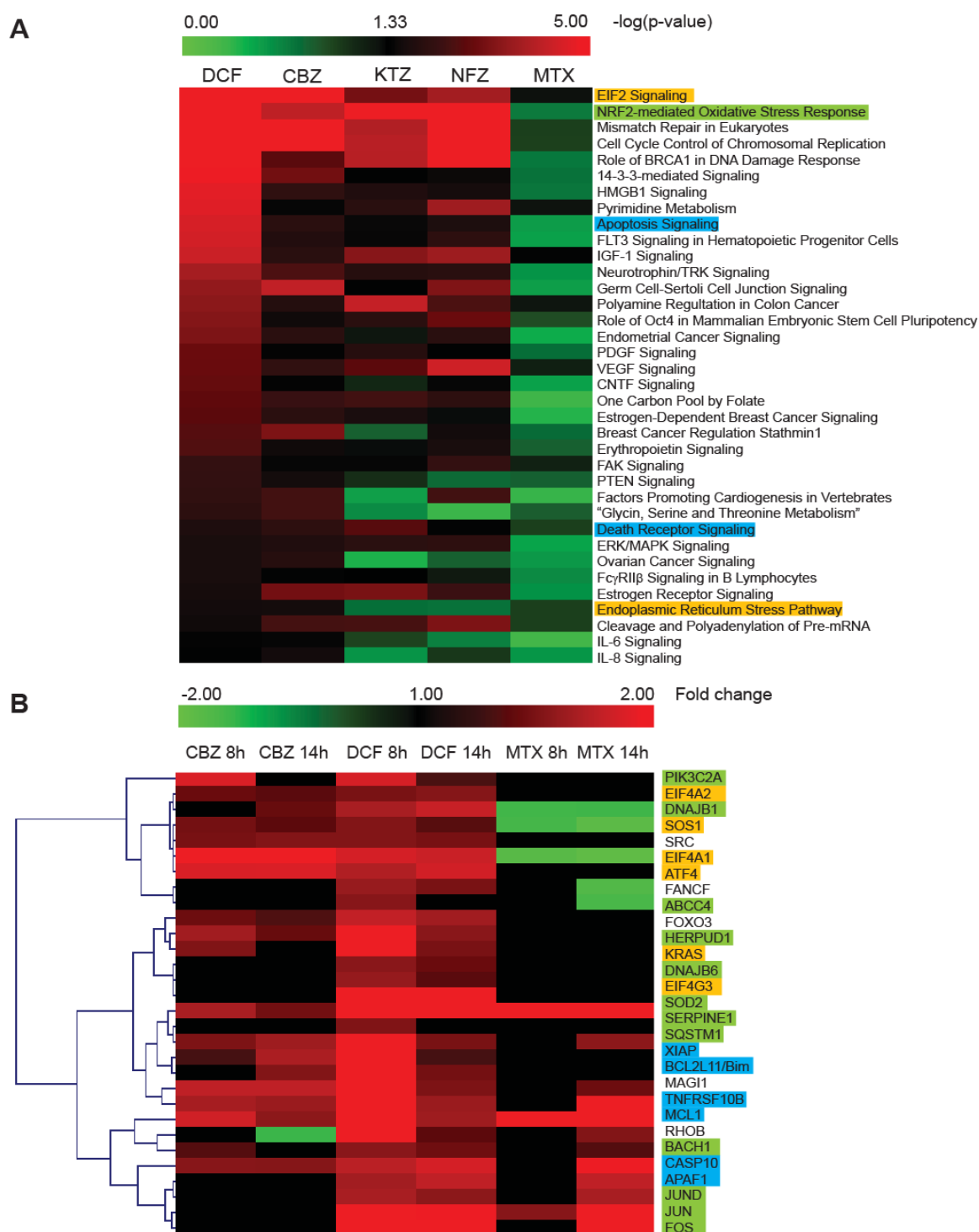


**Figure 2. Identification of CBZ and DCF specific stress responses.** (A) Using IPA® the canonical pathways being significantly affected following exposure to diclofenac (DCF; 500 µM), carbamazepine (CBZ; 500 µM), ketoconazole (KTZ; 75 µM), nefazodone (NFZ; 30 µM) and methotrexate (MTX; 50 µM) for 8 hours were determined. The pathways are ranked by the criteria of being significantly regulated after DCF and CBZ, but not after MTX treatment. The most prominent toxicity pathways are highlighted as follows: EIF2 Signalling/Endoplasmic Reticulum Stress Pathways in yellow, Nrf2-mediated Oxidative Stress response in green and Apoptosis/Death Receptor Signalling in blue. (B) After hierarchical clustering using Pearson correlation and average linkage of the genes representing the pathways in A, the three clusters showing most genes up-regulated under DCF and CBZ conditions but not MTX after 8 and 14h exposure are shown and further clustered using the same method. The colors indicate which pathways they belong to according to the highlighting in A.

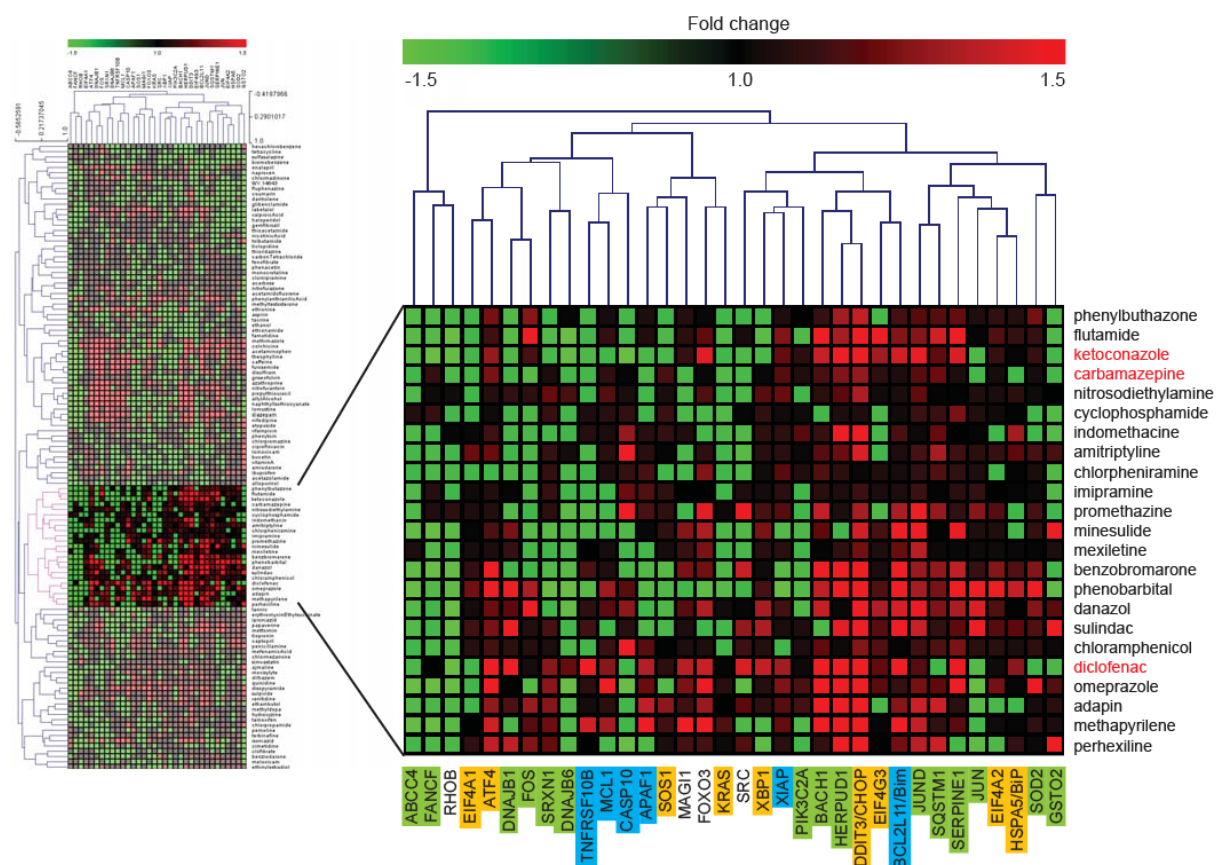


**Figure 3.** Induction of carbamazepine and diclofenac specific stress responses by ~80 DILI compounds in primary human hepatocytes. The expression of the genes presented in Fig. 2B with an addition of typical endoplasmic reticulum (ER)-stress related as well as oxidative stress related genes was investigated in the genes set from TG-GATES. Hierarchical cluster using Pearson Correlation and average linkage resulted in a cluster containing drugs synergizing with TNF $\alpha$  (red).

#### 4.3. PERK activation determines ER stress-mediated hepatotoxicant/TNF $\alpha$ synergistic cell death.

Next we explored the role of the ER stress/UPR pathway in the apoptosis induction after CBZ/TNF $\alpha$  and DCF/TNF $\alpha$  exposure. Pre-treatment of the cells with an ER stressor, tunicamycin, to induce a protective adaptive ER stress response, protected against CBZ/TNF $\alpha$  and DCF/TNF $\alpha$  cell death (Fig. 5A and Supplementary Fig. S3A respectively). Thereafter we systematically analyzed the role of critical upstream signalling components of the ER stress/UPR, inositol-requiring enzyme 1 $\alpha$  (IRE1 $\alpha$ ), activating transcription factor 6 (ATF6) and PERK [118]. Knockdown of IRE1 $\alpha$  and ATF6 led to an enhanced apoptotic response following CBZ/TNF $\alpha$  (Fig. 5B) and DCF/TNF $\alpha$  (Supplementary Fig. S3B) exposure while knockdown of PERK had a protective effect (Fig. 5B [CBZ] and Supplementary Fig. S3B [DCF]). This indicates an exclusive role of the PERK-induced signalling pathway in the onset of apoptosis. In contrast, IRE1 $\alpha$  and ATF6 both have a protective role, most likely related to the control of the cytoprotective heat shock protein family member BiP/HSPA5 [118]. Importantly, activation of PERK could also be observed, which starts as soon as 2 hours after exposure to both CBZ and DCF, independent of TNF $\alpha$  (Fig. 5C).

Next we determined the overall activation of the different ER stress programs after drug exposure, and focused on the PERK/ATF4, IRE1 $\alpha$ /XBP1 and ATF6 pathway activities. For this we



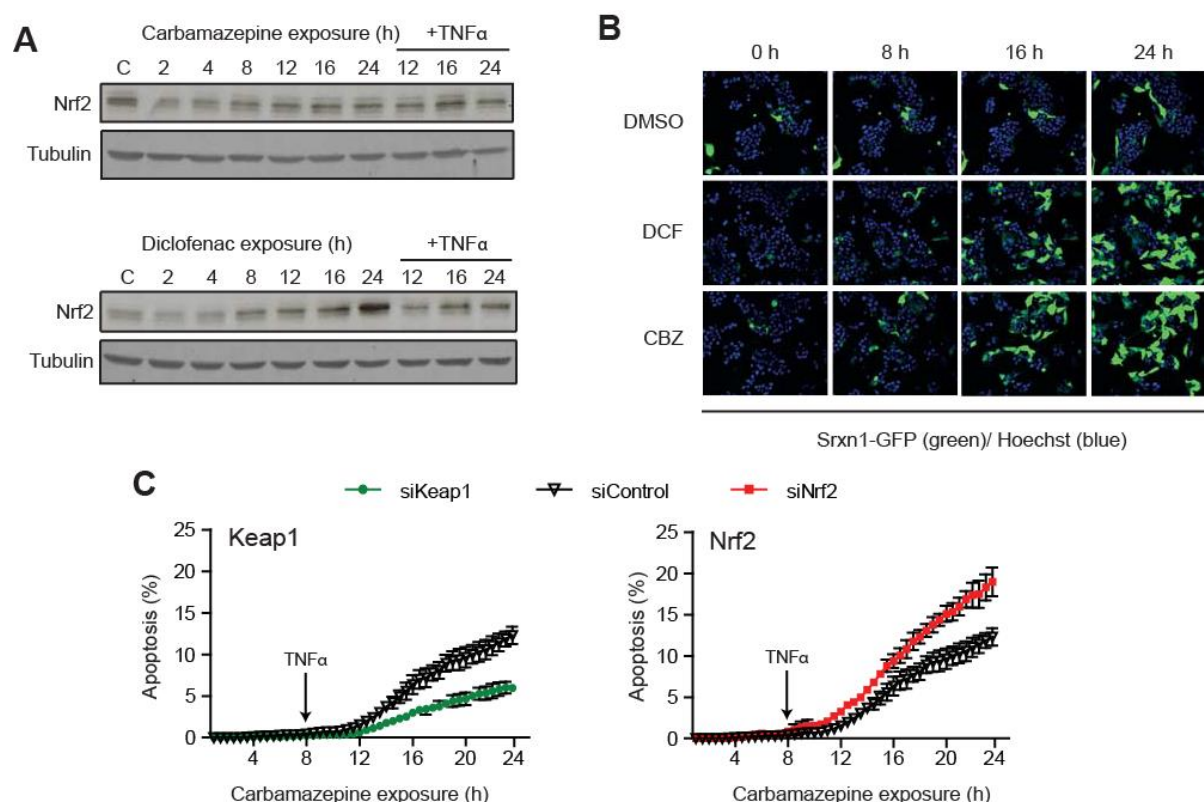


**Figure 4. Carbamazepine and diclofenac induce an Nrf2-response affecting the drug/TNF $\alpha$ -induced apoptosis.** (A) Nrf2 protein levels were investigated by western blot analysis following carbamazepine (CBZ; 500  $\mu$ M) and diclofenac (DCF; 500  $\mu$ M) exposure +/- TNF $\alpha$  addition. "C", controls exposed to vehicle (DMSO) for 12 hours. (B) Nrf2-responsive Srnx1-GFP levels were followed using automated confocal microscopy. Shown are representative images of GFP-Srxn1 (green) HepG2 cells exposed to DMSO, DCF or CBZ for 0, 8, 16 and 24 h. Nuclei are stained by Hoechst (blue). (C) The effect on CBZ/TNF $\alpha$  (10 ng/ml) induced apoptosis after Nrf2 and Keap1 knockdown (SMARTpool) was investigated using live cell imaging of apoptosis. The data are presented as means of three independent experiments +/- SEM or representative of three independent experiments.

evaluated the differential expression of downstream target genes of the transcription factors ATF4, XBP1 and ATF6 after CBZ and DCF exposure. ATF4 showed the strongest up-regulation of downstream targets supporting the hypothesis of a more important role for PERK/ATF4 signalling in the drug-induced toxicity compared to ATF6 and IRE1 $\alpha$ /XBP1 (Fig. 6A). To certify that this main activation of ATF4 after drug exposure was not selective for HepG2 cells, we determined for CBZ and DCF the differential expression of UPR target genes under control of ATF4, XBP1 and ATF6 also three different primary hepatocyte models: precision-cut human liver slices (HLS), primary human hepatocytes (PHM) and primary mouse hepatocytes (PMH). Importantly also in these primary cell systems, the ATF4 transcriptional activity appeared superior to the one of ATF6 and XBP1 after exposure to CBZ or DCF (Fig. 6B, for gene labels see Supplementary Fig. S4).

Finally, we determined whether the PERK/ATF4 pathway was functional in the HepG2 cells. For this we generated a HepG2 bacterial artificial chromosome (BAC)-ATF4-GFP reporter cell line and applied automated live cell confocal microscopy to determine the up-regulation and nuclear translocation of ATF4. ATF4 expression was induced by both DCF and CBZ in time and primarily localized in the nuclear compartment (Fig. 5D) supporting the activation of PERK-mediated UPR signalling pathway and ability to modulate ATF4 target genes.

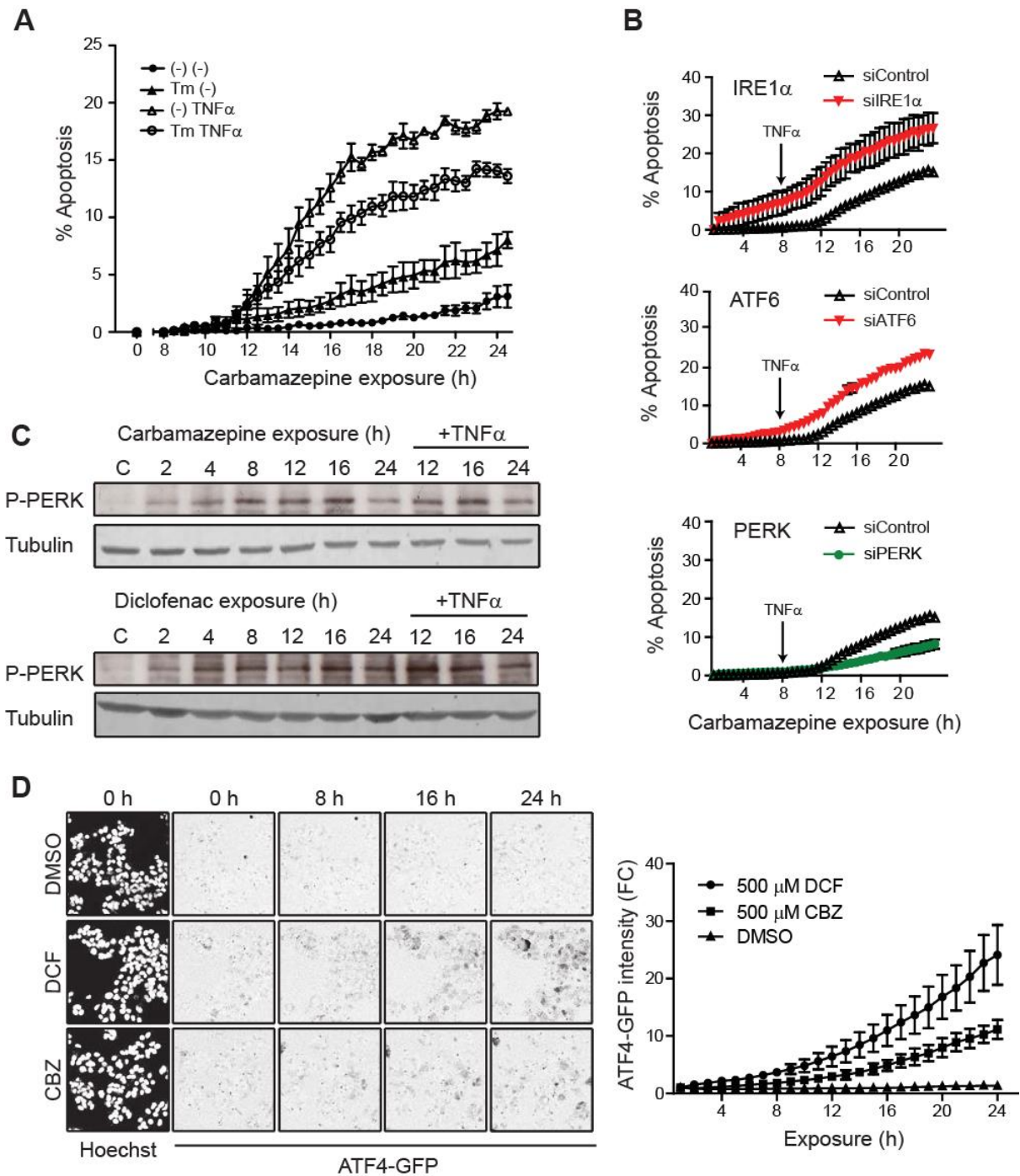


**Figure 5. Carbamazepine and diclofenac induce an ER stress-response affecting the drug/TNF $\alpha$ -induced apoptosis.** (A). HepG2 cells were pre-treated with ER-stressor tunicamycin (Tm; 10  $\mu$ g/ml; A) for 16 hours before treatment with 500  $\mu$ M carbamazepine (CBZ). TNF $\alpha$  (10 ng/ml) was added 8 hours after drug exposure. (B) Apoptosis induced by CBZ/TNF $\alpha$  after knockdown (SMARTpool) of the UPR mediators IRE-1 $\alpha$ , ATF6, and PERK, was followed in time by automated imaging of AnxV-Alexa633 staining (C) PERK activation following CBZ and diclofenac (DCF; 500  $\mu$ M) exposure was followed in time by western blotting for phosphorylated PERK (P-PERK). "C", control exposed to vehicle for 12 hours. (D) HepG2 cells expressing BAC-ATF4-GFP were followed in time after exposure to DCF, CBZ (500  $\mu$ M) or vehicle (DMSO) using automated confocal microscopy. Representative images of Hoechst at 0 and ATF4-GFP (inverted) at 0, 8, 16 and 24 hours after drug exposure are shown as well as the quantification of the increase in ATF4-GFP intensity in time after DCF and CBZ exposure. Values are presented as fold changes (FC) of time-point 0 and the data is presented as means of 3 independent experiments  $\pm$  S.E.M.

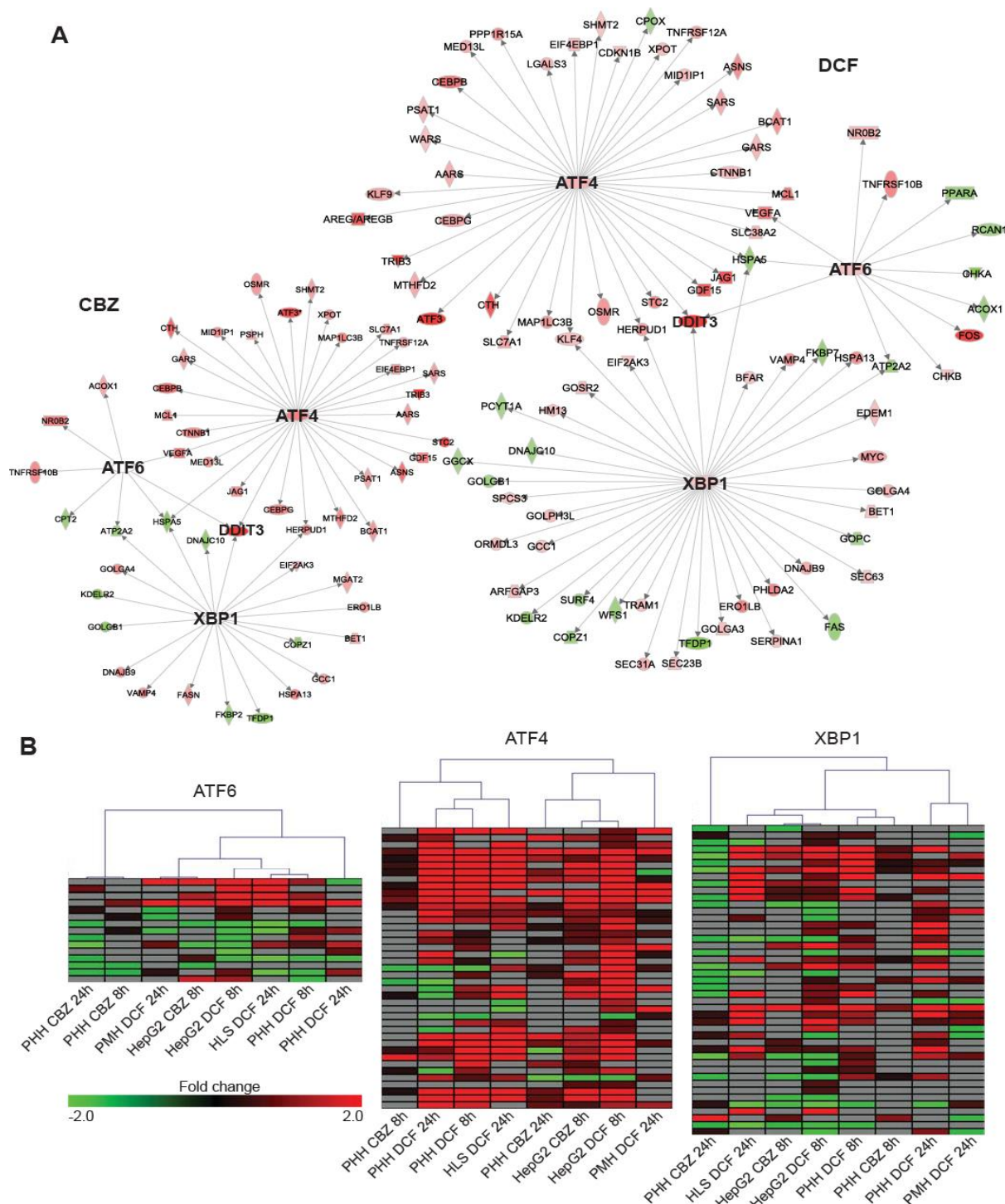


**Figure 6. Diclofenac and carbamazepine exposure mainly induces ATF4 transcription.** (A) Using the IPA® software the genes up- or down-regulated by the transcription factors downstream of the three distinct unfolded protein response pathways, PERK (ATF4), IRE-1 $\alpha$  (XBP1) and ATF6 were determined after 8 hours carbamazepine (CBZ) or diclofenac (DCF) exposure. Red coloring of the shapes indicate up-regulation of the target genes, while green indicate down-regulation. The intensity reflects the fold-change gene expression compared to vehicle-exposed cells. (B) Expression of the genes induced by DCF and CBZ in HepG2 cells was determined by gene array analysis of primary human (PHH), human liver slices (HLS) and primary mouse hepatocytes (PMH) at 8 and/or 24 hours of CBZ and DCF exposure followed by hierarchical clustering of the *in vitro* systems using Pearson correlation and average linkage. Grey color indicates genes that are not regulated at this significance level. A complete figure containing gene names is represented in Supplementary Fig. S4.



#### 4.4. Carbamazepine and diclofenac induce expression of pro-apoptotic CHOP.

A major target of PERK-mediated ATF4 activation is the pro-apoptotic transcription factor C/EBP homologous protein (CHOP)/DDIT3 [121]. We observed a DCF- and CBZ-induced activation of ATF4 (Figs. 5D and 6) and subsequent increased expression of CHOP/DDIT3 to both compounds both in HepG2 cells (Fig. 6A) and in primary cell systems including liver slices (Supplementary Fig. S4). We established a HepG2 BAC-GFP-CHOP reporter cell line and used automated live cell confocal microscopy to monitor the induction of GFP-CHOP. While GFP-CHOP was absent under control conditions, both CBZ and DCF induced the expression of GFP-CHOP in time (Fig. 7A), which was reproduced in parental HepG2 cells by western blotting (Fig. 7B). This CHOP induction was critical for the onset of cell death since siRNA-mediated knockdown of CHOP protected against the apoptosis induced by CBZ/TNF $\alpha$  and DCF/TNF $\alpha$  (Fig. 7C and Supplementary Fig. S3C). These data strongly support the role for the PERK/ATF4/CHOP program in the cell death induced by DCF/TNF $\alpha$  and CBZ/TNF $\alpha$ .

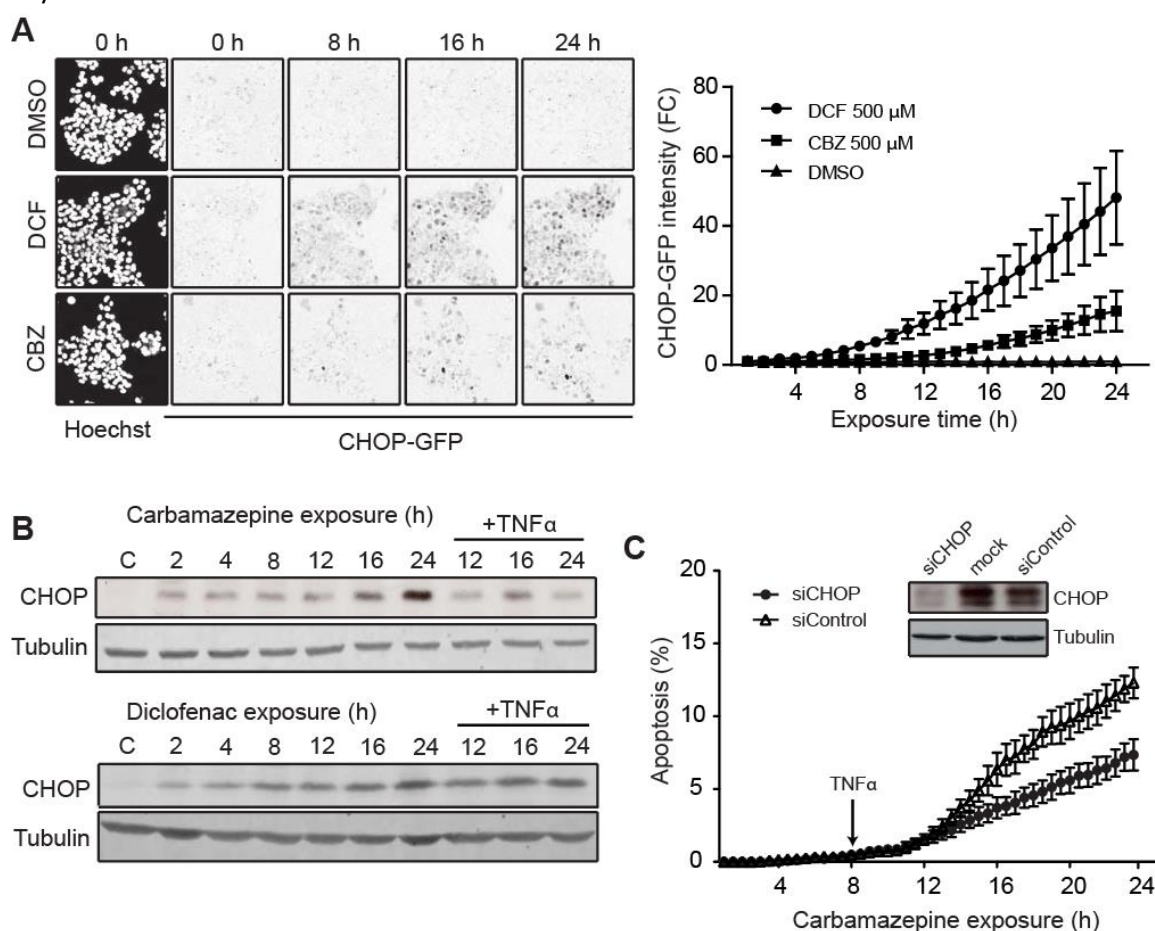


**Figure 7. Carbamazepine- and diclofenac-induced CHOP expression is critical for the apoptosis induction.**

(A) HepG2 cells expressing BAC-CHOP-GFP were followed in time after exposure to diclofenac (DCF; 500  $\mu$ M), carbamazepine (CBZ; 500  $\mu$ M) or vehicle (DMSO) using automated confocal microscopy. Representative images of Hoechst at 0 and CHOP-GFP at 0, 8, 16 and 24 hours after drug exposure (inverted) are shown. The quantification of the increase in CHOP-GFP intensity in time after DCF and CBZ exposure are presented as fold changes (FC) of time-point 0. (B) CHOP induction after carbamazepine and diclofenac exposure was followed in time by western blotting. "C", control exposed to vehicle for 12 hours. Tubulin was used as loading control. (C) Apoptosis induced by CBZ/TNF $\alpha$  after knockdown of CHOP (SMARTpool) was followed in time by automated imaging of AnxV-Alexa633 staining. Data is presented as means of 3 independent experiments  $\pm$  S.E.M.

#### 4.5. Carbamazepine and diclofenac induced Nrf2 activation is independent of ER stress.

Since ER stress can activate the Nrf2 pathway [267] we wanted to determine the link between ER stress and oxidative stress. While PERK and CHOP knockdown protected against cell death (Fig. 5C and 7C), neither PERK nor CHOP knockdown inhibited the expression of the Nrf2 target gene *Srxn1* in the GFP-*Srxn1* HepG2 reporter cells (Fig. 8A). Vice versa, knockdown of Keap1, which stabilized Nrf2, in association with strong *Srxn1* expression and cytoprotection against CBZ/TNF $\alpha$  and DCF/TNF $\alpha$  (see above), did not block the activation of PERK and the expression of CHOP after CBZ exposure (Fig. 8B). Although both important for the DCF/TNF $\alpha$  and CBZ/TNF $\alpha$ -induced cell injury, the role of the oxidative stress response appears to be unrelated to the PERK-initiated ER-stress response.

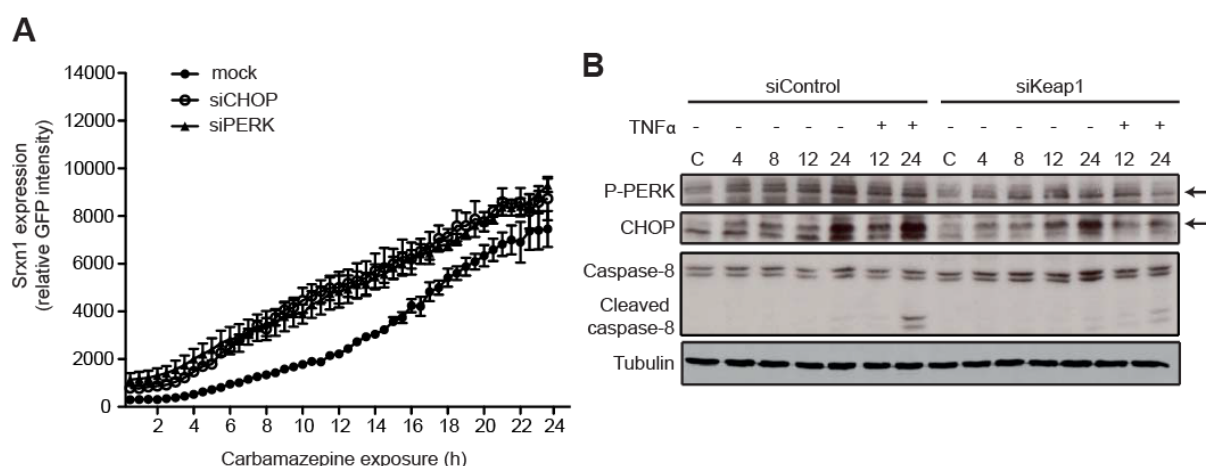


**Figure 8. Carbamazepine and diclofenac induced Nrf2 activation is independent of ER stress.** (A) The effect of PERK and CHOP knockdown on GFP-*Srxn1* induction after carbamazepine (CBZ) exposure was investigated using automated confocal microscopy. GFP intensities were normalized to the area occupied by nuclei as determined by Hoechst staining. (B) ER-stress activation, as measured by protein expression of phosphorylated PERK and CHOP using western blot, was investigated after Keap1 knockdown and a time series of CBZ exposure +/- TNF $\alpha$  addition. Cleavage of caspase-8 is shown for assessment of extrinsic apoptosis induction. Tubulin serves as loading control and "C" is control exposed to vehicle for 12 hours. The data are presented as means of three independent experiments +/- SEM or representative of three independent experiments.

#### 4.6. EIF4A1 controls CHOP expression and thereby apoptosis onset.

Eucaryotic initiation factor (EIF2) signalling in relation to translation initiation was the major pathway affected by CBZ and DCF (see Fig. 2). Salubrinol, an inhibitor of the dephosphorylation of translation initiation factor eIF2 $\alpha$ , which is protective against ER stress induced toxicity [268], inhibited the CBZ and DCF synergy with TNF $\alpha$  (Fig. 9A and Supplementary Fig. S3D) supporting a central role for the translational program in the onset of drug/TNF $\alpha$ -induced apoptosis. To further test this hypothesis we performed a knockdown of the RNA helicase EIF4A1, the translation initiation factor that was found most up-regulated after DCF and CBZ exposure. Depletion of EIF4A1 provided an almost complete protection against both CBZ/TNF $\alpha$ - and DCF/TNF $\alpha$ -induced apoptosis (Fig. 9B and Supplementary Fig. S3E).

Inhibition of global translation is one of the responses for the cell to try to cope with enhanced ER stress [118]. Intriguingly, siEIF4A1 did not affect the PERK activation following CBZ

exposure, yet it almost completely inhibited the induction of CHOP (Fig. 9C). Together these data are indicative for a crucial role for translation in the induction of drug/TNF $\alpha$ -induced apoptosis, which is for a major part related to EIF4A1-mediated translation of ER-stress protein CHOP.

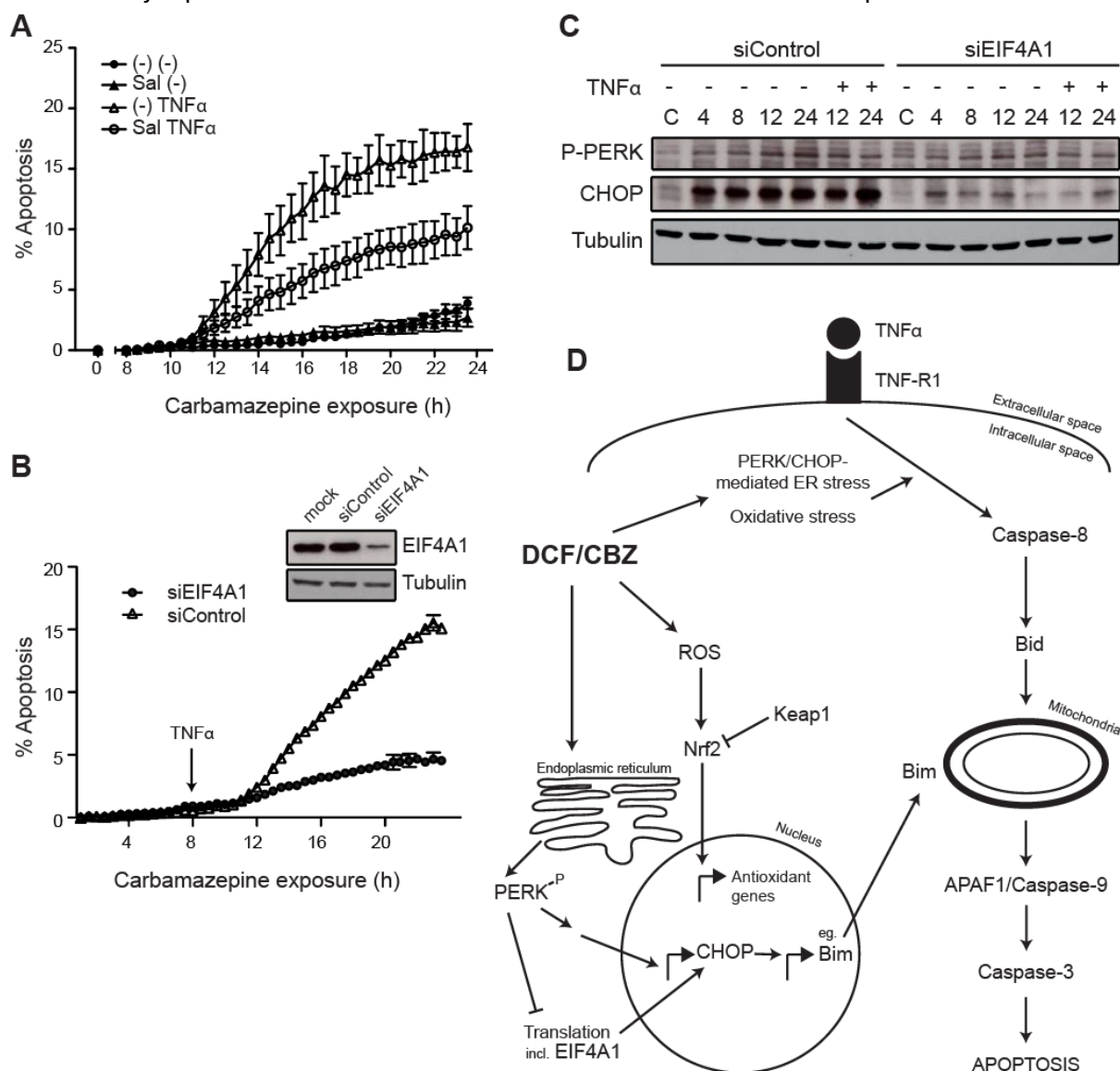


**Figure 9. Translation initiation regulated by EIF4A1 is crucial for carbamazepine/TNF $\alpha$ -apoptosis induction and CHOP expression.** (A) HepG2 cells were pre-treated with an eIF2 $\alpha$  phosphatase inhibitor, salubrinal (Sal; 50  $\mu$ M) for 16 hours before treatment with 500  $\mu$ M carbamazepine (CBZ). TNF $\alpha$  (10 ng/ml) was added 8 hours after drug exposure. (B) Apoptosis induced by CBZ (500  $\mu$ M) and TNF $\alpha$  (10 ng/ml) after EIF4A1 knockdown (SMARTpool) was followed in time using live cell imaging of apoptosis. (C) The effect of EIF4A1 knockdown on the induction of ER-stress proteins P-PERK and CHOP by western blot. The induction caspase-8 cleavage was used as a marker of death receptor induced apoptosis activation. Tubulin served as loading control. All data are presented as means of three independent experiments  $\pm$  SEM or representative for three independent experiments when applicable. (D) Model of the molecular mechanisms of DCF- and CBZ-induced sensitization toward TNF $\alpha$ -induced apoptosis.

## 5. Discussion

Here we studied in detail the underlying molecular mechanisms of the synergistic apoptotic response between hepatotoxic drugs and the pro-inflammatory cytokine tumor necrosis factor  $\alpha$  (TNF $\alpha$ ) using a unique integration of transcriptomics and RNA interference-based functional

genomics. Gene expression analysis of HepG2 cells and primary human and mouse hepatocytes as well as human precision cut liver slices demonstrated the specific activation of the endoplasmic reticulum (ER)-stress/unfolded protein response (UPR) signalling route through the activating transcription factor 4 (ATF4) transcriptional activity by diclofenac (DCF) and carbamazepine (CBZ). Further functional analysis of the role of critical determinants of this pathway identified protein kinase R-like ER kinase (PERK) and C/EBP homologous protein (CHOP) as pivotal players in the onset of drug/TNF $\alpha$ -mediated cytotoxicity in HepG2 cells. Importantly, while oxidative stress modulated the onset of cell death it did not affect the ER-stress/UPR program. On the contrary, the translational machinery of which translation initiation factor EIF4A1 is a critical marker, was manifested as a major determinant of CHOP expression and, thereby, onset of drug/TNF $\alpha$ -mediated toxicity.

Our data demonstrate a clear enhancement of apoptosis with the addition of TNF $\alpha$  to DCF and CBZ treated HepG2 cells, whereby we chose to focus on the toxicity pathways induced by these two compounds. In contrast, in cells pre-exposed to other known idiosyncratic hepatotoxicants the synergism with TNF $\alpha$  was not so clear in the case of ketoconazole (KTZ) and absent in nefazodone (NFZ) and methotrexate (MTX) pre-exposed cells. A synergy in the regulation of the expression of genes directly involved in the apoptosis seems unlikely, since all five compounds synergized in the expression of various candidate genes (Supplementary Fig. S5), although we cannot exclude the role of some individual genes in the DCF/TNF and CBZ/TNF synergistic cytotoxicity. The discrepancy between synergizing and non-synergizing drugs may be explained by the fact that DCF-induced liver injury has been linked to the involvement of an activated immune system [269], and the idiosyncratic nature of CBZ-induced liver injury has been linked to hypersensitivity reactions [270]. However, KTZ, NFZ and MTX, although reported inducers of hepatotoxicity [271-273], have not, to our knowledge, been linked to immune system activation. In addition, supporting our results, absence of TNF $\alpha$  synergism with NFZ and MTX was previously reported in a larger screen of compounds in primary human hepatocytes with and without the addition of pro-inflammatory cytokines including TNF $\alpha$  [146]. Moreover, the current manuscript illustrates the fact that whether or not a compound would synergize with TNF $\alpha$  may lie in the types of stress pathways induced by the drugs alone, where DCF and CBZ affect ER-stress/translation initiation signalling as well as oxidative stress, while NFZ and KTZ are stronger inducers of oxidative stress alone.

Our data indicate that ER stress signalling through the PERK/CHOP pathway is a critical determinant for the hepatotoxicant/TNF $\alpha$  synergy response towards hepatocyte apoptosis. ER stress and the UPR have been implicated in several different liver diseases including drug-induced liver injury (DILI) [252]. Here we present a more selective activation of the PERK-arm of the ER stress/UPR following DCF and CBZ exposure (Figs. 5 and 6), which was directly related to expression of CHOP (Fig. 7), a downstream target of ATF4. Importantly, the up-regulation of ATF4 and CHOP were not only found in our HepG2 cell system after exposure of DCF and CBZ but also in primary human hepatocytes after exposure to a panel of hepatotoxic drugs (Fig. 3) as well as in other primary cell systems after DCF and CBZ exposure (Fig. 6B and Supplementary Fig. S4). Moreover, in primary human hepatocytes we found that many DILI compounds affected the expression of ATF4 and CHOP, while XBP1 and BiP/HSPA5 were less affected. Interestingly, this up-regulation of CHOP and ATF4 was more prominent with drugs related to severe DILI (Fig. 3). Given

our observed critical role of CHOP in the onset of apoptosis, these combined observations suggest that CHOP is a critical player in liver toxicity, in particular in the sensitization for TNF receptor-mediated apoptosis.

The current study highlights the importance of perturbations in the translation initiation program in the hepatotoxicant-induced stress response and onset of cytotoxicity. Firstly, several translation initiation factors, which included EIF4A1, EIF4A2 and EIF4G3 were specifically strongly affected by CBZ and DCF but not the other hepatotoxicants (Fig. 2B and Supplementary Fig. S1A). Secondly, an inhibitor of eIF2 $\alpha$  dephosphorylation, salubrinal, inhibited the drug/TNF $\alpha$ -induced apoptosis (Fig. 9A and Supplementary Fig. S3D). Thirdly, also knockdown of EIF4A1 almost completely abrogated the TNF $\alpha$  synergy with both CBZ and DCF (Fig. 9B and Supplementary Fig. S3E). EIF4A1 and EIF4G3 together with cap-binding protein EIF4E are part of the EIF4F complex that unwinds secondary structures of the 5' untranslated region (UTR) of mRNA to allow ribosomal binding, scanning and thereby translation [274]. The 5' UTR of mRNA can be more or less structured, determining its translation efficiency [275]. EIF4A and EIF4G have also been implicated with cap-independent translation [275]. Interestingly, the translation of several anti- and pro-apoptotic genes such as XIAP, and APAF1 can occur via cap-independent mechanisms [276, 277] and given the drastic effect on drug/TNF $\alpha$ -induced apoptosis we show (Fig. 9B and Supplementary Fig. S3E), EIF4A1 is most likely involved in the expression of other apoptosis-regulating proteins. Here we present that EIF4A1 is a crucial regulator of pro-apoptotic CHOP expression since depletion of EIF4A1 reduced the expression of this protein (Fig. 9C), CHOP protein expression is likely regulated by EIF4A1 cap-independent translation in our model. Of note is that also in the primary human hepatocytes various DILI compounds affected the expression of EIF4A1, EIF4A2 and/or EIF4G3 (Fig. 3). While our combined results emphasize a role of translational control in xenobiotic toxicity further research to uncover the entire (cap-independent) translation-based proteome will provide overall insight in the diversity of molecular networks that underlie the drug/TNF $\alpha$  synergy.

The hepatotoxicant/TNF $\alpha$  synergy was for an important part sensitized by the pro-oxidant properties of both CBZ and DCF (Fig. 4C and Supplementary Fig. S2C). Indeed, our gene expression profiling showed strong up-regulation of nuclear factor-erythroid 2 (NF-E2)-related factor 2 (Nrf2) target genes by both DCF and CBZ, which correlated with strong Nrf2-dependent induction of *Srxn1* (Fig. 4B). Such an up-regulation of *Srxn1* was also observed for human and mouse primary hepatocytes as well as human liver slices (data not shown) which fits with observations for the *in vivo* DCF treated rat liver [269] as well as DCF treated mouse liver [278]. Importantly, knockdown of the endogenous Nrf2-inhibitor Kelch-like ECH-associated protein 1 (Keap1) led to protection against DCF/TNF $\alpha$  and CBZ/TNF $\alpha$ -induced apoptosis (Fig. 4C and Supplementary Fig. 2C). In addition, hepatocyte cell death induced by DCF and CBZ alone are oxidative stress dependent [279, 280]. Despite the fact that Keap1 knockdown was strongly protective against drug/TNF $\alpha$  synergy, it did not affect PERK activation and CHOP expression. This suggests that the drug-induced ER stress/UPR is uncoupled from oxidative stress, and that both stress programs each independently modulate the susceptibility towards TNF $\alpha$ -mediated synergistic drug induced cell killing.

It is of crucial importance to elucidate the connection between ER stress/UPR and the onset of apoptosis by the drug/TNF $\alpha$  combinations. TNF $\alpha$  itself or in combination with CBZ or DCF did



not enhance CHOP protein levels (Fig. 7B), therefore enhancement of CHOP expression is not the sole mechanism behind the enhanced apoptosis observed upon TNF $\alpha$  addition to CBZ and DCF pre-exposed cells. Rather, it seems as if drug-induced CHOP expression leads to sensitization of the HepG2 cells to TNF $\alpha$ -induced apoptosis and since CHOP is a transcription factor, it is likely that downstream target genes is what affects cell susceptibility. Up-regulation of CHOP may lead to apoptosis via up-regulation of pro-apoptotic Bcl-2 family members, including Bim [133]. In our system Bim (BCL2L11) was up-regulated after DCF and CBZ exposure and Bim is induced by different DILI compounds in primary hepatocytes in close association with CHOP expression (Fig. 2 and 3) further emphasizing their close connection. Moreover, siRNA mediated knockdown of Bim rescued both the CBZ/TNF $\alpha$  and DCF/TNF $\alpha$ -induced cytotoxicity (Supplementary Table S1 and reference [38]). In addition to the role of Bim, our current data demonstrate that the CBZ/TNF $\alpha$ -induced apoptosis was inhibited by knockdown of caspase-8, Bid, APAF1, caspase-9 and caspase-3 (Supplementary Table S1). Together these data suggest that drug-induced Bim expression sensitizes the mitochondria to caspase-8-mediated Bid cleavage and activity, causing the synergistic apoptosis-induction with TNF $\alpha$ . We are currently investigating the role of other proteins in this synergistic apoptotic response using an unbiased siRNA screening approach.

In summary, we show that DCF and CBZ, drugs linked to idiosyncratic DILI with activation of the inflammatory system, sensitize liver cells to TNF $\alpha$ -induced apoptosis. We propose an overall working model (Fig. 9D) where CBZ and DCF induce oxidative and ER stress/UPR, which independently sensitize towards apoptosis. The PERK/ATF4/CHOP-dependent ER stress/UPR program enhances the activation of the apoptotic signalling downstream of the TNF receptor in close control by the translation initiation program including EIF4A1. Subsequent expression and/or activation of caspase-8, Bid and Bim drive the activation of the intrinsic apoptotic program controlled by APAF1 and caspase-9 to activate the onset of caspase-3. Our work sheds new light on the mechanism behind the, so far, unpredictable idiosyncratic DILI. Possibly genetic variants in the functionally critical determinants of the cytotoxic response are candidate susceptibility genes that predispose for individual humans to idiosyncratic DILI.

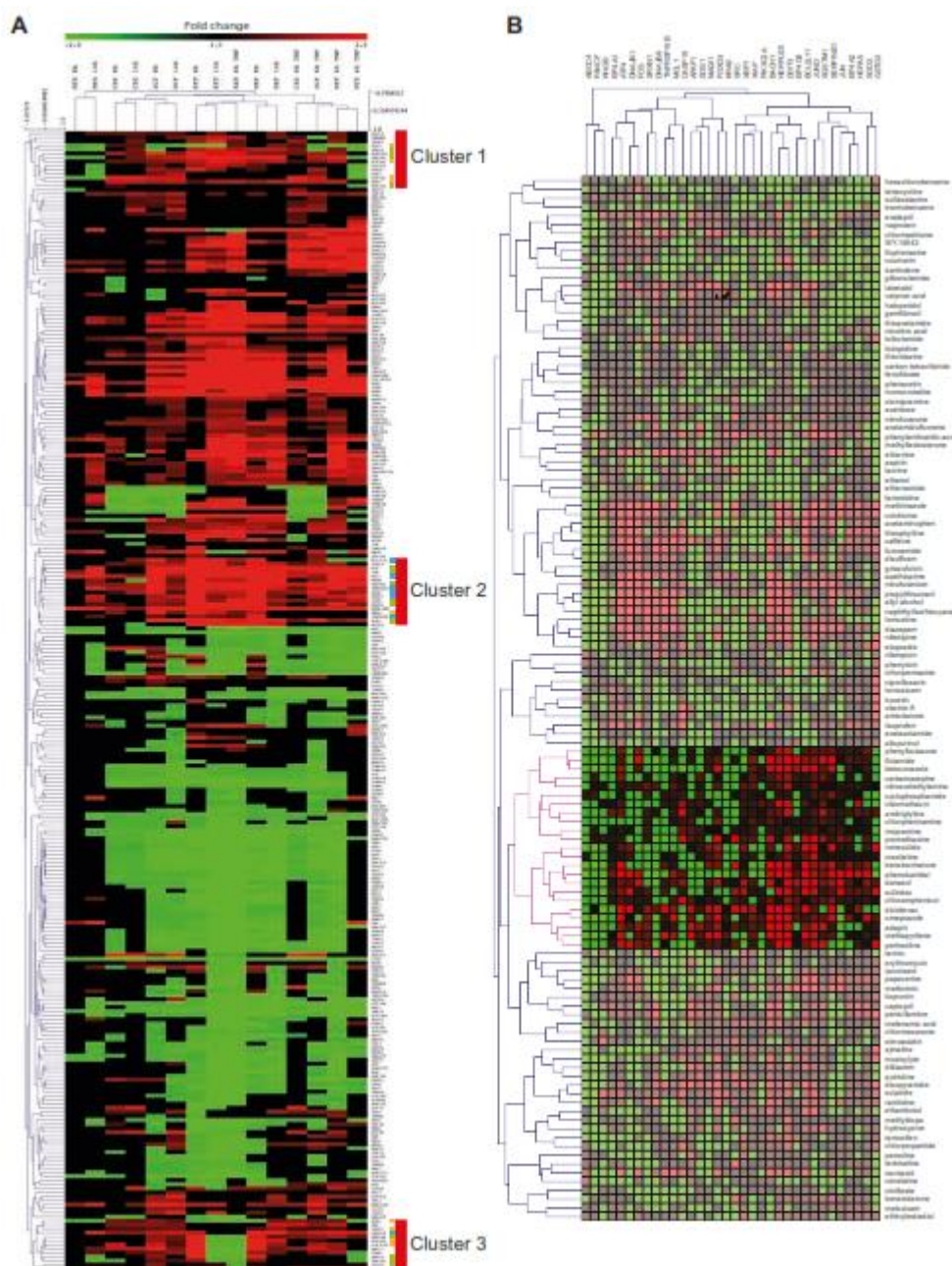
### **Funding**

This work was supported by the Dutch Top Institute Pharma project # D3-201, the FP7 Health SEURAT-1 program DETECTIVE (grant agreement 266838), the Netherlands Genomics Initiative/Netherlands Toxicogenomics Centre and the Innovative Medicine Initiative project MIP-DILI (grant agreement 115336).

### **ACKNOWLEDGEMENTS**

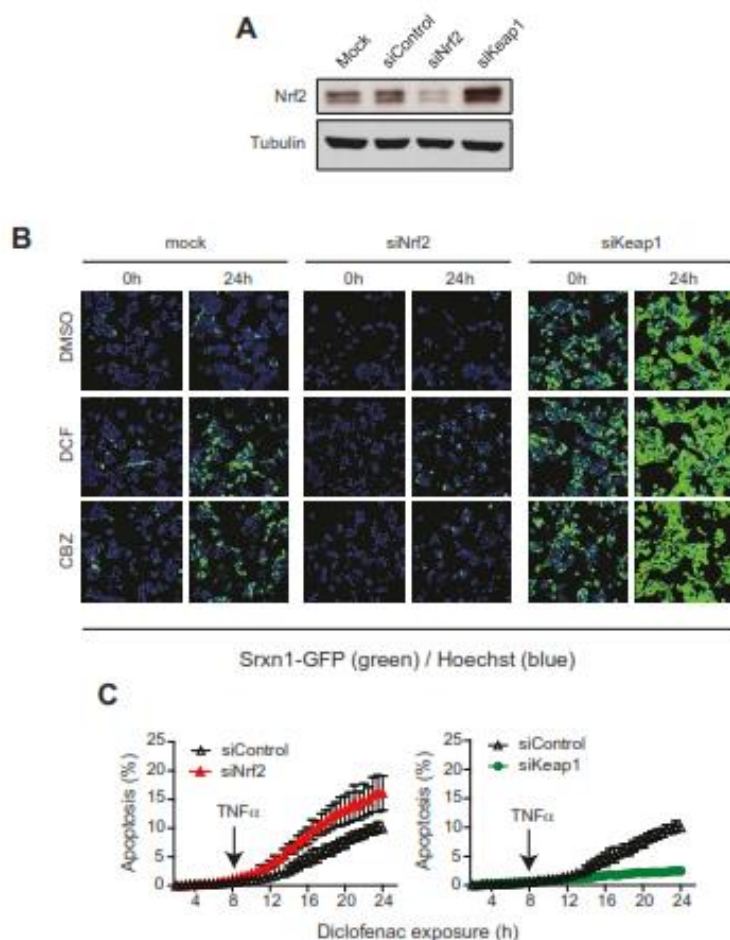
We thank Harry Vrieling and Giel Hendriks for providing the Srxn1-GFP BAC-construct.

## Supplementary Figures

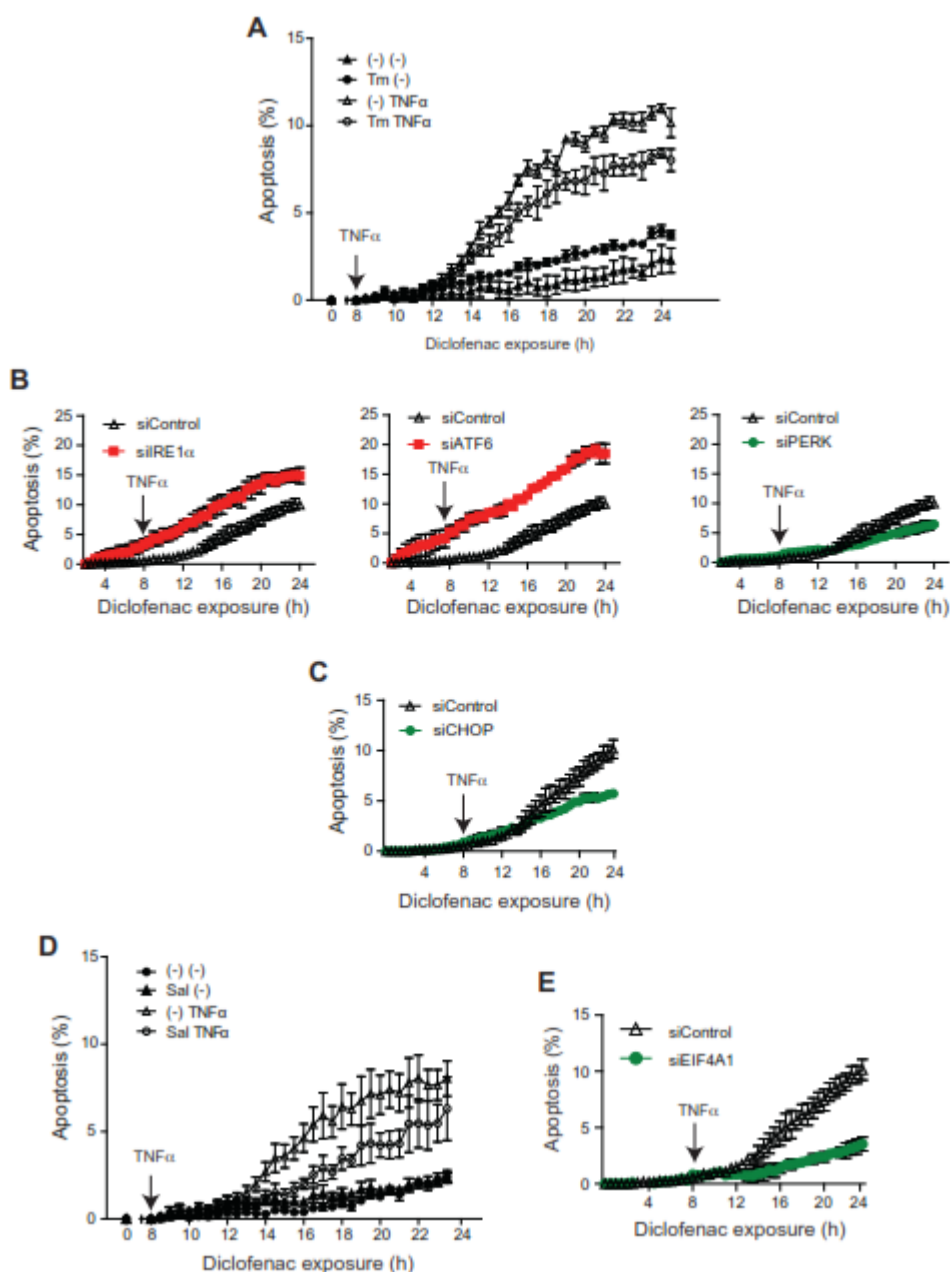


**Supplementary figure S1. Clustering of diclofenac and carbamazepine regulated genes in HepG2 cells confirms specific stress responses which can be induced by ~80 DILI compounds in primary human hepatocytes.** (A) The genes were clustered using Pearson correlation and average linkage in the MultiExperiment Viewer software. Expression values, here presented as fold change of control, from all time points, 8 and 14 hours +/- TNF $\alpha$  (10 ng/ml), and exposure conditions, diclofenac (DCF; 500  $\mu$ M), carbamazepine (CBZ; 500  $\mu$ M), ketoconazole (KTZ; 75  $\mu$ M), nefazodone (NFZ; 30  $\mu$ M) and methotrexate, (MTX; 50  $\mu$ M) were used. The clusters identified as interesting (1-3) contained genes up-regulated after 8 hours DCF and CBZ exposure but down- or non-regulated after MTX treatment. The genes that represent the interesting IPA®-defined canonical pathways presented in Figure 2 were labelled according to their respective pathways; yellow highlight = EIF2-signalling/Endoplasmic Reticulum Stress Pathway; green highlight = NRF2-mediated Oxidative Stress Response; blue highlight = Apoptosis Signalling/Death receptor Signalling. (B) The expression of the genes presented in Fig. 2B with an addition of typical ER-stress related

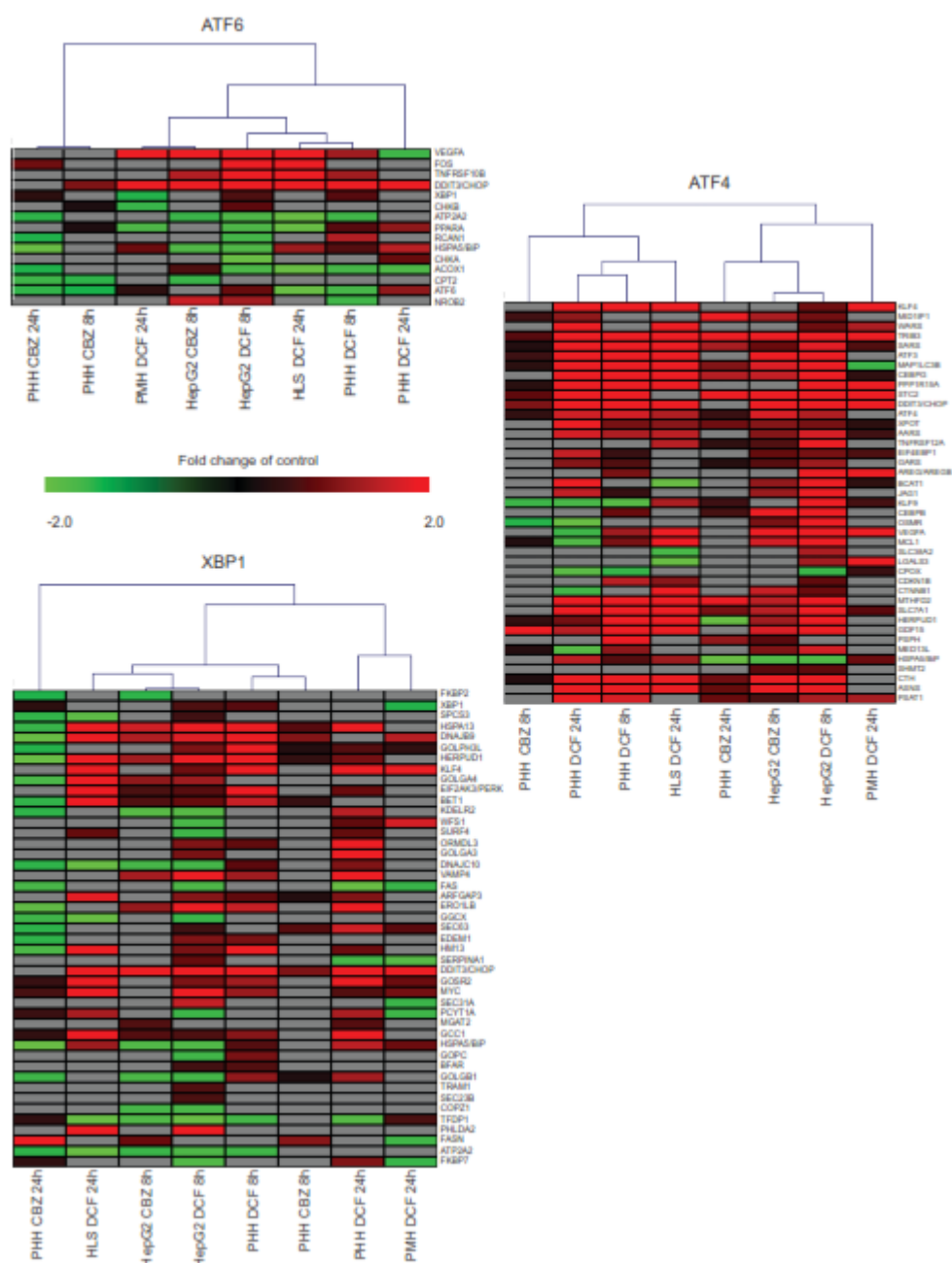
as well as oxidative stress related genes was investigated in the genes set from TG-GATEs. Hierarchical cluster using Pearson Correlation and average linkage resulted in a cluster containing drugs synergizing with TNF $\alpha$  (highlighted).



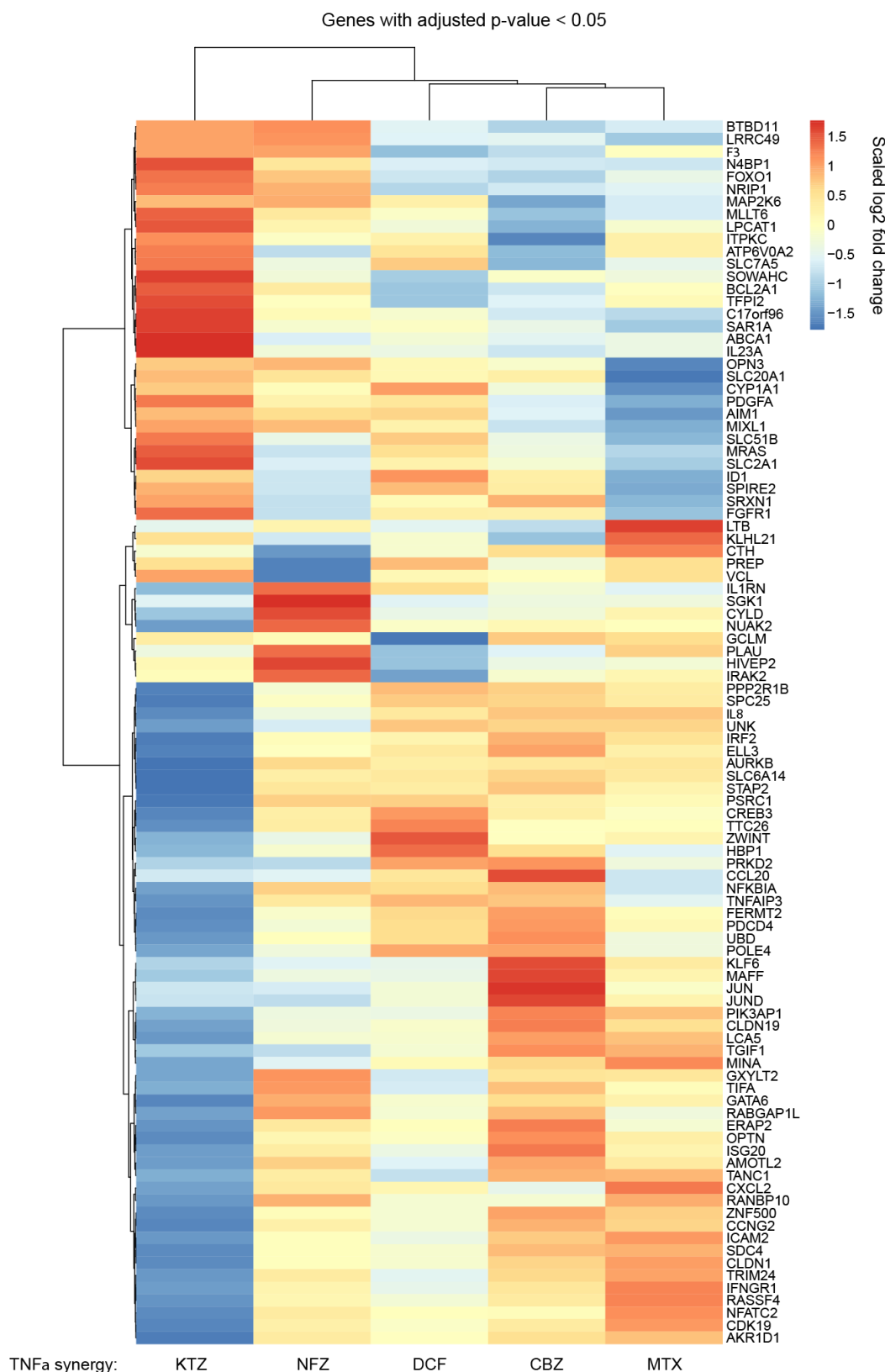
**Supplementary figure S2. Knockdown of Nrf2 and Keap1 affect expression of Nrf2 target gene Srxn1 as well as apoptosis induced by diclofenac/TNF $\alpha$  exposure.** (A) Knockdown (SMARTpool) of Nrf2 and Keap1 in HepG2 cells leads to down- and up-regulation of Nrf2 protein respectively as measured by western blotting. Tubulin served as loading control. (B) Knockdown of Nrf2 and Keap1 leads to down- and up-regulation of Srxn1-GFP respectively in the BAC-Srxn1-GFP HepG2 cell line also after exposure to diclofenac (DCF; 500  $\mu$ M) and carbamazepine (CBZ; 500  $\mu$ M) for 24 hours. (C) Knockdown of Nrf2 and Keap1 leads to enhancement and reduction of DCF/TNF $\alpha$ -induced apoptosis respectively compared to control knockdown cells. Data presented are means of three independent experiments  $\pm$  S.E.M or representative of 3 experiments accordingly.



**Supplementary figure S3. Inhibition of endoplasmic reticulum stress and translation reduces diclofenac/TNF $\alpha$ -induced apoptosis.** (A) HepG2 cells were pre-treated with 5  $\mu$ g/ml tunicamycin (Tm) before replacing the medium with 500  $\mu$ M DCF. After 8 hours of DCF exposure, TNF $\alpha$  (10 ng/ml) was added. (B) The effect of knockdown (SMARTpool) of the main ER-stress related proteins on DCF/TNF $\alpha$ -induced apoptosis was determined. The apoptosis was measured in time using live cell imaging of apoptosis. (C) The effect of knockdown of CHOP/DDIT3 on DCF/TNF $\alpha$ -induced apoptosis was determined by liver cell imaging of apoptosis. (D) HepG2 cells were pre-treated 50  $\mu$ M salubrinal (Sal) before replacing the medium with 500  $\mu$ M DCF. Salubrinal was kept in the medium during the exposure and after 8 hours of DCF treatment, TNF $\alpha$  (10 ng/ml) was added. (E) HepG2 cells were transfected with control or EIF4A1 siRNA and the apoptosis induced by diclofenac (DCF; 500  $\mu$ M) and TNF $\alpha$  (10 ng/ml) was investigated using live cell imaging of apoptosis. Data presented are means of three independent experiments  $\pm$  S.E.M.



**Supplementary figure S4. Diclofenac and carbamazepine exposure induced mainly ATF4 transcription.** The genes that were identified as regulated by ATF6, ATF4 and XBP1 in HepG2 cells after 8-hour exposure to diclofenac (DCF) and carbamazepine (CBZ) (Fig. 5) were investigated for their expression in primary human (PHH), human liver slices (HLS) and primary mouse hepatocytes (PMH) at 8 and/or 24h followed by hierarchical clustering of the *in vitro* systems using Pearson correlation and average linkage. In this figure also the gene names have been included.



**Supplementary figure S5. Synergy between DILI drugs and TNFα to induce the enhanced expression or suppression of target genes.** For the combined treatment/synergistic-effect analysis of carbamazepine (CBZ), diclofenac (DCF), ketoconazole (KTZ), nefazodone (NFZ) and methotrexate (MTX) with TNFα treatment we used a linear modeling approach:  $y_i = \beta_1 x_{iA} + \beta_2 x_{iAB} + \beta_3 x_{iB} + \beta_4 x_{iC} + \epsilon_i$ ,  $i = 1 \dots 16$  and a contrast matrix was set up to test the null-hypothesis;  $H_0: \beta_2 + \beta_4 = \beta_1 + \beta_3$ . (A is the compound treatment, B the TNFα treatment, C the DMSO control and AB is the combined treatment of compound+TNFα, xi is the



model matrix,  $\beta_i$  are the corresponding model-coefficients and  $\epsilon_i$  is the random error term). Differentially synergistic up- or down-regulated genes were determined for all five compounds (adjusted p-value < 0.05). Shown is the row-scaled log2 fold change expression of individual synergistic genes for all five compounds in combination with TNF $\alpha$ .

**Supporting table S1.** siRNAs used in this study, with the significance of the effect knockdown had after exposure to carbamazepine (CBZ) and diclofenac (DCF) respectively and how many of the single siRNAs showed a significant effect by deconvolution.

	siRNA	CBZ (p-value)	DCF (p-value)	Validation (CBZ)
<b>Apoptosis</b>	CASP8	< 0.001	Fredriksson <i>et al.</i>	4/4
	CASP3	< 0.001	Fredriksson <i>et al.</i>	4/4
	CASP9	< 0.001	Fredriksson <i>et al.</i>	2/4
	BCL2L11/Bim	< 0.001	Fredriksson <i>et al.</i>	2/4
	APAF1	< 0.001	Fredriksson <i>et al.</i>	3/4
	CASP10	< 0.001	Fredriksson <i>et al.</i>	1/4
	BID	< 0.001	Fredriksson <i>et al.</i>	2/4
<b>ER stress</b>	DDIT3/CHOP	< 0.001	< 0.05	2/4
	EIF4A1	< 0.001	< 0.001	4/4
	EIF2AK3/PERK	< 0.01	< 0.05	4/4
	ERN1/IRE1 $\alpha$	< 0.001	< 0.001	2/4
	ATF6	< 0.001	< 0.001	2/4
<b>Oxidative stress</b>	KEAP1	< 0.001	< 0.001	2/4
	NRF2	< 0.001	< 0.001	3/4

# Chapter 5

Activation of the Nrf2 response by intrinsic hepatotoxic drugs correlates with suppression of NF- $\kappa$ B activation and sensitizes towards TNF $\alpha$ -induced cytotoxicity.

---

**This chapter has been published as:**

Bram Herpers–\*‡, Steven Wink\*‡, Lisa Fredriksson\*‡, Zi Di\*, Giel Hendriks†, Harry Vrieling†, Hans de Bont\* and Bob van de Water\*§

‡ These authors contributed equally to the manuscript

\*Division of Toxicology, Leiden Academic Centre for Drug Research, Leiden University, Leiden, The Netherlands

†Department of Human Genetics, Leiden University Medical Center, Leiden, The Netherlands

*Activation of the Nrf2 response by intrinsic hepatotoxic drugs correlates with suppression of NF- $\kappa$ B activation and sensitizes towards TNF $\alpha$ -induced cytotoxicity.*

Archives of Toxicology 2015 May 31. [Epub ahead of print]



## 1. Abstract

Drug-induced liver injury (DILI) is an important problem both in the clinic as well as in the development of new safer medicines. Two pivotal adaptation and survival responses to adverse drug reactions are oxidative stress and cytokine signalling based on activation of the transcription factors Nrf2 and NF- $\kappa$ B, respectively. Here we systematically investigated Nrf2 and NF- $\kappa$ B signalling upon DILI-related drug exposure. Transcriptomics analyses of 90 DILI compounds in primary human hepatocytes revealed that a strong Nrf2 activation is associated with a suppression of endogenous NF- $\kappa$ B activity. These responses were translated into quantitative high content live cell imaging of induction of a selective Nrf2 target, GFP-tagged Srxn1, and the altered nuclear translocation dynamics of a subunit of NF- $\kappa$ B, GFP-tagged p65, upon TNFR signalling induced by TNF $\alpha$  using HepG2 cells. Strong activation of GFP-Srxn1 expression by DILI compounds typically correlated with suppression of NF- $\kappa$ B nuclear translocation, yet reversely, activation of NF- $\kappa$ B by TNF $\alpha$  did not affect the Nrf2 response. DILI compounds that provided strong Nrf2 activation, including diclofenac, carbamazepine and ketoconazole, sensitized towards TNF $\alpha$ -mediated cytotoxicity. This was related to an adaptive primary protective response of Nrf2, since loss of Nrf2 enhanced this cytotoxic synergy with TNF $\alpha$ , while KEAP1 down regulation was cytoprotective. These data indicate that both Nrf2 and NF- $\kappa$ B signalling may be pivotal in the regulation of DILI. We propose that the NF- $\kappa$ B inhibiting effects that coincide with a strong Nrf2 stress response likely sensitize liver cells to pro-apoptotic signalling cascades induced by intrinsic cytotoxic pro-inflammatory cytokines.

**Keywords:** Drug-induced liver injury; live-cell imaging; Nrf2 activation; oxidative stress; NF- $\kappa$ B signalling

## 2. Introduction

Drug safety issues that lead to drug-induced liver injury (DILI) are the major reason for drug-related hospitalizations and drug withdrawals. Often with no overt changes in hepatocellular toxicity parameters (e.g. rise in alanine or aspartate aminotransferase (ALT/AST) levels or increased total bilirubin) found in pre-clinical settings, drugs are (unknowingly) safely marketed until more than 1 in 10,000 drug users demonstrate signs of liver failure [6]. Novel, predictive systems for DILI based on mechanistic understanding will be essential to pave the way forward for improved drug safety assessment.

The common notion around DILI is that drugs affect the intracellular biochemistry of liver cells, either elicited by the parent drug, its metabolites or the metabolic shift the drug conveys upon uptake [6, 281]. Although often idiosyncratic there is a need to understand the key events that are critical mechanistic determinants of human DILI. Perturbations of immune mediated signalling seems an important event in DILI [282]. In particular, TNF $\alpha$ -mediated signalling seems an important contributor to sensitize liver cells to drug-induced hepatocyte toxicity both in vitro [244] as well as in vivo [283]. TNF $\alpha$  mediates intracellular signalling through activation of NF- $\kappa$ B transcription factor [284]. NF- $\kappa$ B transiently translocates to the nucleus to activate downstream (cytoprotective) target genes including chemokines, inhibitor of apoptosis proteins family members (IAPs) and anti-apoptotic Bcl2 family members [285]. We demonstrated that for diclofenac the synergy with TNF $\alpha$  to kill hepatocytes is directly related to inhibition of NF- $\kappa$ B

nuclear translocation and activation, and that inhibition of NF- $\kappa$ B signalling sensitizes towards cytotoxicity caused by diclofenac [38].

Bioactivation of drugs contributes to the formation of reactive metabolites which is shown to be a risk factor in DILI [286]. These reactive metabolites typically provoke a cellular oxidative stress environment thereby initiating the stabilization and activation of the transcription factor Nrf2 [287]. Subsequent downstream target gene activation by Nrf2 contributes to adaptation and protection of cells against oxidative stress. Likewise Nrf2 deletion in the liver severely increases the sensitivity towards drug-induced liver failure [113, 288]. In some studies it has been shown that Nrf2 activation can act to suppress NF- $\kappa$ B-based immune signalling responses [289] which is interesting as this would suggest Nrf2 could be involved in NF- $\kappa$ B suppression in certain situations including DILI. So far there is no systematic evaluation on the relationship between Nrf2 and NF- $\kappa$ B activation in DILI.

Here we investigated whether drugs with known risk of DILI invoke specific cellular stress and defense pathways (NF- $\kappa$ B and Nrf2) that predict the degree of drug toxicity and whether associations between these pathways exist. We investigated the transcriptional response to 90 DILI-associated drugs as well as several cytokines/growth factors in primary human hepatocytes (PHH) at multiple concentrations and time-points, based on publicly available data [70]. To translate these findings to high throughput approaches we established novel GFP-based reporter cell lines to quantitatively assess Nrf2 and NF- $\kappa$ B activation on a cell-to-cell basis and amenable for high content high throughput live-cell imaging. Our combined data indicate that the degree of oxidative stress in liver cells negatively correlates with NF- $\kappa$ B activity and that the inability to adequately respond to inflammatory responses upon drug exposure predisposes liver cells towards cell death. We propose that our integration of live cell high content imaging models to determine Nrf2 and NF- $\kappa$ B activation as well as cytotoxicity is likely to contribute to improve the discrimination of novel drug entities that are intrinsically at risk for DILI.

### **3. Materials and Methods**

#### **3.1. Reagents**

All drugs were acquired from Sigma-Aldrich and freshly dissolved in DMSO, except for menadione and naproxen (in PBS). Human TNF $\alpha$  was purchased from R&D systems and stored as 10  $\mu$ g/mL in 0.1% BSA in PBS aliquots.

#### **3.2. Cell culture**

Human hepatoma HepG2 cells were acquired from ATCC (clone HB8065) and maintained and exposed to drugs in DMEM high glucose supplemented with 10% (v/v) FBS, 25U/mL penicillin and 25 $\mu$ g/mL streptomycin. The cells were used between passage 5 and 20. For live cell imaging, the cells were seeded in Greiner black  $\mu$ -clear 96 wells plates, at 20,000 cells per well.

#### **3.3. Gene expression analysis.**

CEL files were downloaded from the Open TG-GATEs database for all DILI-related compounds (see Supplementary Table 1): "Toxicogenomics Project and Toxicogenomics Informatics Project under CC Attribution-Share Alike 2.1 Japan" <http://dbarchive.biosciencedbc.jp/en/open-tggates/desc.html>. Probe annotation was performed using the hthgu133pluspmhsentrezg.db package version 17.1.0 and Probe mapping was performed with hthgu133pluspmhsentrezgcdf

downloaded from NuGO ([http://nmg-r.bioinformatics.nl/NuGO\\_R.html](http://nmg-r.bioinformatics.nl/NuGO_R.html)). Probe-wise background correction (Robust Multi-Array Average expression measure), between-array normalization within each treatment group (quantile normalization) and probe set summaries (median polish algorithm) were calculated with the `rma` function of the Affy package (Affy package, version 1.38.1). [228] The normalized data were statistically analyzed for differential gene expression using a linear model with coefficients for each experimental group within a treatment group. [258]

A contrast analysis was applied to compare each exposure with the corresponding vehicle control. For hypothesis testing the empirical bayes statistics for differential expression was used followed by an implementation of the multiple testing correction of Benjamini and Hochberg [254] using the LIMMA package [259].

### 3.4. Cluster analysis of oxidative stress and inflammation regulated gene sets.

A gene set for oxidative stress and a gene set for inflammatory signalling was generated using several databases (see Supplementary Fig 1). From Ingenuity Pathway Analysis (version 18841524) the genes present in the following pathways were extracted: NRF2-mediated Oxidative Stress Response, Death Receptor Signalling, NF- $\kappa$ B Signalling, TNFR1 Signalling, TNFR2 Signalling and Toll-like Receptor Signalling. From the Gene Ontology project [290], genes associated with the following terms were obtained using AmiGO 2 version: 2.2.0 [291]. For oxidative stress: "response to oxidative stress" GO:0006979 and for inflammatory signalling: "regulation of inflammatory response" GO:0050727, both queries with filters evidence type closure: "experimental evidence" and taxon closure label: "Homo sapiens".

From the Molecular Signatures Database (MSigDB) [292] the following genesets from BioCarta "BIOCARTA NRF2 PATHWAY" for oxidative stress and "BIOCARTA NFKB PATHWAY", "BIOCARTA DEATH PATHWAY", "BIOCARTA TNFR1 PATHWAY", "BIOCARTA TNFR2 PATHWAY" and "BIOCARTA TOLL PATHWAY" for inflammatory signalling.

From Kyoto Encyclopedia of Genes and Genomes (KEGG Release 71.0, July 1, 2014): [293]. "NF-kappa B signalling pathway", "TNF signalling pathway" and "Toll-like receptor signalling pathway" for inflammatory signalling. No entry for Nrf2 or oxidative stress was found. From Reactome (Version 48) [294] "innate immune system" and "detoxification of reactive oxygen species" for the inflammatory and oxidative stress signalling, respectively. From "TRANSFAC® (www.biobase-international.com/transcription-factor-binding-sites) from BIOBASE

Corporation" [295] the genes bound by factor NFE2L2 and RELA. From all databases a total of 490 and 175 unique genes were obtained for inflammatory and oxidative stress signalling, respectively. As a next step to determine if the selected genes are actively transcribed in Primary Human Hepatocytes (PHH) of the TG-GATES dataset another selection step was performed using the oxidative stress model compounds diethyl maleate and butylated hydroxyanisole and inflammatory model treatments TNF $\alpha$ , LPS and interleukin 1 $\beta$ ; both for the high dose 8 hours and 24 hours data. The oxidative stress gene-set was filtered based on a multiple testing corrected p-value of 0.05, minimum average expression of 5 (log2) and a minimum absolute log2 fold change of 1.5 within the oxidative stress model compound subset resulting in 55 genes. The inflammatory signalling gene-set was filtered based on a multiple testing corrected p-value of 0.05, minimum average expression of 5 (log2) and a minimum absolute log2 fold change of 2 within the inflammatory signalling model treatment subset resulting in 82 genes. The log2 fold change values

for all DILI treatments and controls were gathered followed by manhattan distance measure and ward clustering using the NMF package (version 0.20.5) [227]. Different log<sub>2</sub> fold change threshold values were used to obtain similar gene-set sizes.

The DILI-Score annotation was adapted from a manual literature survey performed by Astrazeneca [241]. The DILI concern and SeverityScore was largely based on a text mining study of FDA-labels [264]

### 3.5. Ingenuity Pathway Analysis

Differentially expressed genes for all DILI compounds in the TG-GATEs dataset were selected based on a minimal log<sub>2</sub> fold change of 1.3 (fold change of 2.5 X with respect to matched control), a maximum multiple testing corrected p-value of 0.05 and a minimum average log<sub>2</sub> expression of 7 within the treatment groups (Supplementary Fig 1) Classification of the selected genes according to their biological and toxicological functions were generated through the use of QIAGEN's Ingenuity Pathway Analysis (IPA®, QIAGEN Redwood City, [www.qiagen.com/ingenuity](http://www.qiagen.com/ingenuity))" which finds associated canonical pathways based on the selected gene sets. P-values are calculated using right-tailed Fisher Exact Test and represented as  $-\log_{10}$  (p-values). The p-values were extracted for the "Nrf2-mediated oxidative stress response" pathway representing oxidative stress and as representation for "inflammatory signalling" the average of the p-values of pathways "Toll-like receptor signalling", "death receptor signalling", "TNFR1 signalling", "TNFR2 signalling" and "NF- $\kappa$ B signalling" was calculated. For each treatment the average magnitude of the log<sub>2</sub> fold change values of the genes responsible for the significance of the oxidative stress and inflammatory pathways was calculated and displayed as an arrow vector above the  $-\log_{10}$  p-value bars of the bargraph. The number of genes responsible for the significance of the individual pathways is color coded from blue (low number of genes) to pink (high number of genes).

### 3.6. Generation of GFP-tagged cell lines

HepG2 cells stably expressing human GFP-p65 as described in [38]. Mouse sulfiredoxin (Srxn1) was tagged with GFP at the C-terminus using BAC recombineering [13] and stably introduced into HepG2 cells by transfection and 500  $\mu$ g/ml G-418 selection.

### 3.7. RNA interference

siRNAs against human NFE2L2 (Nrf2) and KEAP1 were acquired from Dharmacon (ThermoFisher Scientific) as siGENOME SMARTpool reagents, as well as in the form of four individual siRNAs. HepG2 cells were transiently transfected with the siRNAs (50nM) using INTERFERin (Polyplus) as described previously [38].

### 3.8. Western blotting

Samples were collected by direct cell lysis (including pelleted apoptotic cells) in 1x sample buffer supplemented with 5% v/v  $\beta$ -mercaptoethanol and heat-denatured at 95°C for 10 minutes. The separated proteins were blotted onto PVDF membranes before antibody incubation in 1% BSA in TBS-Tween20. Antibodies: mouse-anti-GFP (Roche); rabbit-anti-I $\kappa$ B $\alpha$  (Cell Signalling); rabbit-anti-Nrf2 (H300, Santa-Cruz); mouse-anti-Cleaved Caspase-8 (Cell Signalling); rabbit-anti-PARP (Cell Signalling); mouse-anti-Tubulin (Sigma); mouse-anti-actin (Santa-Cruz).

### **3.9. Microscopy**

Real-time cell death induction was determined by monitoring the accumulation of Annexin-V-Alexa633 labeled cells over a 24 hour time period [261]. For this, transmission and Alexa633 images of the same area with cells were taken automatically every 30 minutes using a BD Pathway™ 855 bioimager with CCD camera and a 10x objective with an image resolution of 608X456 (binning 2).

Accumulation of Srxn1-GFP or nuclear oscillation of GFP-p65 was monitored using a Nikon Eclipse Ti confocal microscope (lasers: 488nm and 408nm), equipped with an automated stage, Nikon 20x Dry PlanApo VC NA 0.75 objective and perfect focus system. Images were acquired at 512X512 pixels. Prior to imaging at >20x magnification, HepG2 cells were loaded for 45 minutes with 100ng/mL Hoechst<sub>33342</sub> to visualize the nuclei, upon which the Hoechst-containing medium was washed away to avoid Hoechst phototoxicity [224]. Srxn1-GFP cells were imaged every 30 minutes across a 24 hour time span, GFP-p65 cells every 6 minutes for 6 hours.

### **3.10. Image quantification**

To quantify the total pixel area occupied by cells or the number of cells per field imaged, transmission images and Hoechst images respectively were analyzed using ImagePro 7.0 (Media Cybernetics). The accumulation of dead cells or the appearance of Srxn1-GFP positive cells was quantified as the total number of pixels above background. The Annexin-V-positive pixel total was normalized for the total cell area. The number of adjacent fluorescent Srxn1-GFP pixels above background (with a minimum size of 45 pixels, which is about 1/4th of average cell size) was multiplied by the average density of those pixels as a measure for the GFP signal-intensity increase and normalized for the amount of nuclei.

To quantify the nuclear translocation of GFP-p65, nuclei (Hoechst) masks are segmented and tracked in ImageJ to define the GFP-p65 nuclear intensity, followed by cytoplasm segmentation. The normalized nuclear / cytoplasmic intensity ratio for each cell is recorded and further analyzed for different oscillation features, also using ImageJ, including the number of translocations, time period of each individual peak, intensity of the peaks, delay between peaks, and nuclear entry and exit rates [296].

### **3.11. Statistics**

All experiments are performed at least in triplicate. Error bars indicate Standard Error. Statistical comparisons were done in a one-way ANOVA. P-value indications: P<0.05 (\*); P<0.01 (\*\*); P<0.001 (\*\*\*).

## 4. Results

### 4.1. Enhanced Nrf2 activation is associated with suppression of endogenous NF- $\kappa$ B activity in PHH.

The Japanese Toxicogenomics Project has generated the Open TG-GATEs data repository of gene expression profiles in primary human hepatocytes (PHH) upon exposure to 157 compounds of which many are DILI-related, at 1-3 different concentrations and 1-3 time points (2, 8 and 24 hr), including a few pro-inflammatory cytokines, TNF $\alpha$ , IL1 $\beta$  and LPS [70]. We focused on the NF- $\kappa$ B and Nrf2 signalling related gene sets extracted from several key databases as described in detail the material and methods section. Ingenuity Pathway Analysis (IPA) for oxidative stress and inflammatory signalling was determined for all DILI compounds in the dataset. Typically a significant modulation of these pathways was observed. A major modulation of the “Nrf2-mediated oxidative stress response” overall related to upregulation of genes linked to this pathway. Interestingly, DILI compounds that showed a strong oxidative stress response also showed a modulation of “inflammatory signalling” related to NF- $\kappa$ B activity (26 compounds,  $p < 0.05$ ) although this was typically associated with down regulation of genes (Fig.1A). This effect was strongest after 24 hour treatment, although a similar association was already observed at 8 hour treatment (Supplementary Fig. 2A).

The above observation indicated an opposite direction of Nrf2-mediated signalling versus NF- $\kappa$ B-related inflammatory signalling by DILI compounds in PHH. Indeed, Nrf2 can negatively affect NF- $\kappa$ B activity [297, 298]. Therefore we next performed a more detailed hierarchical clustering analysis of the altered gene expression induced by all DILI compounds associated with both signalling pathways. As a first step based on different annotation databases we systematically selected a set of Nrf2 signalling-related genes as well as a set of inflammatory signalling related genes. To determine which genes are responsive to oxidative stress and inflammatory stimuli in PHH we included a stringent filtering procedure based on the exposures of PHH in the TG-GATEs data to diethyl maleate and butylated hydroxyanisole for Nrf2 signalling, and TNF $\alpha$ , IL-1 $\beta$  and LPS for inflammatory signalling. We then extracted the differential expression levels for all DILI compounds for the selected 55 and 82 genes related to Nrf2 signalling and inflammatory signalling, respectively. Using an unsupervised hierarchical clustering for all genes and DILI compounds at 24 hour we could clearly distinguish Nrf2 clusters (A', B', C' and E') and NF- $\kappa$ B gene clusters (D', F' and G') (Fig. 1B). Moreover, cytokines and LPS (cluster A) clearly induced a different response compared to all DILI compounds (clusters B-E). DILI compound cluster C gave the strongest overall response both at the level of Nrf2 target gene activation as well as inflammation signalling target gene down regulation; this cluster was slightly enriched in compounds that demonstrate ‘fatal hepatotoxicity’. These effects were not as prominent at 8 hour treatment conditions (Supplementary Fig. 2B).

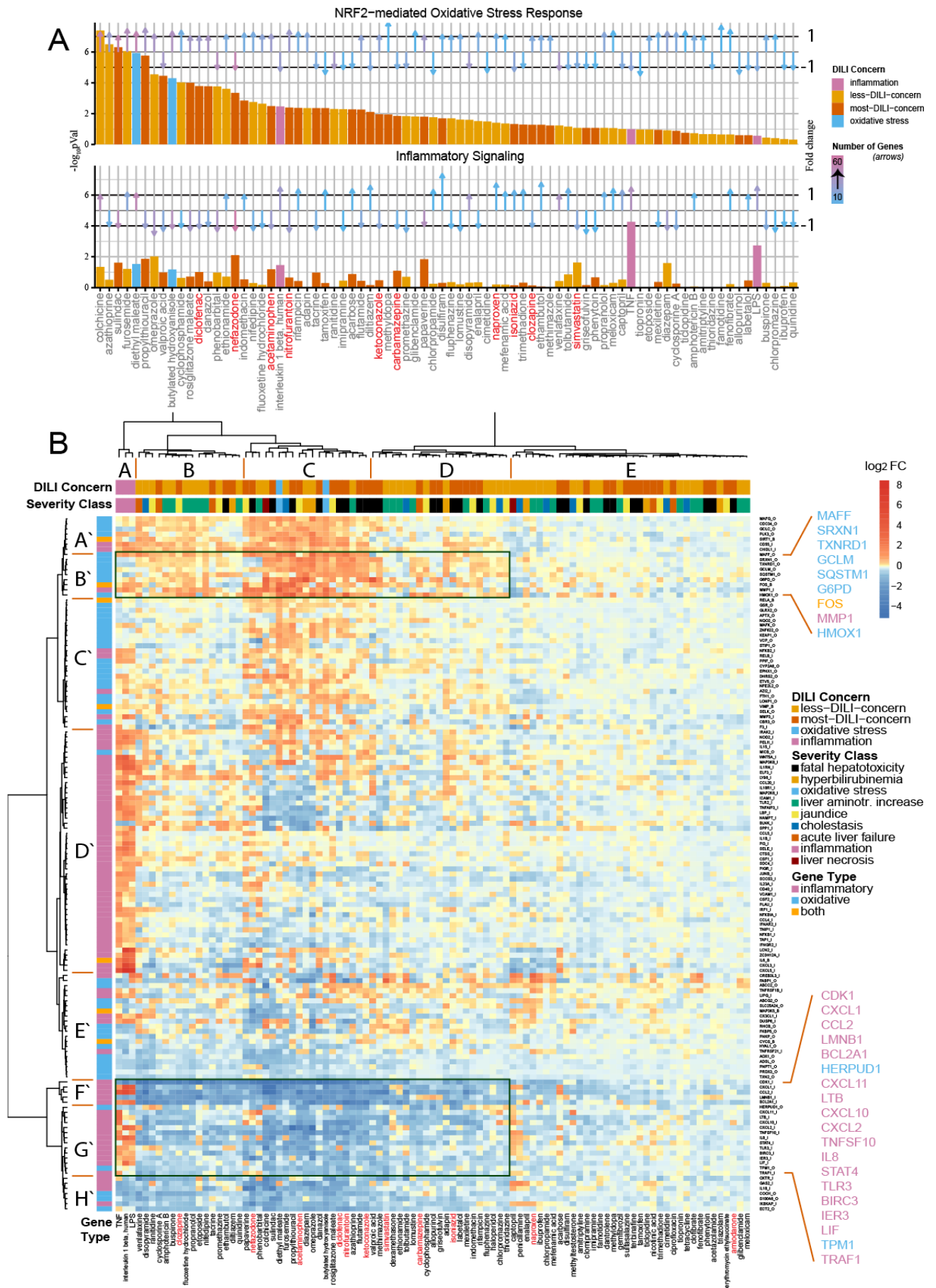
Within the hierarchical cluster analysis two strong gene clusters were prominent in their response to DILI compounds: a first cluster (cluster B') with Nrf2 target genes that were mostly upregulated by DILI compounds but hardly affected by cytokines, including Maff, Srxn1, Txnrd1, GCLM, SQSTM1, G6PD, FOS, MMP1 and HMOX1, mostly prototypical Nrf2 target genes (see Fig. 2 for examples); and a second cluster (clusters F' and G') with inflammatory genes that were strongly upregulated by the cytokines and LPS, but were strongly downregulated by the same DILI compounds that caused upregulation of Nrf2 targets, and included CXCL1, CCL2, BCL2A1, CXCL11,

CXCL2; (see Fig. 2 for examples). To determine the correlation with the DILI severity, we performed a similar cluster analysis for only severe DILI compounds and non-severe DILI compounds based on the FDA drug labeling classification [264] (Supplementary Figs. 3 and 4). Severe DILI compounds mostly mimicked the overall DILI hierarchical cluster analysis showing the strongest inverse relationship between Nrf2 activity and NF- $\kappa$ B suppression and included diclofenac, sulindac, ketoconazole and acetaminophen.

Altogether these findings indicate a strong correlation between the ability of DILI compounds to induce an adaptive Nrf2 response and the suppression of NF- $\kappa$ B activity.



**Figure 1: Gene expression analysis of 24 hours highest concentration primary human hepatocyte subset of the TG-GATES dataset.** (A) Differentially expressed genes were analyzed with ingenuity pathway analysis as described in detail in the material and methods section. In the top panel the  $-\log_{10}$  p-values for the corresponding pathways are displayed for the Nrf2-mediated oxidative stress response. The top panel displays the mean of the p-values for the inflammatory related pathways. Compounds are ordered according to highest significance of the Nrf2-mediated oxidative stress response. The compound labels in red are the compounds chosen in this study. The color of the bars correspond to DILI-severity type or to the oxidative stress/ inflammatory model-compounds (model-compound type). The length of the arrows correspond to the mean fold change of the genes which are responsible for the significance of the corresponding pathways. The direction of the arrow corresponds to either mean up- or down-regulation of these genes. The color of the arrows corresponds to the number of these genes ranging from 10 to 60 genes. (B) Unsupervised hierarchical clustering of all DILI compounds and a selected gene set as described in detail in the material and methods section. Blue corresponds to down-regulated genes and orange to up-regulated genes, the brightness corresponds to the magnitude of the fold changes. The top color-coded bar corresponds to the DILI-Concern or model-compound type. The second top color-coded bar corresponds to the Severity Class or model-compound type. The left color-coded bar corresponds to the gene type- either inflammatory genes, oxidative genes or both. Important clusters on gene-level are represented from A` to H`, and important compound-level clusters with A-E for easy reference from the text. Compounds used in this study are color-coded in red.





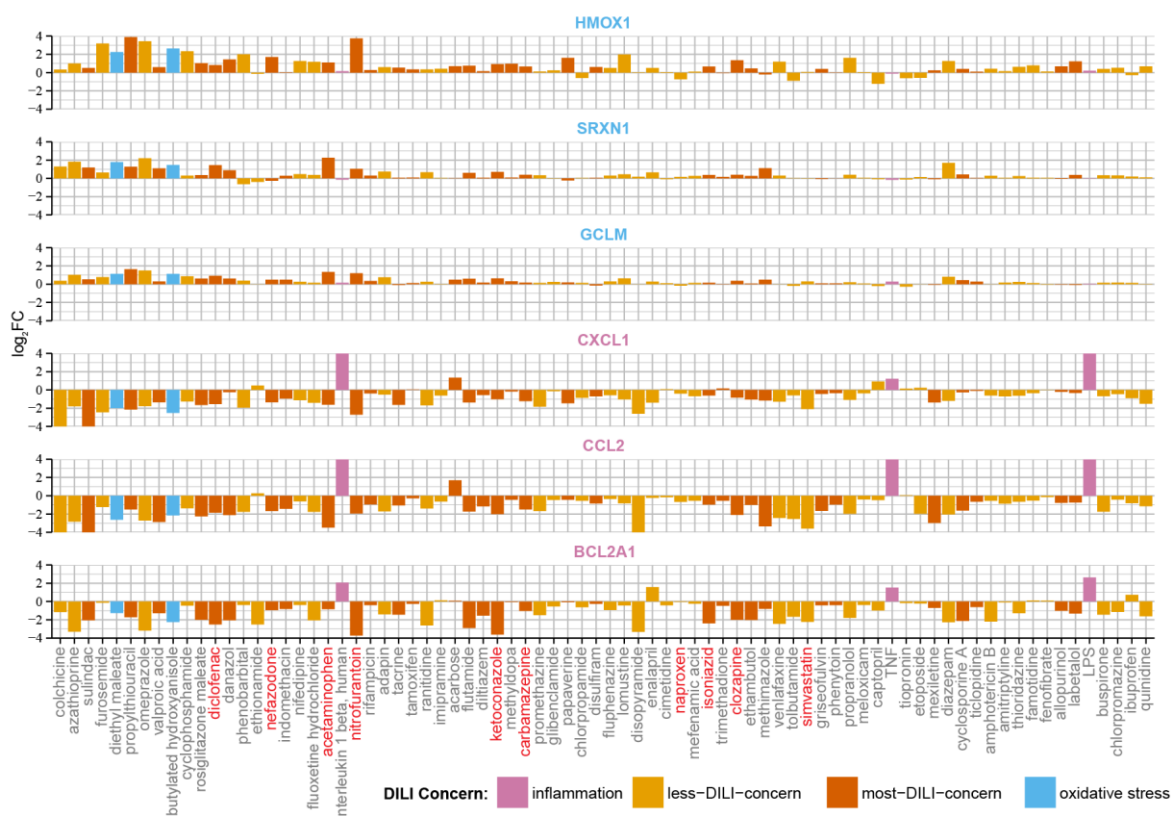


**Figure 2: Fold changes of example genes from the two prominent clusters from the unsupervised hierarchical cluster analysis.** Oxidative stress genes HMOX, SRXN1, GCLM (blue) from cluster B' from Fig. 1B and inflammatory genes CXCL1, CCL2, BCL2A1 (purple) from clusters F' & G'. Color codes are as in Fig. 1.

#### 4.2. A BAC-Srxn1-GFP HepG2 cell line reports xenobiotic-mediated Nrf2 activation.

The most prominent differences between NF- $\kappa$ B and Nrf2 responses in the PHH dataset were observed at high concentrations and at 24 hours of drug exposure. Like all signalling events, the transcriptional activity of Nrf2 and NF- $\kappa$ B are dynamic in nature and may show differential activity over time. Therefore we sought to monitor the activity of these two transcription factors in living cells using GFP-tagging technology allowing their dynamic analysis. As PHH dedifferentiate within 24h *in vitro* when grown in 2D cultures [299] and are not amenable for stable expression of GFP reporter constructs, we chose the liver model cell line HepG2 to generate stable fluorescent reporters for both NF- $\kappa$ B and Nrf2 signalling. As a first step, to enable reliable quantitative measurements of the dynamic effect of drug exposure on Nrf2 activity using live cell imaging, we generated a HepG2 reporter cell line based on bacterial artificial chromosome (BAC) recombineering [48] of the Nrf2 target gene sulfiredoxin (Srxn1) [13] which was part of the predictive DILI cluster. We tagged the Srxn1 gene with GFP at its C-terminus and established a stably expressing HepG2 Srxn1-GFP cell line under control of its own entire promoter region. To monitor for its functionality as an Nrf2 reporter, we exposed the HepG2 cells to menadione (20  $\mu$ M, MEN) and di-ethyl maleate (100  $\mu$ M, DEM) as proto-typical model activators of Nrf2, as well as diclofenac and ketoconazole, of which the PHH data revealed their capacity to strongly activate an Nrf2 response. DEM, MEN, DCF and KTZ all stabilized Nrf2 levels in our cells (Fig. 3B & C). Live-cell imaging by confocal microscopy followed by automated image quantification showed that the Srxn1-GFP reporter is activated with different kinetics by different compounds with MEN and DEM

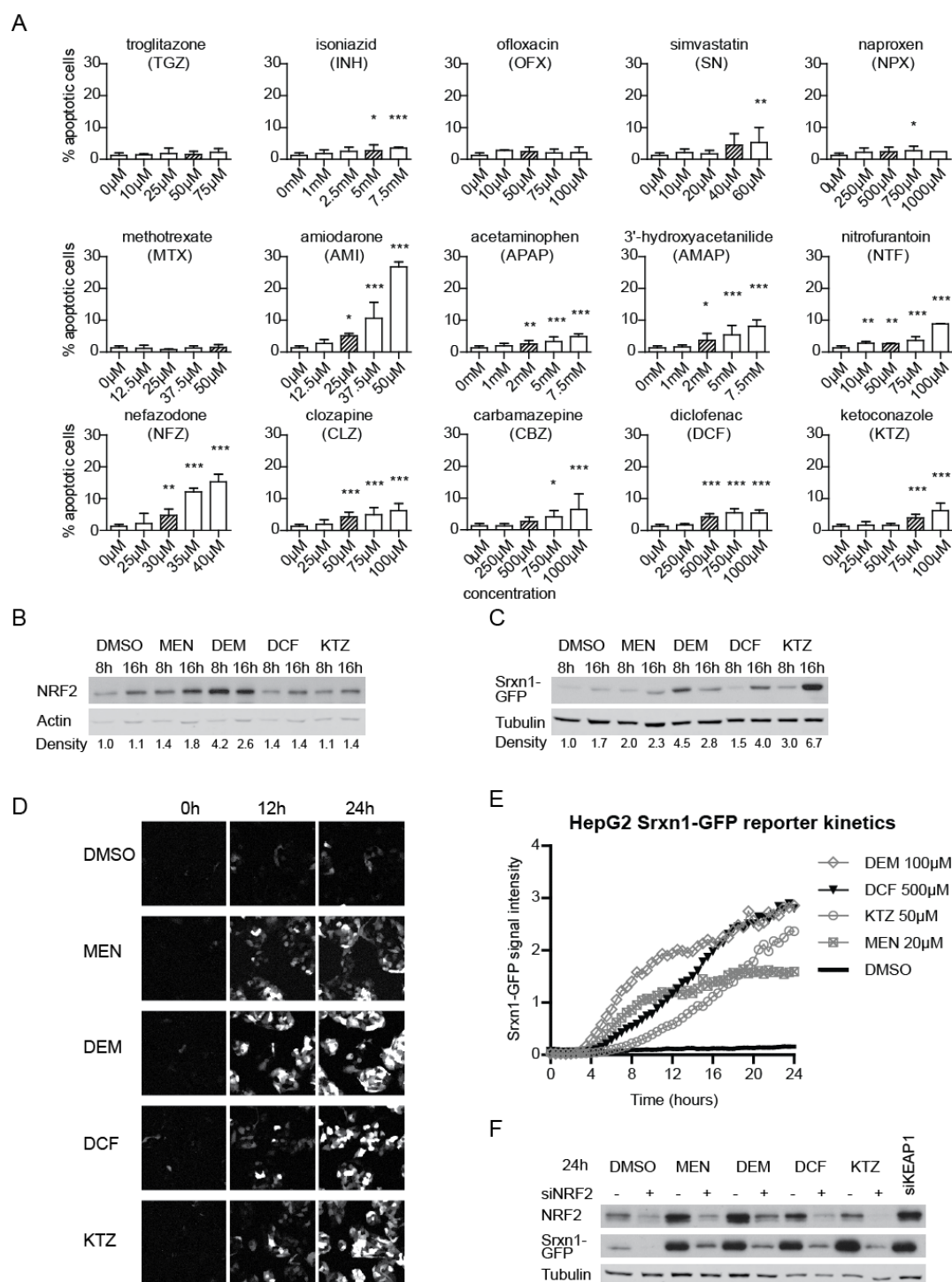


**Figure 3: Srnx1-GFP BAC HepG2 reporter cell line is dependent on Nrf2/KEAP1 signalling.** (A) Cell injury assay using Annexin-V-Alexa-633 staining after 24 hour exposure to our compound set. (B) Western blot of Nrf2 expression in HepG2 cells exposed for 8 or 16 hours to menadione (MEN), diethyl-maleate (DEM), diclofenac (DCF) or ketoconazole (KTZ). Density quantification is relative to Actin levels, normalized to DMSO. (C) Western blot of GFP expression in HepG2 Srnx1-GFP cells as in (B). Density quantification below is relative to tubulin levels. (D) Stills of time-lapse imaging of HepG2 Srnx1-GFP cells exposed to Nrf2 inducers. (E) Quantification of the Srnx1-GFP reporter response kinetics. (F) siRNA-mediated knockdown of Nrf2 (+ siNrf2) or KEAP1 (siKEAP1) or mock treatment (-) in HepG2 Srnx1-GFP cells exposed to DMSO, MEN, DEM, DCF or KTZ for 24h.

being fast inducers, likely related to their direct mode-of-action, and diclofenac and ketoconazole showing a delayed response, possibly related to bioactivation (Fig.3B-E); this effect was directly

related to the expression of the GFP-Srxn1 fusion product. Finally, to confirm that our Srxn1-GFP reporter is under direct control of the KEAP1/Nrf2 pathway, we transiently transfected the HepG2 Srxn1-GFP cells with siRNA oligos targeting Nrf2 or KEAP1. siRNA targeting Nrf2 prevented the stabilization of Nrf2 and consequently inhibited the Srxn1-GFP induction for all compounds. In contrast, as expected KEAP1 knock down itself stimulated Srxn1-GFP expression (Fig. 3F). These data show that the Srxn1-GFP signal intensity depends on the functional KEAP1/Nrf2 pathway.

#### **4.3. Drug-induced cell death of human HepG2 cells.**

Next we selected a set of DILI compounds for further characterization. Since the opposite regulation of Nrf2 versus NF- $\kappa$ B by DILI compounds was largely seen for severe DILI compounds that often require bioactivation, we selected a small panel of compounds that was contained within the TG-GATEs dataset (acetaminophen (APAP), carbamazepine (CBZ), clozapine (CLZ), diclofenac (DCF), ketoconazole (KTZ), nitrofurantoin (NTF) and nefazadone (NFZ)) as well as some DILI compounds that do not require bioactivation and do not activate the Nrf2 pathway much in PHH (amiodarone (AMI), naproxen (NPX) and simvastatin (SN)); we further complemented our compound set with a few additional drugs that fit in these categories but were not included in the TG-GATEs (ofloxacin (OFX), isoniazid (INH), methotrexate (MTX), 3'-hydroxyacetanilide (AMAP) and troglitazone (TGZ)) (Supplementary Table 2). We first tested whether these compounds induced sufficient cell injury that resulted in cell death at similar concentrations as used for the PHH dataset (Fig. 3A). Based on automated live cell imaging of Annexin-V positive cells we identified concentration-dependent HepG2 cell death for AMI, APAP, AMAP, CBZ, CLZ, DCF, KTZ, NFZ, NTF and SN. Little cell death was observed for INH, MTX, NPX, OFX and TGZ. For further experiments we continued with a mildly cytotoxic concentration (<10 % apoptosis onset) for each compound (indicated in Supplementary Fig. 5) to establish the effect on Nrf2 activation, NF- $\kappa$ B signalling and the cytotoxic interaction between DILI compounds and the pro-inflammatory cytokine TNF $\alpha$ .

#### **4.4. DILI compounds activate the Nrf2 stress response independent of TNFR activation.**

The PHH dataset predicted that APAP, CBZ, CLZ, DCF, KTZ and NTF potently activate the Nrf2 response; that INH, NFZ and NPX mildly induce Nrf2 and that AMI and SN weakly activate it (Supplementary Fig. 6). Using live-cell imaging we tested whether these same drugs activated the Srxn1-GFP response in HepG2 cells (Fig. 4A-B). We observed that APAP induced the oxidative stress reporter as soon as 4 hours after compound exposure, which is remarkable considering the low CYP2E1 levels in HepG2 cells however this does indicate that the HepG2 is sensitive to oxidative stress-adaptation signalling. Possibly APAP induces oxidative stress through other means than CYP2E1-mediated bioactivation, possibly involving direct modulation of the mitochondrial respiratory chain. NTF, DCF, KTZ, CLZ, CBZ and NFZ strongly induced the Srxn1-GFP reporter as early as 8 hours after compound exposure. AMI, MTX and NPX showed weak Srxn1-GFP induction with delayed kinetics, around 16 hours after compound exposure. INH, OFX, SN and TGZ did not lead to oxidative stress induction within the 24 hour imaging period in our cell system. These

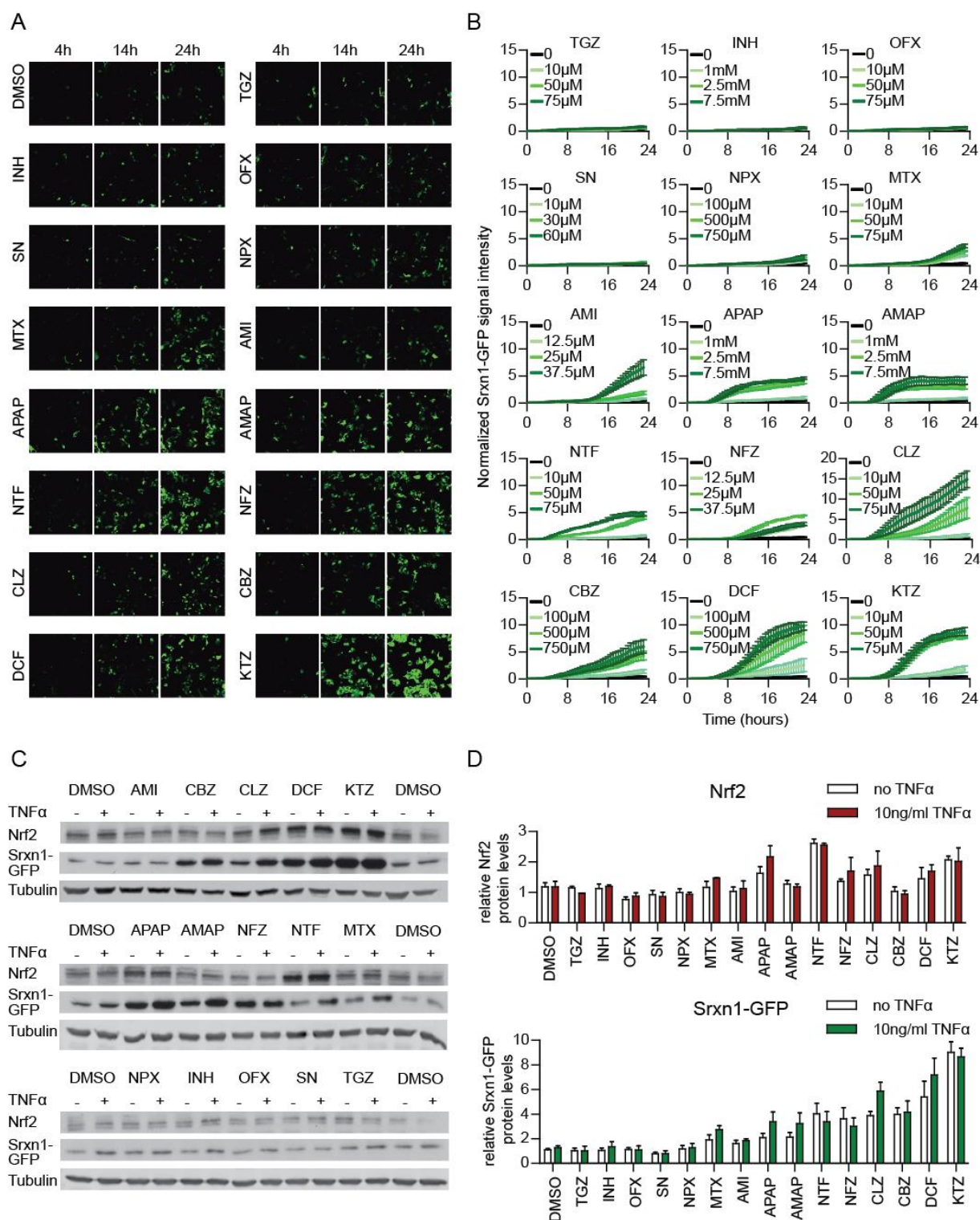


**Figure. 4: Drug exposure induces dynamically divergent Nrf2 responses.** (A) Stills of confocal live-cell imaging in HepG2 Srxn1-GFP cells upon drug exposure (shown are 4, 14 and 24 hours). (B) Quantification of the Srxn1-GFP signal appearing upon exposure to increasing drug doses (averages shown of 4 independent replicates). (C) Western-blots for Nrf2 and GFP expression after 24 hour drug exposure in HepG2 Srxn1-GFP cells, either with or without co-exposure to 10ng/ml TNF $\alpha$ . (D) Quantification of the Nrf2 and Srxn1-GFP protein levels, 24h after drug +/- TNF $\alpha$  exposure (averages of 3 replicates).

findings indicate that the PHH results on the Nrf2 pathway activation correlate well with the HepG2 Srxn1-GFP reporter cell observations.

TNF $\alpha$  promotes NF- $\kappa$ B target gene activation through binding to TNFRSF1A. TNF $\alpha$  binding to its receptor has been suggested to promote Nrf2 activation [300], while the PHH dataset predicted no effect of TNF $\alpha$  on Nrf2 responses. To confirm this we tested whether drug exposure in combination with 10 ng/mL TNF $\alpha$  influenced the drug-induced Nrf2 response (Fig. 4C and D). We observed neither a significant rise nor a decrease in Nrf2 stabilization or Srxn1-GFP expression at 24h when the HepG2 Srxn1-GFP cells were exposed to TNF $\alpha$  alone or in combination with an 8 hour drug pre-exposure. This suggests that TNF $\alpha$ -mediated NF- $\kappa$ B signalling does not influence Nrf2 target gene activation caused by deleterious DILI compounds.

#### 4.5. DILI compounds cause a perturbation of NF- $\kappa$ B signalling.

To test whether Nrf2 activation by DILI compounds is associated with modulation of NF- $\kappa$ B signalling, we made use of a previously established HepG2 cell line expressing GFP-tagged p65/RelA, a subunit of the dimeric transcription factor NF- $\kappa$ B [38]. As reported [38], an 8 hour DCF pre-exposure delays the second translocation event (peaking 26 minutes later than vehicle pre-incubated cells) (Fig. 5A). Also NTF (+29 minutes), KTZ (+26 minutes), AMI (+22 minutes), NFZ (+22 minutes) and CBZ (+20 minutes) delayed the oscillation to a similar extent as DCF. Pretreatment with CLZ and MTX only weakly perturbed the appearance of the second translocation response with a delay of 12 and 9 minutes, respectively. Neither AMAP, APAP, INH, OFX, SN nor TGZ significantly influenced the translocation maximum of the second nuclear translocation event.

Our live cell imaging approach allowed detailed cell population-based quantitative analysis of the translocation response to extract various relevant parameters that describe the NF- $\kappa$ B oscillation pattern invoked by TNF $\alpha$  at the single cell as well as the cell population level [296]. This analysis revealed that pre-treatment with AMI, CBZ, DCF, KTZ, NFZ or NTF significantly delayed the time between the first and second NF- $\kappa$ B nuclear translocation maxima that normally occur at 30 minutes and 150 minutes after TNF $\alpha$  exposure, respectively (Fig. 5B). This effect limits the average number of translocation events observed within the 6 hour imaging window (Fig. 5C). Importantly, by evaluating on average ~1,000 cells per condition, we identified that AMI, CBZ, DCF, KTZ, NFZ and NTF induced a sharp decrease in the percentage of cells that undergo three or more NF- $\kappa$ B nuclear translocation events (Fig. 5D). Together, the results indicate that various DILI compounds affect the TNF $\alpha$ -induced NF- $\kappa$ B activation response by modulating its nuclear translocation dynamics. For the compounds with this delayed translocation event the NF- $\kappa$ B target genes are down regulated (Fig. 1A) and all compounds except amiodarone fall within inhibited NF- $\kappa$ B/activated Nrf2 signalling clusters (clusters B-C, and CBZ cluster D, Fig. 1B) suggesting that the delayed translocation could be indicative for lower NF- $\kappa$ B target gene expression.



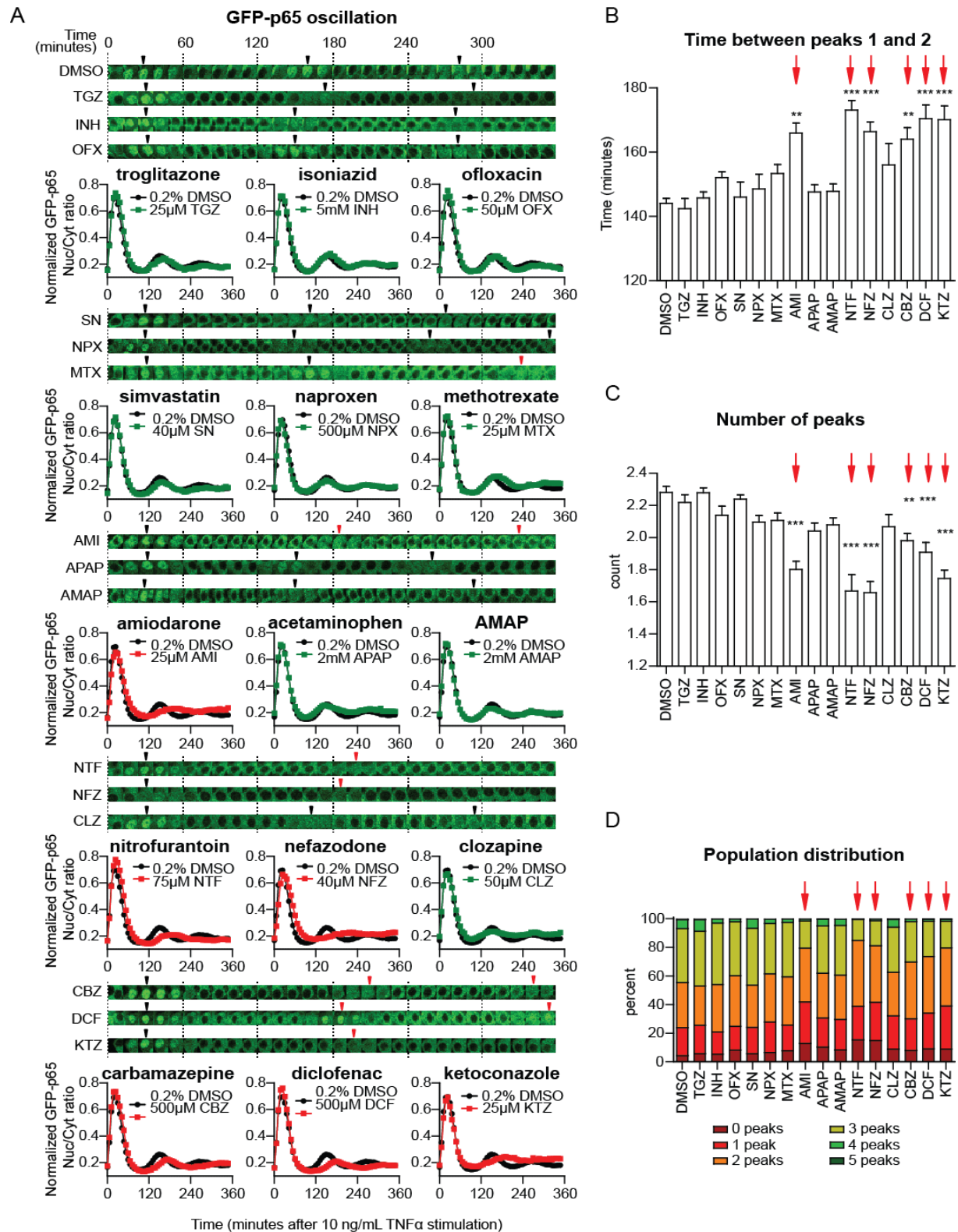


**Figure 5: DILI compounds affect the TNF $\alpha$ -mediated nuclear translocation response of NF- $\kappa$ B.** (A) Time-lapse images of one cell that illustrates NF- $\kappa$ B oscillation upon 10ng/ml TNF $\alpha$  stimulation after an 8 hour drug pre-incubation period. Arrowheads point at the local nuclear translocation maxima ("peaks"). Quantified average of the GFP-p65 nuclear/cytoplasmic intensity ratio (average of 3 experiments, totaling 800-1200 cells), normalized between 0 and 1 to focus on the appearance of the nuclear translocation maxima. (B) Analysis of the NF- $\kappa$ B response: time between peaks 1 and 2. (C) Analysis of the NF- $\kappa$ B response: assessment of the number of peaks. (D) Distribution of the TNF $\alpha$ -stimulated, drug pre-exposed cell population, classified for showing 0 to 5 peaks within the 6 hour imaging period.

#### 4.6. The inhibitory effect of Nrf2 activity on NF- $\kappa$ B signalling promotes the pro-apoptotic role of TNF $\alpha$ in drug-exposed HepG2 cells.

TNF $\alpha$ -mediated signalling seems important in DILI [244, 282]. While TNF $\alpha$ -receptor mediated NF- $\kappa$ B signalling may provide survival signalling through the upregulation of anti-apoptosis genes such as the anti-apoptotic Bcl-2 family member A1 (BCL2A1), activation of the TNFR may in parallel initiate activation of caspase-8 and thereby switch on apoptosis[301]. Since DILI compounds did affect the NF- $\kappa$ B signalling, and therefore possibly suppressed survival signalling, we next investigated whether DILI compounds would also predispose to the onset of TNF $\alpha$ -mediated apoptosis. To address this issue we monitored the rate of HepG2 cell apoptosis by live-cell imaging with Annexin-V-Alexa633 after 8 hour drug pre-exposure and tested whether TNF $\alpha$  co-exposure enhanced the apoptotic response at 24 hours. TNF $\alpha$  enhanced the apoptosis induction upon CBZ and DCF exposure by 18.6% and 9.7% respectively. A smaller increase of 3 to 4% in cell death upon TNF $\alpha$  co-stimulation was found for KTZ, AMI, NFZ and CLZ (Fig. 6A and 6B). Since TNF $\alpha$ -mediated death signalling acts through caspase-8 activation, we anticipated that the synergy for the onset of apoptosis would also be associated with enhanced caspase-8 cleavage. Caspase-8 was markedly increased by TNF $\alpha$  combined with CBZ and DCF, yet for other DILI compounds tested such a caspase-8 activation was not observed, as was expected based on the limited onset of apoptosis (Fig. 6C and 6D). The enhanced caspase-8 cleavage was associated with cleavage of PARP, a well-established caspase substrate which serves as a pivotal marker of onset of apoptosis. This indicates that primarily under CBZ and DCF pretreatment conditions co-treatment with TNF $\alpha$  turns on apoptosis.

**Table 1: Summary of DILI compound modulation of Nrf2 and NF- $\kappa$ B signalling and onset of DILI compound/TNF $\alpha$  cytotoxic synergy.** Full names, abbreviations and function of the drugs chosen for this study. The DILI classification was derived from Chen et al. 2011. The overall results from the current study are summarized as fold induction of the Srxn1-GFP intensity compared to control (Nrf2 response), timing of the GFP-p65 assay, focusing on the delay in the second nuclear translocation event upon TNF $\alpha$  exposure (NF- $\kappa$ B response) and percentage of dead cells as observed by the Annexin-V live assay (including TNF $\alpha$ -enhanced cell death).

Drug name	Abbreviation	Function	DILI label / score	DILI classification	DILI type	DILI concern	Nrf2 response assay (fold induction)	NF- $\kappa$ B oscillation delay upon TNF $\alpha$	Apoptosis assay (+ last 16h TNF $\alpha$ )	Apoptosis effect of TNF $\alpha$ (% increase)	Nrf2 Transcripts up & NF $\kappa$ B Transcripts down
trogliatone	TGZ	antidiabetic	N.A.	N.A.	Acute - cholestatic injury	Most	1.3x	2 min	1.1% (2.6%)	1.5	N.A
isoniazid	INH	antimycobacterial drug	B.W. 8	Fatal hepatotoxicity	Acute - hepatocellular injury	Most	1.0x	2 min	2.8% (3.3%)	0.5	2-9
ofloxacin	OFX	antibiotic	N.A.	N.A.	Acute - hepatocellular injury	Less	1.1x	8 min	2.3% (3.2%)	0.9	N.A
simvastatin	SN	anthyperlipidemic	W/P 3	Liver aminotransferases increase	Acute - hepatocellular injury	Less	1.1x	2 min	2.5% (3.6%)	1.1	2-19
naproxen	NPX	NSAID	W/P 3	Liver aminotransferases increase	Acute - cholestatic injury	Less	1.8x	4 min	2.1% (2.3%)	0.2	2-4
methotrexate	MTX	antineoplastic agent	B.W. 3	Liver aminotransferases increase	Chronic - microvesicular steatosis	Less	3.3x	9 min	1.9% (1.9%)	0	N.A
amiodarone	AMI	antiarrhythmic agent	B.W. 8	Fatal hepatotoxicity	Chronic - steatohepatitis	Most	1.9x	22 min	5.8% (9.0%)	3.2	0-0
acetaminophen	APAP	analgesic and antipyretic	W/P 5	Jaundice	Acute - hepatocellular injury	Most	4.0x	4 min	2.5% (2.5%)	0	12-29
3'-hydroxyacetanilide	AMAP	regionisomer of paracetamol	N.A.	N.A.	N.A.	Less	4.0x	4 min	3.1% (3.4%)	0.3	N.A
nitrofurantoin	NTF	antibacterial	W/P 8	Fatal hepatotoxicity	Chronic - autoimmune hepatitis	Most	4.6x	29 min	2.9% (3.6%)	0.7	15-23
nefazodone	NFZ	antidepressant	B.W. 8	Fatal hepatotoxicity	Acute - hepatocellular injury	Most	4.8x	22 min	3.5% (6.8%)	3.3	13-20
clozapine	CLZ	antipsychotic drug	W/P 25	Cholestasis; steatohepatitis	Acute - cholestatic injury	Most	4.6x	12 min	4.0% (7.7%)	3.7	1-12
carbamazepine	CBZ	antiepileptic drug	W/P 7	Acute Liver Failure	Acute - cholestatic injury	Most	4.1x	20 min	3.9% (22.5%)	18.6	4-9
diclofenac	DCF	NSAID	W/P 8	Fatal hepatotoxicity	Acute - hepatocellular injury	Most	6.7x	26 min	4.5% (14.2%)	9.7	12-23
ketoconazole	KTZ	antifungal antibiotic	B.W. 8	Fatal hepatotoxicity	Acute - hepatocellular injury	Most	8.3x	26 min	5.0% (8.1%)	3.1	9-17

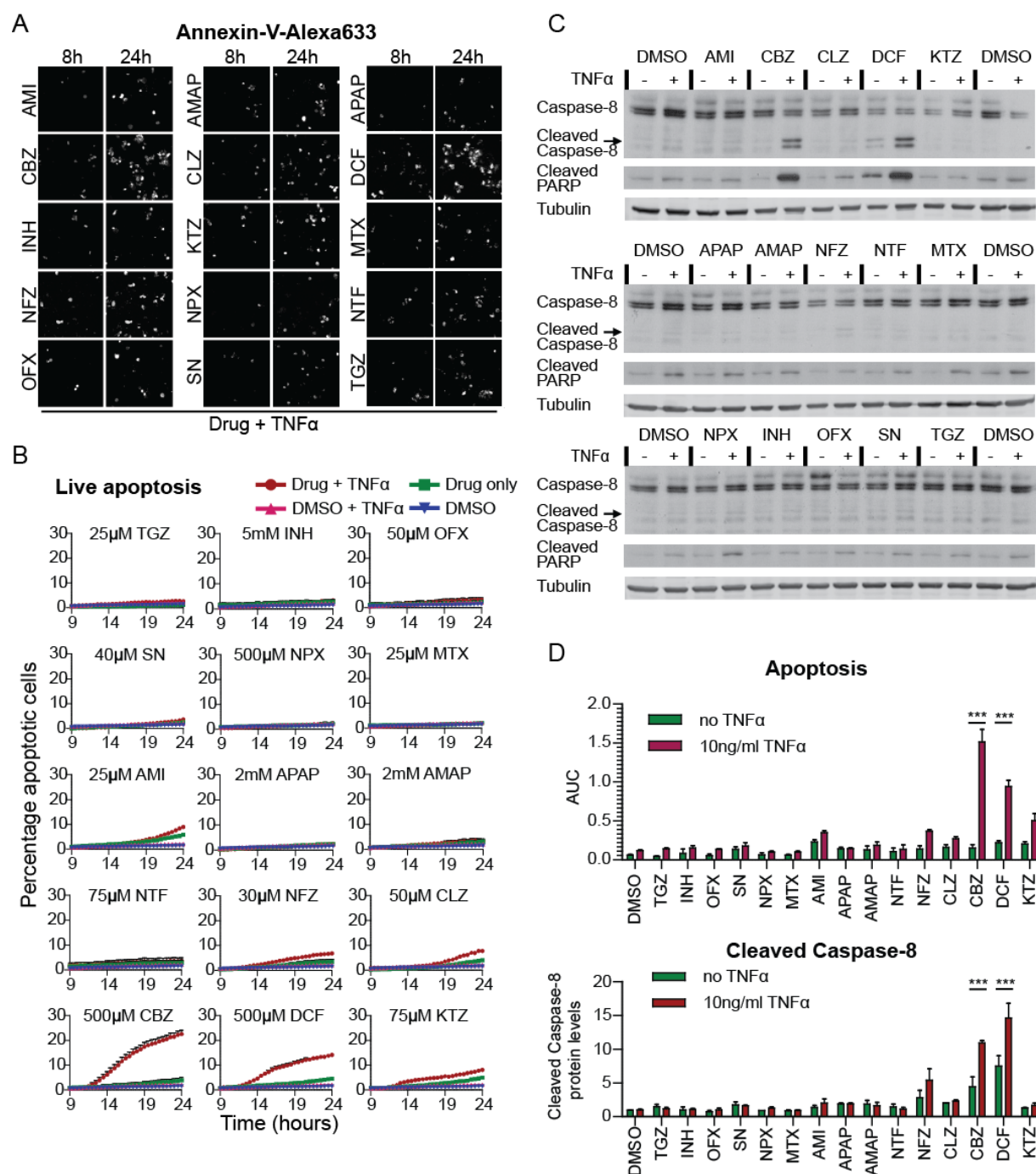


**Figure 6: Adverse DILI compound and TNF $\alpha$  synergy for the onset of cell death.** (A) Still images of time-lapse movies of HepG2 cells exposed to the drugs in co-presence of Annexin-V-Alexa-633, taken at 8 hours (before 10ng/ml TNF $\alpha$  addition) and at 24 hours (16 hours TNF $\alpha$ ). (B) Quantification of the percentage dead cells appearing upon drug only exposure, or in combination with TNF $\alpha$ . Average of 3 to 6 experiments. (C) Western-blot for cleaved caspase-8 and the caspase substrate PARP, induced by 24 hour drug alone or drug-TNF $\alpha$  co-treatment. (D) Comparison of the quantified percentage of dead cells 24 hours after drug (+TNF $\alpha$ ) exposure: the appearance of dead cells in live-cell imaging as area under the curve (AUC) (as in B) and quantification of cleaved caspase-8 protein levels (relative density as in C, average of 3 experiments)



## 5. Discussion

Here we focused on the interplay of two pivotal cellular stress response signalling pathways in drug-induced liver injury: TNF $\alpha$ -mediated NF- $\kappa$ B signalling and chemical stress-induced Nrf2 activation. Extensive transcriptomics data from primary human hepatocyte revealed that the Nrf2 transcriptional program is activated by a majority of different DILI compounds in particular those that are associated with severe DILI. This strong Nrf2 activation correlates with a major downregulation of genes that are under the direct control of NF- $\kappa$ B. We successfully transferred this inverse relationship between Nrf2 activation and NF- $\kappa$ B signalling into a panel of GFP-reporter based high content imaging assays, which now allows the high throughput assessment of their dynamic activation [236]. Using live-cell imaging we established the time-profiles of the activation of these transcription factors and established that various DILI compounds activate Nrf2 activity as well as negatively modulate the NF- $\kappa$ B nuclear oscillation response induced by TNF $\alpha$ . Although no cause and effect relationship between these two signalling pathways has been proven in our study, our data do support an overall working model whereby DILI compounds that strongly affect the Nrf2 response as well as modulate the NF- $\kappa$ B oscillatory response (either directly or indirectly) act in synergy with TNF $\alpha$  to cause a cytotoxic response. An integrated automated high throughput microscopy-based platform that simultaneously measures drug-induced Nrf2 activation, TNF $\alpha$ -induced NF- $\kappa$ B activation and cytotoxicity, will likely contribute to the exclusion or de-prioritization of novel drug entities for further development.

Our data indicate a differential regulation of Nrf2 and NF- $\kappa$ B signalling pathways in primary human hepatocytes (PHH). From the Japanese Toxicogenomics Project a total of 90 DILI compounds have been evaluated. While several DILI compounds caused a strong modulation of most Nrf2 and NF- $\kappa$ B target genes, e.g. nitrofurantoin, diclofenac and ketoconazole, the effect of amiodarone was only modest. Despite the fact that HepG2 cells are notorious for their low level expression of CYP enzymes [207], an enhanced formation of reactive intermediates during drug metabolism may be causative for the activation of the Nrf2 response. However, we cannot exclude the role of other stress response pathways that are intricately linked to the modulation of the Nrf2 response and by themselves are activated by chemical-induced cell injury, including the perturbation of the mitochondria, the endoplasmic reticulum (ER) and the autophagosomes which may result in a secondary source of reactive oxygen species that may initiate an adaptive Nrf2 response [302]. Although the role of these other programs will require further mechanistic investigations, our previous investigations demonstrate that suppression of the Nrf2 adaptive stress response strongly sensitizes cells towards a synergistic toxicity with TNF $\alpha$ , indicating that enhanced oxidative stress predisposes for TNF $\alpha$  sensitization [238].

The PHH transcriptomics data indicated that many DILI compounds themselves suppress the activity of NF- $\kappa$ B target genes. In addition, our imaging data indicate that various DILI compounds suppress the NF- $\kappa$ B oscillatory response. Together this suggests that also under control situations the overall nuclear localization of NF- $\kappa$ B may be limited, thereby precluding the activation of NF- $\kappa$ B target genes. Alternatively a limited activation of NF- $\kappa$ B by DILI compounds possibly influences the expression of modulators that act as feedback suppressors of NF- $\kappa$ B activity, such as I $\kappa$ B $\alpha$ /NFKBIA or A20/TNFAIP3 [303]. Indeed, NF- $\kappa$ B signals through an auto-regulatory negative feedback mechanism that essentially desensitizes a cell for a limited time period against re-activation of the response by an active NF- $\kappa$ B inducing kinase complex (IKK) [304]. Although drug exposure alone

may elicit NF- $\kappa$ B oscillations, this does not limit the primary nuclear translocation event upon TNF $\alpha$  exposure, only the subsequent nuclear translocation events. The later oscillations are less intense and less synchronized due to induction of a second negative feedback regulator, A20. Interestingly, several, but not all, DILI compounds affect the expression of I $\kappa$ B $\alpha$  and A20 in PHH, which often occur in parallel, supporting a similar mechanism of activation (see Supplementary Fig. 7). We therefore turned to our GFP-p65 reporter and tested whether the test drugs can induce NF- $\kappa$ B oscillations on their own. In line with this we found that DCF, CBZ, NFZ, CLZ and KTZ induced a limited NF- $\kappa$ B transition in 2-6% of a given cell population within the first two hours after exposure which was not apparently different from control conditions (Supplementary Fig. 8). This suggests that drug pre-exposure does not directly change the initial balance of NF- $\kappa$ B and its cytoplasmic inhibitor, I $\kappa$ B $\alpha$ , but rather may influence the transcriptional and translational responses required for normal execution of the timing of the NF- $\kappa$ B response after the first nuclear translocation event.

The rationale for the choice of drugs was to investigate whether our live-cell imaging systems were able to discriminate between drugs that are often linked to DILI (TGZ, AMI, INH, KTZ, NFZ, MTX, NTF, CBZ and DCF) and relatively safe drugs (NPX, SN, OFX and CLZ). We have focused on NF- $\kappa$ B signalling, Nrf2 activation and cell death induction and a summary of the different responses is provided in Table 1. As APAP and AMAP induce hepatocellular death through necrosis at high levels of drug concentrations (an EC<sub>50</sub> in PHH of ~25mM), and not apoptosis, these are considered as relatively safe drugs [305]. Based on our results, NPX, SN and OFX are safe (no massive cell death induction, no gross effect on Nrf2 or NF- $\kappa$ B signalling), but clozapine should be re-evaluated: its profile of strong Srxn1-GFP induction, NF- $\kappa$ B delay and slightly higher cell death induced by TNF $\alpha$  co-exposure shows more resemblance to drugs that are more often associated to DILI, such as DCF, CBZ, KTZ, NFZ and NTF.

Our assays have not been able to pick up any mechanistic signs for toxicity for INH and TGZ, two typical idiosyncratic DILI-related drugs (Table 1). The hepatotoxic effect of these two drugs, however, could partly depend on their inhibitory effect on bile acid transport [306, 307], which might only emerge from advanced (3D) hepatocyte culture models [308]. Moreover, lack of strong bioactivation capacity in HepG2 cells could also be a reason why we could not observe any effect for these compounds.

In conclusion, we demonstrate an association between Nrf2 signalling and NF- $\kappa$ B responses in two distinct liver models: PHH and HepG2. Using the live cell imaging of our GFP-based reporter models for Nrf2 and NF- $\kappa$ B signalling we established the inverse relationship between these signalling pathways in relation to DILI compound and TNF $\alpha$  mediated synergistic toxicity. This was only feasible by assessing the quantitative dynamics of the NF- $\kappa$ B responses, underscoring the integration of live cell imaging of stress response pathways in mechanistic studies in relation to DILI assessment.

## Supplementary Materials

Supplementary table 1: TG-GATES compounds and DILI annotations.

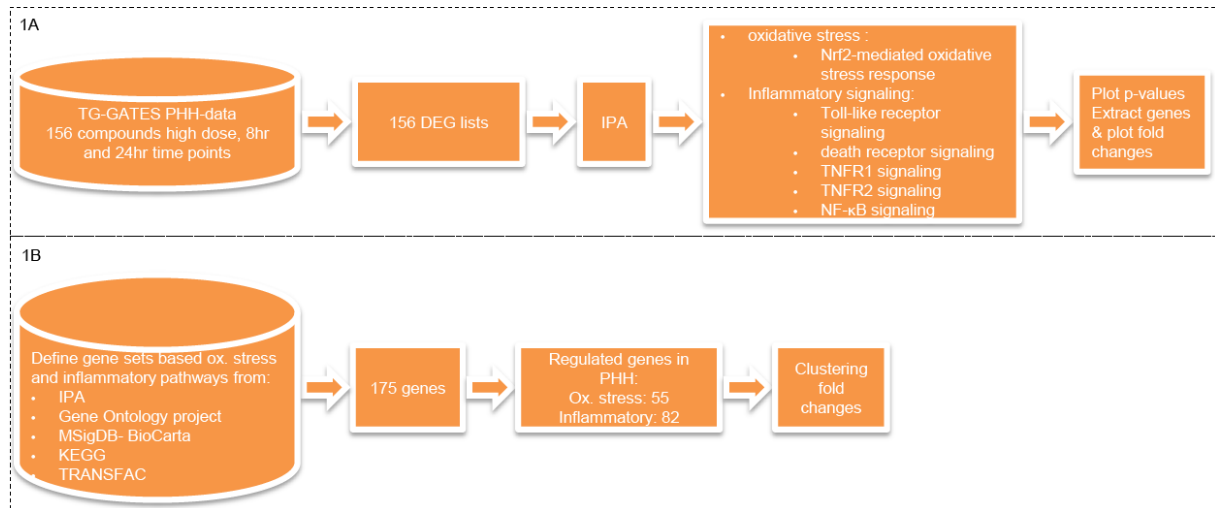
compound	conc.( $\mu$ M)	Severity Class	DILI-Concern	DILI-Score
acetaminophen	5000	5	Most-DILI-Concern	DILI-Reports
isoniazid	10000	8	Most-DILI-Concern	Severe-DILI
phenobarbital	10000	3	Less-DILI-Concern	NA
valproic acid	5000	8	Most-DILI-Concern	Severe-DILI
clofibrate	300	3	Less-DILI-Concern	NA
rifampicin	70	8	Most-DILI-Concern	DILI-Reports
omeprazole	600	4	Less-DILI-Concern	NA
indomethacin	200	5	Most-DILI-Concern	High-Concern
chlorpromazine	20	2	Less-DILI-Concern	DILI-Reports
carbamazepine	300	7	Most-DILI-Concern	High-Concern
diclofenac	400	8	Most-DILI-Concern	High-Concern
nitrofurantoin	125	8	Most-DILI-Concern	High-Concern
diazepam	250	4	Less-DILI-Concern	NA
cyclophosphamide	2000	5	Less-DILI-Concern	NA
phenytoin	60	8	Most-DILI-Concern	NA
allopurinol	140	8	Most-DILI-Concern	NA
propylthiouracil	4000	8	Most-DILI-Concern	NA
gemfibrozil	100	3	Less-DILI-Concern	NA
amiodarone	7	8	Most-DILI-Concern	Severe-DILI
sulfasalazine	150	5	Most-DILI-Concern	NA
cimetidine	300	2	Less-DILI-Concern	NA
haloperidol	20	5	Less-DILI-Concern	NA
fluphenazine	20	3	Less-DILI-Concern	NA
thioridazine	15	5	Less-DILI-Concern	NA
adapin	75	4	Less-DILI-Concern	NA
labetalol	140	8	Most-DILI-Concern	Severe-DILI
methyltestosterone	20	2	Less-DILI-Concern	NA
glibenclamide	20	3	Less-DILI-Concern	DILI-Reports
griseofulvin	20	8	Most-DILI-Concern	NA
flutamide	50	8	Most-DILI-Concern	Severe-DILI
azathioprine	73	3	Less-DILI-Concern	High-Concern
ketoconazole	15	8	Most-DILI-Concern	Severe-DILI
tetracycline	25	2	Less-DILI-Concern	High-Concern
lomustine	120	3	Less-DILI-Concern	NA
ciprofloxacin	25	7	Most-DILI-Concern	NA
tamoxifen	25	8	Most-DILI-Concern	High-Concern
methyldopa	50	8	Most-DILI-Concern	High-Concern
methimazole	10000	8	Most-DILI-Concern	DILI-Reports
tacrine	80	7	Most-DILI-Concern	High-Concern
imipramine	15	3	Less-DILI-Concern	High-Concern
amitriptyline	15	5	Less-DILI-Concern	NA
ibuprofen	150	3	Less-DILI-Concern	DILI-Reports
naproxen	600	3	Less-DILI-Concern	High-Concern
quinidine	50	3	Less-DILI-Concern	NA
furosemide	2500	2	Less-DILI-Concern	DILI-Reports
fenofibrate	30	3	Less-DILI-Concern	NA
chlorpropamide	750	2	Less-DILI-Concern	DILI-Reports
nicotinic acid	10000	7	Most-DILI-Concern	NA
erythromycin ethylsuccinate	5	5	Most-DILI-Concern	NA
ethambutol	4000	8	Most-DILI-Concern	NA
mefenamic acid	150	3	Less-DILI-Concern	NA
famotidine	700	3	Less-DILI-Concern	DILI-Reports
ranitidine	4000	5	Less-DILI-Concern	High-Concern
nifedipine	150	3	Less-DILI-Concern	DILI-Reports
diltiazem	150	4	Most-DILI-Concern	NA
captopril	8000	6	Less-DILI-Concern	NA
enalapril	2000	4	Less-DILI-Concern	High-Concern
papaverine	60	5	Most-DILI-Concern	NA
penicillamine	10000	2	Less-DILI-Concern	NA
sulindac	3000	8	Most-DILI-Concern	High-Concern
disopyramide	3500	2	Less-DILI-Concern	NA
mexiletine	300	3	Most-DILI-Concern	NA

acetazolamide	600	8	Most-DILI-Concern	NA
disulfiram	60	8	Most-DILI-Concern	High-Concern
colchicine	4000	6	Less-DILI-Concern	NA
tolbutamide	2000	2	Less-DILI-Concern	DILI-Reports
acarbose	10000	8	Most-DILI-Concern	NA
simvastatin	30	3	Less-DILI-Concern	High-Concern
meloxicam	50	3	Less-DILI-Concern	NA
ethionamide	600	3	Less-DILI-Concern	NA
ticlopidine	20	4	Most-DILI-Concern	High-Concern
tiopronin	2000	3	Less-DILI-Concern	NA
promethazine	35	5	Less-DILI-Concern	NA
dantrolene	10	8	Most-DILI-Concern	Severe-DILI
clomipramine	10	8	Most-DILI-Concern	DILI-Reports
terbinafine	15	8	Most-DILI-Concern	High-Concern
danazol	35	8	Most-DILI-Concern	NA
etoposide	330	3	Less-DILI-Concern	NA
venlafaxine	1200	7	Less-DILI-Concern	DILI-Reports
clozapine	50	5	Most-DILI-Concern	High-Concern
buspirone	30	3	Less-DILI-Concern	Transaminitis
nefazodone	30	8	Most-DILI-Concern	Severe-DILI
triazolam	10	4	Less-DILI-Concern	NA
trimethadione	10000	5	Most-DILI-concern	NA
cyclosporine A	6	7	Most-DILI-Concern	NA
diethyl maleate	1500	oxidative stress	oxidative stress	NA
LPS	300	inflammation	inflammation	NA
TNF	50	inflammation	inflammation	NA
interleukin 1 beta, human	50	inflammation	inflammation	NA
butylated hydroxyanisole	200	oxidative stress	oxidative stress	NA
amphotericin B	2	3	Less-DILI-Concern	NA
fluoxetine hydrochloride	20	3	Less-DILI-Concern	DILI-Reports
dexamethasone	300	3	Less-DILI-Concern	Transaminitis
rosiglitazone maleate	300	5	Most-DILI-Concern	High-Concern
propranolol	100	3	Less-DILI-Concern	DILI-Reports

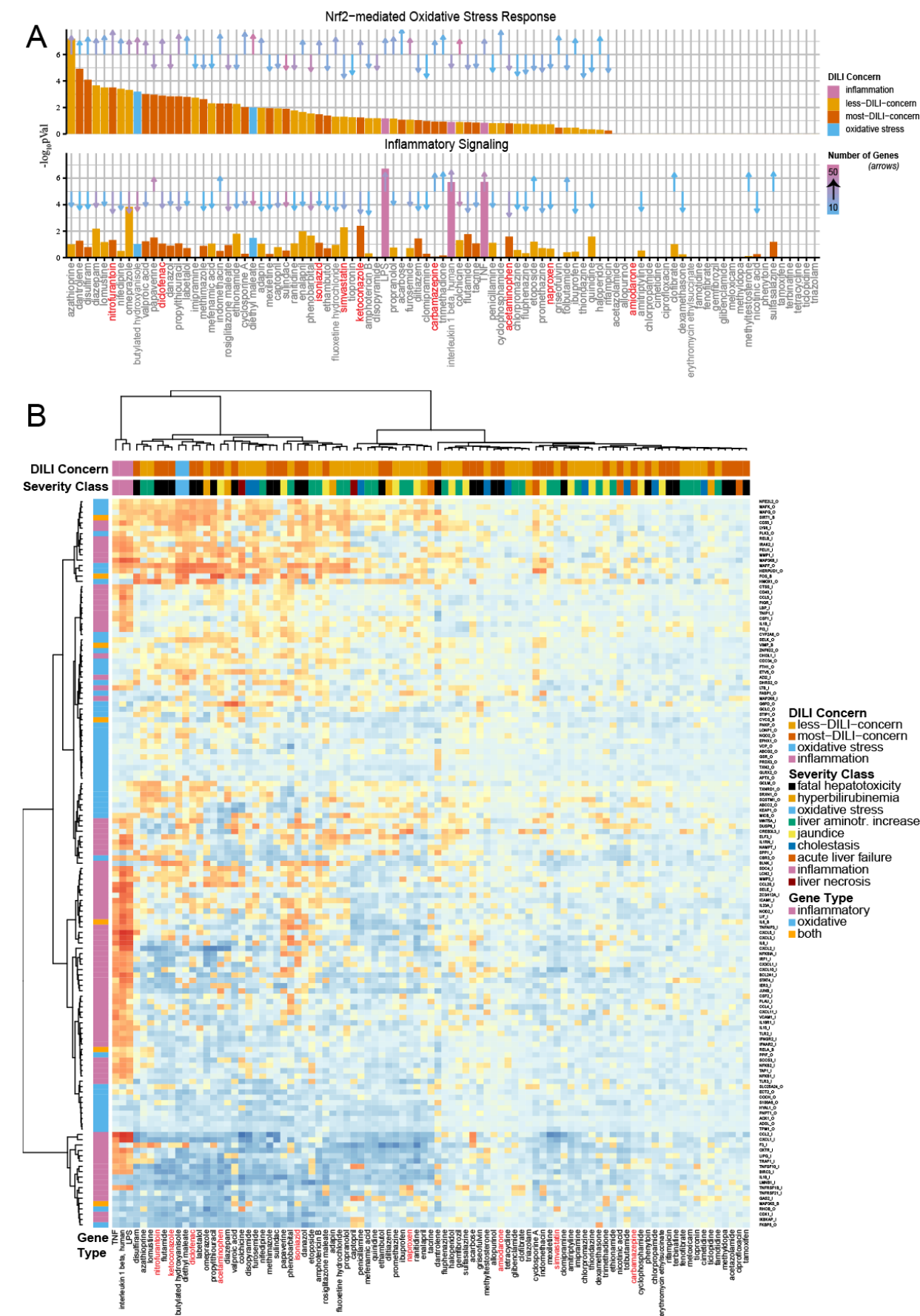
1: steatosis, 2: cholestasis, 3: liver aminotransferases increase, 4: hyperbilirubinemia, 5: Jaundice, 6: liver necrosis, 7: acute liver failure, 8: fatal hepatotoxicity

**Supplementary table 2: Drugs used in this study and their reported adverse effects on the liver.**

Drug name	Abbreviation	Type	Function	Metabolizing enzymes	Adverse reactions in the liver	References
amiodarone	AMI	Positive control	antiarrhythmic agent	CYP3A4; 1A2	ALT/AST elevations; cirrhosis; jaundice; hepatomegaly; hepatitis; phospholipidosis; steatohepatitis; cholestasis	(Lu <i>et al.</i> , 2012; Pollak and Shafer, 2004)
3'-hydroxyacetanilide	AMAP	Negative control	regionisomer of paracetamol	CYP2E1	Does not cause liver failure in mice	(Halmes <i>et al.</i> , 1998; Stamper <i>et al.</i> , 2010)
paracetamol / acetaminophen	APAP	Positive control	analgesic and antipyretic	CYP2E1; 1A2; 2D6; 3A4	Acute liver failure; necrosis	(Jaeschke <i>et al.</i> , 2012; Manyike <i>et al.</i> , 2000; Pirmohamed <i>et al.</i> , 1996)
carbamazepine	CBZ	Positive control	antiepileptic drug	CYP3A4; 2C9; induces CYP3A4	Drug hypersensitivity; acute hepatitis; ALT/AST elevations; chronic hepatitis	(Bjornsson, 2008; Daly, 2012; Phillips and Mallal, 2011; Syn <i>et al.</i> , 2005)
clozapine	CLZ	Positive control	antipsychotic drug	CYP3A4; 1A2; 2D6	ALT/AST elevations; hepatitis; jaundice; necrosis	(Damsten <i>et al.</i> , 2008; Dragovic <i>et al.</i> , 2010; Hummer <i>et al.</i> , 1997; McKnight <i>et al.</i> , 2011; Valevski <i>et al.</i> , 1998)
diclofenac	DCF	Positive control	NSAID	CYP3A4; 2C9 ; 2C8; UGT2B7	Acute hepatitis; necrosis; autoimmune chronic liver injury	(Boelsterli, 2003; Deng <i>et al.</i> , 2009; Fredriksson <i>et al.</i> , 2011)
isoniazid	INH	Positive control	anti-tuberculosis drug	CYP2E1; inhibits CYP2C9 and 3A4	ALT/AST elevation; acute hepatitis; chronic hepatitis; necrosis	(Daly and Day, 2012; Srivastava <i>et al.</i> , 2010; Zand <i>et al.</i> , 1993)
ketoconazole	KTZ	Positive control	antifungal antibiotic	CYP3A4; inhibits CYP3A4 and UGT2B7	acute hepatitis; cholestasis; necrosis	(Bernuau <i>et al.</i> , 1997; Kim <i>et al.</i> , 2003; Lin <i>et al.</i> , 2008)
methotrexate	MTX	Negative control	chemotherapeutic agent	aldehyde oxidase; CYP2E1	ALT/AST elevations; fibrosis; cirrhosis; chronic hepatitis	(Aithal, 2011; West, 1997)
nefazodone	NFZ	Positive control	antidepressant	CYP3A4; inhibits CYP3A4	liver failure; jaundice; hepatitis; hepatocellular necrosis	(Stewart, 2002; Xu <i>et al.</i> , 2008)
naproxen	NPX	Negative control	NSAID	CYP2C9	ALT/AST elevations; cholestasis; acute hepatitis	(Ali <i>et al.</i> , 2011)
nitrofurantoin	NTF	Positive control	antibiotic against urinary tract infections	CYP1A	autoimmune hepatitis; chronic active hepatitis; necrosis	(Boelsterli <i>et al.</i> , 2006; Czaja, 2011)
ofloxacin	OFX	Negative control	antibiotic	CYP1A2; 2C19	hepatocellular necrosis; jaundice; hepatitis	(Blum, 1991)
simvastatin	SN	Positive control	statin	CYP3A4	ALT/AST elevations; jaundice; hepatitis	(Bjornsson <i>et al.</i> , 2012; Law and Rudnicka, 2006)
troglitazone	TGZ	Positive control	antidiabetic	CYP1A1; 2C8; 2C19; 3A4	fulminant hepatitis; acute liver failure	(Jaeschke, 2007; Kaplowitz, 2005)



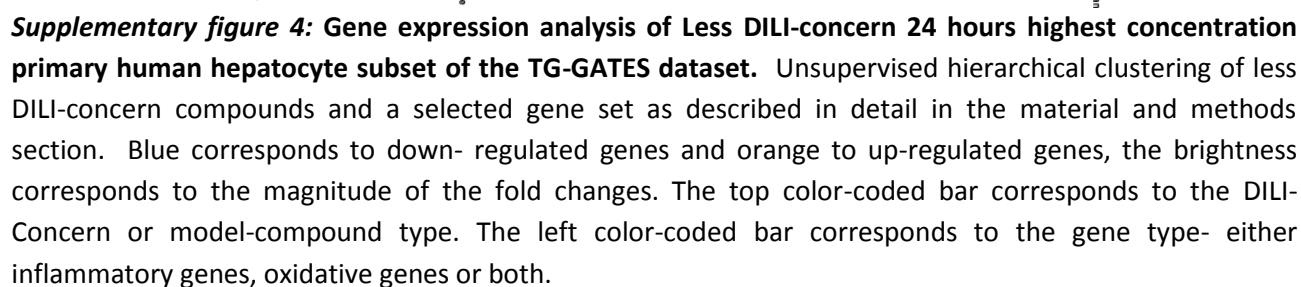
**Supplementary figure 1: Flow diagram of TG-GATES informatics analysis.**

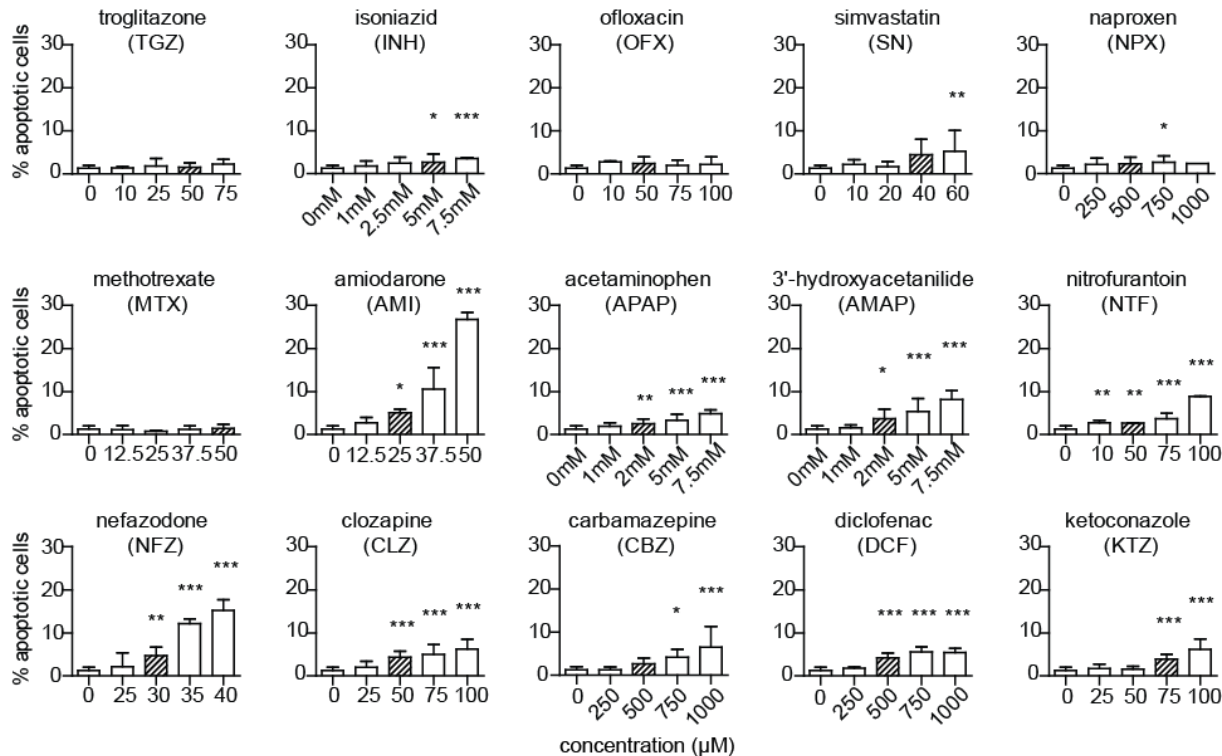


**Supplementary figure 2: Gene expression analysis of 8 hours highest concentration primary human hepatocyte subset of the TG-GATES dataset. (A) Differentially expressed genes were analyzed with**

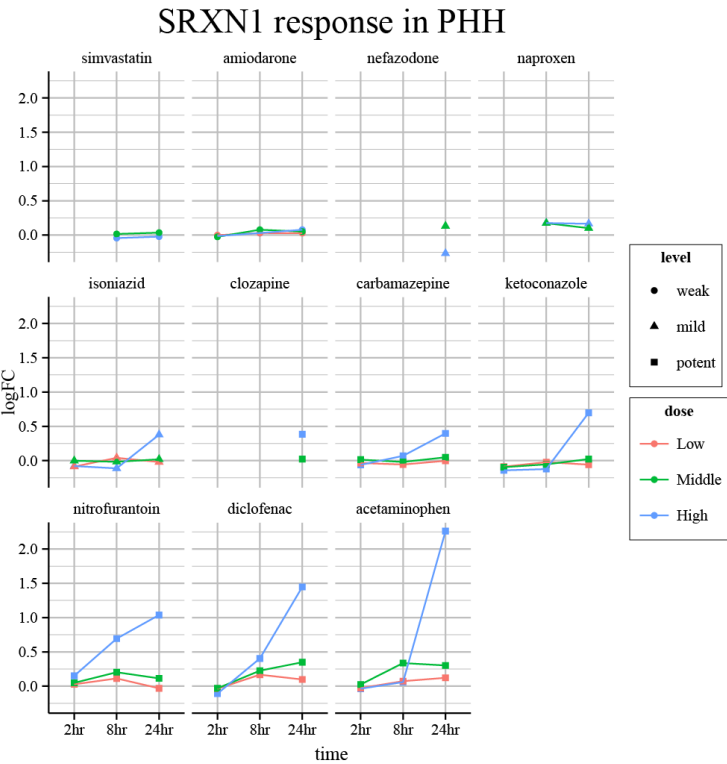




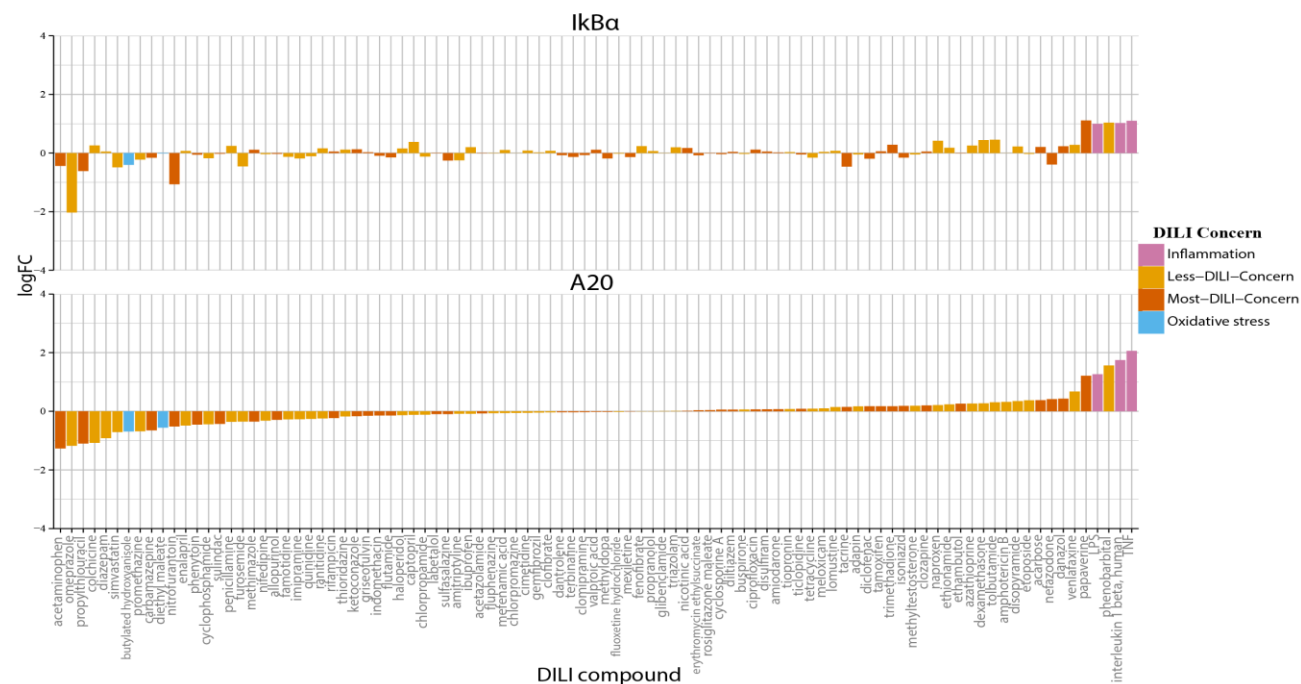




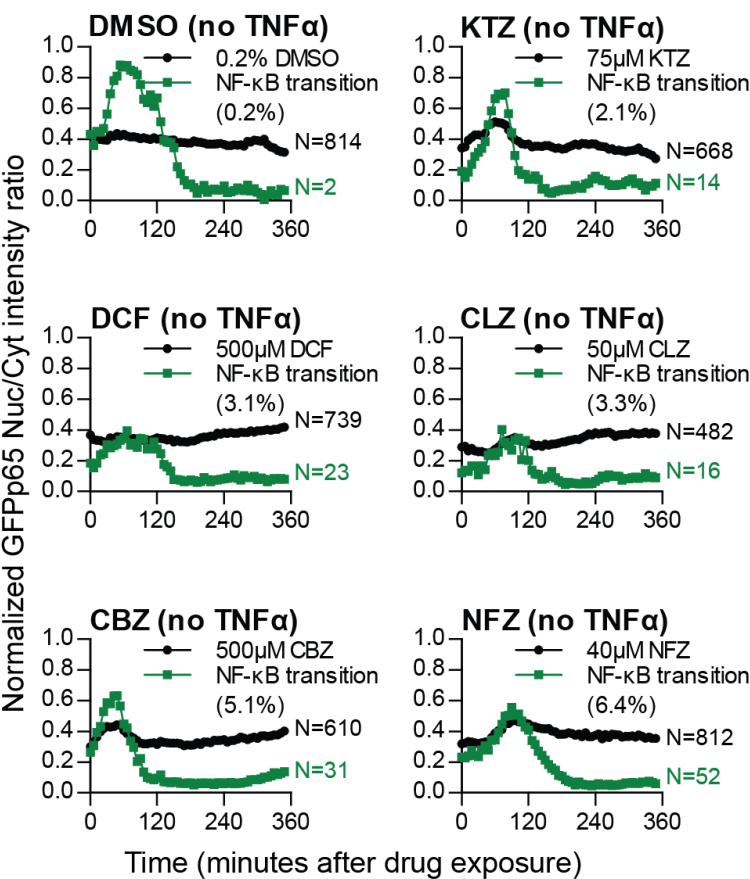
**Supplementary figure 5: Drug-induced cell death of HepG2 cells.** Percentage of dead HepG2 cells at 24 hours after exposure to fifteen different drugs. Concentrations are indicated in  $\mu$ M, except for AMAP, APAP and isoniazid (INH): in mM. "0": 0.2% (v/v) DMSO. Shaded bars: concentration used in subsequent assays.



**Supplementary figure 6: Time course fold change of SRXN1 for PHH highest concentration (TG-GATES).** Time course SRXN1 transcript level in PHH cells from the TG-GATES dataset. Fold change is expressed as  $\log_2$ (FC) as compared to matched vehicle controls. The different concentrations are color coded as low (blue), green (Middle) and red (High).



**Supplementary figure 7: Fold change values for IκBα and A20 for PHH highest concentration (TG-GATES).** Fold change is expressed as log<sub>2</sub>(FC) as compared to matched controls. Compounds are color coded according to DILI concern: inflammatory model compound (purple), oxidative stress model compound (blue), less-DILI-concern (light orange), most-DILI-concern (dark orange). Compounds are sorted according to log<sub>2</sub>(FC) of A20 from low to high.



**Supplementary figure 8: Drug-induced GFP-p65 oscillation in HepG2 cells.** Quantified average of the GFP-p65 nuclear/cytoplasmic intensity ratio, normalized between 0 and 1 to focus on the appearance of the nuclear translocation maxima after exposure to 0.2% (v/v) DMSO (solvent control), 50μM CLZ, 500μM DCF, 500μM CBZ, 75μM KTZ and 40μM NFZ. Black line: average population response; Green line: average response of cells that show NF-κB nuclear translocation within the first 2 hours of compound addition.

# Chapter 6

## **Automated live cell imaging of adaptive stress responses for assessment of drug-induced liver injury (DILI) liabilities.**

---

**This chapter is based on a manuscript in preparation:**

Steven Wink\*‡, Steven W. Hiemstra\*‡, Suzanna Huppelschoten‡\*, Janna E. Klip\*, Bob van de Water\*§

‡Authors contributed equally

\*Division of Toxicology, Leiden Academic Centre for Drug Research, Leiden University, Leiden, The Netherlands

## 1. Abstract

Drug-induced liver injury remains a major concern in the clinic and during drug development. There is an urgent need for improved prediction of DILI liabilities. Many DILI compounds activate cellular adaptive stress response pathways. We have evaluated the application of three BAC-GFP HepG2 reporter cell lines representing oxidative stress (Srxn1-GFP), endoplasmic reticulum stress (CHOP-GFP) and p53-related signalling (p21-GFP) for DILI assessment. More than 170 DILI compounds and reference control compounds (0, 1, 5, 10, 50 and 100 C<sub>max</sub> concentrations) were screened for reporter activation using automated high throughput high content live cell confocal imaging. Quantitative data analysis at the single level revealed activation of the Srxn1-GFP > CHOP-GFP > p21-GFP, with some compounds preferably activating individual reporters. Hierarchical clustering of time course dynamics of all individual reporter responses for all compounds and concentrations, allowed the refinement of primary mode-of-action. Combined integration of concentration responses for both reporters and cell death features resulted in a clustering of 53% of compounds with a most-DILI concern label. The most-DILI concern compounds activated both Srxn1-GFP and the CHOP-GFP. A strong association between HepG2 BAC-GFP reporter activation and primary human hepatocyte mRNA transcript induction was observed. We anticipate that the integration of imaging-based high throughput assays for adaptive stress pathway activation will contribute to DILI assessment and likely chemical safety assessment in general.

## 2. Introduction

Drug-induced liver injury (DILI) is an important problem during drug development, in the clinic and during post-marketing [309]. Various chemical, genetic and life style factors contribute to DILI making it a multi-faceted challenge to predict DILI. This includes compound-specific mode-of-action causing oxidative stress through mitochondrial perturbation, cholestasis due to bile acid transporter inhibition, or steatohepatitis due to altered fat metabolism. Different polymorphisms in cytochrome P450 enzymes or HLA molecules affect drug metabolism and immune responses [310]. While hepatitis or diabetes may affect the susceptibility to DILI onset [311]. The multitude of mechanism contributing to DILI forces a more mechanistic approach in the pre-clinical prediction of DILI liability.

Gene expression analysis has contributed significantly to improve our understanding of DILI [91, 240, 241, 312]. This has led to the identification of various signalling pathways that are activated during DILI and possibly predictive for chemical-induced liver injury. Some of these mechanistic insights have been integrated in high throughput assays, including phospholipidosis [313], cholestasis [314], cytokine induced synergistic apoptosis [38], mitochondrial damage [315], and oxidative stress [84]. However, so far a high throughput approach that more directly integrates the transcriptome-based mode-of-action is missing.

To integrate the mode-of-action in high throughput approaches we propose a more practical approach which focuses on a general biological theme evolved in evolution: the cellular adaptive stress response pathways [45]. Several key adaptive stress response pathways that are essential in the maintenance of cellular homeostasis are the oxidative stress response, the endoplasmic reticulum stress response (ER-stress) / unfolded protein response (UPR) and the DNA damage response (DDR). The TG-GATES transcriptomics dataset indicates that these pathways are often

affected during liver toxicity (Wink *et al.*, manuscript submitted), while mechanistic studies indicate the contribution of these pathways in the pathophysiology of chemical-induced liver failure [238, 316, 317]. Oxidative stress is caused by the oxidation/reduction reactions or alkylation from reactive intermediates or indirect oxidative stress induction by e.g. disruption of endogenous mitochondrial function [318]. Overall, this leads to the modification of KEAP1 followed by the stabilization of the transcription factor Nrf2 which activates the oxidative stress defense gene network including the expression of NQO1 and Srxn1 [217]. Protein alkylation, disruption of protein trafficking or calcium homeostasis in the ER disrupt normal protein folding in the ER and leads to activation of the unfolded protein response [319]. This involves the activation of the kinases IRE1 $\alpha$  and PERK and the proteolytic activation of the transcription factor ATF6; the transcription factors Xbp1 and ATF4 are activated downstream of both kinases [320]. The UPR transcriptional response involves the expression of the chaperone BiP that rescues unfolded proteins in the ER lumen as well as the expression of CHOP/DDIT3, a transcription factor that promotes the expression of pro-apoptotic genes [321]. DNA damage is caused by genotoxic compounds, which are usually electrophiles that directly interact with DNA and form covalent bonds. This involves the activation of p53 followed by activation of downstream target genes including p21 and Btg2. We have previously integrated all the downstream target genes for these three main adaptive stress response pathways in bacterial artificial chromosome (BAC) GFP-based HepG2 reporter cell lines. We showed that these BAC reporters are sensitive and selective for mode-of-action evaluation and can be applied in high throughput – high content live cell imaging to capture the dynamic adaptive stress response activation at the single cell level (Wink *et al.*, manuscript in preparation).

Here we assessed the application of three BAC GFP HepG2 reporter cell lines that represent three major adaptive stress response pathways to predict DILI liability: i.e. Srxn1 (KEAP1/Nrf2), CHOP/DDIT3 (UPR) and p21 (DNA damage response). These three BAC reporters were exposed to more than 170 chemicals at different concentrations covering human exposure levels, and the dynamic stress pathway activation as well as onset of cytotoxicity was followed for 24 hr using automated live cell confocal imaging. All quantitative dynamic GFP reporter data as well as cytotoxicity measurements were integrated to assess DILI liability.

### 3. Materials and methods

#### 3.1. Cell culture

Human hepatoma HepG2 cells were acquired from ATCC (clone HB8065). HepG2 Srxn1, DDIT3 (CHOP) and CDKN1A (p21) BAC GFP reporter were generated according to [48] and have been carefully characterized previously (Wink *et al*, manuscript submitted). HepG2 BAC GFP reporters were maintained and exposed to drugs in DMEM high glucose supplemented with 10% (v/v) FBS, 25U/mL penicillin and 25µg/mL streptomycin. The cell lines were used between passage 5 and 20. For live cell imaging, the cells were seeded in Greiner black µ-clear 384 wells plates, at 8,000 cells per well.

#### 3.2. Reagents

All reference compound chemicals were acquired from Sigma-Aldrich and freshly dissolved in DMSO; except for metformin, fluphenazine, buthionine sulfoxamine, bromoethlyamine (all PBS), acetaminophen and phenobarbital (all DMEM). DILI compounds were a kind gift from the Dr. Weida Tong, NCTR-FDA [264]. All compounds were maintained as 500-fold stock such that final treatments did not exceed 0.2 % v/v DMSO.

#### 3.3. Microscopy

Accumulation of BAC GFP-fusion levels, priopodium iodide (PI) and Annexin-V-Alexa633 (AV) staining was monitored using a Nikon TiE2000 confocal laser microscope (lasers: 647nm, 540nm, 488nm and 408nm), equipped with an automated stage and perfect focus system and at 37 degrees C and humidified atmosphere and 5% CO<sub>2</sub>/air mixture. Prior to imaging at 20x magnification and either 1X, or 2X zoom, HepG2 cells were loaded for 45 minutes with 100 ng/mL Hoechst<sub>33342</sub> to visualize the nuclei, upon which the Hoechst-containing medium was washed away to avoid Hoechst phototoxicity [224] and replaced with medium containing PI and AV to monitor cell death. Each imaged 384-well plate containing one reporter cell line all the compounds used in the screen at one certain concentration (1, 5, 10, 50 or 100 C<sub>max</sub>); for each concentration 2-3 replicates were imaged per reporter cell line.

#### 3.4. Reporter response quantification

Quantitative image analysis was performed with CellProfiler version 2.1.1 [49] with an in house developed module implementing the watershed masked algorithm for segmentation [193]. The watershed separates an image in regions with single cells followed by pixel classification for each region as fore- or background and this method performs well detecting the Hoechst<sub>33342</sub> stained nuclei of the closely packed HepG2 cells. The binary mask containing the segmented nuclei was fed to the *identify-primary-objects* module, *overlap-based-tracking* module and *intensity-nuclei-size-shape-measurement* modules of CellProfiler. For the cytosol location of the Srxn1-GFP reporter the nuclear objects were used as seeds for the *identify-secondary-objects* module set to a propagation method with the MCT algorithm on adaptive (window size approximately 20 pixels) segmentation. Segmentation results were stored as png files for quality control purposes and CellProfiler pipelines were stored for reproducibility. Image analysis results were stored on the local machine as HDF5 files. Data analysis, quality control and graphics was performed using the in house developed R package H5CellProfiler (Wink *et al.*, 2015, manuscript in preparation).

For each reporter the mean intensity and integrated intensity levels of the GFP signal were measured on the single cell level. The mean intensity is less sensitive to size variations of the objects and the integrated intensity is less sensitive for faulty background segmentations within the object. In addition, the nuclear Hoechst<sub>33342</sub> intensity was measured to observe variations in DNA content (e.g. due to apoptosis or necrosis), cell migration speed (which can be affected by compound specific effects), nuclear size (which can vary e.g. due to mitosis inhibition, flattening of cells or changes in the internal osmotic pressure), PI and AV staining per single cell (for cell death detection) and finally the overall cell count. All features were measured with an average one hour intervals; with the exception of the PI and AV which was only measured after completion of the 24 hour live imaging session.

### 3.5. Data analysis

The features of interest were extracted from the HDF5 files and further analyzed using the graphical user interface of the H5CellProfiler package. The mean of the features for each compound, concentration, cell line and replicate combination was calculated. In addition for each plate the mean and standard deviation of the DMSO treated single cell population was calculated to determine background control values: the 2X mean, 3X mean and the mean + 3 standard error values for each plate. Thereafter for each treatment the fraction of cells above these control-values was determined. To account for PI and AV background staining and noise the segmented PI and AV segmentations were masked by a 2 pixel dilated nuclei. The area of these nuclei and the PI and AV objects were divided to obtain the cell death stain to cell area ratio. These ratios were filtered to be at least 10% of the cell size and following this procedure each cells was either flagged as alive or dead in the final time point of the 24 live imaging session. In this manner the fraction of dead cells could be accurately determined. All resultant summarized data was stored as tab delimited text files and further processed for normalization and graphical presentation using R.

Due to automated confocal imaging over a one year period, the time course data required intensity variation plate normalization as well as modeling of the time course-data. The mean and integrated intensity features and the nuclei size and Hoechst<sub>33342</sub> intensity features were first transformed to fold change with respect to the plate- specific DMSO controls at time point 1 and the cell count and cell speed features were transformed to fold change with respect to the plate-specific DMSO controls average over time (diagram 1). Afterwards these value were scaled between 0 and 1 over the entire dataset with the formula  $(x - x_{\min\_screen}) / (x_{\max\_screen} - x_{\min\_screen})$  for the purpose of proper heatmap display. Prior validation of negative and positive control responses preceded this scaling procedure. After the normalization steps the response specific features (integrated and mean intensity and the positive fraction features) were fit separately per replicate with the b-splines method with a degree of freedom of 10 and 3<sup>rd</sup> degree polynomials using the base-r lm function and bs function of the splines package. This allowed resampling the data with equidistant time points for replicate statistics and higher density time point sampling (200 points) for smooth heatmap display. All b-spline fits were stored for verification purposes.

### 3.6. Dose response data transformation

The maximum value of the fold change and normalized, scaled and b-spline modeled mean and integrated intensity features and the b-spline modeled positive GFP fraction features per



compound and concentration combination were selected for the dose response curves. The time course cell numbers, cell speed, Hoechst<sub>33342</sub> intensity and nuclear area features were regressed to the line  $ax + b$  to determine the slope and mean values.

The fraction of dead cells did not require normalization as these features are inherently a plate normalized measure nor did they require transformation as only the final time point was measured. The cytotox features, cell count, Hoechst<sub>33342</sub> intensity and nuclear area also obtained from the final imaging round, were normalized per plate as fold change with respect to DMSO controls and scaled between 0 and 1 for the entire dataset.

### 3.7. Data representation

All HCI data representations were generated or modified with Illustrator CS6, Fiji, ggplot2 [226], the `aheatmap` function of the NMF package [227]. For some of the data clustering the equidistant sample time profile features from the b-spline model were used to calculate a distance matrix for each feature separately using Euclidean distance. A mean distances matrix was calculated and subjected to clustering with the `ward.D` method of the `hclust` function. The columns representing the different features were not subjected to clustering. The same method was applied to the row-clustering, only now the dose response vectors were used for the distance matrixes.

### 3.8. Gene expression analysis

CEL files were downloaded from the Open TG-GATEs database: “Toxicogenomics Project and Toxicogenomics Informatics Project under CC Attribution-Share Alike 2.1 Japan” <http://dbarchive.biosciencedbc.jp/en/open-tggates/desc.html>. Probe annotation was performed using the `hthgu133pluspmhsentrezg.db` package version 17.1.0 and Probe mapping was performed with `hthgu133pluspmhsentrezgcdf` downloaded from NuGO ([http://nmg-r.bioinformatics.nl/NuGO\\_R.html](http://nmg-r.bioinformatics.nl/NuGO_R.html)). Probe-wise background correction (Robust Multi-Array Average expression measure), between-array normalization within each treatment group (quantile normalization) and probe set summaries (median polish algorithm) were calculated with the `rma` function of the Affy package (Affy package, version 1.38.1) (Irizarry, R.A. et al.). The normalized data were statistically analyzed for differential gene expression using a linear model with coefficients for each experimental group within a treatment group [258, 259]. A contrast analysis was applied to compare each exposure with the corresponding vehicle control. For hypothesis testing the empirical bayes statistics for differential expression was used followed by an implementation of the multiple testing correction of [254] using the LIMMA package [259].

## 4. Results

### 4.1. High content adaptive stress response screen with DILI compounds.

To assess the application of adaptive stress pathway activation measurements for the assessment of DILI liability a large high content live cell screen was performed on three BAC reporter cell lines (Srxn1, CHOP and p21) that were described previously (Wink *et. al*, manuscript submitted), with 176 compounds covering mostly DILI related compounds and various reference control compounds. DILI compounds were classified for most-DILI-concern (58), less-DILI-concern (51) or no-DILI-concern (37) (see Table 1). The control reference compounds included negative controls (i.e. DMSO and medium) and positive controls (i.e. alkylating agents, mitochondrial toxicants, inducers of the UPR and DNA damaging agents). All reporters were exposed to five concentrations (1, 5, 10, 50 and 100 Cmax) followed by live cell imaging and automated multi-parametric image analysis (Fig. 1 and 2).

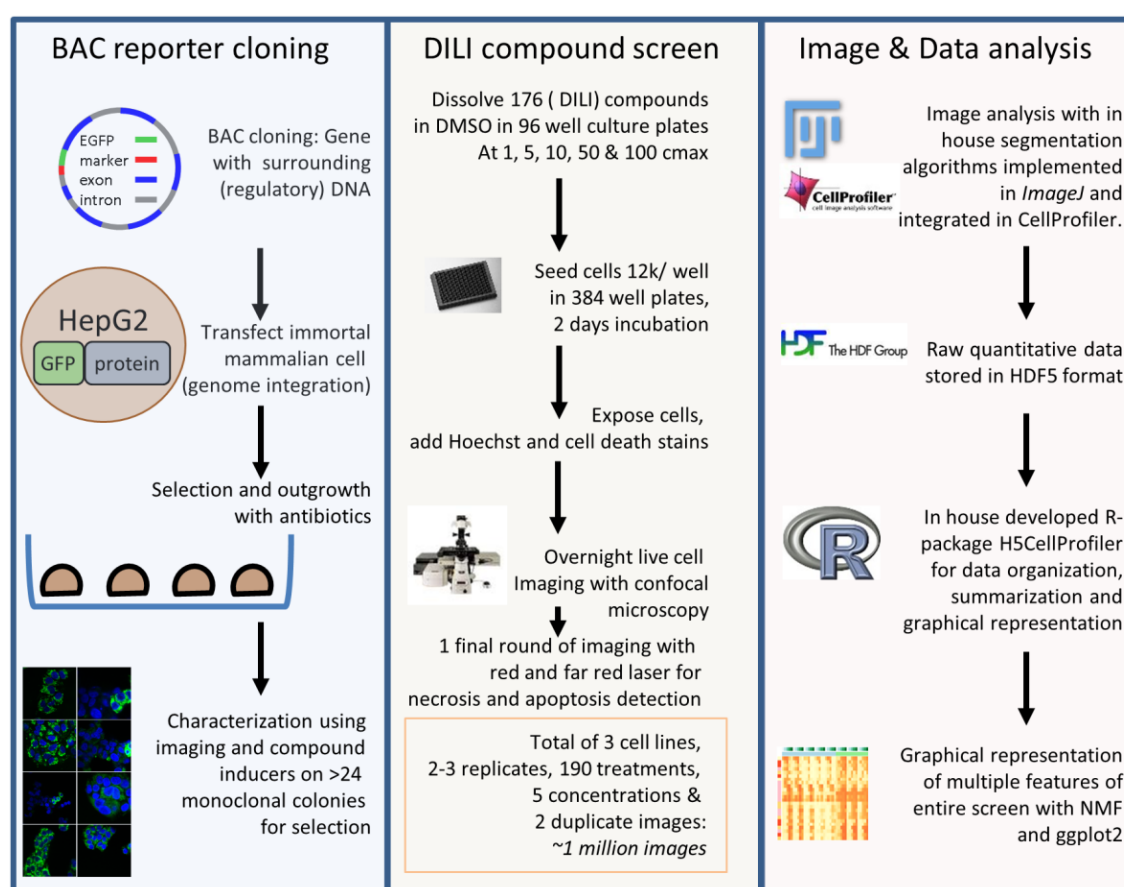


**Figure 1: BAC cloning, BAC reporter DILI screen and analysis pipeline.** Left panel) BAC cloning technology is used to maintain endogenously regulated reporter protein levels and regulation. Monoclonal reporter selection from a high number of clones to ensure endogenous response to positive control stimuli and suitability of reporter for imaging. Middle panel) High content live cell screen of 176 compound at 1, 5, 10, 50 and 100 cmax at 2 or 3 replicates. Right panel) Image and data analysis is performed with CellProfiler/Fiji and R, respectively. Some in-house tools were developed in CellProfiler and R to assist in the quality and analysis of the large data output.

### 4.2. Single cell analysis allows fine tuning of sensitivity versus dynamic range.

For all images single cell analysis was performed to extract a diverse set of quantitative data, including GFP reporter activity, cell migration speed, cell number and cytotoxicity (see Figure 2 for overview of the dataset). The GFP reporter single cell data was used to derive quantitative fitted

data for five different determinants of reporter activity: mean intensity, mean integrated intensity, fraction of cells with GFP intensity 2-fold (GFP\_pos.2m) or 3-fold (GFP\_pos.3m) above average of control, population mean plus three times the standard deviation (GFP\_pos.m3d). Systematic evaluation of these descriptors for the lowest and strongest responding compound for each individual reporter, allowed fine tuning of the sensitivity versus the dynamic range (Figure 3). Based on the mean GFP intensity over the single cell population hydroxurea would not have been defined as a positive in the Srxn1-GFP reporter cell line, because only in a small proportion of cells that contain a higher level of Srxn1-GFP the signal was detected; the GFP\_pos.2m was a more sensitive descriptor that also allowed evaluation of the time course dynamics. Similar observations were made for nitrofurantoin and clozapine for the GFP-CHOP and GFP-p21 reporters, respectively. However for strong inducers of oxidative stress (diethylmaleate; DEM), UPR (thapsigargin) and DNA damage (etoposide), GFP mean intensity already allowed the sensitive detection of the reporter responses, while GFP\_pos.2m caused an early saturation, thereby lowering the dynamic range.

#### **4.3. Temporal order of adaptive stress response activation as indication of primary mode-of-action.**

For evaluation of the reporter activation for the entire compound screen GFP\_pos.2m was selected as the most sensitive initial readout. The b-spline fits of the GFP\_pos.2m time courses were used to calculate the mean of the replicates for Srxn1-GFP, CHOP-GFP and p21-GFP reporter responses for all compounds (Figure 4). Some compounds showed a response in all three reporters, while others only showed a response in one cell line only. Often a specific order in the reporters can be seen in time. For brefeldin A (BFA), CCCP, FCCP, doxycycline (DX), oligomycin A and B (OMA, OMB), thapsigargin (THG), tunicamycin (TUN) and zimelide (ZMI) CHOP-GFP activation was followed by the Srxn1-GFP activation. Yet in other cases Srxn1-GFP did precede CHOP-GFP activation (azathioprine (AZA), benzbromarone (BB), bromfenac (BFC), ethacrynic acid (ETA) and sodium-arsenite (SA)). Simultaneous activation of two reporters was also observed. Interestingly, for some compounds the stress response activation was transient (iodoacetamide; IAA) implicating reversal of the stress response, possibly due to toxicokinetics and/or true cellular adaptation. Few compounds showed direct fluorescence increase starting from the first time point (e.g. tetracyclin (TET), doxorubicin (DOX) and dantrolene (DAN)), suspecting compound autofluorescence. Several compounds showed activation at a lower C-max while a response was absent at higher concentrations indicating that an adaptive stress response preceded cell death. This was verified with the additional markers captured during the live cell imaging: cell number, cell migration speed, nuclear area and DNA content. Although most compounds did not affect these markers, several compounds did, typically in a concentration-dependent manner. Cell migration speed was the most often affected parameter as exemplified by the actin cytoskeleton disrupting agent cytochalasin (Supplemental Figure S1 and S2).

**Table 1: Test compound set.** Alphabetically sorted list of test compounds screened in this study including their c-max values, abbreviations, DILI-concern label and metabolic potential.

compound	cmax (μM)	abbreviation	DILI classification	metabolism	compound	cmax (μM)	abbreviation	DILI classification	metabolism
acarbose	0.15	ACA	Most-DILI-Concern	NM	hydrazine	14.7	HYD	control	NA
acetaminophen	100	APAP	Most-DILI-Concern	YES	hydroxyurea	348	HU	Most-DILI-Concern	YES
adefovir	0.09	ADV	No-DILI-Concern	NM	hydroxyzine	0.27	HYZ	No-DILI-Concern	NM
aflatoxin B1	1.00	AFB1	control	NA	ibuprofen	70.1	IBU	Less-DILI-Concern	YES
allopurinol	13.8	ALLO	Most-DILI-Concern	NM	imipramine	0.29	IM	Less-DILI-Concern	YES
allyl alcohol	2.00	AA	control	NA	indomethacin	5.59	IMN	Most-DILI-Concern	YES
altretamine	3.76	ALM	Less-DILI-Concern	YES	interleukin 6	0.40	IL6	control	NA
amiodarone	0.81	AMIO	Most-DILI-Concern	NM	iodoacetamide	1.00	IAA	control	NA
amoxicillin	22.3	AX	Less-DILI-Concern	NM	isoniazid	45.4	INH	Most-DILI-Concern	YES
antimycin A	0.20	AA	control	NA	isoproterenol	0.01	IPR	No-DILI-Concern	NA
aspirin	1650	ASA	No-DILI-Concern	NM	kanamycin	60.1	KM	No-DILI-Concern	NA
azathioprine	0.34	AZA	Most-DILI-Concern	YES	ketoconazole	6.59	KTZ	Most-DILI-Concern	NM
azidothymidine	3.97	AZT	No-DILI-Concern	NA	ketorolac	3.53	KTL	Less-DILI-Concern	NM
benzbromarone	4.34	BB	Most-DILI-Concern	YES CYP2C9	labetalol	2.68	LABE	Most-DILI-Concern	YES
betaine	940	BET	No-DILI-Concern	NA	maprotiline	0.18	MPT	No-DILI-Concern	NA
brefeldin A	1.00	BFA	control	NA	mebendazole	0.13	MBZ	Less-DILI-Concern	NM
bicalutamide	1.97	BAT	Most-DILI-Concern	YES CYP3A4	meclizine	0.03	MCZ	No-DILI-Concern	NM
bisphenol A	0.80	BPA	No-DILI-Concern	NA	menadione	2.50	MEN	control	NA
bosentan	3.43	BOS	Most-DILI-Concern	YES	mercaptopurine	0.48	6MP	Most-DILI-Concern	YES
bromfenac	18.0	BFC	Most-DILI-Concern	NA	metformin	116	MF	No-DILI-Concern	YES
buspirone	0.02	BUS	Less-DILI-Concern	YES CYP3A4	methimazole	2.62	MTZ	Most-DILI-Concern	YES
busulfan	0.28	BU	Most-DILI-Concern	YES	methotrexate	0.77	MXT	Most-DILI-Concern	NM
buthionine sulfoxamine	0.25	BSO	control	NA	methyldopa	18.9	MD	Most-DILI-Concern	YES
butylated hydroxyanisole	1.00	BHA	control	NA	metoprolol	0.56	MTPL	Less-DILI-Concern	YES
captopril	8.88	CPL	Less-DILI-Concern	YES	metronidazole	237	MTDZ	No-DILI-Concern	NM
carbamazepine	0.00	CBZ	Most-DILI-Concern	NM	mexiletine	3.83	MXT	Most-DILI-Concern	YES
carmustine	60.0	BCNU	Most-DILI-Concern	YES	mitomycin C	7.18	MIT-C	No-DILI-Concern	NM
CCCP	1.00	CCCP	control	NA	moxisylyte	0.16	MOX	Most-DILI-Concern	NA
CCl4	6.50	CCl4	control	NA	naproxen	0.20	NPX	Less-DILI-Concern	YES
CDDO-me	0.01	CDDO	control	NA	nefazodone	0.86	NFZ	Most-DILI-Concern	YES
chloramphenicol	46.4	CAMP	No-DILI-concern	NA	neomycin	0.44	NEO	No-DILI-Concern	NM
chlormezanone	10.6	CMZ	Most-DILI-Concern	NA	nifedipine	0.43	NFP	Less-DILI-Concern	YES
chloroquine diphosphate	0.00	CHQ	No-DILI-concern	MINIMAL	nimesulide	21.1	NMS	Most-DILI-Concern	NA
chlorpromazine	0.94	CPZ	Less-DILI-Concern	YES	nitrofurantoin	6.00	NTF	Most-DILI-Concern	YES
chlorpropamide	130	CHL	Less-DILI-Concern	NM	nizatidine	4.00	NIZ	Less-DILI-Concern	YES
cimetidine	9.00	CMT	Less-DILI-Concern	YES	nocodazole	1.00	NOC	control	NA
ciprofloxacin	6.58	CIPX	Most-DILI-Concern	NM	ochratoxin A	0.05	OTA	No-DILI-Concern	NA
cisplatin	2.00	CDDP	Less-DILI-Concern	NA	ofloxacin	9.96	OFX	Most-DILI-Concern	NM
clofibrate	25.0	CLO	Less-DILI-Concern	YES	oligomycin A	0.50	OMA	control	NA
clotrimazole	0.09	CTZ	No-DILI-Concern	NM	oligomycin B	1.00	OMB	control	NA
clozapine	0.98	CLZ	Most-DILI-Concern	YES	omeprazole	4.70	OMZ	Less-DILI-Concern	YES
colchicine	0.02	CLC	Less-DILI-Concern	YES	oxytetracycline	3.26	OTC	No-DILI-Concern?	NA
coumarin	0.80	COH	control	NA	paroxetine	0.06	PXT	Less-DILI-Concern	YES
cromolyn	0.02	CRO	No-DILI-Concern	NA	penicillamine	27.5	DP	Less-DILI-Concern	NM
cycloheximide	50.0	CHX	Most-DILI-Concern?	NA	perhexiline	2.16	PHX	Most-DILI-Concern	NA
cyclophosphamide	375	CTX	Less-DILI-Concern	YES	phenacetin	0.62	POD	Less-DILI-Concern	NA
cyclosporin A	0.20	CSA	Less-DILI-Concern	YES	phenobarbital	1.46	PBT	Less-DILI-Concern	NM
cytochalasin D	1.00	CDD	control	NA	phenytoin	21.7	PT	Most-DILI-Concern	YES
dacarbazine	20.6	DTIC	Most-DILI-Concern	NM	pioglitazone	2.95	PGZ	Less-DILI-Concern	NM
danazol	0.11	DNZ	Most-DILI-Concern	NM	prednisolone	0.68	PRD	Less-DILI-Concern	NM
dantrolene	7.90	DAN	Most-DILI-Concern	YES	primaquine	0.61	PQ	No-DILI-Concern	NM
deferoxamine	17.8	DFX	No-DILI-Concern	NM	primidone	4.67	PRI	No-DILI-Concern	YES
diethyl maleate	10.0	DEM	control	NA	procydiline	0.40	PCD	No-DILI-Concern	NA
dexamethasone	0.22	DXS	Less-DILI-Concern	NM	propranolol	0.20	PPL	Less-DILI-Concern	YES
dextromethorphan HBr	0.01	DXM	No-DILI-Concern	NA	propylthiouracil	9.10	PTU	Most-DILI-Concern	YES
diclofenac	4.20	DCF	Most-DILI-Concern	YES	ranitidine	1.79	RNT	Less-DILI-Concern	YES
didanosine	9.83	DDL	Most-DILI-Concern	NM	ribavirin	2.61	RBV	No-DILI-Concern	MINIMAL
digoxin	0.00	DIG	No-DILI-Concern	NA	rifampicin	15.0	RFP	Less-DILI-Concern	YES
diltiazem	96.0	DTZ	Most-DILI-Concern	YES	rotenone	0.40	ROT	control	NA
disulfiram	5.40	DIS	Most-DILI-Concern	YES	simvastatin	0.08	SVN	Less-DILI-Concern	YES
DMNQ	0.04	DMNQ	control	NA	sodium-arsenite	10.0	SA	control	NA
DMOG	7.50	DMOG	control	NA	staurosporin	0.01	STAU	control	NA
doxorubicin	1.18	DOX	Less-DILI-Concern	YES	succinylcholine	138	SUCCS	No-DILI-Concern	NA
doxycycline	11.3	DX	Less-DILI-Concern	NM	sulfamethoxazole	217	SMZ	No-DILI-Concern?	YES
edrophonium	60.2	EDR	No-DILI-Concern	NA	sulindac	32.0	SUL	Most-DILI-Concern	YES
enalapril	0.40	ENP	Less-DILI-Concern	YES	tacrine	0.08	TC	Most-DILI-Concern	YES
entacapone	3.93	ECP	No-DILI-Concern	YES	tacrolimus	0.04	TAC	No-DILI-Concern	YES
epinephrine	0.00	EPI	No-DILI-Concern	NA	tamoxifen	0.16	TMX	Most-DILI-Concern	YES
erythromycin	11.0	ERYC	Most-DILI-Concern	NM	terbinafine	4.00	TRB	Most-DILI-Concern	NM
ethacrynic acid	33.0	ETA	No-DILI-Concern	YES	tetracycline	21.0	TET	Less-DILI-Concern	NM
ethambutol	24.5	EMB	Less-DILI-Concern	NM	thapsigargin	0.10	THG	control	NA
ethionine	10.0	ETH	Less-DILI-Concern	NA	thioridazine	0.55	TDZ	Less-DILI-Concern	YES
etodolac	68.5	ELAC	Most-DILI-Concern	YES	ticlopidine	8.07	TPD	Most-DILI-Concern	YES
etoposide	4.04	ETO	Less-DILI-Concern	YES	TNF-α	0.50	TNF	control	NA
famotidine	0.31	FAM	Less-DILI-Concern	YES	TO901317	1.25	TO9	control	NA
FCCP	1.00	FCCP	Less-DILI-Concern	NA	tolbutamide	233	TOLB	Less-DILI-Concern	NM
fenofibrate	4.10	FF	Less-DILI-Concern	NM	tolcapone	22.0	TC	Most-DILI-Concern	YES
fenoprofen	58.2	FPF	Most-DILI-Concern	NA	trazodone	5.06	TZ	Most-DILI-Concern	YES
fialuridine	1.00	FIAU	Most-DILI-Concern	NA	trogilazone	6.39	TRG	Most-DILI-Concern	YES
fluoxetine	0.05	FLX	Less-DILI-Concern	YES	tunicamycin	1.00	TUN	control	NA
flurbiprofen	57.3	FBP	Most-DILI-Concern	NA	valacyclovir	17.4	VACV	No-DILI-Concern	NM
folic acid	0.04	FAM	No-DILI-Concern	NA	valproic acid	243	VA	Most-DILI-Concern	YES
furosemide	3.29	FUR	Less-DILI-Concern	YES	verapamil	0.16	VRP	Less-DILI-Concern	NM
galactosamide	100	GALN	control	NA	warfarin	4.86	WAR	Less-DILI-Concern	NM
ganciclovir	4.62	GCV	No-DILI-Concern	MINIMAL	WY14643	1.25	WY14	control	NA
glimepiride	1.12	GLP	Less-DILI-Concern	NM	ximelagatran	16.9	XML	Most-DILI-Concern	NA
griseofulvin	4.54	GF	Most-DILI-Concern	YES	zafirlukast	1.21	ZFL	Most-DILI-Concern	YES
haloperidol	0.01	HDL	Less-DILI-Concern	YES	zimididine	60.0	ZMI	Less-DILI-Concern	NA

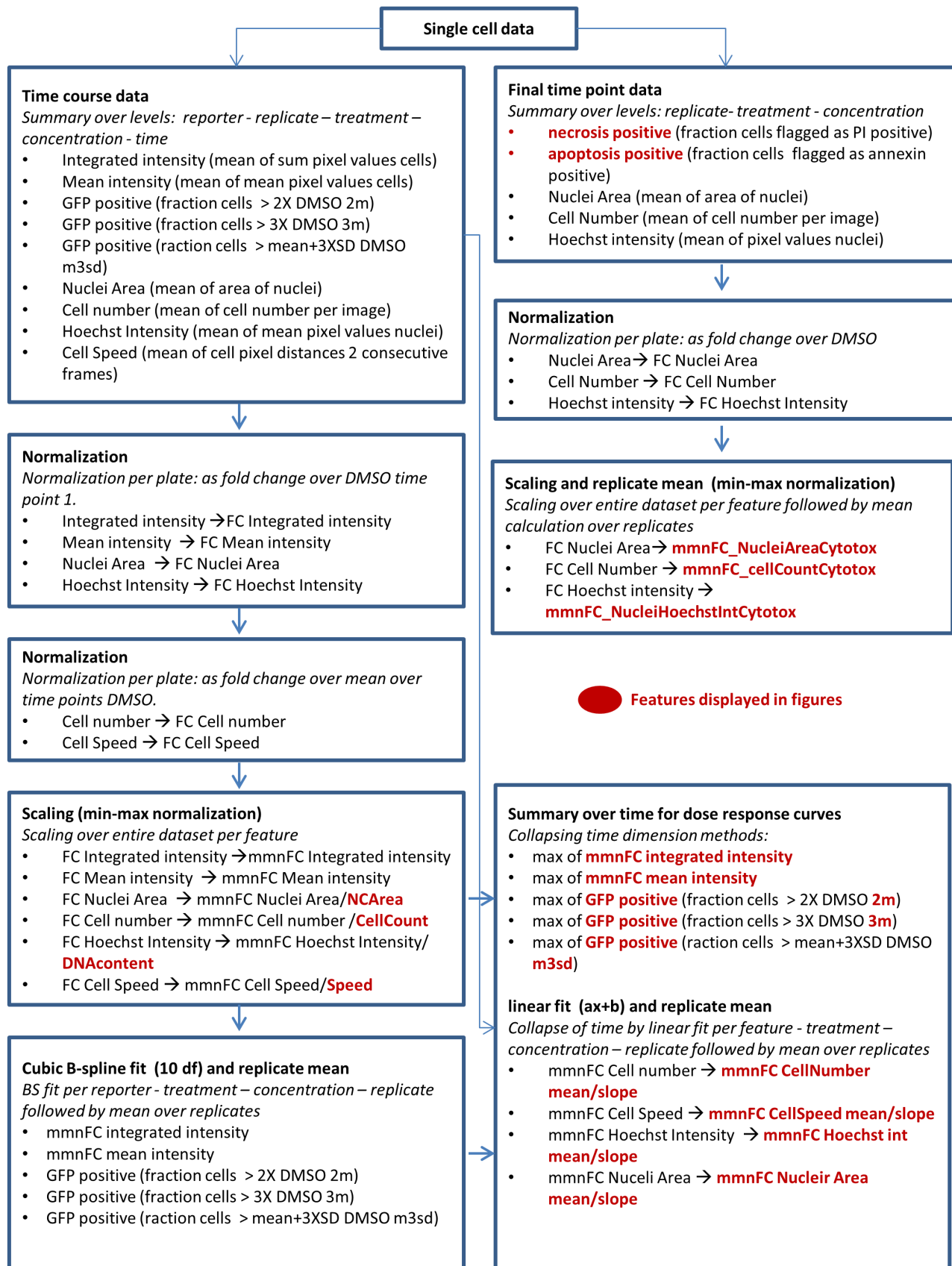


**Figure 2: Data analysis workflow.** The features in red are displayed in the figures of the results section.



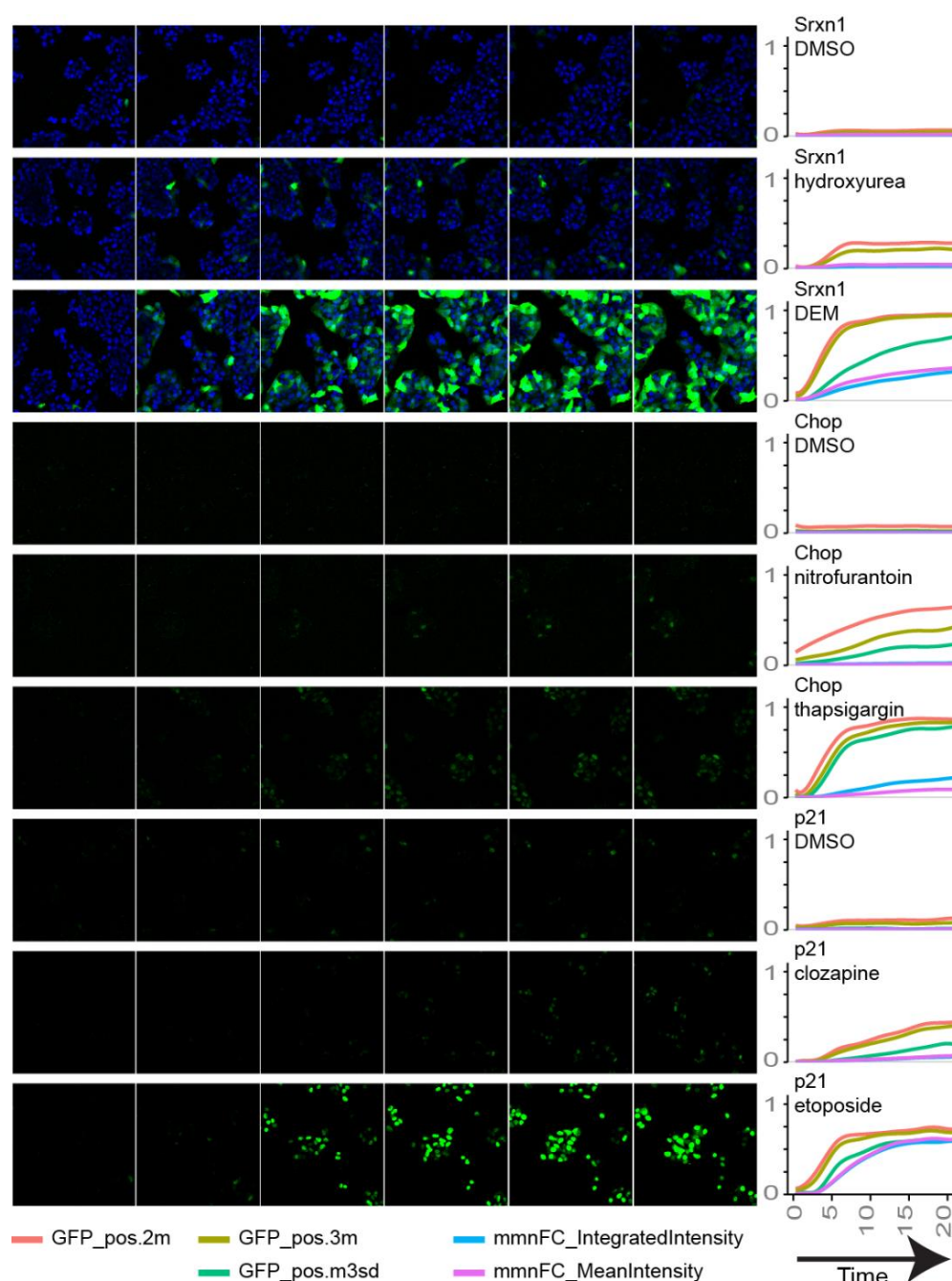


**Figure 3: Dynamics of GFP-Srxn1, GFP-Chop and GFP-p21 reporter activation.** Left panel) Time lapse stills of the reporters exemplifying the importance of single cell analysis which allows fine tuning sensitivity versus dynamic range of BAC-reporter readout. Right panel) quantification of GFP signal of the 3 reporters from a control, a weak reporter-activating compound and a strong reporter-activating compound. The single cell population means of integrated or mean intensity values show no effect for the weak-activating compounds. By counting and determining the fraction of GFP positive cells above a plate-specific threshold; GFP\_pos.2m (twice the DMSO population mean), GFP\_pos.3m (thrice the DMSO population mean) & GFP\_pos.m3sd (population mean plus three times the standard deviation) the sensitivity is increased, at the cost of dynamic range.

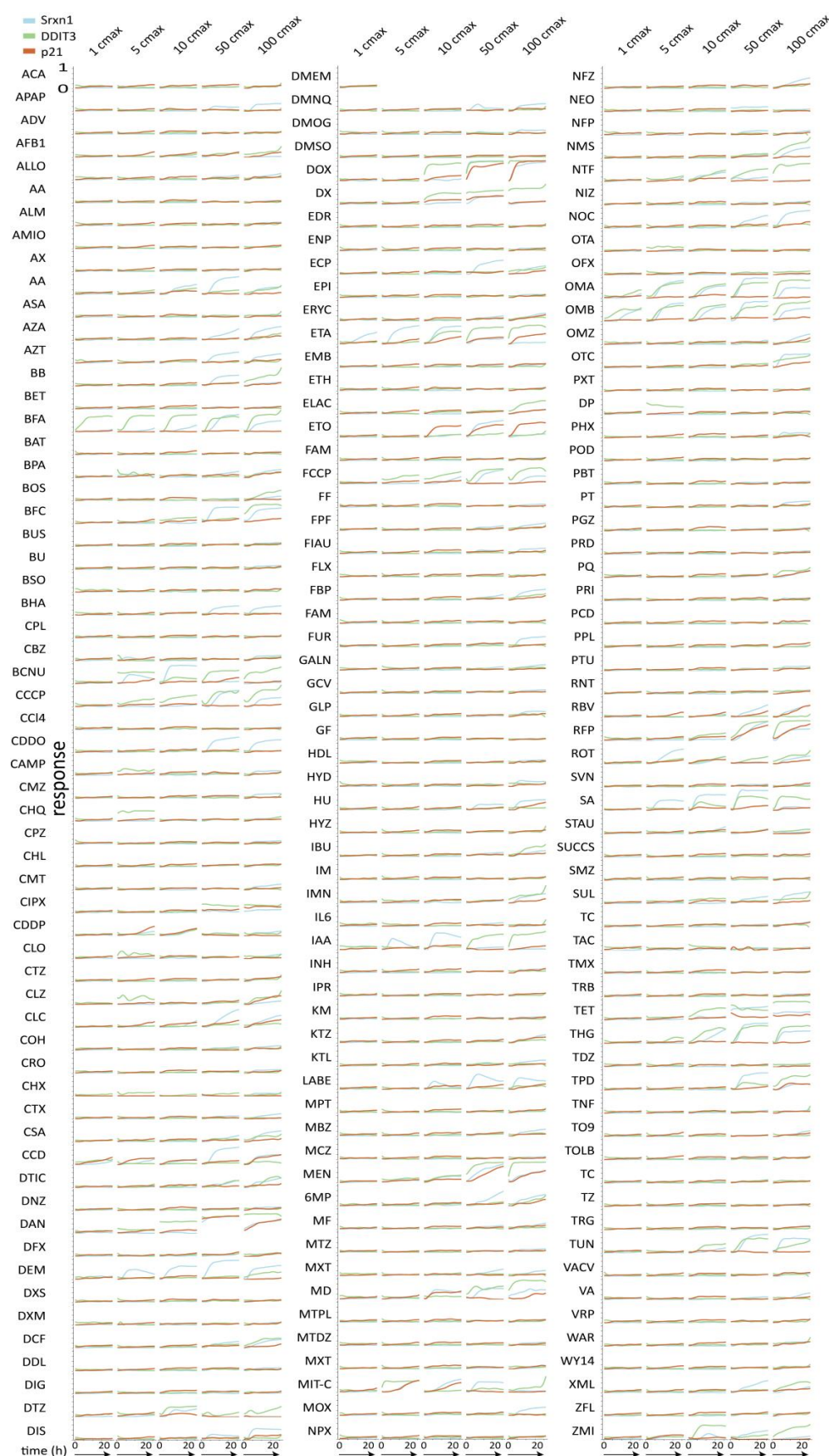
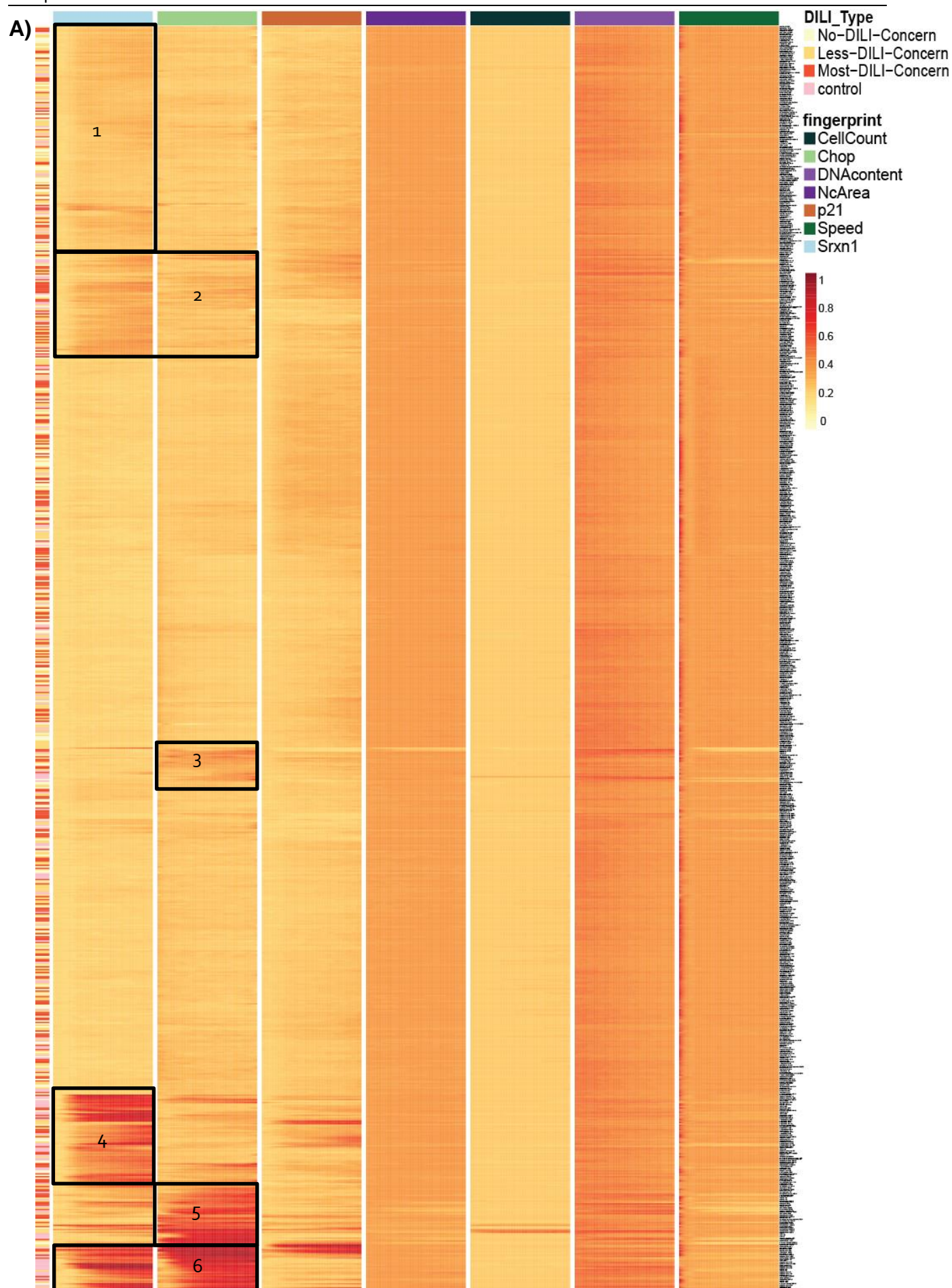


**Figure 4: Concentration time course responses of all compounds for GFP-Srxn1, GFP-Chop and GFP-p21 reporter activation.** For all compounds the reporter activity for the individual reporters was fitted and scaled as described in material and methods section. Shown are the responses for individual concentration (C-max 1, 5, 10, 50 and 100) for the different reporter (GFP-Srxn1: blue; GFP-Chop/DDIT3: green; GFP-p21: red).

#### **4.4. DILI compounds show specific reporter activation with distinct time dynamics and magnitude.**

As a next step we performed hierarchical clustering of all the dynamic information of the 176 concentration-response datasets representing the reporter activities from all BAC-GFP reporter cell lines as well as the viability markers. For this the distance between all time-vectors for each feature were computed separately followed by calculating the mean distances over all features (Figure 5). These mean-distances were used for the ward-clustering. The BAC-GFP reporter responses contributed most to the clustering; as expected the viability measures did only contribute to a minor extent. The clustering distinguished 6 clearly distinct groups: 1) mild Srxn1 activation only; 2) mild Srxn1 and CHOP activation, but no p21 activation; 3) mild CHOP activation only; 4) predominant strong Srxn1 activation; 5) predominantly strong CHOP activation; and 6) strong Srxn1 and CHOP activation. Several compounds also induce p21 strongly (arrows). Since these data include all different concentrations of 1 up to 100 times C-max, we would not expect a defined clustering of all DILI compound exposures, since the lower concentrations were expected not to give a strong response. Regardless, in cluster 4-6 we could see strong responses of 13 of in total 51 (25%) less-DILI concern and 26 of in total 58 (45%) most-DILI concern compounds. 8 of total 37 (22%) non-DILI-concern compounds were in this group, of which ethacrynic acid, mitomycin C, bisphenol A and entecapone are known to be directly cytotoxic to cells and would be defined as reference control compounds. Of relevance, we observed that group 4, i.e. predominant fast and strong activation of the Srxn1-GFP reporter, contained reference control compounds that directly affect the KEAP1/Nrf2 pathway (CDDO-Me and DEM) and other compounds, including DILI compounds, that based on their structure and (in)direct reactivity are likely to affect cellular thiol residues and thus may affect the KEAP1/Nrf2 pathway as well (e.g. carmustine are disulfiram). This illustrates the direct and specific assessment of mode-of-action. Additionally, we observed that several compounds that directly affect mitochondrial function through different mechanisms (oligomycin A and B, FCCP and CCCP) clustered together and strongly affected both the Srxn1-GFP and CHOP-GFP. The p21-GFP was only mildly affected in this screen: only (in)direct DNA damaging agents (etoposide, doxorubicin, mitomycin C, menadione).





B)



**Figure 5: Hierarchical clustering of concentration time course adaptive stress responses of 173 compound treatments.** (A) Time course heatmap of the three response features of the 3 BAC\_GFP adaptive stress response reporters [Srxn1 (blue), Chop (light green) and p21 (brown)] and the four viability markers [nuclear area (dark purple), cell count (black), DNA content (light purple) and cell count (dark green)]. Each of the 7 columns represents a time course of 24 hours. Each line is a separate treatment [compound/concentration]. The red intensity-level represents the magnitude of the feature. All treatments are annotated with the vertical bar on the left as reference control compound (pink), no-DILI (white), less-DILI (light orange) and most-DILI (dark orange). (B) A detail of the clusters 4, 5 and 6 is shown.

#### 4.5. Dose response curves and multiple feature clustering increases mechanistic insight of compound induced cytotoxicity.

As a next step the time profiles of all relevant features were transformed (see also Figure 2). Several features were independent of time (such as cell death fraction at the end of the live imaging session); others required transformation to the maximum in time (to include early response profiles); and for yet other features such as cell speed or cell count the averages and the slopes were determined to get an indication of these features with respect to treatments (with the average) and in time (with the slope). These data transformations allowed visualization of dose response relationships for all compounds and the three BAC-GFP reporters (Figure 6). Half of the compounds induce SRXN1-GFP, about one-third induce CHOP-GFP; much fewer compounds activate p21-GFP. Most responses follow a typical increase concentration level dynamic. Yet, several compounds lead to a decrease in response at higher concentrations; this is likely caused by cytotoxicity and cell death caused by the compounds at the higher concentrations (e.g. ethacrynic acid, nitrofurantoin and iodoacetamide; see also cluster 1 in Figure 7). Interestingly, several compounds at lower concentrations initiate oxidative stress and only at higher concentration the 'secondary' UPR is activated (e.g. dilitiazem, ethacrynic acid, iodoacetamide and simvastatin). Reversely, several compounds activate the UPR CHOP-GFP reporter at lower C-max values followed by 'secondary' SRXN1-GFP induction (e.g. brefeldin A, bromfenac, CCP, FCCP, rifampicin, thapsigargin and tunicamycin).

#### 4.6. Clustering of compound reporter fingerprints allows mode-of-action discrimination.

Next we used the concentration response data from all reporters as well as the biological relevant reporter-independent features for multiple feature-based unsupervised hierarchical clustering of all the DILI compounds together with reference control compounds with known mode-of-action. For the reporter responses we included: 2X mean of DMSO, 3X mean of DMSO, mean + 3X standard deviation of DMSO, mean and integrated intensity; for the reporter-independent responses we included information on: nuclear area, Hoechst intensity, cell speed, number of cells and the PI (necrotic) and AV (apoptosis) positive fraction of cells (Figure 7A and B). Clustering showed two groups with strong reporter activation (see group 1 and 2 in Figure 7A); of importance: cytotoxicity responses are in particular observed in cluster 1.

Group 1 contains 12 DILI compounds (6 less-DILI & 6 most-DILI), 2 non-DILI compounds (ethacrynic acid and mitomycin C) and 10 control compounds. Ethacrynic acid is labeled as non-DILI although this compound is well known to deplete glutathione [322] and rather reflects a reference control compound. Also mitomycin is an alkylating agent causing genotoxicity [323]. The compounds in group 1 showed overt toxicity at higher C-max values and high Srxn1 and CHOP



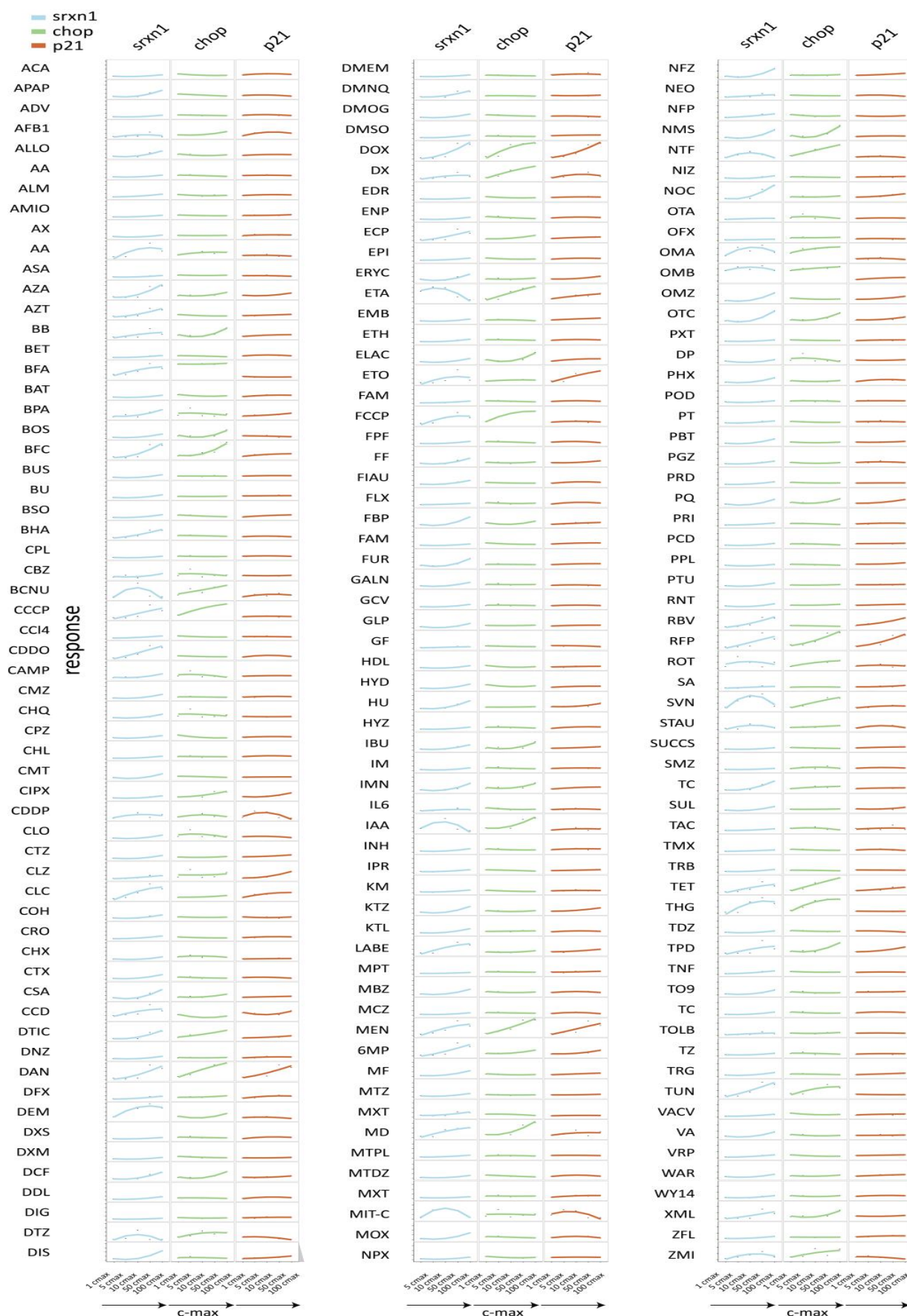
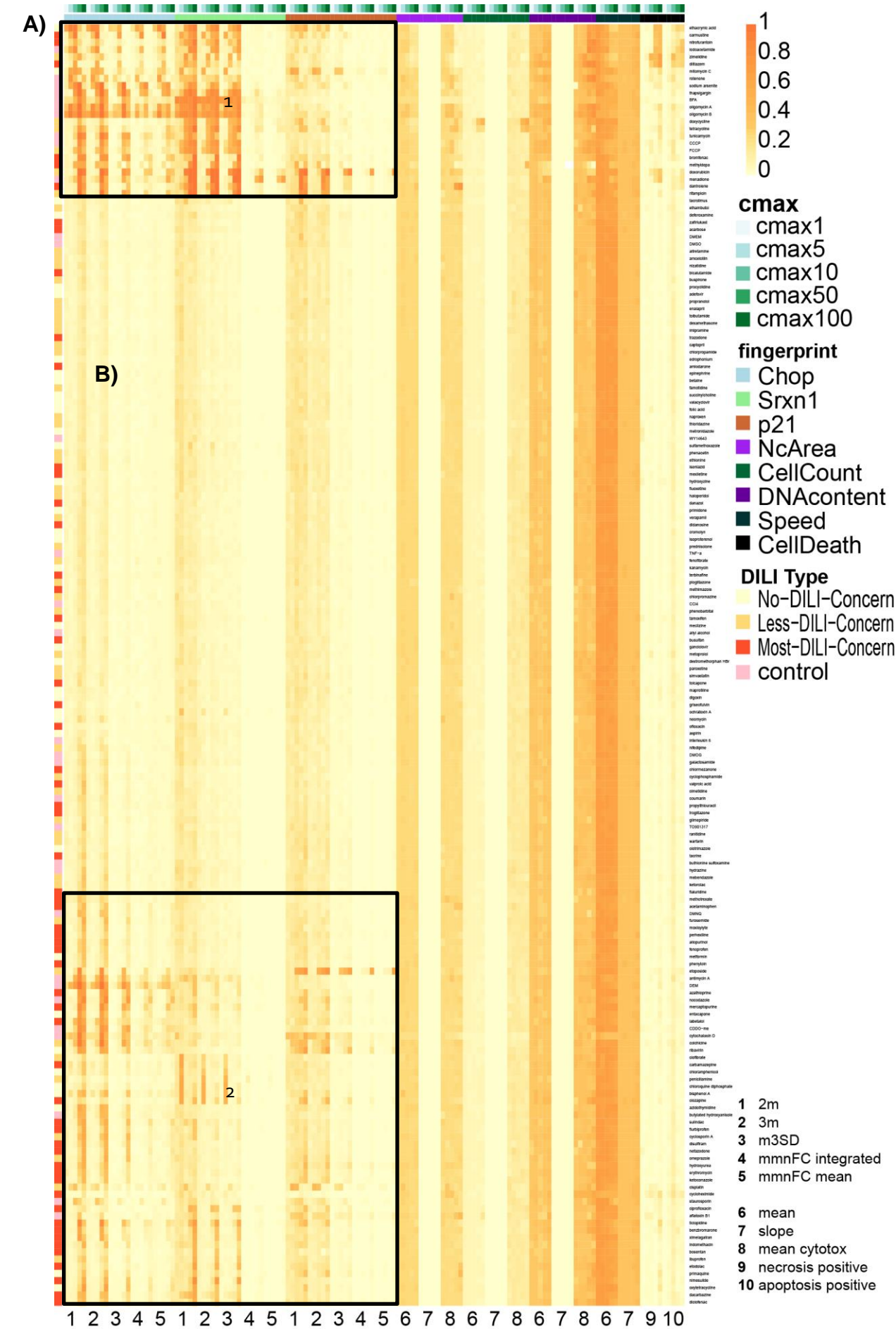


**Figure 6: Dose response curves for all individual compounds and reporters.** Dose response is based on max-in-time of fraction of cells above 2X mean DMSO level for the adaptive stress response proteins Srxn1 (blue), Chop (green) and p21 (red). The compounds are ordered alphabetically, compound abbreviations can be found in Table 1.



responses at lower C-max values. Strikingly both structure-related (e.g. oligomycin A and B, CCCP and FCCP) as well as mode-of-cation-related compounds (brefeldin A, tunicamycin and thapsigargin) clustered together in this group (Figure 7B). Since the reference control compounds in this group are quite reactive and cytotoxic (e.g. iodoacetamide, ethacrynic acid, carmustine, sodium arsenite, rotenone, oligomycin, CCCP, and menadione), we anticipate that the DILI compounds that fall within this cluster are likely to be equally reactive and/or disrupt vital metabolic processes in the cell leading to oxidative stress and UPR activation.

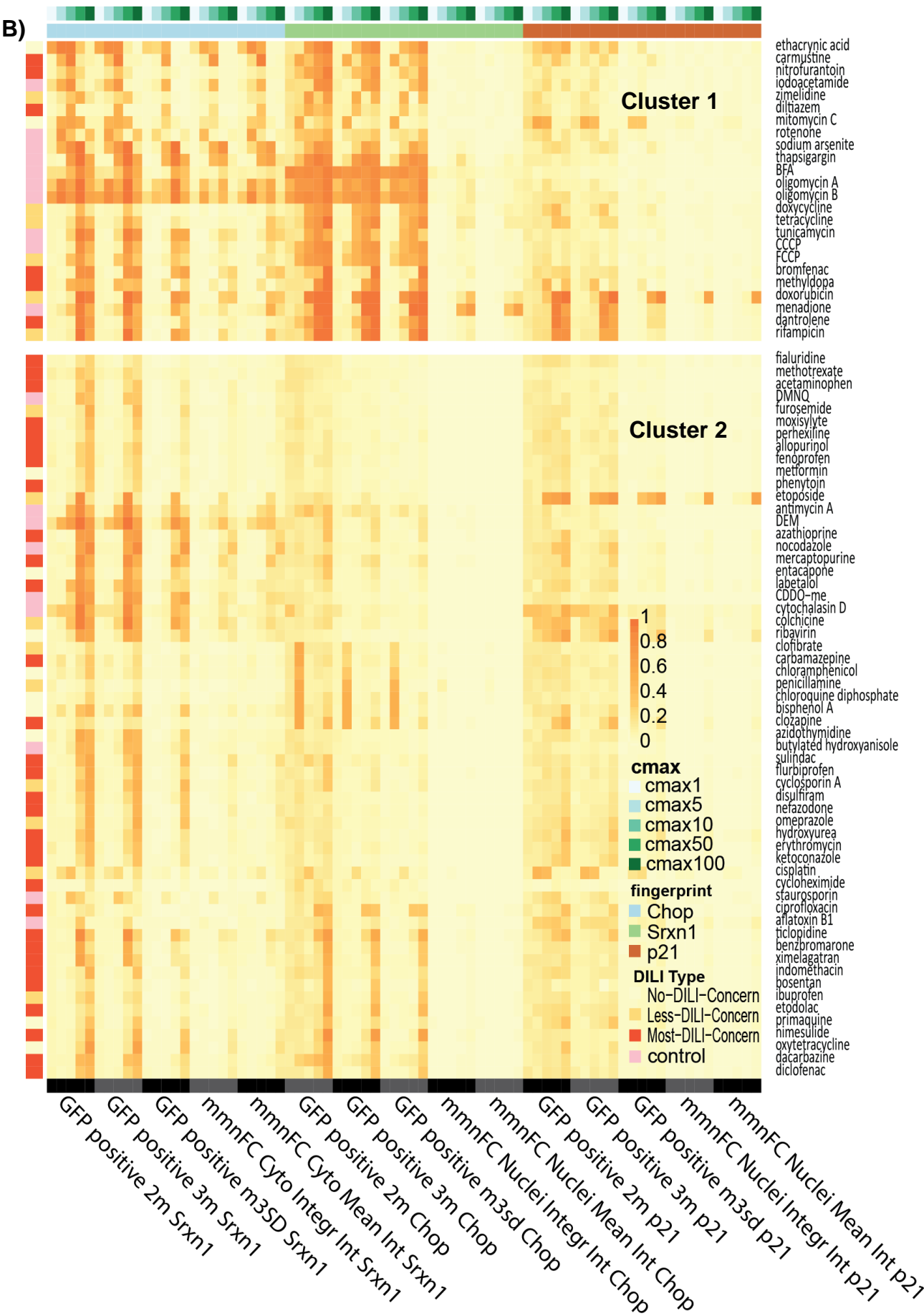
Within group 2 little cytotoxicity was observed within the entire concentration range, indicating that the adaptive stress responses well precede cytotoxic dose ranges. The group 2 compounds are highly enriched with most-DILI concern compounds (31 (53%) of all most-DILI compounds). Several key groups can be identified: i) compounds that predominately induce the SRXN1-GFP reporter, ii) compounds that predominately induce CHOP-GFP reporter activity; and iii) compounds that activate both pathways at closely similar C-max values.

#### 4.7. Multiple adaptive stress response pathway activation and higher C-max values indicate higher risk for DILI.

We further investigated the relationship between concentration and reporter activity. We therefore defined for each compound the actual concentration at which a compound caused at least 25% or 50% induction of GFP-positive cells for individual reporters. Most compounds passed the criteria for the Srxn1-GFP reporter; in particular reference control compounds caused activation of this reporter at sub- $\mu$ M range, whereas most DILI compounds (either less or most concern) caused the activation in the range of 10-100  $\mu$ M; also some non-DILI compounds fell in this range (Figure 8A). Similar observations were made for CHOP-GFP and p21-GFP reporters. Further enrichment of most-DILI compounds occurred for minimally 2 reporter responses with both >25% GFP positive cells, with fewer non-DILI compounds remaining (Figure 8B). Further increasing the stringency (50% GFP-positive cells) overall decreased the number of compounds, and in particular remained Srxn1-GFP and CHOP-GFP, responses (Figure 8C). Interestingly, dual activation under these stringent conditions further reduced the number of compounds, as well as



**Figure 7: Hierarchical clustering of compounds based on concentration responses for all reporter and cell viability features.** A) Clustering results of all features were transformed to single values as described in material and methods. Fingerprint-sets Srxn1 (blue), Chop (light green), p21 (brown), nuclei area (light purple), cell count (dark green), DNA content (dark purple), cell speed (grey) and cell death (black) consist of different features. For reporters: 1) **2m** (fraction of cells above 2 times the mean), 2) **3m** (fraction of cells above 3 times the mean), 3) **m3SD** (3 times the mean or mean plus 3 times standard deviation DMSO population), 4) **mmnFC integrated** (normalized fold change with respect to DMSO population integrated), 5) **mmnFC mean** (normalized fold change with respect to DMSO population integrated). For non-reporter features: 6) **mean** (mean of linear fits of time course data), 7) **slope** (slope of linear fits of time course data), 8) **mean cytotox** (population mean of PI and annexin), 9) **necrosis positive** (fraction of cells stained for PI), 10) **apoptosis positive** (fraction of cells stained annexin-V positive). Each feature shows the concentration range (shades of blue-green [marked on top]) from left to right: 1, 5, 10, 50 and 100 C-max. On the left the compound DILI annotation is indicated as before. B) Zoom of group 1 and group 2 for the different reporter features. B) Zoom of boxes 1 and 2 (displayed on next page)





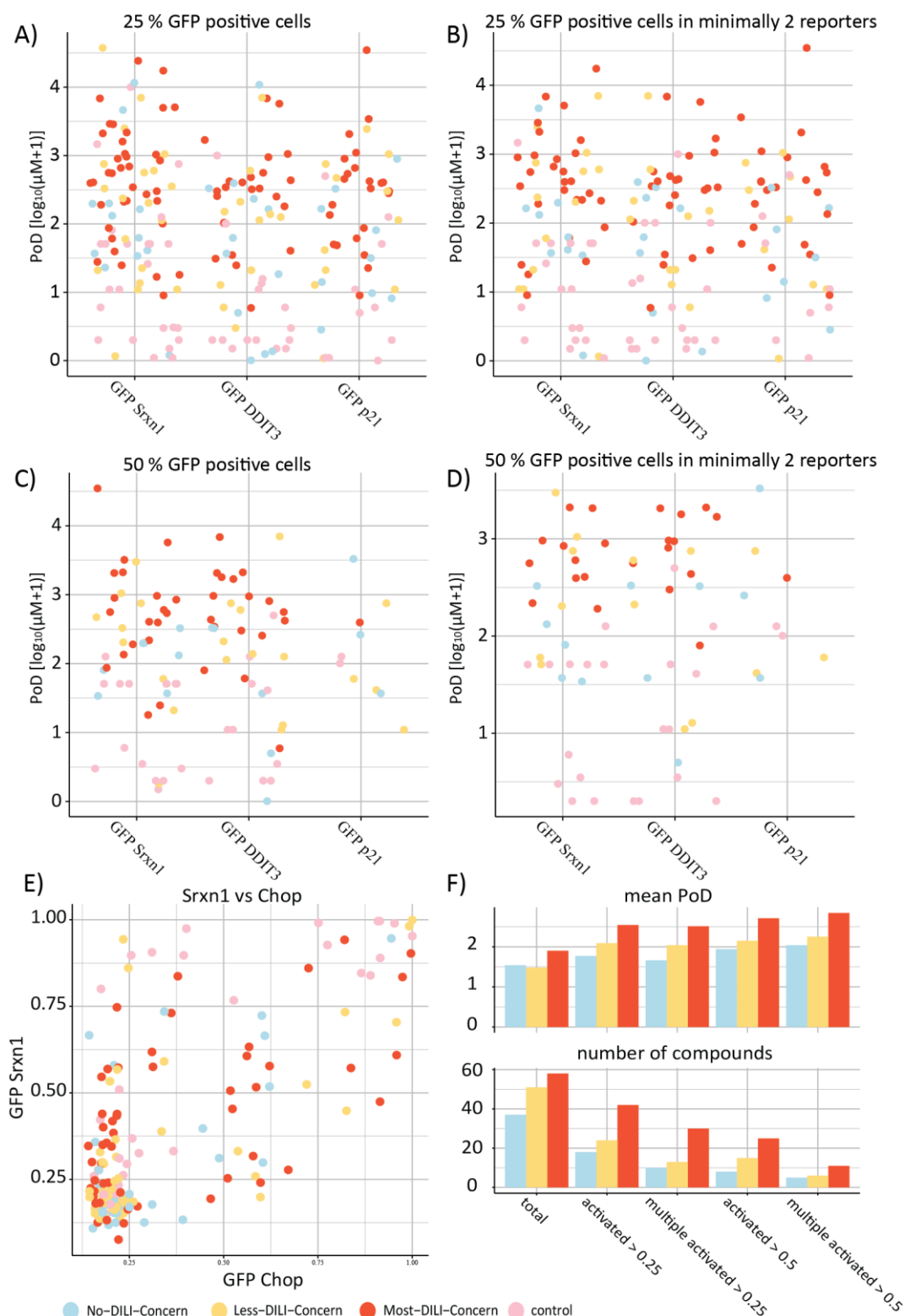


**Figure 8: Relationship between reporter response and DILI labeling.** A) Shown is the lowest concentration where at least 25% cells is “GFP positive” as defined by 2X above population mean of DMSO; only compounds are included for which this is true. B) Lowest concentration where at least 25% of cells is GFP positive in at least two different reporters. C & D) Same as panel A and B, respectively, but now with at least 50% of cells GFP positive. F) summary of panels A-E: top shows the mean Point of Departure (PoD) as the mean of the lowest concentrations of all treatments that activates the reporters. Bottom shows the total number of compounds per DILI category that are activated under these conditions.



further increased the overall concentration at which such a double response was observed (Figure 8D and F). When plotting for all compounds the Srxn1-GFP and CHOP-GFP reporter activities, both most informative, we observed that strong activation of Srxn1 and CHOP was primarily observed for less and most DILI concern compounds (Figure 8E); only one non-DILI compound belonged to this group which was actually ethycrynic acid, a strong soft electrophilic compound directly affecting cellular thiols.

#### **4.8. Concordance between HepG2 BAC-GFP reporters and primary human hepatocytes (PHH).**

To assess the concordance between our reporters and PHH we compared our BAC-GFP reporter data (maximal % GFP positive cells observed) and the fold transcript data in PHH based on the TG-GATEs dataset (highest concentration at 24 hr). In general the response of PHH transcript levels is highly comparable to the HepG2 BAC reporters, in particular for the Srxn1-GFP and CHOP-GFP reporters (Figure 9A). The concordance increased when strong responses were observed in the reporter cells. Interestingly BAC reporters seemed more sensitive than transcript analysis in PHH (Figure 9B). In addition treatments that activate both the HepG2 BAC reporters as well as increase transcript levels are highly enriched in most-DILI concern compounds.

### **5. Discussion**

Here we investigated the integrated application of a panel of three adaptive stress response BAC reporters in high content high throughput screening as a method for DILI liability assessment. We focused on adaptive stress pathway signalling as these defense programs are a universal theme in all life forms, and respond before the onset of overt toxicity. We monitored three downstream target genes for oxidative stress (Srxn1), ER-stress/UPR (CHOP) and DNA damage (p21); these are selective targets for these pathways. Using CellProfiler and R-package H5CellProfiler we quantified all features and performed detailed analysis on the individual contribution to DILI classification. We demonstrate how advanced analysis of live-single cell data can provide key information on the concentration-time course reporter responses that can be applied for DILI liability evaluation. We showed that integration of such mode-of-action assessment using different reporter strongly improves the classification of less- and most-DILI concern compounds.

The current data demonstrate the strength in the application of time-resolved live single cell reporter data. To date toxicity screening efforts using high content imaging have mostly focused on single time point fluorescent dyes or anti-bodies [241] with several real-time based toxicity screening efforts [324]. However with the use of our reporter cell lines biological signalling can be visualized with a high time resolution to more accurately pin-point the primary mode-of-action. The use of dyes and anti-bodies brings additional noise to already very noisy systems as fixation and anti-body binding are likely additional sources of variability; this is not an issue using our reporter models. Time course signalling data also greatly benefits computational modeling efforts as these require detailed time and dose response dynamics, this is only feasible using live cell imaging data.

We have successfully applied a limited set of features for DILI liability assessment. Yet,

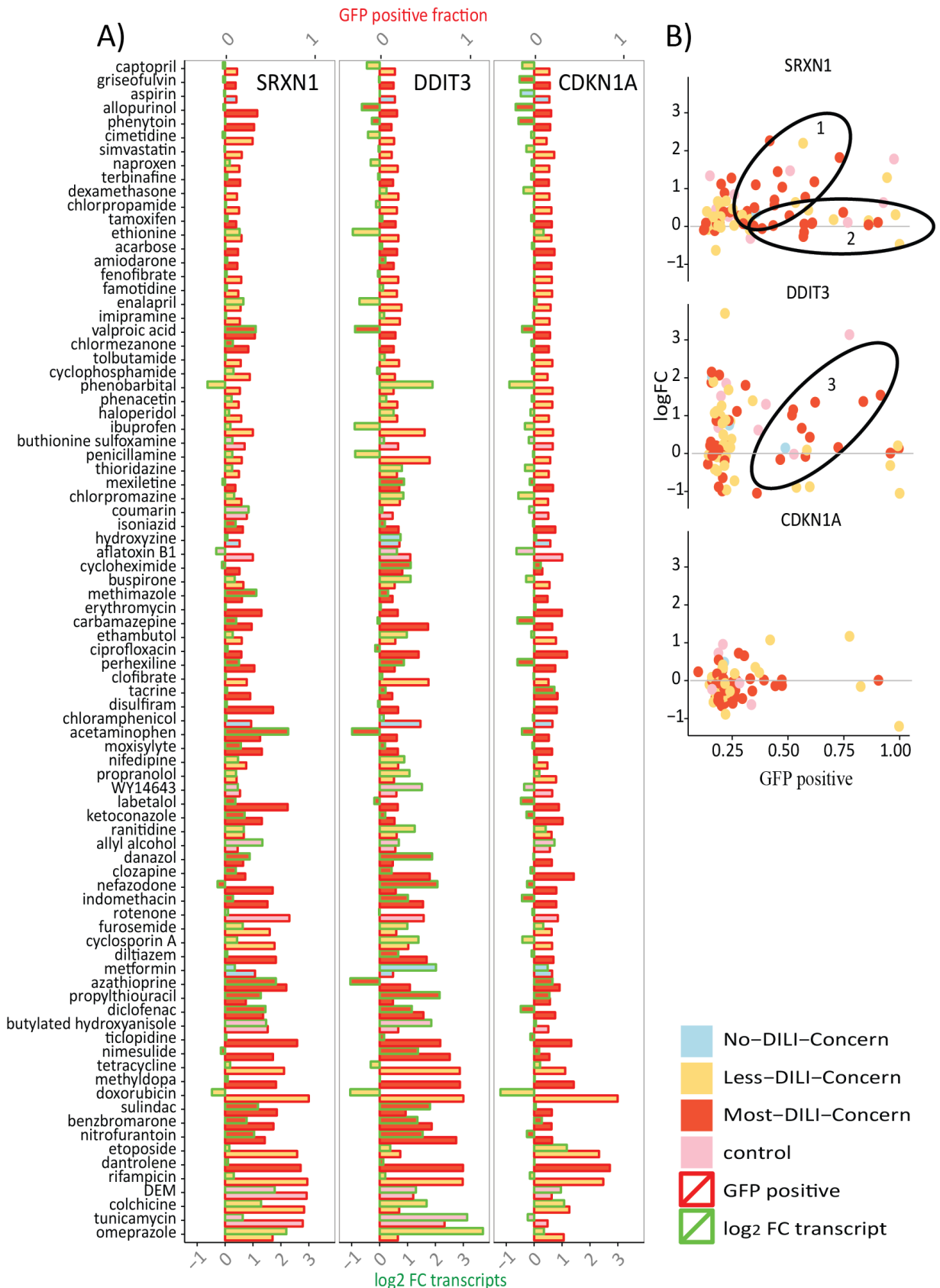


**Figure 9: Concordance between BAC-GFP HepG2 reporter activation and primary human hepatocyte transcript levels.** A) Compounds are ordered from lowest average over *Srxn1*, *Chop* and *p21* to the highest (top). BAC GFP intensity levels are red-lined, transcript fold changes are green-lined. Bar colors correspond to No-DILI-concern (blue), Less-DILI-concern (light orange), Most-DILI-Concern (dark orange) and control compounds (pink). Panel B) GFP positive cells (x-axis) vs transcript levels (y-axis).

another approach to high content imaging is the use of large amounts (up to 700) of measurements/features [325, 326] and use supervised clustering, dimension reduction techniques and/or feature selection to obtain a classifier to predict toxicity or specific compound effects. However several challenges exist with such an approach. It is often difficult to define a biological meaning over certain results beyond co-clustering of compounds of which the toxicity/mechanism is presumed to be known (so called guilt by association). A high-dependency of most of these features exist and this magnifies certain phenotypes over others likely diluting more subtle and possibly important phenotypic changes. We focused on a smaller set of biological interpretable features we believe to be of interest in DILI. This small set of biological interpretable features is a 'fingerprint' as to the cellular state and in the current study includes the activation of: the oxidative stress response, i.e. Srxn1-GFP activation; the ER-stress response (UPR), i.e. CHOP activation; the DNA-damage response, i.e. p21 activation; nuclear area; number of cells; Hoechst intensity; cell speed and cell death (necrosis and apoptosis). This strategy captures together several adaptive stress responses as well as general cellular features. We acknowledge the limitation of these measures, since DILI phenotypes that involve innate and adaptive immune responses, cholestasis or steatosis are likely not covered in our reporters. This possibly explains why the overall sensitivity of the combined assays is not yet sufficient to correctly identify all less- and most-DILI concern compounds. Future integration of other GFP-BAC reporters that would cover these DILI toxicity programs will still be required. At that stage supervised clustering using the pre-defined DILI labels followed by feature selection to establish a most-DILI-concern fingerprint should improve our current approach. Since several DILI compounds induce stress responses with distinct time and reporter activation dynamics, it would be relevant to include the order of reporter activation, the time of the maximum response, the magnitude of the response and the C-max value associated to these dynamics in such supervised clustering efforts. This will be our future research focus. Regardless, our current strategy already allows a near perfect fingerprinting, since oligomycin A and oligomycin B as well as CCCP and FCCP do cluster together. Additional reporter will further improve the compound mode-of-action fingerprinting.

Our data indicate a striking overlap between HepG2 BAC-GFP responses and transcript levels in primary human hepatocyte. Although HepG2 is metabolically incompetent compared to primary hepatocytes, several compounds that involve biotransformation-dependent toxicity do show a Srxn1-GFP oxidative stress response (e.g. acetaminophen and sulindac). Possibly the low metabolic capacity of the HepG2 model is offset to some extent by the increased sensitivity as it is not toxicity that is measured but an adaptive stress responses. Future studies will establish whether our HepG2-based reporter platform would further benefit from improved metabolic competence.

The anti-oxidant response is critical in the protection against oxidative stress and inhibition of this pathways propagates DILI for various compounds [327]. In our study the Srxn1-GFP reporter was activated by about half of the DILI compounds, which fits with the observation that oxidative stress is a major contributor to DILI [328]. Our test compounds may affect this pathway through direct interaction with KEAP1, thus unleashing Nrf2, or through modulation of the mitochondrial respiratory chain. Indeed various reference control compounds that either affect KEAP1 (CDDO, DEM, ethacrynic acid) or the mitochondria (rotenone, CCCP, oligomycin A) do induce Srxn1-GFP activation, supporting both direct and indirect mechanisms for Srxn1-GFP induction. Most notably oxidative stress following UPR activation was also seen for several ER-

stress inducing compounds, including thapsigargin, tunicamycin and brefeldin A. Reversely, oligomycin and CCCP strongly activated the CHOP-GFP activation. Altogether this underscores the connectivity and complexity of adaptive stress response regulation.

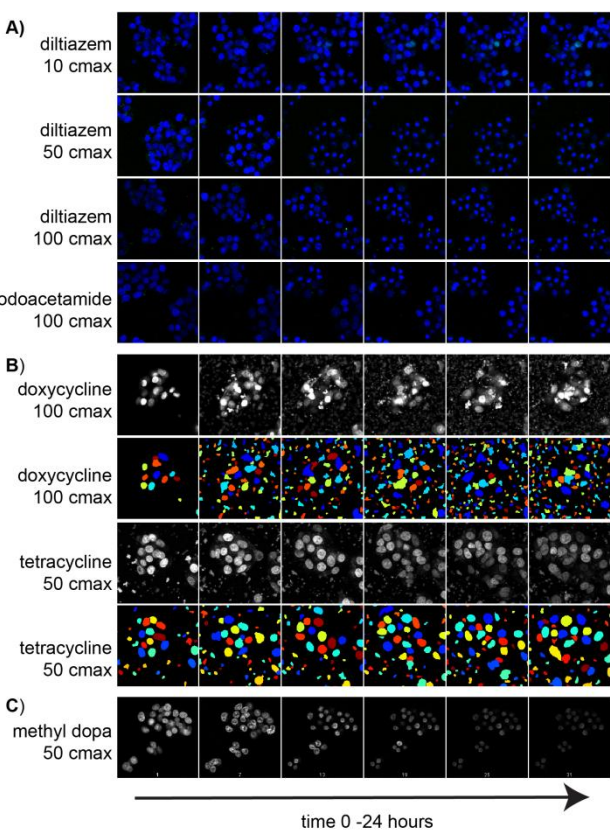
Only several DILI compounds mildly activated the p21 reporter. This is fortunate and expected since direct DNA damaging compounds are terminated early in drug development. Although p21-GFP is activated by DNA damaging agents in our study (e.g. doxorubicin and etoposide), p21 cannot be considered as a sole DNA damage reporter, since its expression is also regulated through other stress responses. Regardless, in our setting, the p21-GFP reporter contributed to the evaluation of DILI responses, be it to a limited level than Srxn1-GFP and CHOP-GFP.

In conclusion, we have shown that BAC-GFP reporter cell lines are a sensitive tool to provide detailed mechanistic information regarding the adaptive stress response activation in a broad compound screening setting using high-content live single cell imaging. Such detailed insights in the perturbations of signalling pathways after chemical exposure provides key information for predictive purposes. We anticipate that our BAC-GFP reporter platform will contribute to the early pre-clinical screening for DILI liabilities and possibly also other chemical safety assessment paradigms.

Supplemental figures

compound[μM]	nuclei area	cell count	DNA content	migration speed
aflatoxin B1 [50]	normal	normal	low	normal
aflatoxin B1 [100]	normal	high	high	normal
benzbromarone [440]	normal	normal	normal	low
carmustine [3000]	low	normal	normal	low
carmustine [6000]	normal	normal	normal	very low
cisplatin [20]	normal	normal	low	normal
cisplatin [100]	normal	normal	normal	bit low
cisplatin [200]	normal	normal	normal	bit low
cyclohexamide [50]	normal	normal	normal	bit low
cyclohexamide [250]	normal	normal	normal	bit low
cyclohexamide [500]	normal	normal	normal	bit low
cyclohexamide [2500]	normal	normal	normal	bit low
cyclohexamide [50]	normal	normal	normal	normal
cyclohexamide [5000]	normal	normal	high	low
cytochalasin D [5]	normal	normal	normal	low
cytochalasin D [10]	normal	normal	normal	low
cytochalasin D [50]	normal	normal	normal	very low
cytochalasin D [100]	normal	normal	normal	very low
digoxin [0.28]	normal	normal	normal	bit low
diltiazem [480]	normal	normal	high	normal
diltiazem [960]	normal	normal	high	low
diltiazem [4800]	low	low	high	very low
diltiazem [9600]	low	low	high	very low
doxycycline [112]	normal	high	normal	normal
doxycycline [560]	normal	high	normal	normal
doxycycline [1125]	normal	high	high	normal
ethacrynic acid [1650]	low	normal	normal	very low
ethacrynic acid [3300]	low	normal	normal	very low
iodoacetamide [50]	low	normal	high	very low
iodoacetamide [100]	low	normal	normal	very low
methyl dopa [950]	low	normal	low	very low
methyl dopa [1900]	normal	normal	low	normal
nitrofurantoin [300]	normal	normal	normal	low
nitrofurantoin [600]	low	normal	normal	very low
perhexiline [215]	normal	normal	normal	normal
rotenone [4]	normal	normal	normal	low
rotenone [20]	normal	normal	high	very low
rotenone [40]	normal	normal	high	very low
staurosporin [0.5]	normal	normal	normal	low
staurosporin [1]	normal	normal	normal	very low
tetracycline [1050]	normal	high	normal	normal
tetracycline [2100]	normal	high	normal	normal
tunicamycin [100]	normal	normal	normal	bit low
zimelidine [600]	normal	normal	high	low
zimelidine [3000]	low	normal	normal	very low
zimelidine [6000]	low	normal	normal	very low

Supplemental Fig. S1



Supplemental Fig. S2

**Supplemental Fig. S1: Cell viability markers-quality control features.** Compound-concentration conditions that were flagged for at least 2 features are displayed. These are flagged as either normal (colored green) or very low (>20% increase), bit low (<30%), low (<50%) and high (>50%) (high-lighted in orange) as determined by visual inspection of figure 7.

**Supplemental Fig. S2: Example images of quality control flagged treatments.** A) Diltiazem at higher c-max values induces cell death; the cells stop moving, the nuclei decrease in number, shrink and the Hoechst intensity increases (top 3 rows). Nuclei shrinkage with migration stop of iodoacetamide at 100-cmax (bottom row). B) Unusual large number of cells of doxycycline and tetracycline due to auto fluorescence. C) low DNA content/ low Hoechst intensity is observed for methyl dopa.

# Chapter 7

## User friendly high-content imaging big-data analysis on a single desktop: R package H5CellProfiler.

---

**This chapter is based on a manuscript in preparation:**

Steven Wink, Joost Beltman and Bob van de Water

Division of Toxicology, Leiden Academic Centre for Drug Research, Leiden University, Leiden, The Netherlands

## 1. Abstract

Technological development has led to ever increasing amounts of data in high content screening. For utilizing such data in an efficient, thorough and user friendly manner we developed the R-package H5CellProfiler. H5CellProfiler is based on R-packages data.table, ggvis, ggplot2 and shiny. H5CellProfiler launches a browser which allows scientists to analyze large single cell datasets and make statistical summaries and graphs on their own local desktop in a fast and memory efficient manner. In addition, single cell track-labels are calculated and broken tracks are re-connected based on user-defined thresholds resulting in unique sets of annotated tracks.

## 2. Introduction

High-throughput high-content automated imaging (HT-HCI) includes image acquisition, image storage, image annotation, image analysis, data analysis and storage of the analysis results. Image acquisition is performed by high-end automated microscopes that are equipped with hardware and software for stage-movement or objective movement and often with an incubation chamber that has temperature and CO<sub>2</sub> regulation allowing live cell imaging. These conditions allow the acquisition of large imaging datasets from multi-well plates capturing the dynamics of cell biological events.

Image annotation can be divided in two categories: first, technical annotation which is automatically generated by the acquisition software and consists of technical acquisition parameters. Second, biological annotation consisting of parameters that the scientist needs to add himself. Biological annotation of images is closely related to data storage of images in a file server, which is managed by a database management system (DBMS). The DBMS allows annotation, organization, querying and often visualization of the acquired images. Well-known image DBM systems are OMERO from the Open Microscopy Environment (OME) [329] and its commercialized version Columbus.

Image analysis can be performed with the aid of commercial or open source software which differ in the offered functionality and flexibility. Several commercial software systems exist that provide easy to use image analysis solutions, sometimes directly combined with image acquisition. Well-known software systems include NIS-Elements (NIKON), Metamorph (Molecular Devices), AxioVision (Zeiss) and Volocity (Perkin-Elmer). Recently, commercial systems have been developed that even combine multiple HT-HCI stages. For example, Columbus from PerkinElmer is able to store, annotate and analyze images and analyze the resultant data with several statistical and graphical tools due to integration with TIBCO Spotfire.

A disadvantage of using commercial software for image analysis is that it is difficult or simply not possible for researchers to modify or extend it because the source code and even the applied image analysis algorithms are hidden in order to secure the commercial product. Commercial systems are therefore best suited for standard image analysis pipelines and mostly used by industry or by labs with relatively basic and fixed image analysis needs.

Labs which frequently change equipment or have specialized image analysis requirements often prefer open source solutions. The most well-known solution is ImageJ [330], which is an important platform for scientific image analysis development. However, it can be challenging to build workflows for automated image analysis because it requires some knowledge in the available ImageJ plugin libraries, a decent understanding of image analysis algorithms and Java

scripting skills. For this reason, some researchers prefer user friendly, GUI-based image analysis software tools. A well-known example is CellProfiler [49], which was developed initially by Carpenter and colleagues. In CellProfiler, parameter optimization can be performed with the help of the GUI and accompanying graphical displays of the segmentation results. Subsequently, image analysis with appropriate parameters can be performed in an automated fashion.

In parallel with recent technological advancements in microscopy, the interest in the analysis of single cell behavior has strongly increased. Indeed, research of the heterogeneity of cell populations [331, 332], of the morphology of subcellular structures [326], of transcription factor oscillatory dynamics [217] or of cell migration [333] all require single cell measurements. As a result, the amount of data has strongly increased with consequences for the handling of image analysis output. A typical overnight live single cell imaging session of an *in vitro* 2D 384-well plate leads to around 20 GB of raw imaging data (approximately 20,000 images) and depending on the features of interest up to 5 GB of analysis data. Memory limitations require data dumps during the analysis by temporary storage in relational databases or hierarchical file based formats. Hence, labs need to set up a dedicated database server which requires maintenance and technical expertise, which can be challenging for biological oriented labs.

Recently, CellProfiler included a feature for storing measurements during the analysis using the file format HDF5 [50], a portable data format without size limitations due to the hierarchical structure. A HDF5 file can be navigated through the use of file paths – strings separated by the forward slash ‘/’ to define the hierarchical structure of the data, analogue to the Unix file system. In addition, the HDF5 format has been implemented specifically for cell-based assays in high-content microscopy in the form of CellH5 which can be used as a format for data exchange. CellH5 and several CellH5 interfaces have been developed by Huber and colleagues [194], allowing for visualization of the stored images and reading and writing of the quantitative data. However, for CellProfiler HDF5 output user friendly solutions do not yet exist. Therefore, we have developed the R-package H5CellProfiler.

H5CellProfiler requires a metadata file with biological annotations and a HDF5 file with the quantitative measurements from CellProfiler. The package loads the data into R-memory and

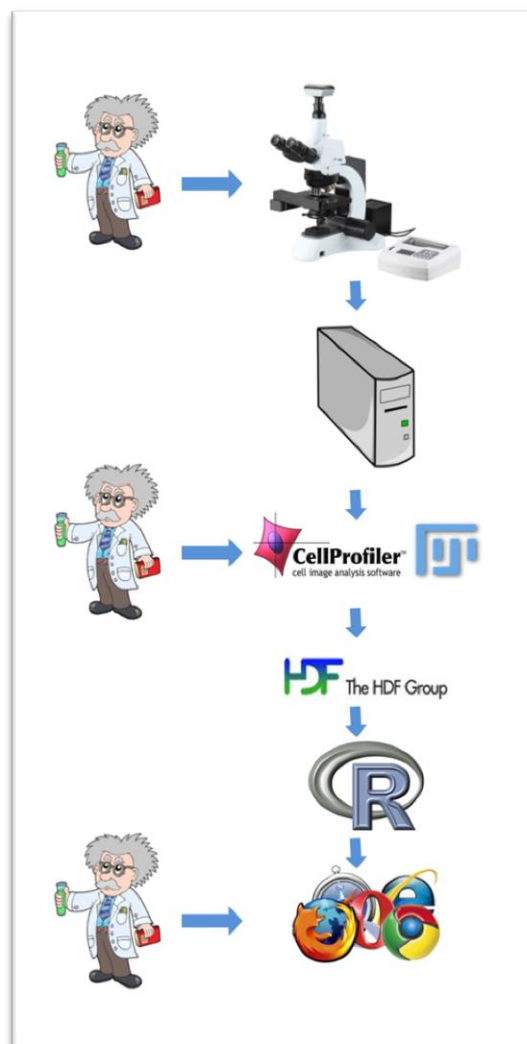


**Figure 1: User-friendly High Content image analysis workflow.** The scientist interacts with the imaging device, sets up the image analysis with GUI-based CellProfiler run on the local desktop, and finally performs the data analysis with a browser based GUI which communicates with the R server (usually on the local desktop).



organizes user-requested features at the level of single cells. Subsequently, a browser is launched and functions as a GUI for the user to manipulate, summarize and display the single cell data. This enables biologists to perform their image analysis with CellProfiler followed by the semi-automated production of single cell data summaries and visualizations that would not be possible using spreadsheets. Thus, H5CellProfiler allows to perform all data operations on a single desktop without the need to set up database and client software and as such makes the entire image analysis workflow user friendly (Fig. 1).

### 3. Results and Discussion

#### 3.1. Description of the H5CellProfiler package.

##### 3.1.1. H5CellProfiler architecture.

H5CellProfiler reads the HDF5 data and uses the input arguments (which can be typed in the R-terminal or provided as a file) and annotation files provided by the user to reformat and summarize the data in a flexible, intelligent and computationally efficient manner (Figure 2). It is flexible because the user guides the reformatting with help of the GUI and has several options: extracting relevant data into a large text file containing a single row per parent object, making a summary for each treatment, writing a text file containing rows per tracked object and columns corresponding to the time points for each time-lapse or plotting graphical displays of the data. The size of the data hardly affects the performance as long as it does not exceed the available memory capacity. This is because all data manipulations are very fast due to parallel computing and ordered indexing. As a result, up to 100GB of data is easily handled by H5CellProfiler.

##### 3.1.2. Parallel computing.

*H5CellProfiler offers parallel processing to speed up the analysis of large datasets. This is achieved with the parallel computing package ‘foreach’ and parallel back-end registration for windows operating systems ‘doSNOW’. The number of parallel sessions that can be initiated for reading and data analysis is limited by the user with a maximum of the number of separate HDF5 files. Parallel computing especially speeds up the summary calculations, the data reshaping for plotting and the re-labeling of tracking data (the number of cores for re-labeling the tracking data is independent of the number of hdf5 files and is set by the user-set argument). Chunks of the data in R memory are divided over the available cores without duplication of the data for each core, thus ensuring memory-efficient parallel computing.*

##### 3.1.3. Reading HDF5 and formatting data.

We employed the recently developed R package ‘rhdf5’[194] for reading and writing HDF5 files. An advantage of using the HDF5 format to store and read data is its annotated hierarchical hyper-rectangular structure. Together with the annotation, this enables the selection of data subsets without the need to query through the entire dataset. As a consequence, very large datasets do not slow down reading significantly.

#### 3.2. Application of R package H5CellProfiler.

Basic knowledge of CellProfiler is required to be able to provide the correct arguments for the H5CellProfiler function and are therefore briefly described here. A detailed manual of CellProfiler can be found on the website [www.cellprofiler.org](http://www.cellprofiler.org).

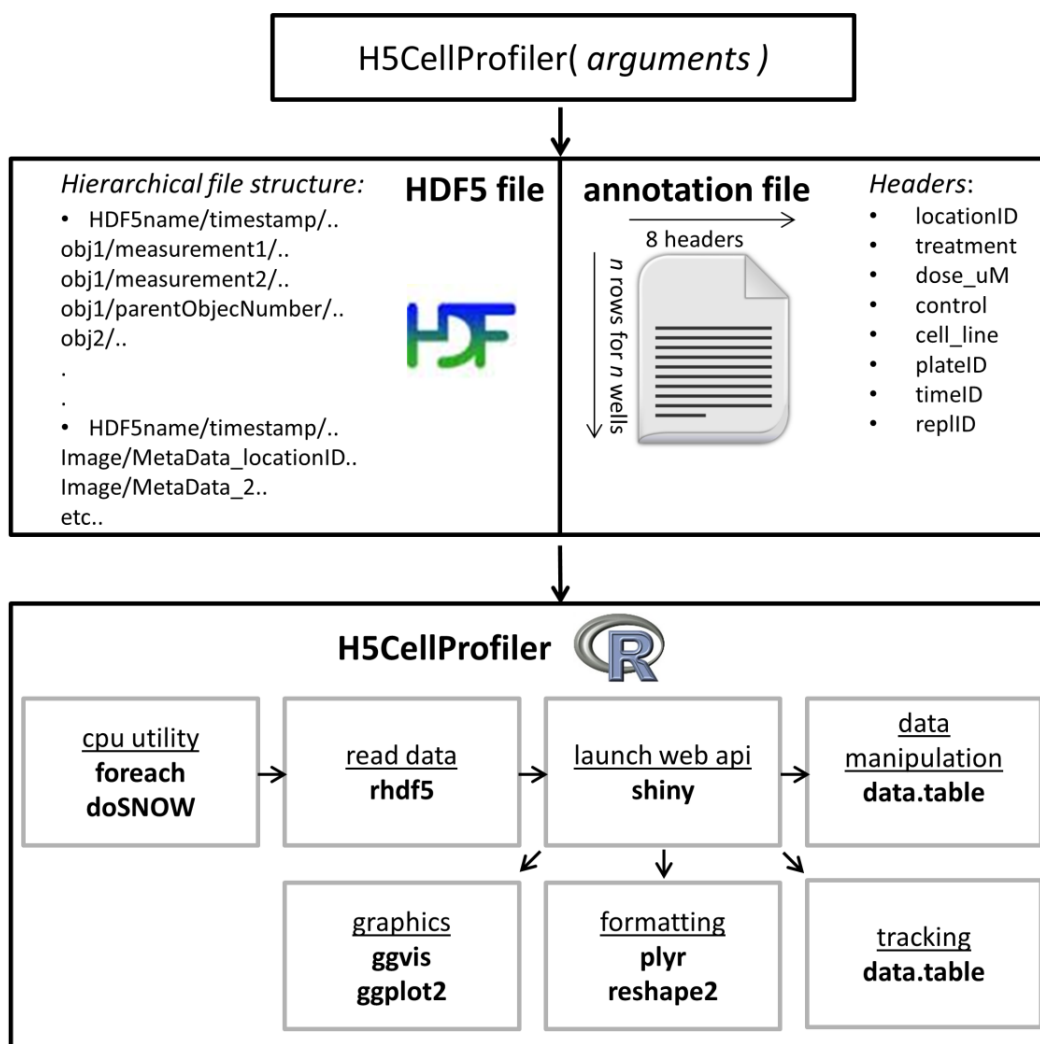


**Figure 2: Architecture of H5CellProfiler.** The main function is run by typing the H5CellProfiler (arguments) function in the terminal or by providing the arguments in a file. H5CellProfiler then uses the HDF5 file containing the image analysis data and the annotation file provided by the user containing the biological annotation. The architecture of the H5CellProfiler package is depicted in the lower panel: the order of the separate internal processes (underlined) using various R-packages (bold) are depicted by the arrows.

### 3.2.1. Regular expressions that enable linkage of biological annotation with image data.

In CellProfiler, variables are captured using a simple collection of regular expressions. For example, for an image named 'xy0013c1t01.tif' and located in a folder named './C03' (according to the well number in the plate), two sets of regular expressions capture this image annotation. In this case, the first regular expression would be `(?P<imageNumber>xy[0-9]4)c[1-4] (?P<tp>t[0-9]).tif` to capture the image number 0013 in the CellProfiler variable 'imageNumber' and the time point 01 in the variable 'tp'. Note that the characters inside the square brackets are the characters to be searched for in the image file names, the numbers inside the curly brackets denote the number of such characters, and the construction with `(?P<variable_name>...)` determines in which CellProfiler variable the contents will be stored. Similarly, the folder name './C03' can be captured by the regular expression `*[\\V](?P<Well>.* )$` or by `(?P<Well>[A-Z] [0-9])$` in the CellProfiler variable 'Well'. In the first expression the construction `*[\\V]` is a regular expression that searches

for a forward slash, the two backward slashes are escape characters for the forward slash. The asterisk '\*' is a wildcard for any character(s). The dollar sign '\$' forces the matching to take place in reverse order (starting at the end). The first expression is flexible, the second is more specific.

The key feature in these examples is that images are automatically annotated by CellProfiler and that this information is stored together with the image analysis results in the HDF5 file. The annotation obtained by the regular expressions are stored in the HDF5 output and the HDF5 file path is defined as 'Metadata\_*variablename*'. Together with a user provided annotation text file, this enables H5CellProfiler to link biological annotation to the image measurements (Figure 2). A tab delimited text file containing the biological annotation is created by the scientist which consists of several columns/headers and a row for each well of all multi-well plates that are simultaneously analyzed with H5CellProfiler. The image analysis results of separate plates can be stored in a single HDF5 or in multiple HDF5 files, depending on how the images were analyzed. In addition to the well (column 'locationID') and plate id (column 'plateID') several optional columns can be entered: the column 'treatment' can be used to enter annotation regarding e.g. compound or siRNA treatment of the well. Moreover, if the column 'dose\_μM' is used to annotate the applied concentrations, dose response curves can be automatically generated at a later stage using the GUI. Furthermore, it is possible to use columns to annotate replicate numbers ('replID') and time information ('timeID') which can be useful for imaging of multiple plates that represent different time points. Finally, the column 'control' can be used to enter control information, which can be useful for plate normalization purposes in the GUI.

### 3.2.2. H5CellProfiler arguments.

The H5CellProfiler package requires several of these metadata HDF5 file paths as arguments to the H5CellProfiler function. At least the 'locationID' and 'imageID' are required, and if multiple plates have been stored in a single HDF5 file also the 'plateID' variable must be provided as a HDF5 file-path. In addition, it is possible to provide a 'timeID' and 'replicateID' if required. The 'plateID', 'timeID' and 'replID' variables can be defined either as a HDF5 file-path or as a constant for a single or for multiple HDF5 files (the latter is only possible if these variables remain the same within a single HDF5 file).

Conversion of the integer values for the time (either by regular expression or manually defined per HDF5 file) to real experimental time is performed based on the two arguments 'exposureDelay' and 'timeBetweenFrames'. These represent the delay of the first image relative to the biological perturbation of interest and the time between two consecutive time points, respectively.

The CellProfiler nomenclature consists of objects and measurements on these objects. Objects can be cells, parts of cells (e.g. cytoplasm) but also the images themselves. Users will segment the objects of interest and define the name of these objects. For each object, several measurement categories can be chosen in CellProfiler, e.g., intensity, texture and morphological measurements can be passed on to H5CellProfiler. Up to ten of these object measurements can be passed on to H5CellProfiler by giving them as argument for the 'myFeaturePathsA' argument. The single entries of these arguments should have an identical format as the CellProfiler output namely '*object/MeasurementCategory\_measurement*'.

Objects are often related to other objects. For example, when there are multiple objects for each cell, a parent object must be defined to link the secondary objects to. In this manner, every object defined by segmentation or object manipulations such as subtraction or shrinking has an object number and an associated parent object number. These object relations are provided to H5CellProfiler as the arguments 'parentObject', 'childObject1', 'childObject2',.....,'childObject5' and 'tertiaryObject', thus defining how the single cell data are organized. The 'tertiaryObject' is a CellProfiler-defined child object defined by other-object manipulations such as subtraction (often the cytosol as defined by cell subtracted by the nucleus). The image and parent object define the primary key of the tables in R-memory and secondary objects are associated to their corresponding parent object and thus on the same row in the table. Thus each row in the table corresponds to a unique parent-object. If multiple secondary objects exist for single parent objects (e.g. multiple organelles belonging to a single parent-nucleus), a summary statistic must be calculated. This summary statistic is by default the mean but can be added as an argument in the form of an r-function. Recommended statistics include the mean or a particular quantile, and is defined as a function, e.g. 'function(x) mean(x, na.rm = TRUE) ' to the argument 'multiplePerParentFunction'.

Finally the number of cpu cores the user wants to assign for all data processing steps can also be provided to H5CellProfiler as the argument 'numberCores'. However this is limited to maximally the number of HDF5 files provided, however for the tracking optimization algorithms this is only limited by the amount of individual locations that were imaged (number of time-lapses)

### 3.2.3. Track re-labeling and optimization.

CellProfiler also performs tracking in the context of time lapse imaging, which means that objects are linked to each other in time. The H5CellProfiler package recognizes tracking parameters automatically using regular expressions, so the user does not need to provide additional arguments. However, the 'fixTrackingFunction' utility from H5CellProfiler offers several options like re-labeling and combining 'broken' tracks based on user input. During tracking with CellProfiler, segmentation errors frequently leads to track interruption for one or several frames. These errors are quite common when cells tend to cluster together while migrating, resulting in an underestimation of the number of segmented objects. Alternatively, overestimation of segmented objects can also cause tracks to break because the tracking label can connect to the spurious cell which will disappear in the next few frames. Tracking errors are maintained in time, meaning that a small percentage of segmentation errors per time point results in accumulation of errors in track labeling. CellProfiler labels a tracked cell based on the object it is estimated to originate from at the previous time step and can assign the same label to multiple objects. Thus, a cell division or a single frame segmentation error results in the same label being assigned to multiple tracks. The 'fixTrackingFunction' re-labels these to new tracks starting at the last time point of imaging, using the track-parent object labels assigned by CellProfiler. Track-parents and track-children correspond to objects related in time, thus the same object tracked through time. When track-child objects lead to an identical track-parent (thus in the previous time point) the track label will be assigned to the closest parent using the x-y coordinates of the parent and child objects. After the re-labeling, the algorithm additionally attempts to reconnect broken tracks over 1-3 time frames if the argument 'reconnect\_frames' is set by the user. In addition, the maximum pixel

distance to reconnect partial tracks can be set with the arguments 'max\_pixel\_reconnect1', 'max\_pixel\_reconnect2' and 'max\_pixel\_reconnect3'. If multiple tracks are within the distance threshold the closest tracks are connected. Finally, the minimal track length can be set with the argument 'minTrackedFrames' which means that only tracks with at least that length after relabeling and reconnection are retained. The tracks can be plotted using the GUI and it is up to the user to validate the reconnect-argument settings by comparing the track plots with the time-lapses.

### 3.2.4. Graphical User Interface.

After the selected data has been read into R-memory and is reorganized with the help of the parent-child object relations and the annotation file, a browser is launched (Figure 3). This utility is based on the package 'shiny', which is an R wrapper for HTML and JavaScript. Shiny requires a server.r and UI.r. The UI.r file defines the layout and functionality of the GUI and generates the tools required for user input and output. The server.r file functions as the R server that performs the operations.

The web application provides a graphical user interface for frequently used data manipulation, summarization and graphical operations. It sends commands to an R-session so the user only indirectly employs R commands. This approach helps to ensure that the data manipulations are performed correctly.

The user can choose a single or multiple variables for summarization, and one or multiple factors over which the summarization takes place. The offered summary functions are the mean, standard deviation, median, sum, minimum, maximum and several quantiles. As soon as these options have been selected the table is calculated using the R-package 'data.table' and takes fractions of a second for tables up to 1GB. The raw measurement variables can also be normalized by z-score, by the plate median or by the min-max method  $(x - x_{\text{plate\_min}}) / (x_{\text{plate\_max}} - x_{\text{plate\_min}})$ . These normalizations are performed over the summarized results as defined by the 'by.what' factors because single cell data contain too many extreme outliers.

Other data manipulations provided by the browser include column division, deletions, filtering, counting and selection. Finally, the modified single cell table and summarized table can both be downloaded as tab-delimited text files. When the summarized table has been created the 'plot' tab (Figure 3, right panel) provides the option to explore the data graphically in an interactive manner (Figure 4). The user can select the treatment to be displayed and the variables to be plotted. Moreover, a third dimension in the data can be visualized with color mapping. and font size. The minimum and maximum values of the x- and y-axis can be set to 'fixed' (i.e. employing the minimum and maximum values of the entire dataset), to 'free' (i.e. specific ranges for each plot), or can be set manually. Finally, the dose values can be set to 'dose-levels' instead of their own specific dose ranges which are usually different for each treatment (see example in Figure 5). Dose level 1 is the lowest value in a dose-range and the highest dose level corresponds to the highest concentration employed for each treatment separately.

The tab 'myTable preview' (Figure 3, right panel) of the GUI displays 100 randomly selected rows of the single cell data table, which is useful to view the table along with the applied modifications.

The R package 'ggplot2' offers faceting of variables which means that multiple graphs can be

## h5CellProfiler GUI

Create summary statistics and make interactive plots of CP generated hdf5 data.

**Choose variables for analysis**

Cytoplasm\_Intensity\_MeanIntensity\_img\_gfp

**Summary Function:**

sum

**Summary by what:**

treatment plateID dose\_uM cell\_line

Calculate summary

**plate normalization method, by display variable:**

MinMax

**negative control string for z-score:**

normalize plates

**nominator column:**

treatment

**denominator column:**

treatment

**denominator addition by mean multiplier:**

0 0.05

0 0.005 0.01 0.015 0.02 0.025 0.03 0.035 0.04 0.045 0.05

Calculate division

**remove column:**

treatment

remove column!

**column to filter, count or select:**

treatment

**> or < (keep/count):**

**filter value**

filter column count data select data

☒ count NA is zero

**new column name**

**path to Rdata file**

table preview update variables reload Data

show barD

**Choose a dataset:**

Summary Data

Download

Calculate Summary plot plotAll myTable preview

	treatment	plateID	dose_uM	cell_line	Cytoplasm_Intensity_MeanIntensity_img_gfp
1	Staurosporin	plate 1	2.500	BTG2 #7	74.495
2	DMSO 25%	plate 1	25.000	BTG2 #7	268.323
3	Tunicamycin	plate 1	2.975	BTG2 #7	151.189
4	Staurosporin	plate 1	5.000	BTG2 #7	102.369
5	Menadione	plate 1	5.000	BTG2 #7	129.712
6	Tunicamycin	plate 1	5.950	BTG2 #7	118.376
7	Staurosporin	plate 1	10.000	BTG2 #7	81.247
8	Menadione	plate 1	10.000	BTG2 #7	142.891
9	Tunicamycin	plate 1	11.900	BTG2 #7	158.761
10	DMSO 100%	plate 1	100.000	BTG2 #7	377.158
11	Menadione	plate 1	20.000	BTG2 #7	95.864
12	DMSO 50%	plate 1	50.000	BTG2 #7	221.441
13	CDDO	plate 1	0.007	BTG2 #7	151.753
14	H2O2	plate 1	125.000	BTG2 #7	138.170
15	Thapsigargin	plate 1	0.250	BTG2 #7	90.327
16	CDDO	plate 1	0.015	BTG2 #7	68.013
17	H2O2	plate 1	250.000	BTG2 #7	135.639
18	Thapsigargin	plate 1	0.500	BTG2 #7	65.405
19	CDDO	plate 1	0.030	BTG2 #7	127.644
20	H2O2	plate 1	500.000	BTG2 #7	124.184
21	Thapsigargin	plate 1	1.000	BTG2 #7	132.085
22	IAA	plate 1	2.500	BTG2 #7	69.755
23	IAA	plate 1	5.000	BTG2 #7	99.639
24	BFA	plate 1	8.925	BTG2 #7	60.875
25	Cisplatin	plate 1	5.000	BTG2 #7	458.840
26	IAA	plate 1	10.000	BTG2 #7	125.701
27	BFA	plate 1	17.850	BTG2 #7	79.748
28	Cisplatin	plate 1	10.000	BTG2 #7	1138.590
29	DEM	plate 1	25.000	BTG2 #7	86.082
30	BFA	plate 1	35.700	BTG2 #7	47.567
31	Cisplatin	plate 1	20.000	BTG2 #7	1013.106
32	DEM	plate 1	50.000	BTG2 #7	131.396
33	DMSO 75%	plate 1	75.000	BTG2 #7	216.991
34	Etoposide	plate 1	6.250	BTG2 #7	693.723
35	DEM	plate 1	100.000	BTG2 #7	81.659
36	Etoposide	plate 1	12.500	BTG2 #7	987.923
37	Etoposide	plate 1	25.000	BTG2 #7	1308.732

Normalization (use by what)

**Figure 3: GUI for HCI data.** Left panel shows an example of a GUI data manipulation and summarization utility page. Utilities include summarization statistics over the requested variables and factors. Further options include choice of plate normalization methods, column division, column deletion, filtering, selection, counting and downloading the modified single cell data or summarized data. Right panel shows an example of a summarized table preview within the browser.

automatically wrapped in a single figure. This option to plot large numbers of graphs at once is offered by the 'plotAll' tab (Figure 4, right panel). In figure 5, an example of graph faceting is shown, together with the input boxes. With this approach it is possible to plot hundreds of graphs in a single figure if the pdf size is sufficient large for the graph annotations to be displayed

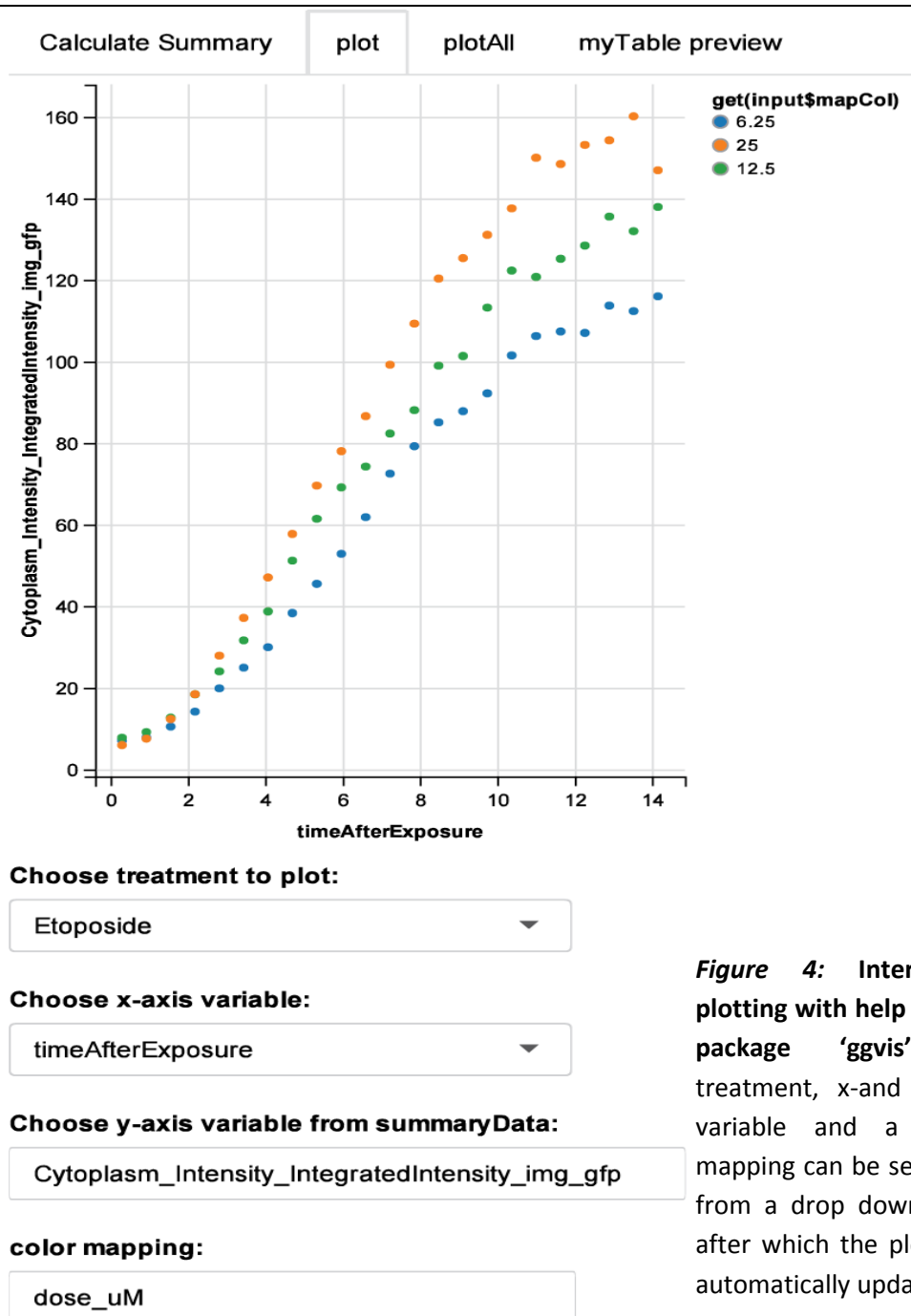


**Figure 4:** Interactive plotting with help of the package 'ggvis'. A treatment, x-and y-axis variable and a color mapping can be selected from a drop down box, after which the plot will automatically update.

correctly (with a small font). Options for multi-facetted plotting include the plot type (line plot or bar plots), variable collapse (i.e., calculation of the mean) and the choice of x and y variables. Moreover, the user can map up to six variables or specific values by employing different color, fill, shape and dot-size. Other options include adding lines between the dots and setting the pdf size



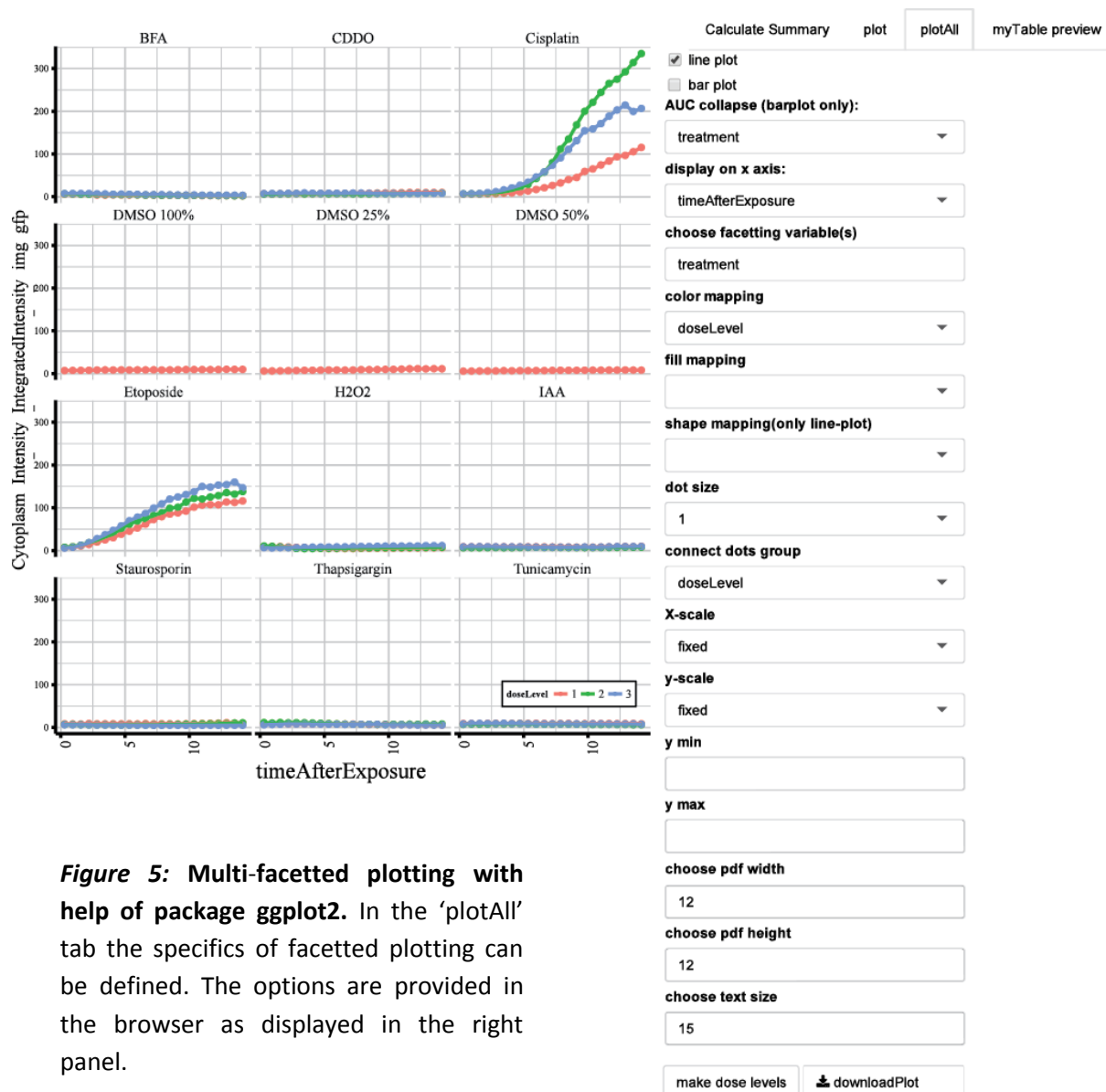


**Figure 5: Multi-facetted plotting with help of package ggplot2.** In the 'plotAll' tab the specifics of facetted plotting can be defined. The options are provided in the browser as displayed in the right panel.

#### 4. Conclusions

High throughput high content image analysis of single cell data leads to large amounts of quantitative data. H5CellProfiler is a user-friendly solution to analyze such data without the requirement of a database. The current implementation of H5CellProfiler is based on the HDF5-output of the popular HCI image analysis tool CellProfiler. The benefit of such an implementation, in contrast to storing the data in a database, is that the entire pipeline can be performed on a single desktop without the need to set up a database and client software.

The current data workflow of CellProfiler is based on exporting the data to a database followed by analysis with CellProfiler Analyst [325] which is based on supervised single cell machine learning approaches. Additionally, the CellProfiler data can be exported in the form of spreadsheets, however this quickly becomes cumbersome in case of large datasets.

We propose the use of the image analysis and data analysis workflow with the use of CellProfiler and R-package CellProfiler for the biologist who prefers to handle their own data analysis and graphics. This will save time in the experimental design to final displayed results cycle, and avoids communication difficulties between the biologist and computational scientists. For the

more computational adherent scientists – H5CellProfiler has the additional benefit of being based on R which is a highly suited platform for data analysis, statistics and graphics.

## 5. Code description

### 5.1. mainFunction

'mainFunction' pulls the user-selected data from HDF5 together with the user provided metadata file and organizes the data into a data.table object with one row per parent object and all associated variables as columns. 'mainFunction' output is a outputList.Rdata file containing a 1 or several list object in the case of multiple HDF5 files. The first list object contains the data.table, metadata, user arguments and a default summary data.table. The outputList.Rdata file is used as the input for the *server.R* and *ui.R* code from the shiny application for the graphical user interface.

### 5.2. mainFunction code description

Argument class, string length, object definitions and relations using regular expressions matching to hdf5 paths (of h5ls of '\$group', see rhdf5 vignette for details) is checked and error messages thrown to inform the user on the type of mistake.

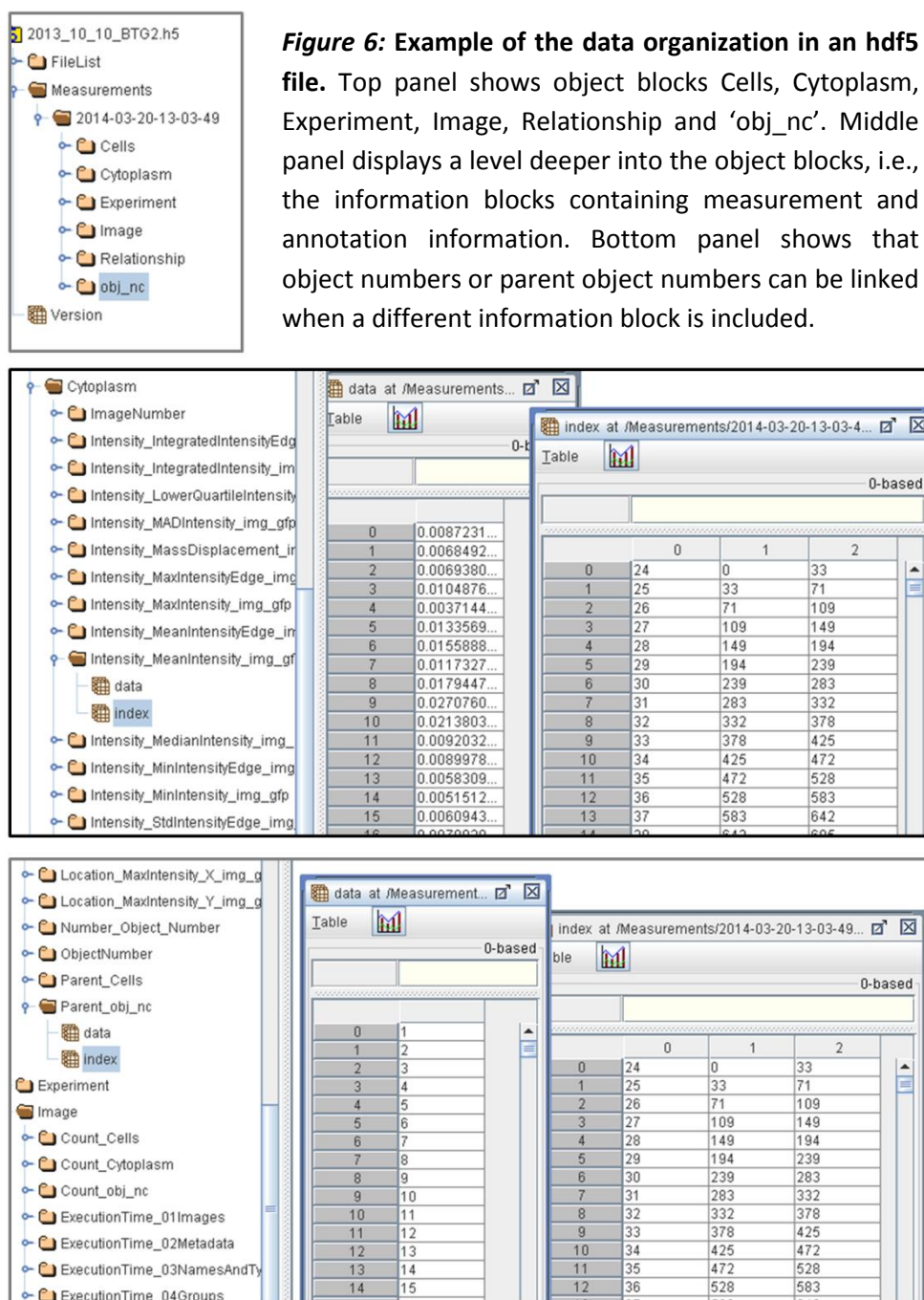
The time stamp of the CellProfiler HDF5 output is extracted with a regular expression.

The tracked object and possibly track distance are extracted from the hdf5 paths and in addition the following track-related paths are defined: tracking label, track parent object numbers, x and y coordinates of tracked object and distance traveled. These track-related hdf5 paths are added to the user defined paths of 'myFeaturesPathsA'.

The 'hdf5IndexFun' pulls data from the hdf5 file and has input 'hdf5path', 'dataname' and 'rowIndName'. 'Hdf5path' points towards the location of the data in the hdf5 file, 'dataname' and 'rowIndName' represent the name of the data inside the object and the name of the object index data of that object, respectively. To understand how the 'hdf5IndexFun' operates, it is important to understand the high level data organization (how it is seen by e.g. the R-interface api).

Each object in the hdf5 file has information blocks; the measurements and metadata e.g. its object numbers and if applicable child or parent object numbers (Figure 6). When pulled from the hdf5 file by the h5read function of the rhdf5 package into R-memory, each information block of a certain object is represented as a list containing a  $1 \times n_{\text{objects}}$  data array and an  $3 \times n_{\text{images}}$  index array with n being the number of unique entries of that particular object. The data array contains the measurements and object numbers or relation specific numbers, the index array contains the image number (first column) and the range of rows within the data array to which this image number belong (2<sup>nd</sup> and 3<sup>rd</sup> columns). To find out which object number a particular set of data points belongs to one must look at the data entries within the 'Number\_Object\_Number' information block. Since a cytoplasm object is a derived secondary object, the parent object number of each object must also be determined to link the measurement to the correct parent object. Hence, depending on the type of object different information about the object is required which explains why the user must provide this information. An alternative solution would be to use regular expressions to search for the 'Parent' and or 'Child' strings to automatically determine these relations.

Note that the order of the measurements and annotation information of the objects within an image is constant, so the data of the image-object, parent object and child objects can be



gathered per image at a time and then merged using the extracted image numbers, object numbers and parent object numbers. The 'hdf5IndFun' reformats the data (unstacks) the index information (index array has an entry for each image) by unstacking the row ranges (which point to the rows in the data array) and these are matched to the row number of the data array. The output is then a 'data.table' object for a single measurement/annotation from a single object containing the data array entries, the image numbers and the row index numbers. The row index numbers are not needed after the merge operation of the data and index arrays because the data.tables for each measurement of that same object will be identical. In addition, merging of the data.tables of the different objects will depend on the extracted data arrays containing the object numbers of the parent objects and the parent object numbers of the child-objects.

### 5.3. mainFunction arguments

hdf5FileNameL

*list of hdf5 file names which serve as input for the function*

locationID

*hdf5 path as provided by user in CellProfiler with regular expressions, serves as linker column together with plateID to merge hdf5 data with metadata file. The locationID in the hdf5 file should be identical to the locaitonID in the metadata file.*

plateID

*list of hdf5 paths or per-hdf5 defined constant, serves as linker column together with locationID to merge hdf5 data with metadata file. The plateID in the hdf5 file or the manually defined plateIDs should be identical to the plateID in the metadata file.*

timeID

*list of hdf5 paths or a constant per hdf5 file containing the time point information. The timeID in the metadata file overrides the provided time argument unless no information in the metadata file is provided.*

imageID

*hdf5 path to image identifier as defined with regular expressions in CellProfiler.*

replID

*list of hdf5 paths or a constant per hdf5 file containing the replicate id constant. The replID in the metadata file overrides the provided time argument unless no information in the metadata file is provided.*

myFeaturePathsA

*List of hdf5 paths that define the measurements the user is interested in. CellProfiler measures everything per user-selected object measurement-class so a selection has to be made to avoid memory problems.*

plateMDFileName

*File name of the user defined metadata file. A tab delimited text file with headers 'locationID', 'treatment', 'control', 'dose\_uM', 'plateID', 'timeID', 'replID'. Only the 'locationID' is obligatory, other columns can be left empty or defined as NA values.*

parentObject

*Parent object as defined by the user in CellProfiler. CellProfiler provides an object as parent by default in relation to other objects that are defined based on this parent. If this is not the case then the user must define the parent-child object using the 'relateObjects' module in CellProfiler. All objects of which measurements are selected for 'myFeaturePathsA', must be defined using the 'parentObject', 'childObject' or 'tertiaryObject' arguments. Note that the 'parentObject' defines the way the data is formatted by 'mainFunction' as each 'parentObject' is assigned a single row in the data.table. The children of the 'parentObject' are summarized by the 'multiplePerParentFunction' argument, only if multiple children exist. This summary function is performed for each parent object even if only a single parent object has multiple children assigned. Therefore the user has to carefully consider the modules used in CellProfiler when assigning object relations. Using the parent object as seed is in general safe, relating multiple parent objects in a parent-child relation could lead to unnecessary computational overhead.*

childObject1-5

*Child of parent object as defined in CellProfiler 'identifySecondaryObject' module or 'relateObjects' module.*

tertiaryObject

*Child based on object derived from parent and/or child as defined in CellProfiler 'identifyTertiaryObject' module.*

multiplePerParentFunction

*User defined function that defines how multiple children per parent object are summarized.*

Oscillation

*Logical argument that enables analogues parameter calculation of in time oscillations (not implemented yet).*

writeSingleCellDataPerWell

*logical argument that enables writing of single cell data per well. Single cell text file data often becomes more manageable in spreadsheets when saved in chunks.*

writeAllSingleCellData

*logical argument that enables writing a single text file of the single cell data.*

h5loop

*numeric, default is the number of hdf5 files. Can be overwritten in case memory issues occur.*

timeBetweenFrames

*string that defines experimental time between consecutive frames. Format is 'hh:mm:ss' (hours, minutes, seconds). Please note that 60 minutes or 60 seconds don't exist in this format, increase the hours (no limit) or minutes by 1 instead.*

exposureDelay

*string that defines the time between the biological perturbation of interest and the first captured image. Note that at this time it is not possible to define time delays within a plate.*



# Chapter 8

## Overall discussion and conclusions.

---

### 1. BAC-GFP reporter systems for prediction of DILI.

In this thesis I have described the application of a diverse set of HepG2 BAC-GFP reporters that represent different adaptive stress response pathways that are implicated in toxicity. In Chapter 3 we first established and characterized the different reporter systems. The rationale to establish this panel of HepG2 BAC reporters for the oxidative, endoplasmic and DNA damage stress responses was to enable the monitoring of these pathways at the 'sensor', 'transcription factor' and 'downstream target' level. The various reporters were all characterized and optimized with a set of reference compounds. In doing so the stress specific compounds in combination with the different stress specific BAC reporters readouts lead to a perfect co-clustering following unsupervised hierarchical clustering.

The next important step for reporter validation was to test a set of clinically relevant DILI-drugs. The rationale for their selection was based on their transcription-level responses of the actual BAC reporter target genes in primary human hepatocytes which were available through the TG-GATES microarray dataset. We successfully established that the primary responses of these selected DILI-drugs involve adaptive stress responses that correlate with the transcriptional responses observed for PHH: 100 % concordance for the Srxn1-GFP response, 80 % concordance for p21-GFP and 50 % for CHOP-GFP and BiP-GFP.

Encouraged by these initial results a compound library of ~170 DILI related drugs including control reference compounds was screened using the Srxn1-GFP, CHOP-GFP and p21-GFP BAC reporters at 1, 5, 10, 50 and 100 C-max with live-cell imaging for 24 hours.

As expected the response levels, the dose-responses and time-dynamics varied within the entire DILI compound set. For many compounds the responses were low to moderate and difficult to detect. However, with a binary method by determining the percentage of GFP-positive cells based on control-level background offsets, the sensitivity of the readout was greatly improved. Yet, this alternative analysis affected the overall dynamic range. We then applied unsupervised clustering of the primary adaptive stress responses time course profiles together with several viability features (see Chapter 7, Figure 4). This allowed the identification of DILI compounds with similar adaptive stress response activation as well as similar time dynamic profiles of these responses. These profiles can be used to determine the primary stress type for compounds that induce multiple stress responses as the corresponding reporter will be activated first. Thus, already from such basic observations general insights into the mechanisms of toxicity can be inferred based on stress type and co-clustering of reference control compounds with known mechanism of action. As all concentration-compound combinations are represented in the clustering of multi-variate time responses the point of departure for the different stress responses can be determined. In addition because of the inclusion of the viability markers technical and



biological outliers can easily be detected, either in an automated fashion or by manual inspection of clustered results.

A next step in such multivariate analysis is often reevaluation from a different angle by data transformation and/or dimension reduction methods. In the current context removing the time dimension was performed by transformation of the time response curves to dose response curves, which serves to decrease the complexity but also enables inclusion of additional features and for example single time point cell death parameters. Visualizing the same dataset from a dose-response angle sets the focus on the critical onset of toxicity based on concentrations. Different sensitivity and dynamic range measures of the adaptive stress response levels together with viability features such as cell count, cell speeds, nuclei area and the cell death features apoptosis-positive-fraction and necrosis-positive-fractions shows a broad cell biologic response to each compound in a dose-response context. Cellular adaptation to stress typically occurs in the form of activation of damage specific adaptive stress responses followed by a decrease in several cell viability markers and finally results in cell death. The point-of-departure (PoD) can be defined in parallel with the point-of-no-return (i.e. cell death). Thus, the compound-specific concentration of these events and, importantly, the concentration differences between these two events are key compound features which pertain how potent a certain compound induces a certain type of stress and how well adaptive programs can combat this stress before cell death occurs, respectively.

Together, our experiments indicate the application of BAC-GFP reporters in the safety assessment of chemicals and their potential for the identification of DILI liabilities.

## **2. Application of BAC-GFP reporter in the understanding of mechanisms of DILI.**

A major theme in DILI is the involvement of immune mediated mechanisms including TNF $\alpha$  induced pro-inflammatory signalling [38]. In Chapter 5 I have studied the role of different stress response pathways and their relationship to DILI in the context of TNF $\alpha$  signalling. As a first step, transcriptomic profiling of the response of HepG2 cells treated with TNF $\alpha$  and co-treated with either one of the hepatotoxicants diclofenac or carbamazepine revealed the involvement of two adaptive stress response pathways: the endoplasmic reticulum (ER) stress/translational initiation signalling and nuclear factor-erythroid 2 (NF-E2)-related factor 2 (Nrf2) antioxidant signalling. Indeed, data mining of the TG-GATES dataset revealed the importance of these adaptive stress responses as the majority of DILI classified drugs affected the corresponding transcription levels in primary in hepatocytes. Following these findings we set out to investigate if these adaptive stress responses have a critical role as drug-induced toxicity pathways that act in synergy with TNF $\alpha$  to cause cell death of liver HepG2 cells.

With the established adaptive stress response BAC-GFP reporter platform a more detailed mechanistic investigation was performed into the involvement of the Nrf2 antioxidant response and ER stress/UPR in TNF $\alpha$ /drug-induced synergy in DILI. Diclofenac and carbamazepine both caused the activation of the ER-stress BAC-GFP HepG2 reporters ATF4-GFP and CHOP-GFP. This ER-stress activation was shown to be independent of TNF $\alpha$  and involved protein kinase R-like ER kinase (PERK). The diclofenac and carbamazepine TNF $\alpha$  synergistic cell death was inhibited when PERK was downregulated. Also siRNA knock down of CHOP inhibited this synergistic cytotoxic onset. Induction of CHOP expression was dependent on the translational initiation factor EIF4A1; and knock down of EIF4A1 also inhibited the cytotoxic response. Thus, ER stress caused by these

two DILI compounds, directly interacts with the pro-apoptotic pathway downstream of the TNF receptor. In contrast to the effect of ER stress, activation of the KEAP1/Nrf2 antioxidant stress response pathway, as evidenced by the induction of the Srxn1-GFP reporter by these two DILI compounds, acted cytoprotective. Thus, knock down of Nrf2 enhanced the synergistic cell death. These data demonstrate the application of the BAC-GFP reporters in mechanistic understanding of DILI compound toxicities.

### **3. Interaction of Nrf2 signalling and NF- $\kappa$ B signalling in DILI.**

The above results suggests that the interaction with TNF signalling is essential for DILI liabilities. Since many DILI compounds also activate the Nrf2 response, we further investigated this interaction and the possible predictivity of these two signalling pathways (Chapter 6). First, a systematic investigation of the Nrf2-mediated oxidative stress signalling and NF- $\kappa$ B-mediated inflammatory signalling pathways in PHH using the TG-GATES microarray dataset revealed a strong correlation between these two pathways in relation to DILI. Strong activation of the Nrf2 pathway was associated with a downregulation of the inflammatory pathway. Following this observation these findings were translated into HCl. Here we combined the HepG2 oxidative stress response reporter Srxn1-GFP and a HepG2 reporter for p65-GFP, a subunit of NF- $\kappa$ B on which we published before. The latter reporter demonstrates nuclear oscillation behavior upon treatment with TNF $\alpha$ . We found that when DILI compounds demonstrate strong activation of the Srxn1-GFP reporter, this was associated with suppression of TNF $\alpha$ -induced NF- $\kappa$ B translocation to the nucleus. Activation of NF- $\kappa$ B signalling by TNF $\alpha$  did not suppress the oxidative stress response in HepG2 cells. Of interest, mainly compounds associated with a strong Nrf2-activation sensitized towards TNF $\alpha$ -mediated cell death. This may indicate that in particular compounds that have a strong cellular stress response are liable for such an interaction. As mentioned above, such an oxidative stress response activation was initially a protective adaptive response, since knock down of Nrf2 enhanced this sensitivity, while on the contrary knock down of the negative regulator of Nrf2, Keap1, acted cytoprotective. Thus, we propose the Nrf2-mediated oxidative stress response as induced by DILI compounds coincides with NF- $\kappa$ B suppressions and that this results in liver cells that are more sensitive to pro-apoptotic signalling induced by immune cell released cytokines such as TNF $\alpha$ . We anticipate that by monitoring in early drug development the effect of novel drug candidates on oxidative stress activation (Srxn1-GFP reporter), TNF $\alpha$  signalling (p65-GFP reporter oscillation) and synergistic cell death, may reduce the number of compounds that will enter the clinic with DILI liabilities.

### **4. Implications of the BAC-GFP reporters in understanding DILI and assessment of chemical safety.**

In Chapter 3 we determined that monitoring only three adaptive stress response pathways using endogenously regulated BAC-GFP reporter HepG2 cells together with several cell-viability features using HCl, allows the identification of a biological “fingerprint”. This was evidenced by the co-clustering of highly structural similar compounds: oligomycin A and oligomycin B, CCCP and FCCP; as well as compounds with similar mode-of-action: thapsigargin, tunicamycin and brefeldin A. Does this infer that these are *the* major adaptive stress response pathways in cellular defense and that these pathways are key in DILI? Yes and no. Oxidative stress has been shown in numerous

studies to be the main source of damage implicated in DILI [328]. ER-stress is emerging as another important player in DILI, especially the role of cell death signalling via PERK and CHOP resulting from prolonged ER-stress [334, 335]. DNA damage is known in several cases of DILI, but this pathway is general not a main player in DILI, as was also indicated by our DILI screen results [336, 337]. In our DILI screen in Chapter 7 we also observed that a large set of compounds did not induce any of the three adaptive stress response reporters; this indicates that it is likely that different types of stress and signalling do occur in DILI. Regardless, as a proof-of concept we demonstrate that both the time-dynamics and concentration-response profiles that can be obtained from HCI of the reporter platform provides detailed information on: 1) the primary mode-of-action; 2) the resultant secondary stress responses; 3) the point-of-departure (i.e. lowest observed effect level at which an activation of a response occurs); 4) the consequently point-of-no-return at which *maladaptation* or cell death occurs. The HCI data is multi-dimensional and therefore complex automation in the form of an analysis pipeline which displays such data in heatmaps can simplify the analysis and interpretation of such data. At this point adaptive stress response fingerprints that are associated with diverse DILI classes would need to be established first.

Although not included in our screening efforts so far, the development of the inflammatory signalling BAC-GFP reporters (Chapter 5) now allows inclusion of the highly relevant NF- $\kappa$ B signalling pathway in our HCI DILI screening efforts. The NF- $\kappa$ B pathway acts as a pivotal survival signalling node but can also contribute to or initiate cell death pathways. In the lab, we have also established BAC-GFP reporters for several downstream targets of NF- $\kappa$ B, including A20-GFP and ICAM-GFP, respectively early and late target genes. Our HCI BAC-GFP reporter panel is an ideal platform to investigate the interaction between multiple pivotal pathways related to DILI (i.e. the Nrf2 antioxidant/ oxidative stress response and the NF- $\kappa$ B pathway, in Chapter 6). The possibility to quantify the Nrf2 mediated oxidative stress response together with the oscillation patterns of NF- $\kappa$ B in live cells following exposure to DILI-drugs and inflammatory signalling activation by TNF $\alpha$  is only possible with the high temporal and spatial resolution that HCI provides. The sensitivity required to detect incremental changes in endogenously regulated *Srxn1* levels as the result of slight increase in Nrf2-mediated oxidative stress signalling and more importantly the detection of subtle changes in NF- $\kappa$ B nuclei-cytosol oscillation patterns in single cells is only possible using HCI, in particular using state-of-the-art optics and detection which are available on confocal microscope systems that we have used in our investigations.

The complexity and the diversity of responses of biological systems to chemical exposure is evident. The involvement and interconnectivity of multiple pathways in DILI has been demonstrated in previous work and in this thesis. More importantly, however, is our demonstration of how several key regulatory components can be used to determine the primary response of cells to chemical exposure. Since adaptive stress responses are upstream in these biological regulatory programs, exploring additional adaptive stress responses will prove to be of high value to create more BAC-GFP reporters for their integration in HCI.

## 5. Improvements to be considered.

Some key features on the implementation of the current HCI-imaging based reporter platform are warranted. At this stage, as a proof-of-concept, we focused on several reporter cell lines that were

based on HepG2 cells. This cell line was selected since it is easy to genetically modify, it is robust and easy to maintain and transfer to a commercial setting. However, the HepG2 cell line has limited biotransformation capacity which is required for reactive metabolite formation. Secondly, these cells are grown in two-dimensional conditions; under these conditions the cells divide rapidly which is not representative for the *in vivo* conditions. The cells lack the other differentiated features of normal primary cultured hepatocytes including bile-duct formation. Thirdly the culture system lacks the multi-cellularity which is often key in the pathophysiology of DILI. Thus, the liver resident macrophages, Kupffer cells, pit cells, stellate cells, sinusoidal cells and cholangiocytes all contribute in their own way to DILI. Future work should involve both the culturing of our reporter cell lines in 3D and/or in co-cultures with other liver cell types. Indeed, we have been successful to culture the various BAC-GFP HepG2 reporters as spheroid cultures in a 3D matrigel environment. The phenotype of the different reporters in 3D spheroids mimics the phenotype as observed for wild type HepG2 3D spheroids.

Additional we have started to explore the use of human induced pluripotent stem cells. Inclusion of reporters in these cells will involve the CRISPR/Cas9 technology. hiPSC will allow the differentiation of the ultimate fluorescent reporter cells into multiple cell types including hepatocyte-like cells followed by integration in high content imaging.

An additional shortcoming of our current model is the lack of prolonged repeated dosing possibilities for up to several weeks. A repeated dosing scheme would be in particular interesting when considering the concepts of sensitization or desensitization after onset of the adaptive stress response programs. Will repeated dosing create a new steady state of the stress response, thus ensuring true adaptation? Or will repeated drug exposure create a sustained ever increasing stress response that is doomed to end with a point of no-return? These are questions that are difficult to answer using our 2D culture BAC-GFP reporter approach. The above already mentioned non-proliferative 3D HepG2 spheroid cultures would be ideally suited for this purpose [14]. Such strategies are currently being explored in our lab and are beyond the scope of this thesis.

A final current shortcoming worth mentioning are the costs, time and expertise involved in setting up the required hardware and software infrastructures. Moreover the complexity of the datasets requires rigid image and data analysis protocols to obtain reliable and reproducible end-of-the-pipeline results so that the risk assessor might actually use such data.

## **6. Adaptive stress responses and cell biology: implications for prediction.**

In this thesis I focused on the application of reporters that reflect cellular adaptation programs. In view of the adaptation versus the point-of-no-return one can consider cellular systems in a continuous dynamic state of acquiring damage and repairing damage with the ultimate goal to maintain cellular homeostasis. One step further leads us to a hypothesis where all cellular and organ adversity is the inability of biological repair systems to cope with the acquired damage. The biological repair mechanisms consist of intrinsic repair such as during DNA transcription coupled repair, normal cellular protein turnover through proteosomal degradation, or malformed proteins that are rescued by chaperones already present in cells under normal physiological conditions. An adaptive stress response program is then the detection of damage and signalling response of biological systems to increase these intrinsic repair mechanism to a specific damage type to a higher level. If this is true, how can we use reporter based systems of the adaptive stress response

pathways that control these repair mechanisms to better predict DILI? The employed approach of Chapter 7 of clustering compounds by similarity of their corresponding biological fingerprints has shown promise in the enrichment in most-DILI concern compounds: they caused a strong activation of the Nrf2-mediated oxidative stress response and ER-stress/UPR response within a 24 hour time period. However, other most-DILI concern compounds did not induce one of the adaptive stress response programs in this time period. Our current simplified working hypothesis is that all DILI is the result of failed adaptation programs due to overwhelming damage. Since this is not observed this leads to several explanations. Firstly, the 2D HepG2 cells are immortalized dedifferentiated liver cells that lack many physiological and structural properties of a the actual liver, and, thus, limiting the coverage of 'all' pathophysiological programs involved in DILI. Secondly, only three adaptive stress programs have been monitored leading to the possibility that certain damage types are overlooked in the current reporter platform. We need to integrate other stress programs in our platform as well. Thirdly, the toxicodynamics is likely different than the physiological dynamics in the human liver and this will for certain compounds likely be key in the compound induced toxicity. Repeated dosing and longer time courses for accumulation of the compound or its metabolites have been shown to be key mechanisms [14, 15]. And, fourthly, compounds that directly interact with cell death or survival pathways and sensitize cells to stress induced cell death could lead to adversity without inducing adaptive stress response pathways to higher than significantly detectable levels.

## **7. Practical implementation of the technologies.**

We believe the current proof of concept methodology can directly be applied in an industrial setting. Several pharmaceutical companies have jointly performed promising pilot studies on DILI related compound sets. On one hand the BAC-GFP reporter platform can be used for early screening for the purpose of hazard identification for early lead termination. Such a system could be simple: e.g. a single/multiple time point(s) and single/multiple concentration(s) on a small set of primary adaptive stress response reporters, including oxidative stress and ER-stress reporters. Compounds that induce these stress types at the pre-determined concentration can be terminated simply by the notion that they induce these pathways at a too low concentration. Such an approach might lead to identification of false positives. This may be undesirable because compounds may have optimal pharmacodynamics and pharmacokinetic properties or there may not be that many compounds to start with. In this case a more detailed screening effort can be performed using multiple reporters and time points to gather more information as to what constitutes a high-hazard high-risk biological fingerprint. Such a high risk-fingerprint includes the point of departure concentration for several key adaptive stress response pathways, the concentration where adaptation changes to maladaptation and cell death. To obtain such a fingerprint, or multiple fingerprints, two strategies should be considered. Firstly, the expert knowledge based method where the data such as activation of (multiple) pathways at certain point of departures are interpreted in the context of the compound application for hazard identification or even risk assessment. This would however require much experience in the understanding and interpretation of such data; without this prior knowledge the reporter screening concept is not likely to be incorporated in toxicity screening programs in the first place.

The second strategy would be a supervised clustering methodology where a large set of DILI compounds versus a large set of non-DILI compounds is used to optimize a fingerprint that functions as classifier for these two groups. Such a classifier would evolve as more data becomes available, and indeed the foundations for such a biological fingerprint have already been made in this thesis. The difficulty does however remain in the ground-truth classification of DILI compounds as well as the complexity and variety of the mode-of-action of different DILI compounds. With such a complexity we would propose to simplify as much as possible the application of the reporter platform. One can envision an initial screen with single time points and a small range of concentrations in several HepG2 BAC-GFP reporters where only strong evidence is used to terminate sets of compounds flagged as hazardous by their corresponding fingerprints. This would be followed by a more elaborate screen with the inclusion of the time dynamics and concentration response.

Will all drug-related DILI be translated to some form of adaptive stress response? This is not likely as for example phospholipidosis or cholestasis might initially not lead to any or sufficient high perturbation levels to induce one of the adaptive stress responses to increase significantly above endogenous levels. This would therefore require the integration of additional reporters that need to be developed and/or characterized further in the future. Reporters that have already been established as BAC-GFP clones include several additional adaptive stress responses including the heat shock response and the metal stress response. In addition, also reporters that represent the structure of different organelles have been established and include: 1) a CYC1-GFP reporter which visualizes the mitochondria and mitochondrial networks. As compounds that affect the oxidative phosphorylation process and likely the metabolism in general are expected to influence the size, number and network structure of mitochondria. 2) EEA1-GFP which is a marker of early endosomes and LAMP1-GFP which is a marker of the lysosomes; these markers could be of interest in monitoring phospholipidosis. 3) LC3-GFP which visualizes the autophagosomes 4) LAMIN A-GFP markers of the nuclear envelope, 5) PDIA6-GFP which serves as a morphological marker of the endoplasmic reticulum. 6) BSEP-GFP and MRP2-GFP reporters that are involved in cholestasis and are located at the bile canaluculis. 7) CYP3A4-GFP that is induced by various xenobiotics. 8) cytochrome-c (CYCS-GFP) and Bid-GFP that are relevant to monitor early onset of cell death commitment.

## **8. Final concluding remarks.**

Our long term vision is to establish an imaging-based platform that can quantitatively assess the activation of individual key events relevant to AOPs. The focus of my thesis was on adaptive stress response pathways, that are typically part of AOPs and related to adverse drug reactions. In this thesis, we have established and characterized various reporter cell lines. We have developed the infrastructure for automated imaging and image analysis of the BAC reporters. We have used the quantitative output of the HCI from these reporters for the mechanistic understanding and improved prediction of DILI. While still further development is required for implementation of the technologies as well as broadening the panel of reporters, I anticipate that the HCI-based safety testing strategies will find its place in DILI liability assessment and/or the chemical safety evaluation in general.

## References

1. Lazarou, J., B.H. Pomeranz, and P.N. Corey, *Incidence of adverse drug reactions in hospitalized patients: a meta-analysis of prospective studies*. JAMA, 1998. **279**(15): p. 1200-5.
2. Einarson, T.R., *Drug-related hospital admissions*. Ann Pharmacother, 1993. **27**(7-8): p. 832-40.
3. Johnson, J.A. and J.L. Bootman, *Drug-related morbidity and mortality. A cost-of-illness model*. Arch Intern Med, 1995. **155**(18): p. 1949-56.
4. Stevens, J.L. and T.K. Baker, *The future of drug safety testing: expanding the view and narrowing the focus*. Drug Discov Today, 2009. **14**(3-4): p. 162-7.
5. Kola, I. and J. Landis, *Can the pharmaceutical industry reduce attrition rates?* Nature Reviews Drug Discovery, 2004. **3**(8): p. 711-715.
6. Kaplowitz, N., *Idiosyncratic drug hepatotoxicity*. Nat Rev Drug Discov, 2005. **4**(6): p. 489-99.
7. Regev, A., *Drug-induced liver injury and drug development: industry perspective*. Semin Liver Dis, 2014. **34**(2): p. 227-39.
8. Olson, H., et al., *Concordance of the toxicity of pharmaceuticals in humans and in animals*. Regul Toxicol Pharmacol, 2000. **32**(1): p. 56-67.
9. Donato, M.T., et al., *Cell lines: a tool for in vitro drug metabolism studies*. Curr Drug Metab, 2008. **9**(1): p. 1-11.
10. Polster, B.M., et al., *Use of potentiometric fluorophores in the measurement of mitochondrial reactive oxygen species*. Methods Enzymol, 2014. **547**: p. 225-50.
11. Grandl, M. and G. Schmitz, *Fluorescent high-content imaging allows the discrimination and quantitation of E-LDL-induced lipid droplets and Ox-LDL-generated phospholipidosis in human macrophages*. Cytometry A, 2010. **77**(3): p. 231-42.
12. Tolosa, L., et al., *High-content screening of drug-induced mitochondrial impairment in hepatic cells: effects of statins*. Arch Toxicol, 2015. **89**(10): p. 1847-60.
13. Hendriks, G., et al., *The ToxTracker assay: novel GFP reporter systems that provide mechanistic insight into the genotoxic properties of chemicals*. Toxicol Sci, 2012. **125**(1): p. 285-98.
14. Ramaiahgari, S.C., et al., *A 3D in vitro model of differentiated HepG2 cell spheroids with improved liver-like properties for repeated dose high-throughput toxicity studies*. Arch Toxicol, 2014. **88**(5): p. 1083-95.
15. Materne, E.M., et al., *The multi-organ chip--a microfluidic platform for long-term multi-tissue coculture*. J Vis Exp, 2015(98): p. e52526.
16. Godoy, P., et al., *Recent advances in 2D and 3D in vitro systems using primary hepatocytes, alternative hepatocyte sources and non-parenchymal liver cells and their use in investigating mechanisms of hepatotoxicity, cell signalling and ADME*. Arch Toxicol, 2013. **87**(8): p. 1315-530.
17. Hadi, M., et al., *Human precision-cut liver slices as an ex vivo model to study idiosyncratic drug-induced liver injury*. Chem Res Toxicol, 2013. **26**(5): p. 710-20.
18. Ruffner, H. and J. Lichtenberg, *3D cell culture systems--towards primary drug discovery platforms: an interview with Heinz Ruffner (Novartis) and Jan Lichtenberg (InSphero)*. Biotechnol J, 2012. **7**(7): p. 833-4.
19. Krueger, W., U.A. Boelsterli, and T.P. Rasmussen, *Stem Cell Strategies to Evaluate Idiosyncratic Drug-induced Liver Injury*. J Clin Transl Hepatol, 2014. **2**(3): p. 143-52.
20. Jan, Y.H., et al., *Acetaminophen reactive intermediates target hepatic thioredoxin reductase*. Chem Res Toxicol, 2014. **27**(5): p. 882-94.
21. Jaeschke, H., et al., *Mechanisms of hepatotoxicity*. Toxicol Sci, 2002. **65**(2): p. 166-76.
22. Kalinec, G.M., et al., *Acetaminophen and NAPQI are toxic to auditory cells via oxidative and endoplasmic reticulum stress-dependent pathways*. Hear Res, 2014. **313**: p. 26-37.
23. Silva, M.F., et al., *Valproic acid metabolism and its effects on mitochondrial fatty acid oxidation: a review*. J Inherit Metab Dis, 2008. **31**(2): p. 205-16.
24. Cotariu, D. and J.L. Zaidman, *Valproic acid and the liver*. Clin Chem, 1988. **34**(5): p. 890-7.
25. Kesterson, J.W., G.R. Granneman, and J.M. Machinist, *The hepatotoxicity of valproic acid and its metabolites in rats. I. Toxicologic, biochemical and histopathologic studies*. Hepatology, 1984. **4**(6): p. 1143-52.
26. Labbe, G., D. Pessayre, and B. Fromenty, *Drug-induced liver injury through mitochondrial dysfunction: mechanisms and detection during preclinical safety studies*. Fundam Clin Pharmacol, 2008. **22**(4): p. 335-53.
27. Porceddu, M., et al., *Prediction of liver injury induced by chemicals in human with a multiparametric assay on isolated mouse liver mitochondria*. Toxicol Sci, 2012. **129**(2): p. 332-45.
28. Begriche, K., et al., *Drug-induced toxicity on mitochondria and lipid metabolism: mechanistic diversity and deleterious consequences for the liver*. J Hepatol, 2011. **54**(4): p. 773-94.



29. Kamei, J. and Y. Kasuya, *The effect of hydrochlorothiazide on the enhanced coughing associated with treatment with enalapril*. Eur J Pharmacol, 1992. **213**(1): p. 137-9.
30. Aluvila, S., et al., *Organization of the mitochondrial apoptotic BAK pore: oligomerization of the BAK homodimers*. J Biol Chem, 2014. **289**(5): p. 2537-51.
31. Vinken, M., et al., *Drug-induced liver injury: mechanisms, types and biomarkers*. Curr Med Chem, 2013. **20**(24): p. 3011-21.
32. Deniaud, A., et al., *Endoplasmic reticulum stress induces calcium-dependent permeability transition, mitochondrial outer membrane permeabilization and apoptosis*. Oncogene, 2008. **27**(3): p. 285-99.
33. Bertolotti, A., et al., *Dynamic interaction of BiP and ER stress transducers in the unfolded-protein response*. Nat Cell Biol, 2000. **2**(6): p. 326-32.
34. Di Sano, F., et al., *Endoplasmic reticulum stress induces apoptosis by an apoptosome-dependent but caspase 12-independent mechanism*. J Biol Chem, 2006. **281**(5): p. 2693-700.
35. Kobayashi, E., et al., *Halothane-induced liver injury is mediated by interleukin-17 in mice*. Toxicol Sci, 2009. **111**(2): p. 302-10.
36. Pirmohamed, M., D.A. Ostrov, and B.K. Park, *New genetic findings lead the way to a better understanding of fundamental mechanisms of drug hypersensitivity*. J Allergy Clin Immunol, 2015. **136**(2): p. 236-44.
37. Matsuo, K., et al., *Involvement of oxidative stress and immune- and inflammation-related factors in azathioprine-induced liver injury*. Toxicol Lett, 2014. **224**(2): p. 215-24.
38. Fredriksson, L., et al., *Diclofenac inhibits tumor necrosis factor-alpha-induced nuclear factor-kappaB activation causing synergistic hepatocyte apoptosis*. Hepatology, 2011. **53**(6): p. 2027-41.
39. Roberts, R.A., et al., *Role of the Kupffer cell in mediating hepatic toxicity and carcinogenesis*. Toxicol Sci, 2007. **96**(1): p. 2-15.
40. Klaassen, C.D. and J.Y. Cui, *Review: Mechanisms of How the Intestinal Microbiota Alters the Effects of Drugs and Bile Acids*. Drug Metab Dispos, 2015. **43**(10): p. 1505-21.
41. Krauskopf, J., et al., *Global MicroRNA Analysis in Primary Hepatocyte Cultures*. Methods Mol Biol, 2015. **1250**: p. 241-50.
42. Pennings, J.L., et al., *Gene set assembly for quantitative prediction of developmental toxicity in the embryonic stem cell test*. Toxicology, 2011. **284**(1-3): p. 63-71.
43. Hochstenbach, K., et al., *Transcriptomic fingerprints in human peripheral blood mononuclear cells indicative of genotoxic and non-genotoxic carcinogenic exposure*. Mutat Res, 2012. **746**(2): p. 124-34.
44. Kamp, H., et al., *Reproducibility and robustness of metabolome analysis in rat plasma of 28-day repeated dose toxicity studies*. Toxicol Lett, 2012. **215**(2): p. 143-9.
45. Jennings, P., et al., *An overview of transcriptional regulation in response to toxicological insult*. Arch Toxicol, 2013. **87**(1): p. 49-72.
46. Igarashi, Y., et al., *Open TG-GATEs: a large-scale toxicogenomics database*. Nucleic Acids Res, 2015. **43**(Database issue): p. D921-7.
47. Ganter, B., et al., *Toxicogenomics in drug discovery and development: mechanistic analysis of compound/class-dependent effects using the DrugMatrix database*. Pharmacogenomics, 2006. **7**(7): p. 1025-44.
48. Poser, I., et al., *BAC TransgeneOmics: a high-throughput method for exploration of protein function in mammals*. Nature Methods, 2008. **5**(5): p. 409-15.
49. Kametsky, L., et al., *Improved structure, function and compatibility for CellProfiler: modular high-throughput image analysis software*. Bioinformatics, 2011. **27**(8): p. 1179-80.
50. Fraser, W.D., *Storing and Processing Complex Data Sets with HDF5*. Aerosp Med Hum Perform, 2015. **86**(7): p. 659-61.
51. Davern, T.J., *Drug-induced liver disease*. Clin. Liver Dis., 2012. **16**(2): p. 231-45.
52. Holt, M.P. and C. Ju, *Mechanisms of drug-induced liver injury*. AAPS J., 2006. **8**(1): p. E48-54.
53. Silva, F.G., *Chemical-induced nephropathy: a review of the renal tubulointerstitial lesions in humans*. Toxicol. Pathol., 2004. **32 Suppl 2**: p. 71-84.
54. Wolf, J. and W.R. Levis, *The study of simple chemicals in animals and man: mechanisms of contact sensitivity*. J. Drugs. Dermatol., 2012. **11**(10): p. 1166-73.
55. Hayes, A. and S. Bakand, *Inhalation toxicology*. EXS, 2010. **100**: p. 461-88.
56. Mariussen, E., *Neurotoxic effects of perfluoroalkylated compounds: mechanisms of action and environmental relevance*. Arch Toxicol, 2012. **86**(9): p. 1349-67.
57. Kinter, L.B. and J.P. Valentin, *Safety pharmacology and risk assessment*. Fundam Clin Pharmacol, 2002. **16**(3): p. 175-82.
58. Hall, A.P., et al., *Liver hypertrophy: a review of adaptive (adverse and non-adverse) changes--conclusions from the 3rd International ESTP Expert Workshop*. Toxicol Pathol, 2012. **40**(7): p. 971-94.

59. Liefvendahl, E. and H.J. Arnqvist, *Mitogenic effect of the insulin analogue glargine in malignant cells in comparison with insulin and IGF-I*. *Horm Metab Res*, 2008. **40**(6): p. 369-74.
60. Andersen, M.E., et al., *The future of toxicity testing*. *J Toxicol Environ Health B Crit Rev*, 2010. **13**(2-4): p. 163-96.
61. van Vliet, E., *Current standing and future prospects for the technologies proposed to transform toxicity testing in the 21st century*. *ALTEX*, 2011. **28**(1): p. 17-44.
62. *National Research Council: Toxicity testing in the 21st century: a vision and a strategy*.
63. Ankley, G.T., et al., *Adverse outcome pathways: a conceptual framework to support ecotoxicology research and risk assessment*. *Environ Toxicol Chem*, 2010. **29**(3): p. 730-41.
64. Peters, T.S., *Do preclinical testing strategies help predict human hepatotoxic potentials?* *Toxicol Pathol*, 2005. **33**(1): p. 146-54.
65. Ramirez, T., et al., *Metabolomics in toxicology and preclinical research*. *ALTEX*, 2013. **30**(2): p. 209-25.
66. Chen, M., et al., *A decade of toxicogenomic research and its contribution to toxicological science*. *Toxicol Sci*, 2012. **130**(2): p. 217-28.
67. Zhang, M., M. Chen, and W. Tong, *Is toxicogenomics a more reliable and sensitive biomarker than conventional indicators from rats to predict drug-induced liver injury in humans?* *Chem Res Toxicol*, 2012. **25**(1): p. 122-9.
68. Ellinger-Ziegelbauer, H., et al., *Application of toxicogenomics to study mechanisms of genotoxicity and carcinogenicity*. *Toxicol Lett*, 2009. **186**(1): p. 36-44.
69. Ryan, T.P., J.L. Stevens, and C.E. Thomas, *Strategic applications of toxicogenomics in early drug discovery*. *Curr Opin Pharmacol*, 2008. **8**(5): p. 654-60.
70. Uehara, T., et al., *The Japanese toxicogenomics project: application of toxicogenomics*. *Mol Nutr Food Res*, 2010. **54**(2): p. 218-27.
71. Yamada, F., et al., *Toxicogenomics discrimination of potential hepatocarcinogenicity of non-genotoxic compounds in rat liver*. *J Appl Toxicol*, 2012.
72. Hirode, M., et al., *Gene expression profiling in rat liver treated with compounds inducing elevation of bilirubin*. *Hum Exp Toxicol*, 2009. **28**(4): p. 231-44.
73. Hirode, M., et al., *Gene expression profiling in rat liver treated with various hepatotoxic-compounds inducing coagulopathy*. *J Toxicol Sci*, 2009. **34**(3): p. 281-93.
74. Carreras Puigvert, J., et al., *Systems biology approach identifies the kinase Csnk1a1 as a regulator of the DNA damage response in embryonic stem cells*. *Sci Signal*, 2013. **6**(259): p. ra5.
75. Pines, A., et al., *Global phosphoproteome profiling reveals unanticipated networks responsive to cisplatin treatment of embryonic stem cells*. *Mol Cell Biol*, 2011. **31**(24): p. 4964-77.
76. von Stechow, L., et al., *Identification of Cisplatin-regulated metabolic pathways in pluripotent stem cells*. *PLoS One*, 2013. **8**(10): p. e76476.
77. Porter, E., et al., *Use of an avian hepatocyte assay and the avian ToxChip PCR array for testing prioritization of 16 organic flame retardants*. *Environ Toxicol Chem*, 2013.
78. Krutzik, P.O., et al., *Phospho flow cytometry methods for the analysis of kinase signalling in cell lines and primary human blood samples*. *Methods Mol Biol*, 2011. **699**: p. 179-202.
79. LeCluyse, E.L., et al., *Organotypic liver culture models: meeting current challenges in toxicity testing*. *Crit Rev Toxicol*, 2012. **42**(6): p. 501-48.
80. Gerlier, D. and N. Thomasset, *Use of MTT colorimetric assay to measure cell activation*. *J Immunol Methods*, 1986. **94**(1-2): p. 57-63.
81. Malich, G., B. Markovic, and C. Winder, *The sensitivity and specificity of the MTS tetrazolium assay for detecting the in vitro cytotoxicity of 20 chemicals using human cell lines*. *Toxicology*, 1997. **124**(3): p. 179-92.
82. Miret, S., E.M. De Groene, and W. Klaffke, *Comparison of in vitro assays of cellular toxicity in the human hepatic cell line HepG2*. *J Biomol Screen*, 2006. **11**(2): p. 184-93.
83. Fernandez-Cruz, E., et al., *Hepatocyte damage induced by lymphocytes from patients with chronic liver diseases, as detected by LDH release*. *Clin Exp Immunol*, 1978. **31**(3): p. 436-42.
84. Tolosa, L., et al., *Development of a multiparametric cell-based protocol to screen and classify the hepatotoxicity potential of drugs*. *Toxicol Sci*, 2012. **127**(1): p. 187-98.
85. Zanella, F., J.B. Lorens, and W. Link, *High content screening: seeing is believing*. *Trends Biotechnol*, 2010. **28**(5): p. 237-45.
86. Thomas, N., *High-content screening: a decade of evolution*. *J Biomol Screen*, 2010. **15**(1): p. 1-9.
87. Steinberg, P., *High-throughput screening methods in toxicity testing*. xv, 552 pages.
88. Zhang, G., et al., *Early detection of apoptosis using a fluorescent conjugate of annexin V*. *Biotechniques*, 1997. **23**(3): p. 525-31.
89. Listenberger, L.L. and D.A. Brown, *Fluorescent detection of lipid droplets and associated proteins*. *Curr Protoc Cell Biol*, 2007. **Chapter 24**: p. Unit 24 2.

90. van de Water, F.M., et al., *High content screening analysis of phospholipidosis: validation of a 96-well assay with CHO-K1 and HepG2 cells for the prediction of in vivo based phospholipidosis*. *Toxicol In Vitro*, 2011. **25**(8): p. 1870-82.
91. O'Brien, P.J., et al., *High concordance of drug-induced human hepatotoxicity with in vitro cytotoxicity measured in a novel cell-based model using high content screening*. *Arch Toxicol*, 2006. **80**(9): p. 580-604.
92. Peyker, A., O. Rocks, and P.I. Bastiaens, *Imaging activation of two Ras isoforms simultaneously in a single cell*. *Chembiochem*, 2005. **6**(1): p. 78-85.
93. Violin, J.D., et al., *A genetically encoded fluorescent reporter reveals oscillatory phosphorylation by protein kinase C*. *J Cell Biol*, 2003. **161**(5): p. 899-909.
94. Imamura, H., et al., *Visualization of ATP levels inside single living cells with fluorescence resonance energy transfer-based genetically encoded indicators*. *Proc Natl Acad Sci U S A*, 2009. **106**(37): p. 15651-6.
95. Huang, R., et al., *Chemical genomics profiling of environmental chemical modulation of human nuclear receptors*. *Environ Health Perspect*, 2011. **119**(8): p. 1142-8.
96. Raymond, J. and D. Segre, *The effect of oxygen on biochemical networks and the evolution of complex life*. *Science*, 2006. **311**(5768): p. 1764-7.
97. Ma, Q., *Transcriptional responses to oxidative stress: pathological and toxicological implications*. *Pharmacol Ther*, 2010. **125**(3): p. 376-93.
98. Forman, H.J. and M. Torres, *Reactive oxygen species and cell signalling: respiratory burst in macrophage signalling*. *Am J Respir Crit Care Med*, 2002. **166**(12 Pt 2): p. S4-8.
99. Talalay, P., A.T. Dinkova-Kostova, and W.D. Holtzclaw, *Importance of phase 2 gene regulation in protection against electrophile and reactive oxygen toxicity and carcinogenesis*. *Adv Enzyme Regul*, 2003. **43**: p. 121-34.
100. James, L.P., P.R. Mayeux, and J.A. Hinson, *Acetaminophen-induced hepatotoxicity*. *Drug Metab Dispos*, 2003. **31**(12): p. 1499-506.
101. Barve, A., et al., *Gamma-tocopherol-enriched mixed tocopherol diet inhibits prostate carcinogenesis in TRAMP mice*. *Int J Cancer*, 2009. **124**(7): p. 1693-9.
102. Pool-Zobel, B., S. Veeriah, and F.D. Bohmer, *Modulation of xenobiotic metabolising enzymes by anticarcinogens -- focus on glutathione S-transferases and their role as targets of dietary chemoprevention in colorectal carcinogenesis*. *Mutat Res*, 2005. **591**(1-2): p. 74-92.
103. Kumaraguruparan, R., et al., *Chemoprevention of rat mammary carcinogenesis by black tea polyphenols: modulation of xenobiotic-metabolizing enzymes, oxidative stress, cell proliferation, apoptosis, and angiogenesis*. *Mol Carcinog*, 2007. **46**(9): p. 797-806.
104. Lee, S.B., et al., *Induction of the phase II detoxification enzyme NQO1 in hepatocarcinoma cells by lignans from the fruit of Schisandra chinensis through nuclear accumulation of Nrf2*. *Planta Med*, 2009. **75**(12): p. 1314-8.
105. Venugopal, R. and A.K. Jaiswal, *Nrf1 and Nrf2 positively and c-Fos and Fra1 negatively regulate the human antioxidant response element-mediated expression of NAD(P)H:quinone oxidoreductase1 gene*. *Proc Natl Acad Sci U S A*, 1996. **93**(25): p. 14960-5.
106. Ma, Q. and X. He, *Molecular basis of electrophilic and oxidative defense: promises and perils of Nrf2*. *Pharmacol Rev*, 2012. **64**(4): p. 1055-81.
107. Itoh, K., et al., *Keap1 represses nuclear activation of antioxidant responsive elements by Nrf2 through binding to the amino-terminal Neh2 domain*. *Genes Dev*, 1999. **13**(1): p. 76-86.
108. Talalay, P., M.J. De Long, and H.J. Prochaska, *Identification of a common chemical signal regulating the induction of enzymes that protect against chemical carcinogenesis*. *Proc Natl Acad Sci U S A*, 1988. **85**(21): p. 8261-5.
109. Dinkova-Kostova, A.T., et al., *Potency of Michael reaction acceptors as inducers of enzymes that protect against carcinogenesis depends on their reactivity with sulfhydryl groups*. *Proc Natl Acad Sci U S A*, 2001. **98**(6): p. 3404-9.
110. Zhang, D.D., et al., *Keap1 is a redox-regulated substrate adaptor protein for a Cul3-dependent ubiquitin ligase complex*. *Mol Cell Biol*, 2004. **24**(24): p. 10941-53.
111. Hong, F., M.L. Freeman, and D.C. Liebler, *Identification of sensor cysteines in human Keap1 modified by the cancer chemopreventive agent sulforaphane*. *Chem Res Toxicol*, 2005. **18**(12): p. 1917-26.
112. Rushmore, T.H., M.R. Morton, and C.B. Pickett, *The antioxidant responsive element. Activation by oxidative stress and identification of the DNA consensus sequence required for functional activity*. *J Biol Chem*, 1991. **266**(18): p. 11632-9.
113. Liu, J., et al., *Nrf2 protection against liver injury produced by various hepatotoxicants*. *Oxid Med Cell Longev*, 2013. **2013**: p. 305861.
114. Patterson, A.D., et al., *Disruption of Thioredoxin Reductase 1 Protects Mice from Acute Acetaminophen-Induced Hepatotoxicity through Enhanced NRF2 Activity*. *Chem Res Toxicol*, 2013.

115. Copple, I.M., et al., *The hepatotoxic metabolite of acetaminophen directly activates the Keap1-Nrf2 cell defense system*. Hepatology, 2008. **48**(4): p. 1292-301.
116. Kansanen, E., et al., *The Keap1-Nrf2 pathway: Mechanisms of activation and dysregulation in cancer*. Redox Biol, 2013. **1**(1): p. 45-49.
117. Shelton, P. and A.K. Jaiswal, *The transcription factor NF-E2-related factor 2 (Nrf2): a protooncogene?* FASEB J, 2013. **27**(2): p. 414-23.
118. Hetz, C., *The unfolded protein response: controlling cell fate decisions under ER stress and beyond*. Nat Rev Mol Cell Biol, 2012. **13**(2): p. 89-102.
119. Ron, D. and P. Walter, *Signal integration in the endoplasmic reticulum unfolded protein response*. Nat Rev Mol Cell Biol, 2007. **8**(7): p. 519-29.
120. Shen, J., et al., *ER stress regulation of ATF6 localization by dissociation of BiP/GRP78 binding and unmasking of Golgi localization signals*. Dev Cell, 2002. **3**(1): p. 99-111.
121. Harding, H.P., et al., *Regulated translation initiation controls stress-induced gene expression in mammalian cells*. Mol Cell, 2000. **6**(5): p. 1099-108.
122. Ameri, K. and A.L. Harris, *Activating transcription factor 4*. Int J Biochem Cell Biol, 2008. **40**(1): p. 14-21.
123. Travers, K.J., et al., *Functional and genomic analyses reveal an essential coordination between the unfolded protein response and ER-associated degradation*. Cell, 2000. **101**(3): p. 249-58.
124. Han, D., et al., *IRE1alpha kinase activation modes control alternate endoribonuclease outputs to determine divergent cell fates*. Cell, 2009. **138**(3): p. 562-75.
125. Kroemer, G., G. Marino, and B. Levine, *Autophagy and the integrated stress response*. Mol Cell, 2010. **40**(2): p. 280-93.
126. Kang, S.W., et al., *Substrate-specific translocational attenuation during ER stress defines a pre-emptive quality control pathway*. Cell, 2006. **127**(5): p. 999-1013.
127. Haze, K., et al., *Mammalian transcription factor ATF6 is synthesized as a transmembrane protein and activated by proteolysis in response to endoplasmic reticulum stress*. Mol Biol Cell, 1999. **10**(11): p. 3787-99.
128. Yamamoto, K., et al., *Transcriptional induction of mammalian ER quality control proteins is mediated by single or combined action of ATF6alpha and XBP1*. Dev Cell, 2007. **13**(3): p. 365-76.
129. Averous, J., et al., *Induction of CHOP expression by amino acid limitation requires both ATF4 expression and ATF2 phosphorylation*. J Biol Chem, 2004. **279**(7): p. 5288-97.
130. Zhang, H., et al., *Selective, potent blockade of the IRE1 and ATF6 pathways by 4-phenylbutyric acid analogues*. Br J Pharmacol, 2013. **170**(4): p. 822-34.
131. Ma, Y. and L.M. Hendershot, *Herp is dually regulated by both the endoplasmic reticulum stress-specific branch of the unfolded protein response and a branch that is shared with other cellular stress pathways*. J Biol Chem, 2004. **279**(14): p. 13792-9.
132. Yamaguchi, H. and H.G. Wang, *CHOP is involved in endoplasmic reticulum stress-induced apoptosis by enhancing DR5 expression in human carcinoma cells*. J Biol Chem, 2004. **279**(44): p. 45495-502.
133. Puthalakath, H., et al., *ER stress triggers apoptosis by activating BH3-only protein Bim*. Cell, 2007. **129**(7): p. 1337-49.
134. Back, S.H., et al., *Translation attenuation through eIF2alpha phosphorylation prevents oxidative stress and maintains the differentiated state in beta cells*. Cell Metab, 2009. **10**(1): p. 13-26.
135. Tamaki, N., et al., *CHOP deficiency attenuates cholestasis-induced liver fibrosis by reduction of hepatocyte injury*. Am J Physiol Gastrointest Liver Physiol, 2008. **294**(2): p. G498-505.
136. Hur, K.Y., et al., *IRE1alpha activation protects mice against acetaminophen-induced hepatotoxicity*. J Exp Med, 2012. **209**(2): p. 307-18.
137. Racanelli, V. and B. Rehermann, *The liver as an immunological organ*. Hepatology, 2006. **43**(2 Suppl 1): p. S54-62.
138. Tian, Z., Y. Chen, and B. Gao, *Natural killer cells in liver disease*. Hepatology, 2013. **57**(4): p. 1654-62.
139. Lukacs-Kornek, V. and D. Schuppan, *Dendritic cells in liver injury and fibrosis: shortcomings and promises*. J Hepatol, 2013. **59**(5): p. 1124-6.
140. Shaw, P.J., P.E. Ganey, and R.A. Roth, *Tumor necrosis factor alpha is a proximal mediator of synergistic hepatotoxicity from trovafloxacin/lipopolysaccharide coexposure*. The Journal of pharmacology and experimental therapeutics, 2009. **328**(1): p. 62-8.
141. Zou, W., et al., *Sulindac metabolism and synergy with tumor necrosis factor-alpha in a drug-inflammation interaction model of idiosyncratic liver injury*. The Journal of pharmacology and experimental therapeutics, 2009. **331**(1): p. 114-21.
142. Landstrom, M., *The TAK1-TRAF6 signalling pathway*. The international journal of biochemistry & cell biology, 2010. **42**(5): p. 585-9.
143. Dinarello, C.A., *Immunological and inflammatory functions of the interleukin-1 family*. Annual review of immunology, 2009. **27**: p. 519-50.

144. Corsini, A., et al., *Current challenges and controversies in drug-induced liver injury*. Drug safety : an international journal of medical toxicology and drug experience, 2012. **35**(12): p. 1099-117.
145. Eliceiri, K.W., et al., *Biological imaging software tools*. Nat Methods, 2012. **9**(7): p. 697-710.
146. Cosgrove, B.D., et al., *Synergistic drug-cytokine induction of hepatocellular death as an in vitro approach for the study of inflammation-associated idiosyncratic drug hepatotoxicity*. Toxicology and applied pharmacology, 2009. **237**(3): p. 317-30.
147. Ramm, S. and A. Mally, *Role of drug-independent stress factors in liver injury associated with diclofenac intake*. Toxicology, 2013. **312C**: p. 83-96.
148. Kastan, M.B. and J. Bartek, *Cell-cycle checkpoints and cancer*. Nature, 2004. **432**(7015): p. 316-23.
149. Hartwell, L.H. and T.A. Weinert, *Checkpoints: controls that ensure the order of cell cycle events*. Science, 1989. **246**(4930): p. 629-34.
150. Lagerwerf, S., et al., *DNA damage response and transcription*. DNA Repair (Amst), 2011. **10**(7): p. 743-50.
151. Shiloh, Y., *ATM and related protein kinases: safeguarding genome integrity*. Nat Rev Cancer, 2003. **3**(3): p. 155-68.
152. FitzGerald, J.E., M. Grenon, and N.F. Lowndes, *53BP1: function and mechanisms of focal recruitment*. Biochem Soc Trans, 2009. **37**(Pt 4): p. 897-904.
153. Zhou, B.B. and S.J. Elledge, *The DNA damage response: putting checkpoints in perspective*. Nature, 2000. **408**(6811): p. 433-9.
154. Li, L. and L. Zou, *Sensing, signalling, and responding to DNA damage: organization of the checkpoint pathways in mammalian cells*. J Cell Biochem, 2005. **94**(2): p. 298-306.
155. Banin, S., et al., *Enhanced phosphorylation of p53 by ATM in response to DNA damage*. Science, 1998. **281**(5383): p. 1674-7.
156. Khosravi, R., et al., *Rapid ATM-dependent phosphorylation of MDM2 precedes p53 accumulation in response to DNA damage*. Proc Natl Acad Sci U S A, 1999. **96**(26): p. 14973-7.
157. Riley, T., et al., *Transcriptional control of human p53-regulated genes*. Nat Rev Mol Cell Biol, 2008. **9**(5): p. 402-12.
158. Yu, J. and L. Zhang, *No PUMA, no death: implications for p53-dependent apoptosis*. Cancer Cell, 2003. **4**(4): p. 248-9.
159. Chipuk, J.E., et al., *PUMA couples the nuclear and cytoplasmic proapoptotic function of p53*. Science, 2005. **309**(5741): p. 1732-5.
160. Vousden, K.H. and C. Prives, *Blinded by the Light: The Growing Complexity of p53*. Cell, 2009. **137**(3): p. 413-31.
161. Brady, C.A. and L.D. Attardi, *p53 at a glance*. J Cell Sci, 2010. **123**(Pt 15): p. 2527-32.
162. Bieganski, K.T. and L.D. Attardi, *Deconstructing p53 transcriptional networks in tumor suppression*. Trends Cell Biol, 2012. **22**(2): p. 97-106.
163. Liang, S.H. and M.F. Clarke, *Regulation of p53 localization*. Eur J Biochem, 2001. **268**(10): p. 2779-83.
164. Tao, W. and A.J. Levine, *Nucleocytoplasmic shuttling of oncoprotein Hdm2 is required for Hdm2-mediated degradation of p53*. Proc Natl Acad Sci U S A, 1999. **96**(6): p. 3077-80.
165. Jayaraman, L. and C. Prives, *Covalent and noncovalent modifiers of the p53 protein*. Cell Mol Life Sci, 1999. **55**(1): p. 76-87.
166. Tibbetts, R.S., et al., *A role for ATR in the DNA damage-induced phosphorylation of p53*. Genes Dev, 1999. **13**(2): p. 152-7.
167. Shieh, S.Y., et al., *DNA damage-induced phosphorylation of p53 alleviates inhibition by MDM2*. Cell, 1997. **91**(3): p. 325-34.
168. Sakaguchi, K., et al., *Damage-mediated phosphorylation of human p53 threonine 18 through a cascade mediated by a casein 1-like kinase. Effect on Mdm2 binding*. J Biol Chem, 2000. **275**(13): p. 9278-83.
169. Harper, J.W. and S.J. Elledge, *The DNA damage response: ten years after*. Mol Cell, 2007. **28**(5): p. 739-45.
170. Bartek, J., J. Bartkova, and J. Lukas, *DNA damage signalling guards against activated oncogenes and tumour progression*. Oncogene, 2007. **26**(56): p. 7773-9.
171. Moudry, P., et al., *Nucleoporin NUP153 guards genome integrity by promoting nuclear import of 53BP1*. Cell Death Differ, 2012. **19**(5): p. 798-807.
172. Levav-Cohen, Y., S. Haupt, and Y. Haupt, *Mdm2 in growth signalling and cancer*. Growth Factors, 2005. **23**(3): p. 183-92.
173. Lahav, G., *Oscillations by the p53-Mdm2 feedback loop*. Adv Exp Med Biol, 2008. **641**: p. 28-38.
174. Westerheide, S.D. and R.I. Morimoto, *Heat shock response modulators as therapeutic tools for diseases of protein conformation*. J Biol Chem, 2005. **280**(39): p. 33097-100.
175. Voellmy, R. and F. Boellmann, *Chaperone regulation of the heat shock protein response*. Adv Exp Med Biol, 2007. **594**: p. 89-99.

176. Kampinga, H.H., et al., *Guidelines for the nomenclature of the human heat shock proteins*. Cell Stress Chaperones, 2009. **14**(1): p. 105-11.
177. Simmons, S.O., C.Y. Fan, and R. Ramabhadran, *Cellular stress response pathway system as a sentinel ensemble in toxicological screening*. Toxicol Sci, 2009. **111**(2): p. 202-25.
178. Gunther, V., et al., *A conserved cysteine cluster, essential for transcriptional activity, mediates homodimerization of human metal-responsive transcription factor-1 (MTF-1)*. Biochim Biophys Acta, 2012. **1823**(2): p. 476-83.
179. Carpena, E., G. Andreani, and G. Isani, *Metallothionein functions and structural characteristics*. J Trace Elem Med Biol, 2007. **21 Suppl 1**: p. 35-9.
180. Wang, Y., et al., *Metal-responsive transcription factor-1 (MTF-1) is essential for embryonic liver development and heavy metal detoxification in the adult liver*. FASEB J, 2004. **18**(10): p. 1071-9.
181. Lee, K.A., R.A. Roth, and J.J. LaPres, *Hypoxia, drug therapy and toxicity*. Pharmacol Ther, 2007. **113**(2): p. 229-46.
182. Li, Y., et al., *HUMMR, a hypoxia- and HIF-1alpha-inducible protein, alters mitochondrial distribution and transport*. J Cell Biol, 2009. **185**(6): p. 1065-81.
183. Sparkenbaugh, E.M., et al., *The role of hypoxia-inducible factor-1alpha in acetaminophen hepatotoxicity*. J Pharmacol Exp Ther, 2011. **338**(2): p. 492-502.
184. Li, F., et al., *Human PXR modulates hepatotoxicity associated with rifampicin and isoniazid co-therapy*. Nat Med, 2013. **19**(4): p. 418-20.
185. Picard, M., et al., *Mitochondrial morphology transitions and functions: implications for retrograde signalling?* Am J Physiol Regul Integr Comp Physiol, 2013. **304**(6): p. R393-406.
186. Rimessi, A., et al., *Perturbed mitochondrial Ca signals as causes or consequences of mitophagy induction*. Autophagy, 2013. **9**(11).
187. Lenna, S. and M. Trojanowska, *The role of endoplasmic reticulum stress and the unfolded protein response in fibrosis*. Curr Opin Rheumatol, 2012. **24**(6): p. 663-8.
188. Huveneers, S., et al., *Integrins uncouple Src-induced morphological and oncogenic transformation*. J Biol Chem, 2008. **283**(19): p. 13243-51.
189. van de Water, B., et al., *Cleavage of the actin-capping protein alpha -adducin at Asp-Asp-Ser-Asp633-Ala by caspase-3 is preceded by its phosphorylation on serine 726 in cisplatin-induced apoptosis of renal epithelial cells*. J Biol Chem, 2000. **275**(33): p. 25805-13.
190. Schneider, C.A., W.S. Rasband, and K.W. Eliceiri, *NIH Image to ImageJ: 25 years of image analysis*. Nat Methods, 2012. **9**(7): p. 671-5.
191. Carpenter, A.E., et al., *CellProfiler: image analysis software for identifying and quantifying cell phenotypes*. Genome Biol, 2006. **7**(10): p. R100.
192. *The HDF Group Hierarchical data format version 5*. 2000-2010.
193. Di, Z., et al., *Automated analysis of NF-kappaB nuclear translocation kinetics in high-throughput screening*. PLoS One, 2012. **7**(12): p. e52337.
194. Sommer, C., et al., *CellH5: a format for data exchange in high-content screening*. Bioinformatics, 2013. **29**(12): p. 1580-2.
195. Dougherty, M.T., et al., *Unifying Biological Image Formats with HDF5*. Commun ACM, 2009. **52**(10): p. 42-47.
196. Warren, S.C., et al., *Rapid global fitting of large fluorescence lifetime imaging microscopy datasets*. PLoS One, 2013. **8**(8): p. e70687.
197. Michael R. Berthold, N.C., Fabian Dill, Thomas R. Gabriel, Tobias Kötter, Thorsten Meinl, Peter Ohl, Christoph Sieb, Kilian Thiel, Bernd Wiswedel, *KNIME: The Konstanz Information Miner*. Studies in Classification, Data Analysis, and Knowledge Organization (GfKL 2007). Springer.
198. ToxCast™. <http://www.epa.gov/ncct/toxcast/>. Available from: <http://www.epa.gov/ncct/toxcast/>.
199. Yates, M.S., et al., *Pharmacodynamic characterization of chemopreventive triterpenoids as exceptionally potent inducers of Nrf2-regulated genes*. Mol Cancer Ther, 2007. **6**(1): p. 154-62.
200. Laine, L., et al., *How common is diclofenac-associated liver injury? Analysis of 17,289 arthritis patients in a long-term prospective clinical trial*. The American journal of gastroenterology, 2009. **104**(2): p. 356-62.
201. Yano, A., et al., *Involvement of immune-related factors in diclofenac-induced acute liver injury in mice*. Toxicology, 2012. **293**(1-3): p. 107-14.
202. Basak, S., M. Behar, and A. Hoffmann, *Lessons from mathematically modeling the NF-kappaB pathway*. Immunol Rev, 2012. **246**(1): p. 221-38.
203. Jain, A., et al., *p62/SQSTM1 is a target gene for transcription factor NRF2 and creates a positive feedback loop by inducing antioxidant response element-driven gene transcription*. J Biol Chem, 2010. **285**(29): p. 22576-91.
204. Li, Y., J.D. Paonessa, and Y. Zhang, *Mechanism of chemical activation of Nrf2*. PLoS One, 2012. **7**(4): p. e35122.

205. McMahon, M., et al., *Redox-regulated turnover of Nrf2 is determined by at least two separate protein domains, the redox-sensitive Neh2 degron and the redox-insensitive Neh6 degron*. J Biol Chem, 2004. **279**(30): p. 31556-67.
206. Westerink, W.M. and W.G. Schoonen, *Phase II enzyme levels in HepG2 cells and cryopreserved primary human hepatocytes and their induction in HepG2 cells*. Toxicol In Vitro, 2007. **21**(8): p. 1592-602.
207. Westerink, W.M. and W.G. Schoonen, *Cytochrome P450 enzyme levels in HepG2 cells and cryopreserved primary human hepatocytes and their induction in HepG2 cells*. Toxicol In Vitro, 2007. **21**(8): p. 1581-91.
208. Nakamura, K., et al., *Expression of albumin and cytochrome P450 enzymes in HepG2 cells cultured with a nanotechnology-based culture plate with microfabricated scaffold*. J Toxicol Sci, 2011. **36**(5): p. 625-33.
209. Katsuda, T., Y. Sakai, and T. Ochiya, *Induced pluripotent stem cell-derived hepatocytes as an alternative to human adult hepatocytes*. J Stem Cells, 2012. **7**(1): p. 1-17.
210. Tox21. <http://www.epa.gov/ncct/Tox21/>. Available from: <http://www.epa.gov/ncct/Tox21/>.
211. Vinken, M., *The adverse outcome pathway concept: a pragmatic tool in toxicology*. Toxicology, 2013. **312**: p. 158-65.
212. Venugopal, R. and A.K. Jaiswal, *Nrf2 and Nrf1 in association with Jun proteins regulate antioxidant response element-mediated expression and coordinated induction of genes encoding detoxifying enzymes*. Oncogene, 1998. **17**(24): p. 3145-56.
213. Kim, R., et al., *Role of the unfolded protein response in cell death*. Apoptosis, 2006. **11**(1): p. 5-13.
214. Reed, M., et al., *The C-terminal domain of p53 recognizes DNA damaged by ionizing radiation*. Proc Natl Acad Sci U S A, 1995. **92**(21): p. 9455-9.
215. Girinsky, T., et al., *Attenuated response of p53 and p21 in primary cultures of human prostatic epithelial cells exposed to DNA-damaging agents*. Cancer Res, 1995. **55**(17): p. 3726-31.
216. Mazur, W., et al., *Cell-specific elevation of NRF2 and sulfiredoxin-1 as markers of oxidative stress in the lungs of idiopathic pulmonary fibrosis and non-specific interstitial pneumonia*. APMIS, 2010. **118**(9): p. 703-12.
217. Herpers, B., et al., *Activation of the Nrf2 response by intrinsic hepatotoxic drugs correlates with suppression of NF-kappaB activation and sensitizes toward TNFalpha-induced cytotoxicity*. Arch Toxicol, 2015.
218. Takayanagi, S., et al., *Gene regulatory network of unfolded protein response genes in endoplasmic reticulum stress*. Cell Stress Chaperones, 2013. **18**(1): p. 11-23.
219. Reinke, V. and G. Lozano, *Differential activation of p53 targets in cells treated with ultraviolet radiation that undergo both apoptosis and growth arrest*. Radiat Res, 1997. **148**(2): p. 115-22.
220. d'Adda di Fagagna, F., et al., *A DNA damage checkpoint response in telomere-initiated senescence*. Nature, 2003. **426**(6963): p. 194-8.
221. Knasmuller, S., et al., *Use of human-derived liver cell lines for the detection of environmental and dietary genotoxicants; current state of knowledge*. Toxicology, 2004. **198**(1-3): p. 315-28.
222. Maness, S.C., D.P. McDonnell, and K.W. Gaido, *Inhibition of androgen receptor-dependent transcriptional activity by DDT isomers and methoxychlor in HepG2 human hepatoma cells*. Toxicol Appl Pharmacol, 1998. **151**(1): p. 135-42.
223. Lin, Z. and Y. Will, *Evaluation of drugs with specific organ toxicities in organ-specific cell lines*. Toxicol Sci, 2012. **126**(1): p. 114-27.
224. Purschke, M., et al., *Phototoxicity of Hoechst 33342 in time-lapse fluorescence microscopy*. Photochem Photobiol Sci, 2010. **9**(12): p. 1634-9.
225. Du, G., et al., *Spatial dynamics of DNA damage response protein foci along the ion trajectory of high-LET particles*. Radiat Res, 2011. **176**(6): p. 706-15.
226. Wickham, H., *ggplot2: elegant graphics for data analysis*. 2009.
227. Gaujoux, R. and C. Seoighe, *A flexible R package for nonnegative matrix factorization*. BMC Bioinformatics, 2010. **11**: p. 367.
228. Irizarry, R.A., et al., *Exploration, normalization, and summaries of high density oligonucleotide array probe level data*. Biostatistics, 2003. **4**(2): p. 249-64.
229. Itoh, K., K.I. Tong, and M. Yamamoto, *Molecular mechanism activating Nrf2-Keap1 pathway in regulation of adaptive response to electrophiles*. Free Radic Biol Med, 2004. **36**(10): p. 1208-13.
230. Hetz, C., E. Chevet, and S.A. Oakes, *Proteostasis control by the unfolded protein response*. Nat Cell Biol, 2015. **17**(7): p. 829-38.
231. Gulow, K., D. Bienert, and I.G. Haas, *BiP is feed-back regulated by control of protein translation efficiency*. J Cell Sci, 2002. **115**(Pt 11): p. 2443-52.
232. Lee, D.H., et al., *Dephosphorylation enables the recruitment of 53BP1 to double-strand DNA breaks*. Mol Cell, 2014. **54**(3): p. 512-25.
233. Yang, L., et al., *Neuroprotective effects of the triterpenoid, CDDO methyl amide, a potent inducer of Nrf2-mediated transcription*. PLoS One, 2009. **4**(6): p. e5757.

234. Li, L. and G.K. Hu, *Pink1 protects cortical neurons from thapsigargin-induced oxidative stress and neuronal apoptosis*. Biosci Rep, 2015. **35**(1).
235. Yoshida, H., *Unconventional splicing of XBP-1 mRNA in the unfolded protein response*. Antioxid Redox Signal, 2007. **9**(12): p. 2323-33.
236. Wink, S., et al., *Quantitative high content imaging of cellular adaptive stress response pathways in toxicity for chemical safety assessment*. Chem Res Toxicol, 2014. **27**(3): p. 338-55.
237. Limonciel, A., et al., *Transcriptomics hit the target: Monitoring of ligand-activated and stress response pathways for chemical testing*. Toxicol In Vitro, 2015.
238. Fredriksson, L., et al., *Drug-induced endoplasmic reticulum and oxidative stress responses independently sensitize toward TNFalpha-mediated hepatotoxicity*. Toxicol Sci, 2014. **140**(1): p. 144-59.
239. Loo, L.H., L.F. Wu, and S.J. Altschuler, *Image-based multivariate profiling of drug responses from single cells*. Nat Methods, 2007. **4**(5): p. 445-53.
240. Persson, M., et al., *A high content screening assay to predict human drug-induced liver injury during drug discovery*. J Pharmacol Toxicol Methods, 2013. **68**(3): p. 302-13.
241. Garside, H., et al., *Evaluation of the use of imaging parameters for the detection of compound-induced hepatotoxicity in 384-well cultures of HepG2 cells and cryopreserved primary human hepatocytes*. Toxicol In Vitro, 2014. **28**(2): p. 171-81.
242. Roth, R.A. and P.E. Ganey, *Animal models of idiosyncratic drug-induced liver injury--current status*. Crit Rev Toxicol, 2011. **41**(9): p. 723-39.
243. Shaw, P.J., et al., *Lipopolysaccharide and trovafloxacin coexposure in mice causes idiosyncrasy-like liver injury dependent on tumor necrosis factor-alpha*. Toxicol Sci, 2007. **100**(1): p. 259-66.
244. Cosgrove, B.D., et al., *Synergistic drug-cytokine induction of hepatocellular death as an in vitro approach for the study of inflammation-associated idiosyncratic drug hepatotoxicity*. Toxicol Appl Pharmacol, 2009. **237**(3): p. 317-30.
245. Lu, J., et al., *Amiodarone exposure during modest inflammation induces idiosyncrasy-like liver injury in rats: role of tumor necrosis factor-alpha*. Toxicol Sci, 2012. **125**(1): p. 126-33.
246. Cosgrove, B.D., et al., *Cytokine-associated drug toxicity in human hepatocytes is associated with signalling network dysregulation*. Mol Biosyst, 2010. **6**(7): p. 1195-206.
247. Cui, Y. and R.S. Paules, *Use of transcriptomics in understanding mechanisms of drug-induced toxicity*. Pharmacogenomics, 2010. **11**(4): p. 573-85.
248. Jaiswal, A.K., *Nrf2 signalling in coordinated activation of antioxidant gene expression*. Free Radic Biol Med, 2004. **36**(10): p. 1199-207.
249. Kobayashi, A., et al., *Oxidative stress sensor Keap1 functions as an adaptor for Cul3-based E3 ligase to regulate proteasomal degradation of Nrf2*. Mol Cell Biol, 2004. **24**(16): p. 7130-9.
250. Okawa, H., et al., *Hepatocyte-specific deletion of the keap1 gene activates Nrf2 and confers potent resistance against acute drug toxicity*. Biochem Biophys Res Commun, 2006. **339**(1): p. 79-88.
251. Woehlbier, U. and C. Hetz, *Modulating stress responses by the UPRosome: a matter of life and death*. Trends Biochem Sci, 2011. **36**(6): p. 329-37.
252. Dara, L., C. Ji, and N. Kaplowitz, *The contribution of endoplasmic reticulum stress to liver diseases*. Hepatology, 2011. **53**(5): p. 1752-63.
253. van Kesteren, P.C., et al., *Deregulation of cancer-related pathways in primary hepatocytes derived from DNA repair-deficient Xpa-/-p53+/- mice upon exposure to benzo[a]pyrene*. Toxicol Sci, 2011. **123**(1): p. 123-32.
254. Hochberg, Y. and Y. Benjamini, *More powerful procedures for multiple significance testing*. Stat Med, 1990. **9**(7): p. 811-8.
255. Saeed, A.I., et al., *TM4: a free, open-source system for microarray data management and analysis*. Biotechniques, 2003. **34**(2): p. 374-8.
256. Edgar, R., M. Domrachev, and A.E. Lash, *Gene Expression Omnibus: NCBI gene expression and hybridization array data repository*. Nucleic Acids Res, 2002. **30**(1): p. 207-10.
257. Huber, W., et al., *Variance stabilization applied to microarray data calibration and to the quantification of differential expression*. Bioinformatics, 2002. **18 Suppl 1**: p. S96-104.
258. Wolfinger, R.D., et al., *Assessing gene significance from cDNA microarray expression data via mixed models*. J Comput Biol, 2001. **8**(6): p. 625-37.
259. Smyth, G.K., J. Michaud, and H.S. Scott, *Use of within-array replicate spots for assessing differential expression in microarray experiments*. Bioinformatics, 2005. **21**(9): p. 2067-75.
260. Smyth, G.K., *Linear models and empirical bayes methods for assessing differential expression in microarray experiments*. Stat Appl Genet Mol Biol, 2004. **3**: p. Article3.
261. Puigvert, J.C., et al., *High-throughput live cell imaging of apoptosis*. Curr Protoc Cell Biol, 2010. **Chapter 18**: p. Unit 18 10 1-13.



262. van De Water, B., et al., *Distinct endoplasmic reticulum signalling pathways regulate apoptotic and necrotic cell death following iodoacetamide treatment*. Chem Res Toxicol, 1999. **12**(10): p. 943-51.
263. Xu, J.J., et al., *Cellular imaging predictions of clinical drug-induced liver injury*. Toxicol Sci, 2008. **105**(1): p. 97-105.
264. Chen, M., et al., *FDA-approved drug labeling for the study of drug-induced liver injury*. Drug Discov Today, 2011. **16**(15-16): p. 697-703.
265. Zou, W., et al., *Sulindac metabolism and synergy with tumor necrosis factor-alpha in a drug-inflammation interaction model of idiosyncratic liver injury*. J Pharmacol Exp Ther, 2009. **331**(1): p. 114-21.
266. Soriano, F.X., et al., *Transcriptional regulation of the AP-1 and Nrf2 target gene sulfiredoxin*. Mol Cells, 2009. **27**(3): p. 279-82.
267. Cullinan, S.B. and J.A. Diehl, *Coordination of ER and oxidative stress signalling: the PERK/Nrf2 signalling pathway*. Int J Biochem Cell Biol, 2006. **38**(3): p. 317-32.
268. Boyce, M., et al., *A selective inhibitor of eIF2alpha dephosphorylation protects cells from ER stress*. Science, 2005. **307**(5711): p. 935-9.
269. Deng, X., et al., *Gene expression profiles in livers from diclofenac-treated rats reveal intestinal bacteria-dependent and -independent pathways associated with liver injury*. J Pharmacol Exp Ther, 2008. **327**(3): p. 634-44.
270. Leeder, J.S., *Mechanisms of idiosyncratic hypersensitivity reactions to antiepileptic drugs*. Epilepsia, 1998. **39 Suppl 7**: p. S8-16.
271. Stricker, B.H., et al., *Ketoconazole-associated hepatic injury. A clinicopathological study of 55 cases*. J Hepatol, 1986. **3**(3): p. 399-406.
272. West, S.G., *Methotrexate hepatotoxicity*. Rheum Dis Clin North Am, 1997. **23**(4): p. 883-915.
273. Choi, S., *Nefazodone (Serzone) withdrawn because of hepatotoxicity*. CMAJ, 2003. **169**(11): p. 1187.
274. Parsyan, A., et al., *mRNA helicases: the tacticians of translational control*. Nat Rev Mol Cell Biol, 2011. **12**(4): p. 235-45.
275. Jackson, R.J., C.U. Hellen, and T.V. Pestova, *The mechanism of eukaryotic translation initiation and principles of its regulation*. Nat Rev Mol Cell Biol, 2010. **11**(2): p. 113-27.
276. Holcik, M., et al., *A new internal-ribosome-entry-site motif potentiates XIAP-mediated cytoprotection*. Nat Cell Biol, 1999. **1**(3): p. 190-2.
277. Coldwell, M.J., et al., *Initiation of Apaf-1 translation by internal ribosome entry*. Oncogene, 2000. **19**(7): p. 899-905.
278. Cantoni, L., et al., *Induction of hepatic heme oxygenase-1 by diclofenac in rodents: role of oxidative stress and cytochrome P-450 activity*. J Hepatol, 2003. **38**(6): p. 776-83.
279. Gomez-Lechon, M.J., et al., *Diclofenac induces apoptosis in hepatocytes by alteration of mitochondrial function and generation of ROS*. Biochem Pharmacol, 2003. **66**(11): p. 2155-67.
280. Santos, N.A., et al., *Involvement of oxidative stress in the hepatotoxicity induced by aromatic antiepileptic drugs*. Toxicol In Vitro, 2008. **22**(8): p. 1820-4.
281. Han, D., et al., *Regulation of drug-induced liver injury by signal transduction pathways: critical role of mitochondria*. Trends in Pharmacological Sciences, 2013. **34**(4): p. 243-253.
282. Steuerwald, N.M., et al., *Profiles of serum cytokines in acute drug-induced liver injury and their prognostic significance*. PLoS One, 2013. **8**(12): p. e81974.
283. Shaw, P.J., et al., *Lipopolysaccharide and trovafloxacin coexposure in mice causes idiosyncrasy-like liver injury dependent on tumor necrosis factor-alpha*. Toxicological Sciences, 2007. **100**(1): p. 259-66.
284. Mercurio, F., et al., *IKK-1 and IKK-2: cytokine-activated I kappa B kinases essential for NF-kappa B activation*. Science, 1997. **278**(5339): p. 860-6.
285. Liu, Z.G., et al., *Dissection of TNF receptor 1 effector functions: JNK activation is not linked to apoptosis while NF-kappa B activation prevents cell death*. Cell, 1996. **87**(3): p. 565-76.
286. Leung, L., A.S. Kalgutkar, and R.S. Obach, *Metabolic activation in drug-induced liver injury*. Drug Metab Rev, 2012. **44**(1): p. 18-33.
287. Li, J., et al., *Stabilization of Nrf2 by tBHQ confers protection against oxidative stress-induced cell death in human neural stem cells*. Toxicological Sciences, 2005. **83**(2): p. 313-28.
288. Liu, F., et al., *Increased susceptibility of Nrf2-null mice to 1-bromopropane-induced hepatotoxicity*. Toxicological Sciences, 2010. **115**(2): p. 596-606.
289. Chen, X.L., et al., *Activation of Nrf2/ARE pathway protects endothelial cells from oxidant injury and inhibits inflammatory gene expression*. Am J Physiol Heart Circ Physiol, 2006. **290**(5): p. H1862-70.
290. Ashburner, M., et al., *Gene ontology: tool for the unification of biology. The Gene Ontology Consortium*. Nature Genetics, 2000. **25**(1): p. 25-9.
291. Carbon, S., et al., *AmiGO: online access to ontology and annotation data*. Bioinformatics, 2009. **25**(2): p. 288-9.

292. Liberzon, A., et al., *Molecular signatures database (MSigDB) 3.0*. Bioinformatics, 2011. **27**(12): p. 1739-40.
293. Kanehisa, M., et al., *Data, information, knowledge and principle: back to metabolism in KEGG*. Nucleic acids research, 2014. **42**(Database issue): p. D199-205.
294. Croft, D., et al., *The Reactome pathway knowledgebase*. Nucleic Acids Research, 2014. **42**(Database issue): p. D472-7.
295. Qian, Z., Y.D. Cai, and Y. Li, *Automatic transcription factor classifier based on functional domain composition*. Biochemical and Biophysical Research Communications, 2006. **347**(1): p. 141-4.
296. Di, Z., et al., *Automated Analysis of NF- $\kappa$ B Nuclear Translocation Kinetics in High-Throughput Screening*. PLoS One, 2012. **7**(12): p. e52337.
297. Yu, M., et al., *Nuclear factor p65 interacts with Keap1 to repress the Nrf2-ARE pathway*. Cellular Signalling, 2011. **23**(5): p. 883-892.
298. Liu, G.H., J. Qu, and X. Shen, *NF-kappaB/p65 antagonizes Nrf2-ARE pathway by depriving CBP from Nrf2 and facilitating recruitment of HDAC3 to MafK*. Biochimica et biophysica acta, 2008. **1783**(5): p. 713-27.
299. Boess, F., et al., *Gene expression in two hepatic cell lines, cultured primary hepatocytes, and liver slices compared to the in vivo liver gene expression in rats: possible implications for toxicogenomics use of in vitro systems*. Toxicological sciences : an official journal of the Society of Toxicology, 2003. **73**(2): p. 386-402.
300. Rushworth, S.A., S. Shah, and D.J. MacEwan, *TNF mediates the sustained activation of Nrf2 in human monocytes*. Journal of immunology, 2011. **187**(2): p. 702-7.
301. Hsu, H., et al., *TRADD-TRAF2 and TRADD-FADD interactions define two distinct TNF receptor 1 signal transduction pathways*. Cell, 1996. **84**(2): p. 299-308.
302. Sano, R. and J.C. Reed, *ER stress-induced cell death mechanisms*. Biochimica et biophysica acta, 2013. **1833**(12): p. 3460-70.
303. Hutti, J.E., et al., *IkappaB kinase beta phosphorylates the K63 deubiquitinase A20 to cause feedback inhibition of the NF-kappaB pathway*. Molecular and Cellular Biology, 2007. **27**(21): p. 7451-61.
304. Hinz, M. and C. Scheidereit, *The IkappaB kinase complex in NF-kappaB regulation and beyond*. EMBO Rep, 2014. **15**(1): p. 46-61.
305. Hadi, M., et al., *AMAP, the alleged non-toxic isomer of acetaminophen, is toxic in rat and human liver*. Archives of Toxicology, 2013. **87**(1): p. 155-165.
306. Cheng, J., et al., *CYP2E1-dependent elevation of serum cholesterol, triglycerides, and hepatic bile acids by isoniazid*. Toxicology and Applied Pharmacology, 2013. **266**(2): p. 245-253.
307. Foster, J.R., et al., *Differential Effect of Troglitazone on the Human Bile Acid Transporters, MRP2 and BSEP, in the PXB Hepatic Chimeric Mouse*. Toxicol Pathol, 2012.
308. Malinen, M.M., et al., *Peptide nanofiber hydrogel induces formation of bile canaliculi structures in three-dimensional hepatic cell culture*. Tissue engineering. Part A, 2012. **18**(23-24): p. 2418-25.
309. Raschi, E. and F. De Ponti, *Drug- and herb-induced liver injury: Progress, current challenges and emerging signals of post-marketing risk*. World J Hepatol, 2015. **7**(13): p. 1761-71.
310. Tang, S., et al., *Cytochrome P450 2E1 gene polymorphisms/haplotypes and anti-tuberculosis drug-induced hepatitis in a Chinese cohort*. PLoS One, 2013. **8**(2): p. e57526.
311. Ramachandran, R. and S. Kakar, *Histological patterns in drug-induced liver disease*. J Clin Pathol, 2009. **62**(6): p. 481-92.
312. Adeleye, Y., et al., *Implementing Toxicity Testing in the 21st Century (TT21C): Making safety decisions using toxicity pathways, and progress in a prototype risk assessment*. Toxicology, 2015. **332**: p. 102-11.
313. Park, S., Y.J. Choi, and B.H. Lee, *In vitro validation of drug-induced phospholipidosis*. J Toxicol Sci, 2012. **37**(2): p. 261-7.
314. Chatterjee, S., et al., *Hepatocyte-based in vitro model for assessment of drug-induced cholestasis*. Toxicol Appl Pharmacol, 2014. **274**(1): p. 124-36.
315. Dick, S.H., L.A. Tremere, and D.D. Rasmusson, *Calcitonin gene-related peptide and neuropeptide Y in the raccoon cuneate nucleus*. Brain Res Bull, 1998. **47**(4): p. 387-91.
316. Liu, Y., et al., *Role for the endoplasmic reticulum stress sensor IRE1alpha in liver regenerative responses*. J Hepatol, 2015. **62**(3): p. 590-8.
317. Mulder, J.E., et al., *The impact of chronic Aflatoxin B1 exposure and p53 genotype on base excision repair in mouse lung and liver*. Mutat Res, 2015. **773**: p. 63-8.
318. Bhat, A.H., et al., *Oxidative stress, mitochondrial dysfunction and neurodegenerative diseases; a mechanistic insight*. Biomed Pharmacother, 2015. **74**: p. 101-10.
319. Kaufman, R.J., *Orchestrating the unfolded protein response in health and disease*. J Clin Invest, 2002. **110**(10): p. 1389-98.
320. Ma, Y. and L.M. Hendershot, *The unfolding tale of the unfolded protein response*. Cell, 2001. **107**(7): p. 827-30.
321. Brenner, C., et al., *Decoding cell death signals in liver inflammation*. J Hepatol, 2013. **59**(3): p. 583-94.

322. Nagy, T., et al., *Inhibition of Glutathione S-Transferase by Ethacrynic Acid Augments Ischemia-Reperfusion Damage and Apoptosis and Attenuates the Positive Effect of Ischemic Postconditioning in a Bilateral Acute Hindlimb Ischemia Rat Model*. J Vasc Res, 2015. **52**(1): p. 53-61.
323. Suresh Kumar, G., et al., *Mitomycin C-DNA adducts generated by DT-diaphorase. Revised mechanism of the enzymatic reductive activation of mitomycin C*. Biochemistry, 1997. **36**(46): p. 14128-36.
324. Kim, J.A., et al., *Real-time concurrent monitoring of apoptosis, cytosolic calcium, and mitochondria permeability transition for hypermulticolor high-content screening of drug-induced mitochondrial dysfunction-mediated hepatotoxicity*. Toxicol Lett, 2012. **214**(2): p. 175-81.
325. Jones, T.R., et al., *CellProfiler Analyst: data exploration and analysis software for complex image-based screens*. BMC Bioinformatics, 2008. **9**: p. 482.
326. Di, Z., et al., *Ultra high content image analysis and phenotype profiling of 3D cultured micro-tissues*. PLoS One, 2014. **9**(10): p. e109688.
327. Goldring, C.E., et al., *Activation of hepatic Nrf2 in vivo by acetaminophen in CD-1 mice*. Hepatology, 2004. **39**(5): p. 1267-76.
328. Stephens, C., R.J. Andrade, and M.I. Lucena, *Mechanisms of drug-induced liver injury*. Curr Opin Allergy Clin Immunol, 2014. **14**(4): p. 286-92.
329. Allan, C., et al., *OMERO: flexible, model-driven data management for experimental biology*. Nat Methods, 2012. **9**(3): p. 245-53.
330. Schindelin, J., et al., *Fiji: an open-source platform for biological-image analysis*. Nat Methods, 2012. **9**(7): p. 676-82.
331. Forslund, E., et al., *Novel Microchip-Based Tools Facilitating Live Cell Imaging and Assessment of Functional Heterogeneity within NK Cell Populations*. Front Immunol, 2012. **3**: p. 300.
332. Pauwels, E., et al., *A probabilistic model for cell population phenotyping using HCS data*. PLoS One, 2012. **7**(8): p. e42715.
333. van Roosmalen, W., et al., *Tumor cell migration screen identifies SRPK1 as breast cancer metastasis determinant*. J Clin Invest, 2015. **125**(4): p. 1648-64.
334. Uzi, D., et al., *CHOP is a critical regulator of acetaminophen-induced hepatotoxicity*. J Hepatol, 2013. **59**(3): p. 495-503.
335. Pfaffenbach, K.T., et al., *Linking endoplasmic reticulum stress to cell death in hepatocytes: roles of C/EBP homologous protein and chemical chaperones in palmitate-mediated cell death*. Am J Physiol Endocrinol Metab, 2010. **298**(5): p. E1027-35.
336. Beggs, K.M., et al., *Trovafloxacin-induced replication stress sensitizes HepG2 cells to tumor necrosis factor-alpha-induced cytotoxicity mediated by extracellular signal-regulated kinase and ataxia telangiectasia and Rad3-related*. Toxicology, 2015. **331**: p. 35-46.
337. Alkreathy, H.M., et al., *CCl4 induced genotoxicity and DNA oxidative damages in rats: hepatoprotective effect of Sonchus arvensis*. BMC Complement Altern Med, 2014. **14**: p. 452.

## List of abbreviations

---

ADR: Adverse Drug Reaction  
AMAP: 3'-hydroxyacetanilide  
AMI: amiodarone  
AOP: Adverse Outcome Pathway  
APAP: acetaminophen/ paracetamol  
BAC: Bacterial Artificial Chromosome  
BFA: Brefeldin A  
CBZ: carbamazepine  
CDDO-Me: bardoxolone methyl (methyl-2-cyano 3,12-dioxooleano-1,9-dien-28-oate)  
CLZ: clozapine  
DCF: diclofenac  
DDR: DNA damage response  
DEM: di-ethyl maleate  
DEM: Diethylmaleate  
DILI: Drug-Induced Liver Injury  
ER-stress Endoplasmic Reticulum stress  
IAA: Iodoacetamide  
INH: isoniazid  
H<sub>2</sub>O<sub>2</sub>: hydrogen peroxide  
HCI: High Content Imaging  
HTS: High Throughput Screening  
HTI: High Throughput Imaging  
HTM: High Throughput Microscopy  
KTZ: ketoconazole  
MEN: menadione  
MTX: methotrexate  
NFZ: nefazodone  
NPX: naproxen  
NTF: nitrofurantoin  
OFX: ofloxacin  
OSR: Oxidative stress response/ antioxidant pathways  
PHH: primary human hepatocytes  
PI: propidium iodide  
ROS: reactive oxygen species  
SN: simvastatin  
siRNA: small interfering RNA  
Tc: Tunicamycin  
Tg: Thapsigargin  
TGZ: troglitazone  
UPR: Unfolded Protein Response

# Samenvatting

## Waarom dit onderzoek

Veel geneesmiddelen, met name antibiotica-, ontstekingsremmers-, antischimmel-, anti-psychose- en antikankergeneesmiddelen en bepaalde alternatieve geneeskruiden kunnen bij sommige individuen leiden tot ernstige leverschade. De lever is het orgaan dat het meest beschadigd raakt door toxische verbindingen omdat al de opgenomen voedselcomponenten uiteindelijk via de lever in de bloedcirculatie komen. Bovendien is de lever verantwoordelijk voor het metaboliseren en detoxificeren van schadelijke verbindingen. Soms leidt metabolisme juist tot de vorming van reactieve metabolieten afkomstig van een anders onschadelijke verbinding.

De door medicijn-geïnduceerde leverschade is globaal in zeven verschillende typen te onderscheiden: 1) Fibrose: cellen genaamd “hepatische stellaat cellen” maken bindweefsel met als doel de lever te repareren maar de vorming hiervan kan verstoord worden door sommige geneesmiddelen. 2) Cirrose of leverontsteking: langdurige leverschade of problemen met de productie van bindweefsel in de lever kan leiden tot overmatig veel littekenweefsel. Dit wordt cirrose genoemd en is meestal het gevolg van een chronische primaire pathologie. 3) Cholestase: problemen met galzuur metabolisme of transport in de lever leiden tot stapeling van galzuren in de lever en tot schade in de levercellen. 4) Steatose/ steatosis hepatis: als een probleem met metabolisme of transport van vetten plaatsvindt waardoor er een ophoping van deze vetten (voornamelijk triglyceriden) ontstaat, heet dit steatose. Wanneer er als gevolg hiervan ontstekingen in de lever plaatsvinden dan wordt dit steatosis hepatis genoemd. Het vaakst komt deze leveraandoening door alcoholmisbruik maar ook geneesmiddelen kunnen deze pathologie induceren. 5) Fosfolipidose: een vorm van steatose met ophoping van fosfolipiden als gevolg van problemen met liposomale verwerking van vet. 6) Necrose: celdood van levercellen op een ongecontroleerde wijze. Tot slot 7) Apoptose: celdood van levercellen op een door cellen gecontroleerde wijze.

Blootstelling aan sommige geneesmiddelen leidt tot iets mildere vormen van leverschade, zoals steatose en cholestase, dat pas op de langere termijn tot cirrose kan leiden. Echter, sommige geneesmiddelen die tot massale leverceldood leiden, in de vorm van necrose of apoptose, zorgen voor imminente ernstige complicaties waarbij een snelle levertransplantatie nodig is.

Met behulp van allerlei methoden, met cellen (*in vitro*), met bepaalde proefdieren (*in vivo*) en klinisch onderzoek, proberen wetgever en farmaceutische bedrijven te voorkomen dat dergelijke leverschade-inducerende geneesmiddelen op de markt komen. Soms gebeurt het dat geneesmiddelen op de markt komen die bij sommige individuen (ernstige) leverschade veroorzaken. Dit gebeurt bij één op enkele tot vele duizenden patiënten, afhankelijk van het geneesmiddel. Een dergelijke zeldzame ongewenste reactie op een geneesmiddel noemt men een idiosyncratische reactie. De oorzaak van idiosyncratische reacties is niet helemaal bekend en verschilt van individu tot individu (*i.e.* genetisch). Verschillen in milieumomstandigheden en externe factoren, zoals predispositie door activatie van het immuunsysteem, zijn in de literatuur vaak genoemde oorzaken. Naast de zogenaamde idiosyncratische reacties zijn er de algemene

levertoxische verbindingen. Deze toxiciteit is concentratie-afhankelijk en daarom beter te voorspellen als de toxiciteit eenmaal in mensen is geconstateerd. Echter, het ontwikkelen van geneesmiddelen is zeer kostbaar (dit kan oplopen tot meer dan een miljard euro en hoe verder in de ontwikkeling een medicijn is voordat de toxiciteit ervan duidelijk wordt, hoe hoger de kosten zullen zijn). Het is daarom zeer wenselijk voor de farmaceutische industrie, de consumenten en ook de gehele gezondheidszorg om nauwkeurig en vroeg in de ontwikkeling van een medicijn (lever) toxiciteit te kunnen voorspellen. Bovendien is het zeer gewenst deze vroege voorspellingen met behulp van *in vitro*-methoden te doen. Deze methoden kunnen namelijk vroeg in de ontwikkeling van nieuwe kandidaat-geneesmiddelen gebruikt worden wanneer het aantal nog zeer groot is. Dit doordat het mogelijk is 'high-throughput' te werken, in tegenstelling tot onderzoek met dierproeven en klinisch onderzoek.

### *Ons idee voor het bijdragen van het voorspellen van leverschade van nieuwe geneesmiddelen.*

Nieuwe wetenschappelijke methoden en inzichten hebben geleid tot een beter begrip van hoe de verschillende cellen in ons lichaam reageren op bepaalde verbindingen. Met technieken zoals 'microarray chips', 'proteomics' en 'metabolomics' die respectievelijk genen, eiwitten en metabolieten meten zijn de belangrijkste signaalroutes die cellen gebruiken om zichzelf in leven te houden of juist celdood initiëren in kaart gebracht. Verschillende essentiële signaaltransductie-routes die hieruit zijn voortgekomen zijn o.a. de adaptieve stress response signaaltransductie cascade; 1) de Nrf2-gemedieerde oxidatieve stress signaaltransductie cascade (Nrf2-cascade), 2) de endoplasmatisch reticulum ongevouwen eiwitten signaaltransductie cascade (ER-cascade) en 3) de p53-gemedieerde DNA-schade signaaltransductie cascade (DNA-cascade). Naast de adaptieve stress responsen is er de NF- $\kappa$ B gemedieerde immuun-signaltransductie cascade (NF- $\kappa$ B-cascade), dat een belangrijke rol bij celoverleving speelt.

De adaptieve stress response signaaltransductie cascades zijn evolutionair behouden celmechanismen die zorgen voor een endogene fysiologisch intracellulair milieu, zodat de cellen goed kunnen blijven functioneren als onderdeel van een orgaan.

Het is belangrijk dat cellen deze adaptieve mechanismen hebben om stress te neutraliseren dat wordt veroorzaakt door geneesmiddelen. Echter, het is van belang te beseffen dat de primaire rol van deze adaptieve mechanismen is om fysiologisch geïnduceerde stress te neutraliseren veroorzaakt door onder andere beweging, eten of ziekte. Zo zorgt de Nrf2-cascade bij oxidatieve stress ervoor dat er antioxidanteiwitten tot expressie komen om o.a. vrije radicalen en alkyliserende verbindingen op te ruimen en daarmee de beschadiging van macromoleculen, zoals eiwitten en DNA, maar ook beschadiging van celmembranen door lipide peroxidatie, tegen te gaan. De ER-cascade is een cellulair adaptief mechanisme dat bij problemen met het vouwen van aminozuurketens tot functionele eiwitten, in het endoplasmatisch reticulum, geactiveerd wordt. Deze activatie leidt tot het tot expressie brengen van meer zogenaamde chaperones. Deze chaperones helpen bij het op de juiste manier vouwen van de aminozuurketens, zodat het risico op de vorming van eiwitaggregaten verkleind wordt. Bovendien wordt bij de activatie van de ongevouwen eiwit response translatie gestopt. Bij langdurige activatie wordt de cel aangestuurd om in apoptose te gaan. Tot slot zorgt de DNA-cascade ervoor dat er bij schade aan het DNA

eiwitten tot expressie worden gebracht die de DNA-schade proberen te repareren. Daarnaast wordt celdeling een halt toegeroepen. Pas als het DNA gerepareerd is zal de cel weer kunnen delen.

Echter in tegenstelling tot cellulaire aanpassing en overleving is het ook belangrijk dat cellen de beslissing kunnen nemen om in apoptose te gaan. Dit om de gezondheid van een orgaan als geheel niet te belemmeren. Als een cel DNA-schade, eiwit aggregaten of andere beschadigingen na celdeling doorgeeft leidt dat tot ernstige problemen voor een orgaan en daarmee de gezondheid van het individu. De essentiële signaaltransductie cascade die bij de overleving van een cel een rol speelt is de NF- $\kappa$ B-cascade. Deze signaal cascade zorgt onder fysiologische omstandigheden ervoor dat een individuele cel niet in apoptose gaat. Echter kan bij bepaalde signalen, bijvoorbeeld na langdurige activatie van de ER-cascade of bij een virale of bacteriële infectie, dit er voor zorgen dat immuuncellen het paracrien cytokine TNF $\alpha$  signaal uitscheiden. Deze TNF $\alpha$  activeert de TNF $\alpha$ -receptor waardoor de NF- $\kappa$ B-cascade verstoord wordt.

De verschillende signaaltransductie-routes zorgen tezamen dus voor adaptatie en herstel nadat het biochemisch evenwicht is verstoord. Mochten de adaptieve stress response cascades het evenwicht niet kunnen herstellen, omdat de biochemische perturbatie of schade te groot was, dan zorgt o.a. de TNF $\alpha$ -receptor-route ervoor dat de cel in apoptose gaat.

Onze hypothese is dan ook dat alle soorten cellulaire schade, veroorzaakt door geneesmiddelen of andere verbindingen, gedetecteerd worden en leiden tot activatie van verschillende repareermechanismen in de cel.

Wij monitoren in levende cellen gedurende een bepaalde periode deze adaptieve stress cascades en de NF- $\kappa$ B-cascade gebruikmakend van fluorescerende eiwitten, de zogenaamde 'Green fluorescent protein' (GFP). Deze eiwitten zijn gefuseerd met eiwitten die zich op cruciale posities in de signaaltransductie cascades bevinden. De gefuseerde eiwitten zijn in een van de lever afgeleid celtype gebouwd, de HepG2 cellijn. Deze 'HepG2 reporter' cellijnen worden in incubatiebakjes gekweekt en blootgesteld aan verbindingen die ingedeeld zijn in de mate die deze lever-schade induceren. Met behulp van geautomatiseerde confocale microscopen hebben wij vervolgens de cellen gedurende 24 uur gevolgd, met als gevolg heel veel plaatjes in de tijd (filmpjes) met daarbij ook de mogelijkheid voor het onderscheiden van allerlei (morfologische) fenotypen na blootstelling aan de chemische stoffen. Deze fenotypen zijn bijvoorbeeld; de grootte van de kern, de migratiesnelheid, wanneer er bij welke concentratie de genoemde cascades worden geactiveerd en wanneer er bij welke concentratie de cellen in apoptose dan wel necrose gaan. Deze methode en de beargumentering van onze hypothese staat beschreven in hoofdstuk 2. In hoofdstuk 3 worden deze HepG2 reporter cellijnen getest op referentieverbindingen waarvan we weten wat voor type cellulaire schade deze induceren. Zo kon de gevoeligheid en selectiviteit van verschillende HepG2 reporter cellijnen geverifieerd worden. In hoofdstuk 4 is gedetailleerd onderzoek gedaan naar de invloed van de Nrf2-cascade en ER-cascade in de context van de immuun-cel cytokine TNF $\alpha$ , om de oxidatieve stress en ER-cascade activatie onder simulatie van een (bijvoorbeeld) infectie te simuleren. Hoofdstuk 5 sluit aan op hetzelfde principe en beschrijft het onderzoek naar de interactie tussen de NF- $\kappa$ B-cascade en Nrf2-cascade in de context van geneesmiddelen die leverschade induceren. Daarnaast is er een groep HepG2 reporter cellijnen gebruikt om een set van 180 geneesmiddelen en andere verbindingen te testen. De resultaten van dit microscopisch-fenotypisch onderzoek zijn gecorreleerd aan de mate waarin geneesmiddelen

leverschade induceren. Tot slot is de ontwikkeling van een gebruikersvriendelijke browser-gebaseerde interface voor het analyseren van de kwantitatieve data resulterend van de geautomatiseerde confocale microscopen beschreven in hoofdstuk 7.

## *Resultaten van dit onderzoek*

### *Hoofdstuk 3: Hoog-gehalte beelden gebaseerde BAC-GFP adaptieve stress responsen voor de evaluatie van de toxiciteits-risico van chemicaliën.*

Als eerste zijn de HepG2 reporter cellijnen gekloond door aan eiwitten die op cruciale locaties in de adaptieve stress cascades gepositioneerd zijn een fluorescent eiwit te fuseren. Vervolgens is het signaal detectie niveau (de gevoeligheid) en selectiviteit, voor ofwel oxidatieve stress, ofwel endoplasmatisch reticulum stress, ofwel DNA schade stress getest bij drie verschillende concentraties van een set referentie verbindingen waarvan het type toxiciteit bekend is. Het bleek dat de HepG2 reporter cellijnen in een concentratie afhankelijke wijze reageerden op de referentie verbindingen. Daarnaast bleken ze gevoelig genoeg om detectie mogelijk te maken en selectief aangezet te worden door hun corresponderende stress inducerende verbindingen. Bovendien bleek door het gebruik van microscopie-techniek de tijdsresolutie hoog genoeg zodat nauwkeurig bepaald kon worden in welke volgorde de adaptieve stress response cascades geactiveerd worden. Dit maakte het mogelijk de primaire stress type van de hierop volgende secundaire stress te scheiden. Tot slot is naar het RNA-niveau gekeken onder vergelijkbare condities in een publiek beschikbare micro-array dataset gebaseerd op primair humane hepatocyten. Primair humane hepatocyten worden beschouwd als een 'gouden standaard' model omdat het geïsoleerde levercellen van donoren zijn en daarom meer eigenschappen bezitten van een fysiologische lever. Het bleek dat de GFP gefuseerde eiwitten van HepG2 reporter cellijnen op een vergelijkbare manier reageerden ten opzichte van het RNA niveau van de primair humane hepatocyten.

### *Hoofdstuk 4: Geneesmiddelen-geïnduceerde endoplasmatisch reticulum- en oxidatieve stress responsen predisponeren naar TNF $\alpha$ geïnduceerde hepatotoxiciteit.*

In dit hoofdstuk zijn de onderliggende mechanismen van de synergistische respons van hepatotoxische geneesmiddelen en TNF $\alpha$  onderzocht gebruikmakend van een unieke combinatie van geïntegreerde transcriptomics en RNA-interferentie. Genexpressie analyse van HepG2 cellen, primaire humane- en muis hepatocyten en dunne menselijke leverplakjes demonstreerden dat specifieke activatie van de ER-cascade geschiedde door middel van activatie van de ATF4 transcriptie factor. Door gebruik te maken van RNA-interferentie, imaging en de HepG2-reporter cellijnen bleek een bepaalde arm van de ER-cascade, namelijk PERK-CHOP, cruciaal te zijn voor het geneesmiddel-TNF $\alpha$  geïnduceerde synergistische celdood. Oxidatieve stress zorgde voor een additionele impuls voor HepG2 celdood. Echter beïnvloedde deze oxidatieve stress niet de mate van ER-cascade activatie. De translatie inhibitie marker EIF4A1 bleek wel cruciaal voor de activatie van CHOP en daarmee het geobserveerde geneesmiddel/TNF $\alpha$  geïnduceerde celdood.

### *Hoofdstuk 5 Activatie van de Nrf2-cascade door intrinsieke hepatotoxische geneesmiddelen correleert met suppressie van NF- $\kappa$ B-cascade activatie en predisponeert naar TNF $\alpha$ -geïnduceerde cytotoxiciteit.*



Analyse van een grote transcriptomics dataset van primaire humane hepatocyten leidde tot het inzicht dat veel geneesmiddelen die ernstige leverschade kunnen veroorzaken ook een sterke Nrf2-cascade response kunnen induceren. Bovendien bleek dat deze Nrf2-cascade activatie correleerde met een lagere mate van NF- $\kappa$ B activatie. Dit inzicht is verder uitgewerkt gebruikmakend van een set van HepG2 reporters voor deze twee signaaltransductie cascades. Inderdaad, aan de hand van de tijdprofielen van activatie van deze twee cascades bleek dat TNF $\alpha$  geïnduceerde NF- $\kappa$ B activatie geremd werd door (met name sterk-leverschade inducerende) geneesmiddelen die een sterke Nrf2-response activeerden. Omdat NF- $\kappa$ B activatie belangrijk is voor cellen om te overleven bij TNF $\alpha$  stimulatie, zou de suppressie van deze signaaltransductie cascade een mogelijke verklaring kunnen zijn voor de synergistische celdood geïnduceerd door geneesmiddel/TNF $\alpha$ . Dankzij onze imaging-technieken met behulp van de HepG2-reporters was het mogelijk het oscillatoire gedrag van NF- $\kappa$ B te kwantificeren. Het bleek dat de remming van de NF- $\kappa$ B activatie bestond uit een vertraging van het herhaalde transport van NF- $\kappa$ B naar de kern. Daarom stellen wij voor deze vertraging als een bio-marker mee te nemen in toekomstige toxiciteit onderzoeken.

#### *Hoofdstuk 6 Geautomatiseerde 'live'-cel imaging van adaptieve stress responsen voor de bepaling van geneesmiddel- geïnduceerde leverschade.*

Gebruikmakend van drie HepG2-reporter cellijnen, namelijk; Srxn1 voor oxidatieve stress, CHOP voor ER-stress geïnduceerde ongevouwen eiwit response-activatie en p21 voor DNA-schade stress, is een groot aantal leverschade inducerende geneesmiddelen op stress-response activatie en additionele fenotypen die het niveau van toxiciteit laten zien weergegeven. Bijna de helft van alle leverschade inducerende geneesmiddelen activeerden een van de drie stress-responsen. Het merendeel van de geactiveerde stress-responsen bestond uit de Nrf2-cascade, gevolgd door de ER-cascade en een klein deel DNA-cascade activatie. Concentratie- en tijdresponsen van de stress response activatie gaf mechanistische informatie over het type stress, primaire/secundaire stress en bij welke concentraties dit geschiedde. Een belangrijke observatie, de gehele dataset in ogenschouw nemend, is dat onderzoek naar slechts enkele adaptieve stress cascades al een goede indicatie geeft over de potentieel tot ernstige leverschade die veroorzaakt kan worden door een verbinding. Dit onderbouwt ons concept dat toxiciteit mede veroorzaakt wordt door het tekortkomen van repareermechanismen en dat het kwantitatief meten van deze repareermechanismen gebruikt kan worden voor de voorspelling van het mogelijk optreden van toxiciteit. Aan de andere kant waren er geen repareermechanismen in werking gezet bij ongeveer de helft van alle geteste verbindingen en een derde van de leverschade inducerende geneesmiddelen. Dit is mogelijk omdat niet alle adaptieve repareermechanismen door ons onderzocht zijn in onze screening. Een andere verklaring kan zijn dat ons celmodel niet volledig representatief is. Wij zijn dan ook hard bezig met het maken van additionele reporter cellijnen die o.a. vet en galzuur metabolisme weergeven. Daarnaast proberen we deze reporters in te bouwen in andere celtypen.

Wij verwachten dat de in dit project ontwikkelde paneel van HepG2-reporters en afgeleide kwantitatieve data als 'biologische vingerafdruk' gebruikt kan worden voor het toekomstig 'high-throughput' screenen van verbindingen op hun potentie om levertoxiciteit te veroorzaken bij de mens.

## List of publications

### Quantitative high content imaging of cellular adaptive stress response pathways in toxicity for chemical safety assessment.

**Wink S**, Hiemstra S, Huppelschoten S, Danen E, Niemeijer M, Hendriks G, Vrieling H, Herpers B, van de Water B. *Chem Res Toxicol*. 2014 Mar 17;27(3):338-55. doi: 10.1021/tx4004038. Epub 2014 Feb 5. Review.  
PMID: 24450961

### Activation of the Nrf2 response by intrinsic hepatotoxic drugs correlates with suppression of NF-κB activation and sensitizes toward TNFα-induced cytotoxicity.

Herpers B, **Wink S**, Fredriksson L, Di Z, Hendriks G, Vrieling H, de Bont H, van de Water B. *Arch Toxicol*. 2015 May 31. [Epub ahead of print]  
PMID: 26026609

### Drug-induced endoplasmic reticulum and oxidative stress responses independently sensitize toward TNFα-mediated hepatotoxicity.

Fredriksson L, **Wink S**, Herpers B, Benedetti G, Hadi M, de Bont H, Groothuis G, Luijten M, Danen E, de Graauw M, Meerman J, van de Water B. *Toxicol Sci*. 2014 Jul;140(1):144-59. doi: 10.1093/toxsci/kfu072. Epub 2014 Apr 20.  
PMID: 24752500

### Alternative signalling network activation through different insulin receptor family members caused by pro-mitogenic antidiabetic insulin analogues in human mammary epithelial cells.

Ter Braak B, **Wink S**, Koedoot E, Pont C, Siezen CL, Van der Laan JW, Van de Water B. *Breast Cancer Res*. 2015 Jul 19;17:97. doi: 10.1186/s13058-015-0600-5.  
PMID: 26187749

### Toxicogenomics directory of chemically exposed human hepatocytes.

Grinberg M, Stöber RM, Edlund K, Rempel E, Godoy P, Reif R, Widera A, Madjar K, Schmidt-Heck W, Marchan R, Sachinidis A, Spitkovsky D, Hescheler J, Carmo H, Arbo MD, van de Water B, **Wink S**, Vinken M, Rogiers V, Escher S, Hardy B, Mitic D, Myatt G, Waldmann T, Mardinoglu A, Damm G, Seehofer D, Nüssler A, Weiss TS, Oberemm A, Lampen A, Schaap MM, Luijten M, van Steeg H, Thasler WE, Kleinjans JC, Stierum RH, Leist M, Rahnenführer J, Hengstler JG. *Arch Toxicol*. 2014 Dec;88(12):2261-87. doi: 10.1007/s00204-014-1400-x. Epub 2014 Nov 16.  
PMID: 25399406

### 3D cell culture improves liver-specific characteristics of HepG2 cells: a gene expression analysis-based comparison HepG2 spheroids and other liver models.

Sreenivasa Ramaiahgari<sup>1</sup>, Steven Wink<sup>1</sup>, Maarten Coonen<sup>2,3</sup>, Mackenzie Hadi<sup>3</sup>, John Meerman<sup>1</sup>, Mirjam Luijten<sup>4</sup>, Geny Groothuis<sup>5</sup>, Danyel Jennen<sup>2,3</sup>, Joost van Delft<sup>2,3</sup>, Leo Price<sup>1</sup> and Bob van de Water<sup>1</sup>  
<sup>1</sup>Division of Toxicology, Leiden Academic Centre for Drug Research, Leiden University, Leiden, The Netherlands.  
<sup>2</sup>Department of Toxicogenomics, Maastricht University, Maastricht, The Netherlands.  
<sup>4</sup>Laboratory for Health Protection Research, National Institute for Public Health and the Environment, Bilthoven, The Netherlands.  
<sup>5</sup>Division of Pharmacokinetics, Toxicology and Targeting, Department of Pharmacy, University of Groningen, Groningen, The Netherlands.  
Manuscript in preparation

### High Content Imaging-based BAC-GFP Toxicity Pathway Reporters to Assess Chemical Adversity Liabilities.

Steven Wink<sup>\*†</sup>, Steven Hiemstra<sup>\*†</sup>, Suzanna Huppelschoten<sup>\*</sup>, Bram Herpers<sup>\*</sup>, Bob van de Water<sup>\*§</sup>  
<sup>†</sup>Both authors contributed equally  
<sup>\*</sup>Division of Toxicology, Leiden Academic Centre for Drug Research, Leiden University, Leiden, The Netherlands  
Submitted to Archives of Toxicology (November 2015)

**Automated live cell imaging of adaptive stress responses for assessment of drug-induced liver injury (DILI) liabilities.**

Steven Wink\*‡, Steven W. Hiemstra\*‡, Suzanna Huppelschoten‡\*, Janna E. Klip\*, Bob van de Water\*§

\*Division of Toxicology, Leiden Academic Centre for Drug Research, Leiden University, Leiden, The Netherlands

‡authors contributed equally

Manuscript in preparation

**User friendly high-content imaging big-data analysis on a single desktop: R package H5CellProfiler.**

Steven Wink, Joost Beltman and Bob van de Water

Division of Toxicology, Leiden Academic Centre for Drug Research, Leiden University, Leiden, The Netherlands

Manuscript in preparation

**Functional analysis of high-content high-throughput imaging data.**

Xiaoqi Jiang<sup>a</sup>, Steven Wink<sup>b</sup>, Annette Kopp-Schneider<sup>a</sup>

<sup>a</sup>Division of Biostatistics, German Cancer Research Center, Im Neuenheimer Feld 280, 69120 Heidelberg, Germany

<sup>b</sup>Division of Toxicology, Leiden Academic Centre for Drug Research, Leiden University, Leiden, The Netherlands

Submitted to Journal of Applied Statistics (November 2015)

## Curriculum Vitae

Steven Wink was born in Warnsveld, the Netherlands, on April 2<sup>nd</sup> 1980. He went to the Scholengemeenschap Lelystad, where he obtained his VWO diploma in 2000.

In 2000, he started his study Life Science & Technology at the Technical University of Delft and Leiden University. After completion of his first semester he worked as a full time post-office servant followed by independent travel through Europe by bicycle. From 2001 to 2002 he took up residence in Basel, Switzerland, where he worked just across the border in Germany as a waiter and as a German-English translator. After two years studying earth sciences and biology in Utrecht he came back to his study Life Science & Technology. During his studies he worked part time as a junior researcher at a small biotech company where he was involved in optimizing sludge reduction by aquatic worms.

For his master thesis he modeled the kinetics of storage metabolites during dynamic feast famine cycles, based on <sup>13</sup>C intermittent feeding experiments with *Penicillium chrysogenum*. He obtained his master in biochemical engineering in 2011.

In 2011 he started working as a PhD student at the Leiden Academic Center for Drug Research at the Leiden University, on the project “Automated High Content Imaging of Cell Organelle Morphometry and Function in Cellular Stress Responses”. This project was carried out under the supervision of prof. dr. Bob van de Water.

From January 2016 he will work as a business intelligence consultant for Dimensional Insight in Leiden.